Kinetic modeling and experiments on gas uptake and chemical transformation of organic aerosol in the atmosphere

Dissertation zur Erlangung des Grades eines

`Doktor rerum naturalium (Dr. rer. nat.)'

der Fachbereiche:

09 - Chemie, Pharmazie und Geowissenschaften

der Johannes Gutenberg-Universität

Max Planck Graduate Center

vorgelegt von

Manabu Shiraiwa

geb. am 27.04.1983 in Japan

Mainz, 2011

Bibliografische Information der Deutschen Nationalbibliothek

Die Deutsche Nationalbibliothek verzeichnet diese Publikation in der Deutschen Nationalbibliografie; detaillierte bibliografische Daten sind im Internet über http://dnb.d-nb.de abrufbar.

Dissertationen aus:
International Max Planck Research School for Atmospheric Chemistry and Physics

Herausgegeben von:

MPI für Chemie, IMPRS
Postfach 3060
D-55020 Mainz, Germany
www.atmosphere.mpg.de/school

Titelbild: Christopher Pöhlker

ISBN 978-3-939262-12-1

1. Auflage 2011

I hereby declare that I wrote the dissertation submitted without any unauthorized external assistance and used only sources acknowledged in the work. All textual passages which are appropriated verbatim or paraphrased from published and unpublished texts as well as all information obtained from oral sources are duly indicated and listed in accordance with bibliographical rules. In carrying out this research, I compiled with the rules of standard scientific practice as formulated in the statutes of Johannes Gutenberg University Mainz to insure standard scientific practice.

Contents

Abstract

Aerosol particles affect climate by scattering and absorption of radiation and as nuclei for clouds and precipitation. Moreover, aerosols have a large impact on air pollution and human health. Gas-particle interactions are key processes because they can significantly change the physical and chemical properties of aerosols such as optical parameters, hygroscopicity and toxicity. Due to a lack of experimental data and rigorous model formalisms, however, the mechanisms and kinetics of gas uptake and chemical aging of organic aerosol are not well constrained. Moreover, the chemical transformation and adverse health effects of toxic and allergenic air particulate matter, such as soot, polycyclic aromatic hydrocarbons (PAHs) and proteins, are not well understood.

In this study, kinetic flux models for aerosol surface and bulk chemistry were developed based on the Pöschl-Rudich-Ammann framework for aerosol and cloud surface chemistry and gas-particle interactions. A kinetic double-layer model of surface chemistry (K2-SURF) was developed and applied to describe the degradation of PAHs on aerosol particles exposed to ozone, nitrogen dioxide, water vapor, hydroxyl and nitrate radicals. Competitive adsorption and chemical transformation of the surface lead to a strong non-linear dependence of gas uptake and PAH decay on gas phase composition. Under atmospheric conditions, the chemical half-life of PAHs is expected to range from a few minutes on the surface of soot to multiple hours on organic and inorganic solid particles and days on liquid particles.

A kinetic multi-layer model of surface and bulk chemistry (KM-SUB) was developed and applied to describe the chemical transformation of organic aerosol particles. KM-SUB explicitly resolves mass transport and chemical reaction at the surface and in the bulk of aerosol particles. Unlike earlier models, it does not require simplifying assumptions about steady-state conditions and radial mixing. In combination with literature data and new experimental results, KM-SUB was used to resolve the effects of interfacial and bulk transport on the ozonolysis and nitration of protein macromolecules, oleic acid and related organic compounds. The kinetic models developed in this study shall serve as a basis for the development of a comprehensive master mechanism of aerosol chemistry as well as for the derivation of simplified but realistic parameterizations for large-scale atmospheric and climate models.

The experiments and model calculations performed in this study provide evidence for the formation of long-lived reactive oxygen intermediates (ROIs) in the heterogeneous reaction of ozone with aerosol particles. The chemical lifetime of these intermediates exceeds 100 s, which is much longer than the surface residence time of molecular O_3 (~10^{-9} s). The ROIs explain and resolve apparent discrepancies between earlier quantum mechanical calculations and kinetic experiments. They play a key role in the chemical transformation and adverse health effects of toxic and allergenic air particulate matter, such as soot, PAHs and proteins. ROIs may also be involved in the decomposition of ozone on mineral dust and in the formation and growth of secondary organic aerosols. Moreover, they provide a link between atmospheric and biospheric multiphase processes (chemical and biological aging).

Organic substances can adopt an amorphous solid or semi-solid state, influencing the rate of heterogeneous reactions and multiphase processes in atmospheric aerosols. Flow tube experiments performed in this study show that the ozone uptake and oxidative aging of amorphous protein is kinetically limited by bulk diffusion. The reactive gas uptake exhibits a pronounced increase with relative humidity, which can be explained by a decrease of viscosity due to hygroscopic water uptake transforming the amorphous organic matrix from a glassy to a semi-solid state (moisture-induced phase transition). The chemical lifetime of reactive compounds in atmospheric particles can increase from seconds to days as the rate of diffusion in semi-solid phases can decrease by multiple orders of magnitude in response to low temperature or low relative humidity. The findings of this study demonstrate how amorphous semi-solid phases can influence the effects of organic aerosols on air quality, public health, and climate.

Zusammenfassung

Aerosolpartikel beeinflussen das Klima durch Streuung und Absorption von Strahlung sowie als Nukleations-Kerne für Wolkentröpfchen und Eiskristalle. Darüber hinaus haben Aerosole einen starken Einfluss auf die Luftverschmutzung und die öffentliche Gesundheit. Gas-Partikel-Wechselwirkunge sind wichtige Prozesse, weil sie die physikalischen und chemischen Eigenschaften von Aerosolen wie Toxizität, Reaktivität, Hygroskopizität und optische Eigenschaften beeinflussen. Durch einen Mangel an experimentellen Daten und universellen Modellformalismen sind jedoch die Mechanismen und die Kinetik der Gasaufnahme und der chemischen Transformation organischer Aerosolpartikel unzureichend erfasst. Sowohl die chemische Transformation als auch die negativen gesundheitlichen Auswirkungen von toxischen und allergenen Aerosolpartikeln, wie Ruß, polyzyklische aromatische Kohlenwasserstoffe (PAK) und Proteine, sind bislang nicht gut verstanden.

Kinetische Fluss-Modelle für Aerosoloberflächen- und Partikelbulk-Chemie wurden auf Basis des Pöschl-Rudich-Ammann-Formalismus für Gas-Partikel-Wechselwirkungen entwickelt. Zunächst wurde das kinetische Doppelschicht-Oberflächenmodell K2-SURF entwickelt, welches den Abbau von PAK auf Aerosolpartikeln in Gegenwart von Ozon, Stickstoffdioxid, Wasserdampf, Hydroxyl- und Nitrat-Radikalen beschreibt. Kompetitive Adsorption und chemische Transformation der Oberfläche führen zu einer stark nicht-linearen Abhängigkeit der Ozon-Aufnahme bezüglich Gaszusammensetzung. Unter atmosphärischen Bedingungen reicht die chemische Lebensdauer von PAK von wenigen Minuten auf Ruß, über mehrere Stunden auf organischen und anorganischen Feststoffen bis hin zu Tagen auf flüssigen Partikeln.

Anschließend wurde das kinetische Mehrschichtenmodell KM-SUB entwickelt um die chemische Transformation organischer Aerosolpartikel zu beschreiben. KM-SUB ist in der Lage, Transportprozesse und chemische Reaktionen an der Oberfläche und im Bulk von Aerosol-partikeln explizit aufzulösen. Es erforder im Gegensatz zu früheren Modellen keine vereinfachenden Annahmen über stationäre Zustände und radiale Durchmischung. In Kombination mit Literaturdaten und neuen experimentellen Ergebnissen wurde KM-SUB eingesetzt, um die Effekte von Grenzflächen- und Bulk-Transportprozessen auf die Ozonolyse und Nitrierung von Protein-Makromolekülen, Ölsäure, und verwandten organischen Verbin-dungen aufzuklären. Die in dieser Studie entwickelten kinetischen Modelle sollen als Basis für

die Entwicklung eines detaillierten Mechanismus für Aerosolchemie dienen sowie für das Herleiten von vereinfachten, jedoch realistischen Parametrisierungen für großskalige globale Atmosphären- und Klima-Modelle.

Die in dieser Studie durchgeführten Experimente und Modellrechnungen liefern Beweise für die Bildung langlebiger reaktiver Sauerstoff-Intermediate (ROI) in der heterogenen Reaktion von Ozon mit Aerosolpartikeln. Die chemische Lebensdauer dieser Zwischenformen beträgt mehr als 100 s, deutlich länger als die Oberflächen-Verweilzeit von molekularem O_3 ($\sim 10^{-9}$ s). Die ROIs erklären scheinbare Diskrepanzen zwischen früheren quantenmechanischen Berechnungen und kinetischen Experimenten. Sie spielen eine Schlüsselrolle in der chemischen Transformation sowie in den negativen Gesundheitseffekten von toxischen und allergenen Feinstaubkomponenten, wie Ruß, PAK und Proteine. ROIs sind vermutlich auch an der Zersetzung von Ozon auf mineralischem Staub und an der Bildung sowie am Wachstum von sekundären organischen Aerosolen beteiligt. Darüber hinaus bilden ROIs eine Verbindung zwischen atmosphärischen und biosphärischen Mehrphasenprozessen (chemische und biologische Alterung).

Organische Verbindungen können als amorpher Feststoff oder in einem halbfesten Zustand vorliegen, der die Geschwindigkeit von heterogenen Reaktionenen und Mehrphasenprozessen in Aerosolen beeinflusst. Strömungsrohr-Experimente zeigen, dass die Ozonaufnahme und die oxidative Alterung von amorphen Proteinen durch Bulk-Diffusion kinetisch limitiert sind. Die reaktive Gasaufnahme zeigt eine deutliche Zunahme mit zunehmender Luftfeuchte, was durch eine Verringerung der Viskosität zu erklären ist, bedingt durch einen Phasenübergang der amorphen organischen Matrix von einem glasartigen zu einem halbfesten Zustand (feuchtigkeitsinduzierter Phasenübergang). Die chemische Lebensdauer reaktiver Verbindungen in organischen Partikeln kann von Sekunden bis zu Tagen ansteigen, da die Diffusionsrate in der halbfesten Phase bei niedriger Temperatur oder geringer Luftfeuchte um Größenordnungen absinken kann. Die Ergebnisse dieser Studie zeigen wie halbfeste Phasen die Auswirkung organischeer Aerosole auf Luftqualität, Gesundheit und Klima beeinflussen können.

1. Introduction

1.1. Aerosol chemistry

Aerosols are ubiquitous in the atmosphere and have strong effects on climate and public health (Pöschl, 2005; IPCC, 2007; Finlayson-Pitts, 2010). Depending on chemical composition, phase state and surface properties, they can act as nuclei for cloud droplets and ice crystals, and they can affect the abundance of trace gases through heterogeneous chemical reactions (Ammann et al., 1998; Fuzzi et al., 2006; Andreae and Rosenfeld, 2008; Pöschl et al., 2010). Gas-particle interactions can also significantly change the physical and chemical properties of aerosols such as toxicity, reactivity, hygroscopicity and radiative properties (Rudich, 2003; Enami et al., 2008; Shiraiwa et al., 2008; Wiedensohler et al., 2009; Shiraiwa et al., 2011). Chemical reactions and mass transport lead to continuous transformation and changes in the composition of atmospheric aerosols ("chemical aging") (Schwartz and Freiberg, 1981; Hanson, 1997; Smith et al., 2003; Maria et al., 2004; Ammann and Poschl, 2007; Jimenez et al., 2009; Shiraiwa et al., 2010; Kroll et al., 2011). Heterogeneous reactions of ozone with aerosol particles have been studied extensively, but the molecular mechanism and kinetics remained unresolved (Pöschl et al., 2001; Maranzana et al., 2005; Rudich et al., 2007; Finlayson-Pitts, 2009; McCabe and Abbatt, 2009; Kolb et al., 2010).

Chemical reactions can occur both at the surface and in the bulk of liquid and (semi-)solid particles. It is often difficult to discriminate surface and bulk reactions, and the relative importance of surface and bulk processes is not well understood (e.g., Moise and Rudich, 2000; Hearn et al., 2005; Pfrang et al., 2010). Resistor model formulations are widely used to describe and investigate heterogeneous reactions and multiphase processes in laboratory, field and model studies of atmospheric chemistry (Hanson, 1997; Finlayson-Pitts and Pitts, 2000; Worsnop et al., 2002; Anttila et al., 2006; King et al., 2009; and references therein). The traditional resistor models, however, are usually based on simplifying assumptions such as steady state conditions, homogeneous mixing, and limited numbers of non-interacting species and processes.

In order to overcome these limitations, Pöschl, Rudich and Ammann have developed a kinetic model framework (PRA framework) with a double-layer surface concept and universally applicable rate equations and parameters for mass transport and chemical reactions at the gas-particle interface of aerosols and clouds (Pöschl et al., 2007). Ammann and Pöschl (2007)

provided first examples on how the PRA framework can be applied to describe various physico-chemical processes in aerosols and clouds such as reactive gas uptake on solid particles and solubility saturation of liquid droplets under transient or steady-state conditions.

Atmospheric particles consist of a wide variety of organic and inorganic chemical compounds which can exist in different liquid or (semi-)solid states (crystalline, amorphous, glassy, ultraviscous, gel-like) (Seinfeld and Pandis, 1998; Finlayson-Pitts and Pitts, 2000; Martin, 2000; Zobrist et al., 2008; Mikhailov et al., 2009). Carbonaceous combustion aerosol particles such as soot and related substances are known to be quasi-solid and undergo chemical reactions at the surface rather than in the bulk (black or elemental carbon, graphene, polycyclic aromatic hydrocarbons) (Pöschl, 2005; Sadezky et al., 2005; Andreae and Gelencser, 2006; Shiraiwa et al., 2009). Until recently, secondary organic aerosol (SOA) particles formed in the atmosphere from condensable oxidation products of volatile organic compounds were assumed to be liquid (Pankow, 1994; Kanakidou et al., 2005; Hallquist et al., 2009). Virtanen et al. (2010), however, showed that biogenic SOA particles formed in plant chamber experiments and in new particle formation events over boreal forests can adopt an amorphous semi-solid state, which is in line with the observed presence of oligomers or other organic compounds with high molecular mass and low volatility in SOA (Kalberer et al., 2004; Russell et al., 2011). Many organic substances, including carboxylic acids, carbohydrates and proteins, tend to form amorphous phases upon cooling or drying of aqueous solution droplets (Mikhailov et al., 2009). Depending on viscosity and microstructure, the amorphous phases can be classified as glasses, rubbers, gels, or ultra-viscous liquids (Mikhailov et al., 2009).

1.2. Impact of aerosols on human health

Airborne particulates and gaseous pollution are important environmental issues because they affect human health. Asthma and allergy are major health problems in most modern societies and numerous studies indicate that allergic diseases have been increasing during the past decades (Krämer et al., 1999; Wahn, 2000). Immune responses can be affected by air pollutants including atmospheric particles, semi-volatile hydrocarbons and exhaust gases, which drive proallergic inflammation through the generation of oxidative stress (Saxon and Diaz-Sanchez, 2005). Traffic-related air pollution such as ozone and nitrogen dioxide and particulate

matter less than 10 or 2.5 μm in size appears to link allergic diseases and childhood respiratory health (Miguel et al., 1999; Brunekreef and Sunyer, 2003; Janssen et al., 2003). However, the effects of air pollution on the occurrence of allergic diseases are not yet well-understood (Ring et al., 2001).

Proteins contained in biogenic aerosol particles account for up to 5% of urban air particulate matter (Jaenicke, 2005; Fröhlich-Nowoisky et al., 2009; Huffman et al., 2010). They are not only contained in coarse biological particles (e.g., pollen, spores) but also in the fine fraction of air particulate matter (Schäppi et al., 1997). Several studies have shown that ozone can promote the nitration of protein molecules contained in primary biological aerosol particles (Franze et al., 2005; Yang et al., 2010). Nitration of protein leads to the formation of 3-nitrotyrosine residues, which is a posttranslational modification (Zhang et al., 2010). Indeed, nitrated proteins were detected in dust samples from various urban environments (Franze et al., 2005). Inhalation and deposition of these nitrated proteins in the human respiratory tract may lead to the adverse health effects. Accumulating data suggest a strong link between protein 3-nitrotyrosine and the mechanism involved in disease development (Souza et al., 2008). This posttranslational modification provides a molecular rationale for the enhancement of allergic diseases by traffic-related air pollution in urban and rural environments, which has been observed in epidemiological studies but remains to be elucidated on a molecular level (Franze et al., 2005; Gruijthuijsen et al., 2006; Traidl-Hoffmann et al., 2009).

Reactive oxygen species (ROS) play important roles in atmospheric chemistry as well as in physiological processes; ozone photochemistry, oxidative self-cleaning of the atmosphere, biological aging, metabolism, and oxidative stress (Finkel and Holbrook, 2000; Apel and Hirt, 2004; Pöschl, 2005). In physiology and biochemistry, the umbrella term ROS has been broadly defined to comprise a wide range of oxygen-centered and related free radicals, ions, and molecules (Finkel and Holbrook, 2000; Apel and Hirt, 2004; Venkatachari and Hopke, 2008). Different types of ROS are closely coupled by radical reactions and cyclic transformation (Finlayson-Pitts and Pitts, 2000; Pöschl, 2005; George and Abbatt, 2010). The coupling and exchange of atmospheric and physiological ROS can proceed through various interfaces like plant surfaces and the human respiratory tract (emission and deposition of trace gas and particle deposition). The biomedical definition of ROS includes also reactive nitrogen species (RNS) like NO, NO_2, and ONO_2^- (Finkel and Holbrook, 2000). In atmospheric science, however, reactive

nitrogen species are usually treated separately from oxy, hydroxy and peroxy radicals (Seinfeld and Pandis, 1998; Finlayson-Pitts and Pitts, 2000). The term reactive oxygen intermediates (ROIs) was adopted to describe the subset of ROS potentially involved in the reaction of ozone with aerosol particles, including organic and inorganic species with reactive oxygen atoms or groups (O, RO, RO_2, etc.) (Shiraiwa et al., 2011).

Polycyclic aromatic hydrocarbons (PAHs) are one of the most prominent groups of toxic air pollutants related to health effects. They are an integral component of soot and related carbonaceous combustion aerosol particles in the submicron size range that can penetrate deep into human lungs (Finlayson-Pitts and Pitts, 2000). Chemical transformation can change the toxicity of PAHs and modify the hygroscopic properties and climate effects of combustion aerosol particles (Finlayson-Pitts and Pitts, 2000; George and Abbatt, 2010). PAH oxidation products (quinones, phenols, etc.) are also involved in physiological processes leading to the adverse health effects of traffic-related air pollution (Finkel and Holbrook, 2000; Pöschl, 2002; Nel, 2005; Pöschl, 2005). Moreover, PAH as well as its oxygenated or nitrated derivatives are well defined model substances for the molecular structure of soot, which is the black solid product of incomplete combustion or pyrolysis of organic matter (Homann, 1998; Messerer et al., 2005; Sadezky et al., 2005).

1.3. Research objectives and activities

For a reliable assessment of aerosol effects on climate and public health, it is necessary to understand and quantify the transformation of organic aerosols in the atmosphere. So far, however, the elucidation of multiphase processes in aerosols is limited by a lack of experimental data and rigorous mathematical model formalisms of mass transport and chemical reaction. Thus, the research activities of this thesis have two dimensions: (1) the development of kinetic models for aerosol surface and bulk chemistry, and (2) experimental investigations and model applications for systems and processes that are relevant for the atmosphere and human health. The specific objectives and activities of the PhD work can be summarized as follows:

1. Develop a comprehensive kinetic model for aerosol surface chemistry. Describe the degradation of polycyclic aromatic hydrocarbons (PAHs), a prominent group of toxic air pollutants, on various organic and inorganic substrates by atmospheric oxidants such as

O_3, NO_2, NO_3, and OH radicals. The model development and application were based on literature data.

2. Develop detailed and simplified kinetic models for aerosol surface and bulk chemistry. Describe the effects of surface-bulk exchange, bulk diffusion and surface crust formation on the ozonolysis of oleic acid. Oleic acid is a common model system of organic aerosol chemistry. The model developments and applications were based on literature data and performed in collaboration with Dr. C. Pfrang (University of Reading, UK).
3. Investigate the detailed molecular mechanism and kinetics of heterogeneous reaction of ozone with aerosol particles. Resolve the discrepancies between quantum mechanical calculations and kinetic experiments to PAH ozonolysis. Elucidate the formation of allergenic nitro-proteins by reaction of protein macromolecules with ozone and nitrogen dioxide. Laboratory experiments using flow reactors and radioactive tracer techniques were performed in collaboration with Dr. M. Ammann (Paul-Scherrer-Institut, Villigen, CH). The experimental results were analyzed by kinetic surface model taking into literature data and quantum mechanical calculations results.
4. Investigate the influence of amorphous semi-solid phases on the gas uptake and chemical aging of organic aerosol particles. Flow tube experiments of ozone uptake by amorphous protein were performed at different relative humidities, and diffusion coefficients were extracted by kinetic surface and bulk model calculations taking into account literature data and models of diffusivity, viscosity, and hygroscopicity. This work was done in collaboration with Dr. M. Ammann and Prof. T. Koop (University of Bielefeld, D).

2. Results and Conclusions

2.1. Overview

The results of the PhD project are described in 7 manuscripts for peer-reviewed publication in international scientific journals (5 first-author and 2 second-author papers). The manuscripts are attached in Appendix B of this thesis, and 6 of them have already been published. An overview of the studies and of the connections between them is given in Figure 1. The main results and conclusions of each study are summarized below.

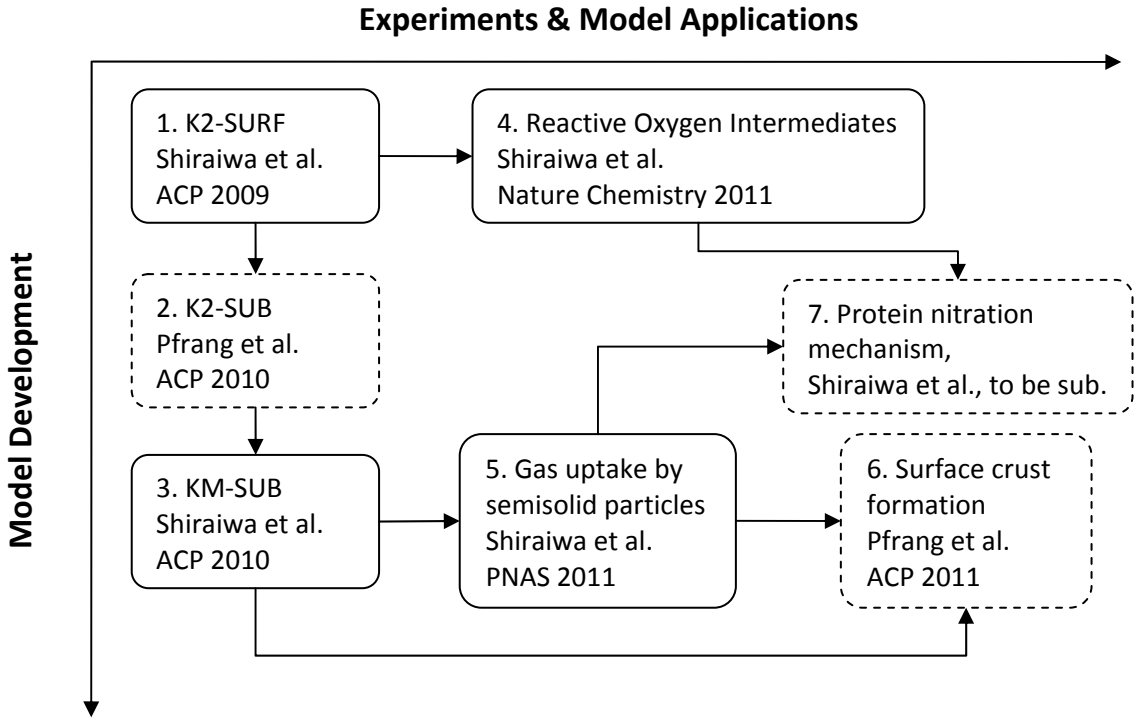

Figure 1. Structure and results of the PhD project evolving in two dimensions: model development vs. experiments & model applications. Each box represents a manuscript for peer-reviewed publication in an international scientific journal. Solid frames indicate published first-author papers; dashed frames indicate published second-author papers and a manuscript to be submitted. Arrows show connections between studies.

2.2. Individual Studies

2.2.1. K2-SURF

A new kinetic double-layer surface model (K2-SURF) was developed to describe the chemical degradation of polycyclic aromatic hydrocarbons (PAHs) on aerosol particles exposed to O_3, NO_2, H_2O, OH and NO_3 radicals. The model consistently simulates the decay of 8 PAHs (benzo[a]pyrene, pyrene, anthracene, etc.) on various organic and inorganic substrates (soot, azelaic acid, octanol, ZnSe, etc.). K2-SURF is the first atmospheric process model resolving multiple types of parallel and sequential surface reactions between multiple gaseous and particle-bound chemical species. For details see Appendix B1: Shiraiwa et al., *Atmospheric Chemistry and Physics* (*ACP*), 2009.

2.2.2. K2-SUB

Kinetic double-layer model for aerosol surface and bulk chemistry (K2-SUB) was developed and applied to the interaction of ozone with oleic acid. K2-SUB allows de-convoluting surface and bulk processes, however, due to the wide range of rate coefficients reported from different experimental studies, the exact proportions between surface and bulk reaction rates remain uncertain. Sensitivity studies show that the surface accommodation coefficient of the gas-phase reactant has a strong non-linear influence on both surface and bulk chemical reactions. For details see Appendix B2: Pfrang et al., *Atmospheric Chemistry and Physics* (*ACP*), 2010.

2.2.3. KM-SUB

Kinetic multi-layer model (KM-SUB) was developed that explicitly resolves mass transport and chemical reaction at the surface and in the bulk of aerosol particles. Unlike earlier models, KM-SUB does not require simplifying assumptions about steady-state conditions and radial mixing. The temporal evolution and concentration profiles of volatile and non-volatile species at the gas-particle interface and in the particle bulk was modeled along with surface concentrations and gas uptake coefficients. Sensitivity studies suggest that in fine air particulate matter oleic acid and compounds with similar reactivity against ozone (carbon-carbon double bonds) can reach chemical lifetimes of many hours only if they are embedded in a (semi-)solid matrix with very low diffusion coefficients ($\leq 10^{-10}$ cm^2 s^{-1}). For details see Appendix B3: Shiraiwa et al., *Atmospheric Chemistry and Physics* (*ACP*), 2010.

2.2.4. Reactive Oxygen Intermediates

Based on new experimental data and K2-SURF model calculations, the evidence of formation of long-lived reactive oxygen intermediates (ROIs) on the aerosol particles was provided. The chemical lifetime of these intermediates exceeds 100 seconds, which is much longer than the surface residence time of molecular O_3 ($\sim 10^{-9}$ s). The ROIs explain and resolve apparent discrepancies between earlier quantum mechanical calculations and kinetic experiments. They play a key role in the chemical transformation and adverse health effects of toxic and allergenic air particulate matter, such as soot, polycyclic aromatic hydrocarbons and proteins. For details see Appendix B4: Shiraiwa et al., *Nature Chemistry*, 2011.

2.2.5. Gas uptake by semi-solid particles

Based on flow tube experiments, ozone uptake and oxidative aging of amorphous protein are found to be kinetically limited by bulk diffusion and the reactive gas uptake exhibits a pronounced increase with relative humidity due to moisture-induced phase transition. The reaction rate depends on the condensed phase diffusion coefficients of both the oxidant and the organic reactant molecules, which can be described by KM-SUB but not by the traditional resistor model approach. The chemical lifetime of reactive compounds in atmospheric particles can increase from seconds to days as the rate of diffusion in semisolid phases can decrease by multiple orders of magnitude in response to low temperature or low relative humidity. For details see Appendix B5: Shiraiwa et al., *Proceedings of the National Academy of Sciences USA* (*PNAS*), 2011.

2.2.6. Surface crust formation

The impact of diffusivity on the ageing of multi-component reactive organic particles was investigated applying extended KM-SUB to a 12-component organic mixture. It was demonstrated that solidification and crust formation at the particle surface due to formation of oligomers changes the diffusivity of oxidant in the particle and affect the chemical transformation of organic aerosols significantly. For details see Appendix B6: Pfrang et al., *Atmospheric Chemistry and Physics* (*ACP*), 2011.

2.2.7. Protein nitration mechanism

Reaction kinetics and mechanism of the nitration of aerosolized protein by O_3 and NO_2 were investigated using a radioactive tracer technique. In the absence of O_3, uptake coefficients of NO_2 was below detection limit ($\gamma_{NO2} < \sim 10^{-6}$). In the presence of O_3, however, the γ_{NO2} were of the order of 10^{-5} and enhance up to $\sim 1 \times 10^{-4}$ with the increase of the O_3 concentration. The products analysis of protein exposed to ozone suggests phenoxy radical derivatives of amino acid tyrosine as chemical identity of reactive oxygen intermediates. For details see Appendix B7: Shiraiwa et al., to be submitted.

2.3. Summary and Outlook

The kinetic flux models developed in this PhD project are powerful tools for analyzing experimental data of gas uptake and chemical transformation of aerosol particles and for elucidating the molecular mechanisms of aerosol surface and bulk chemistry. Depending on the complexity of the investigated system, unlimited numbers of volatile and non-volatile species and chemical reactions can be included and treated consistently. The models shall serve as a basis for the development of a detailed master mechanism of aerosol chemistry as well as for the derivation of simplified but realistic parameterizations for large scale models of the atmosphere, climate and the Earth system.

Ongoing developments extending the model applicability to condensation and evaporation will enable detailed investigations of the molecular processes involved in the formation and growth of secondary organic aerosol (SOA). Important aspects are the effects of phase state and multi-phase chemistry on SOA formation, as well as size-dependent particle growth and evaporation kinetics. A universal kinetic multi-layer model for gas-particle interactions in aerosols and clouds shall be capable of simulating the chemical transformation of aerosol particles as well as the activation of cloud condensation and ice nuclei on molecular scales.

3. References

Ammann, M., Kalberer, M., Jost, D. T., Tobler, L., Rossler, E., Piguet, D., Gäggeler, H. W. and Baltensperger, U.: Heterogeneous production of nitrous acid on soot in polluted air masses, Nature, 395, 157-160, 1998.

Ammann, M. and Poschl, U.: Kinetic model framework for aerosol and cloud surface chemistry and gas-particle interactions - Part 2: Exemplary practical applications and numerical simulations, Atmos Chem Phys, 7, 6025-6045, 2007.

Andreae, M. O. and Gelencser, A.: Black carbon or brown carbon? The nature of light-absorbing carbonaceous aerosols, Atmos. Chem. Phys., 6, 3131-3148, 2006.

Andreae, M. O. and Rosenfeld, D.: Aerosol-cloud-precipitation interactions. Part 1. The nature and sources of cloud-active aerosols, Earth-Sci. Rev., 89, 13-41, 10.1016/j.earscirev.2008.03.001, 2008.

Anttila, T., Kiendler-Scharr, A., Tillmann, R. and Mentel, T. F.: On the reactive uptake of gaseous compounds by organic-coated aqueous aerosols: Theoretical analysis and application to the heterogeneous hydrolysis of N_2O_5, J. Phys. Chem. A, 110, 10435-10443, 10.1021/jp062403c, 2006.

Apel, K. and Hirt, H.: Reactive oxygen species: Metabolism, oxidative stress, and signal transduction, Annu. Rev. Plant Biol., 55, 373-399, 2004.

Brunekreef, B. and Sunyer, J.: Asthma, rhinitis and air pollution: is traffic to blame?, European Respiratory Journal, 21, 913-915, 10.1183/09031936.03.00014903, 2003.

Enami, S., Hoffmann, M. R. and Colussi, A. J.: Acidity enhances the formation of a persistent ozonide at aqueous ascorbate/ozone gas interfaces, Proc Natl Acad Sci USA, 105, 7365-7369, 10.1073/pnas.0710791105, 2008.

Finkel, T. and Holbrook, N. J.: Oxidants, oxidative stress and the biology of ageing, Nature, 408, 239-247, 2000.

Finlayson-Pitts, B. J.: Reactions at surfaces in the atmosphere: integration of experiments and theory as necessary (but not necessarily sufficient) for predicting the physical chemistry of aerosols, Phys. Chem. Chem. Phys., 11, 7760-7779, 10.1039/b906540g, 2009.

Finlayson-Pitts, B. J.: Atmospheric Chemistry, Proc Natl Acad Sci USA, 107, 6566-6567, 10.1073/pnas.1003038107, 2010.

Franze, T., Weller, M. G., Niessner, R. and Pöschl, U.: Protein nitration by polluted air, Environ. Sci. Technol., 39, 1673-1678, 10.1021/es0488737, 2005.

Fröhlich-Nowoisky, J., Pickersgill, D. A., Despres, V. R. and Pöschl, U.: High diversity of fungi in air particulate matter, Proc Natl Acad Sci USA, 106, 12814-12819, 10.1073/pnas.0811003106, 2009.

Fuzzi, S., Andreae, M. O., Huebert, B. J., et al.: Critical assessment of the current state of scientific knowledge, terminology, and research needs concerning the role of organic aerosols in the atmosphere, climate, and global change, Atmos. Chem. Phys., 6, 2017-2038, 2006.

George, I. J. and Abbatt, J. P. D.: Heterogeneous oxidation of atmospheric aerosol particles by gas-phase radicals, Nature Chem., 2, 713-722, 10.1038/nchem.806, 2010.

Gruijthuijsen, Y. K., Grieshuber, I., Stocklinger, A., et al.: Nitration enhances the allergenic potential of proteins, Int. Arch. Allergy Immunol., 141, 265-275, 10.1159/000095296, 2006.

Hallquist, M., Wenger, J. C., Baltensperger, U., et al.: The formation, properties and impact of secondary organic aerosol: current and emerging issues, Atmos. Chem. Phys., 9, 5155-5235, 2009.

Hanson, D. R.: Surface-specific reactions on liquids, J. Phys. Chem. B, 101, 4998-5001, 1997.

Hearn, J. D., Lovett, A. J. and Smith, G. D.: Ozonolysis of oleic acid particles: evidence for a surface reaction and secondary reactions involving Criegee intermediates, Phys. Chem. Chem. Phys., 7, 501-511, 10.1039/b414472d, 2005.

Homann, K. H.: Fullerenes and soot formation - New pathways to large particles in flames, Angew. Chem.-Int. Edit., 37, 2435-2451, 1998.

Huffman, J. A., Treutlein, B. and Pöschl, U.: Fluorescent biological aerosol particle concentrations and size distributions measured with an ultraviolet aerodynamic particle sizer (UV-APS) in Central Europe, Atmos. Chem. Phys., 10, 3215-3233, 2010.

Jaenicke, R.: Abundance of cellular material and proteins in the atmosphere, Science, 308, 73-73, 10.1126/science.1106335, 2005.

Janssen, N. A. H., Brunekreef, B., van Vliet, P., Aarts, F., Meliefste, K., Harssema, H. and Fischer, P.: The relationship between air pollution from heavy traffic and allergic sensitization, bronchial hyperresponsiveness, and respiratory symptoms in Dutch schoolchildren, Environ. Health Perspect., 111, 1512-1518, 10.1289/ehp.6243, 2003.

Jimenez, J. L., Canagaratna, M. R., Donahue, N. M., et al.: Evolution of Organic Aerosols in the Atmosphere, Science, 326, 1525-1529, 10.1126/science.1180353, 2009.

Kalberer, M., Paulsen, D., Sax, M., et al.: Identification of polymers as major components of atmospheric organic aerosols, Science, 303, 1659-1662, 2004.

Kanakidou, M., Seinfeld, J. H., Pandis, S. N., et al.: Organic aerosol and global climate modelling: a review, Atmos. Chem. Phys., 5, 1053-1123, 2005.

King, M. D., Rennie, A. R., Thompson, K. C., Fisher, F. N., Dong, C. C., Thomas, R. K., Pfrang, C. and Hughes, A. V.: Oxidation of oleic acid at the air-water interface and its potential effects on cloud critical supersaturations, Phys. Chem. Chem. Phys., 11, 7699-7707, 10.1039/b906517b, 2009.

Kolb, C. E., Cox, R. A., Abbatt, J. P. D., et al.: An overview of current issues in the uptake of atmospheric trace gases by aerosols and clouds, Atmos. Chem. Phys., 10, 10561-10605, 10.5194/acp-10-10561-2010, 2010.

Krämer, U., Behrendt, H., Dolgner, R., Ranft, U., Ring, J., Willer, H. and Schlipkoter, H. W.: Airway diseases and allergies in East and West German children during the first 5 years after reunification: time trends and the impact of sulphur dioxide and total suspended particles, Int. J. Epidemiol., 28, 865-873, 1999.

Kroll, J. H., Donahue, N. M., Jimenez, J. L., et al.: Carbon oxidation state as a metric for describing the chemistry of atmospheric organic aerosol, Nature Chem., 3, 133-139, 2011.

Maranzana, A., Serra, G., Giordana, A., Tonachini, G., Barco, G. and Causa, M.: Ozone interaction with polycyclic aromatic hydrocarbons and soot in atmospheric processes: Theoretical density functional study by molecular and periodic methodologies, J. Phys. Chem. A, 109, 10929-10939, 10.1021/jp053672q, 2005.

Maria, S. F., Russell, L. M., Gilles, M. K. and Myneni, S. C. B.: Organic aerosol growth mechanisms and their climate-forcing implications, Science, 306, 1921-1924, 10.1126/science.1103491, 2004.

Martin, S. T.: Phase transitions of aqueous atmospheric particles, Chem. Rev., 100, 3403-3453, 10.1021/cr990034t, 2000.

McCabe, J. and Abbatt, J. P. D.: Heterogeneous Loss of Gas-Phase Ozone on n-Hexane Soot Surfaces: Similar Kinetics to Loss on Other Chemically Unsaturated Solid Surfaces, J. Phys. Chem. C, 113, 2120-2127, 10.1021/jp806771q, 2009.

Messerer, A., Rothe, D., Niessner, R. and Pöschl, U.: Kinetic observations and model calculations on continuous regeneration of NFZ diesel carbon particle precipitation systems, Chemie Ingenieur Technik, 77, 881-886, 10.1002/cite.200500038, 2005.

Miguel, A. G., Cass, G. R., Glovsky, M. M. and Weiss, J.: Allergens in paved road dust and airborne particles, Environ. Sci. Technol., 33, 4159-4168, 1999.

Mikhailov, E., Vlasenko, S., Martin, S. T., Koop, T. and Pöschl, U.: Amorphous and crystalline aerosol particles interacting with water vapor: conceptual framework and experimental evidence for restructuring, phase transitions and kinetic limitations, Atmos. Chem. Phys., 9, 9491-9522, 2009.

Moise, T. and Rudich, Y.: Reactive uptake of ozone by proxies for organic aerosols: Surface versus bulk processes, J. Geophys. Res.-Atmos., 105, 14667-14676, 2000.

Nel, A.: Air pollution-related illness: Effects of particles, Science, 308, 804-806, 10.1126/science.1108752, 2005.

Pankow, J. F.: An absorption-model of the gas aerosol partitioning involved in the formation of secondary organic aerosol, Atmos. Environ., 28, 189-193, 1994.

Pfrang, C., Shiraiwa, M. and Pöschl, U.: Coupling aerosol surface and bulk chemistry with a kinetic double layer model (K2–SUB): an exemplary study of the oxidation of oleic acid by ozone, Atmos. Chem. Phys., 10, 4537-4557, 2010.

Pöschl, U., Letzel, T., Schauer, C. and Niessner, R.: Interaction of ozone and water vapor with spark discharge soot aerosol particles coated with benzo[a]pyrene: O_3 and H_2O adsorption, benzo[a]pyrene degradation, and atmospheric implications, J. Phys. Chem. A, 105, 4029-4041, 2001.

Pöschl, U.: Formation and decomposition of hazardous chemical components contained in atmospheric aerosol particles, J. Aerosol. Med., 15, 203-212, 2002.

Pöschl, U.: Atmospheric aerosols: Composition, transformation, climate and health effects, Angew. Chem.-Int. Edit., 44, 7520-7540, 10.1002/anie.200501122, 2005.

Pöschl, U., Rudich, Y. and Ammann, M.: Kinetic model framework for aerosol and cloud surface chemistry and gas-particle interactions - Part 1: General equations, parameters, and terminology, Atmos. Chem. Phys., 7, 5989-6023, 2007.

Pöschl, U., Martin, S. T., Sinha, B., et al.: Rainforest Aerosols as Biogenic Nuclei of Clouds and Precipitation in the Amazon, Science, 329, 1513-1516, 10.1126/science.1191056, 2010.

Ring, J., Kramer, U., Schafer, T. and Behrendt, H.: Why are allergies increasing?, Curr. Opin. Immunol., 13, 701-708, 2001.

Rudich, Y.: Laboratory perspectives on the chemical transformations of organic matter in atmospheric particles, Chem. Rev., 103, 5097-5124, 10.1021/cr020508f, 2003.

Rudich, Y., Donahue, N. M. and Mentel, T. F.: Aging of organic aerosol: Bridging the gap between laboratory and field studies, Annu. Rev. Phys. Chem., 58, 321-352, 10.1146/annurev.physchem.58.032806.104432, 2007.

Russell, L. M., Bahadur, R. and Ziemann, P. J.: Identifying organic aerosol sources by comparing functional group composition in chamber and atmospheric particles, Proc Natl Acad Sci USA, 108, 3516-3521, 10.1073/pnas.1006461108, 2011.

Sadezky, A., Muckenhuber, H., Grothe, H., Niessner, R. and Pöschl, U.: Raman microspectroscopy of soot and related carbonaceous materials: Spectral analysis and structural information, Carbon, 43, 1731-1742, 2005.

Saxon, A. and Diaz-Sanchez, D.: Air pollution and allergy: you are what you breathe, Nat. Immunol., 6, 223-226, 10.1038/ni0305-223, 2005.

Schäppi, G. F., Suphioglu, C., Taylor, P. E. and Knox, R. B.: Concentrations of the major birch tree allergen Bet v 1 in pollen and respirable fine particles in the atmosphere, J. Allergy Clinical Immunol., 100, 656-661, 1997.

Schwartz, S. E. and Freiberg, J. E.: Mass-transport limitation to the rate of reaction of gases in liquid droplets - Application to oxidation of SO_2 in aqueous-solutions, Atmos. Environ., 15, 1129-1144, 1981.

Seinfeld, J. H. and Pandis, S. N.: Atmospheric chemistry and physics - From air pollution to climate change, John Wiley & Sons, Inc., New York, 1998.

Shiraiwa, M., Kondo, Y., Moteki, N., Takegawa, N., Sahu, L. K., Takami, A., Hatakeyama, S., Yonemura, S. and Blake, D. R.: Radiative impact of mixing state of black carbon aerosol in Asian outflow, J. Geophys. Res.-Atmos., 113, D24210, 10.1029/2008jd010546, 2008.

Shiraiwa, M., Garland, R. M. and Pöschl, U.: Kinetic double-layer model of aerosol surface chemistry and gas-particle interactions (K2-SURF): Degradation of polycyclic aromatic hydrocarbons exposed to O_3, NO_2, H_2O, OH and NO_3, Atmos. Chem. Phys., 9, 9571-9586, 2009.

Shiraiwa, M., Pfrang, C. and Pöschl, U.: Kinetic multi-layer model of aerosol surface and bulk chemistry (KM-SUB): the influence of interfacial transport and bulk diffusion on the oxidation of oleic acid by ozone, Atmos. Chem. Phys., 10, 3673-3691, 2010.

Shiraiwa, M., Sosedova, Y., Rouviere, A., Yang, H., Zhang, Y., Abbatt, J. P. D., Ammann, M. and Pöschl, U.: The role of long-lived reactive oxygen intermediates in the reaction of ozone with aerosol particles, Nature Chem., 3, 291-295, 10.1038/nchem.988, 2011.

Smith, G. D., Woods, E., Baer, T. and Miller, R. E.: Aerosol uptake described by numerical solution of the diffusion - Reaction equations in the particle, J. Phys. Chem. A, 107, 9582-9587, 10.1021/jp021843a, 2003.

Souza, J. M., Peluffo, G. and Radi, R.: Protein tyrosine nitration - Functional alteration or just a biomarker?, Free Radical Biol. Med., 45, 357-366, 10.1016/j.freeradbiomed.2008.04.010, 2008.

Traidl-Hoffmann, C., Jakob, T. and Behrendt, H.: Determinants of allergenicity, J. Allergy Clinical Immunol., 123, 558-566, 10.1016/j.jaci.2008.12.003, 2009.

Venkatachari, P. and Hopke, P. K.: Development and evaluation of a particle-bound reactive oxygen species generator, J. Aerosol Sci., 39, 168-174, 10.1016/j.jaerosci.2007.11.003, 2008.

Virtanen, A., Joutsensaari, J., Koop, T., et al.: An amorphous solid state of biogenic secondary organic aerosol particles, Nature, 467, 824-827, doi:10.1038/nature09455, 2010.

Wahn, U.: What drives the allergic march?, Allergy, 55, 591-599, 2000.

Wiedensohler, A., Cheng, Y. F., Nowak, A., et al.: Rapid aerosol particle growth and increase of cloud condensation nucleus activity by secondary aerosol formation and condensation: A case study for regional air pollution in northeastern China, J. Geophys. Res.-Atmos., 114, D00G08, 10.1029/2008jd010884, 2009.

Worsnop, D. R., Morris, J. W., Shi, Q., Davidovits, P. and Kolb, C. E.: A chemical kinetic model for reactive transformations of aerosol particles, Geophys. Res. Lett., 29, 57-51-54, 10.1029/2002gl015542, 2002.

Yang, H., Zhang, Y. and Pöschl, U.: Quantification of nitrotyrosine in nitrated proteins, Anal. Bioanal. Chem., 397, 879-886, 10.1007/s00216-010-3557-3, 2010.

Zhang, Y., Yang, H. and Pöschl, U.: Analysis of nitrated proteins and tryptic peptides by HPLC-chip-MS/MS: site-specific quantification, nitration degree, and reactivity of tyrosine residues, Anal. Bioanal. Chem., 1-13, 10.1007/s00216-010-4280-9, 2010.

Zobrist, B., Marcolli, C., Pedernera, D. A. and Koop, T.: Do atmospheric aerosols form glasses?, Atmos. Chem. Phys., 8, 5221-5244, 2008.

Appendix A. Personal List of Publications

Journal article

1. Kulmala, M., A. Asmi, H. K. Lappalainen, U. Baltensperger, J. L. Brenguier, M. C. Facchini, H. C. Hansson, Ø. Hov, C. D. O'Dowd, U. Pöschl, A. Wiedensohler, R. Boers, O. Boucher, G. de Leeuw, H. Denier van den Gon, J. Feichter, R. Krejci, P. Laj, H. Lihavainen, U. Lohmann, G. McFiggans, T. Mentel, C. Pilinis, I. Riipinen, M. Schulz, A. Stohl, E. Swietlicki, E. Vignati, M. Amann, C. Alves, S. Arabas, P. Artaxo, D. C. S. Beddows, R. Bergström, J. P. Beukes, M. Bilde, J. F. Burkhart, F. Canonaco, S. Clegg, H. Coe, S. Crumeyrolle, B. D'Anna, S. Decesari, S. Gilardoni, M. Fischer, A. M. Fjæraa, C. Fountoukis, C. George, L. Gomes, P. Halloran, T. Hamburger, R. M. Harrison, H. Herrmann, T. Hoffmann, C. Hoose, M. Hu, U. Hõrrak, Y. Iinuma, T. Iversen, M. Josipovic, M. Kanakidou, A. Kiendler-Scharr, A. Kirkevåg, G. Kiss, Z. Klimont, P. Kolmonen, M. Komppula, J. E. Kristjánsson, L. Laakso, A. Laaksonen, L. Labonnote, V. A. Lanz, K. E. J. Lehtinen, R. Makkonen, G. McMeeking, J. Merikanto, A. Minikin, S. Mirme, W. T. Morgan, E. Nemitz, D. O'Donnell, T. S. Panwar, H. Pawlowska, A. Petzold, J. J. Pienaar, C. Pio, C. Plass-Duelmer, A. S. H. Prévôt, S. Pryor, C. L. Reddington, G. Roberts, D. Rosenfeld, J. Schwarz, Ø. Seland, K. Sellegri, X. J. Shen, M. Shiraiwa, H. Siebert, B. Sierau, D. Simpson, J. Y. Sun, D. Topping, P. Tunved, P. Vaattovaara, V. Vakkari, J. P. Veefkind, A. Visschedijk, H. Vuollekoski, R. Vuolo, B. Wehner, J. Wildt, S. Woodward, D. R. Worsnop, G. J. van Zadelhoff, A. A. Zardini, K. Zhang, P. G. van Zyl, V. M. Kerminen, K. S. Carslaw and S. N. Pandis. General overview: European Integrated project on Aerosol Cloud Climate and Air Quality interactions (EUCAARI) – integrating aerosol research from nano to global scales. ***Atmospheric Chemistry and Physics Discussions***. 11(6): 17941-18160, 2011.

2. Pfrang, C., M. Shiraiwa, and U. Pöschl, Chemical ageing and transformation of diffusivity in semi-solid multi-component organic aerosol particles, ***Atmospheric Chemistry and Physics*****,** 11, 7343-7354, 2011.

3. Shiraiwa, M., M. Ammann, T. Koop and U. Pöschl, Gas uptake and chemical aging of semi-solid organic aerosol particles, ***Proceedings of the National Academy of Sciences of the United States of America***, 108, 11003-11008, 2011.

4. Shiraiwa, M., Y. Sosedova, A. Rouviere, H. Yang, Y. Zhang, J.P.D. Abbatt, M. Ammann, U. Pöschl, The role of long-lived reactive oxygen intermediates in the reaction of ozone with aerosol particles, ***Nature Chemistry*****,** 3, 291-295, 2011.

5. Kondo, Y, N. Takegawa, H. Matsui, T. Miyakawa, M. Koike, Y. Miyazaki, Y. Kanaya, M. Mochida, M. Kuwata, Y. Morino and M. Shiraiwa , Formation and transport of aerosols in Tokyo in relation to their physical and chemical properties: A review, ***Journal of Meteorological Society of Japan,*** 88, 4, 597-624, 201*0.*

6. Pfrang, C., M. Shiraiwa, and U. Pöschl, Coupling aerosol surface and bulk chemistry with a kinetic double layer model (K2-SUB): oxidation of oleic acid by ozone, ***Atmospheric Chemistry and Physics,*** 10, 4537-4557, 2010.

7. Shiraiwa, M., C. Pfrang and U. Pöschl, Kinetic multi-layer model of aerosol surface and bulk chemistry (KM-SUB): the influence of interfacial transport and bulk diffusion on the oxidation of oleic acid by ozone ***Atmospheric Chemistry and Physics,*** 10, 3673-3691, 2010.

8. Shiraiwa, M., Y. Kondo, T. Iwamoto, and K. Kita, Amplification of light absorption of black carbon by organic coating, ***Aerosol Science and Technology***,44: 1, 46 – 54, 2010.

9. Shiraiwa, M., R. M. Garland, and U. Pöschl, Kinetic double-layer model of aerosol surface chemistry and gas-particle interactions (K2-SURF): degradation of polycyclic aromatic hydrocarbons exposed to O_3, NO_2, H_2O, OH and NO_3, ***Atmospheric Chemistry and Physics,*** 9, 9571-9586, 2009.

10. Shimizu, R., T. Hitosugi, K. S. Nakayama, T. Sakurai, M. Shiraiwa, T. Hasegawa, and T. Hashizume, Preparation of atomically flat TiO_2(110) substrate, ***Japanese Journal of Applied Physics***, 48, 125506, 2009.

11. Miyazaki, Y., Y. Kondo, M. Shiraiwa, N. Takegawa, T. Miyakawa, S. Han, K. Kita, M. Hu, Z. Q. Deng, Y. Zhao, N.Sugimoto, D. R. Blake, and R. J. Weber, Chemical characterization of water-soluble organic carbon aerosols at a rural site in the Pearl River Delta, China, in the summer of 2006, ***Journal of Geophysical Research - Atmospheres,*** 114, D14208, 2009.

12. Shiraiwa, M., Y. Kondo, N. Moteki, N. Takegawa, L. K. Sahu, A. Takami, S. Hatakeyama, S. Yonemura and D. R. Blake, Radiative impact of mixing state of black carbon in Asian outflow, ***Journal of Geophysical Research - Atmospheres,*** 113, D24210, 2008.

13. Shiraiwa, M., Y. Kondo, N. Moteki, N. Takegawa, Y. Miyazaki, and D. R. Blake, Evolution of mixing state of black carbon in polluted air from Tokyo, ***Geophysical Research Letters,*** 34, L16803, 2007.

Oral Presentations.

1. Shiraiwa, M., Y. Sosedova, A. Rouviere, H. Yang, Y. Zhang, J.P.D. Abbatt, M. Ammann, U. Pöschl, Long-lived reactive oxygen intermediates in the reaction of ozone with aerosol particles and aerosol health effects, European Aerosol Conference, Manchester, UK, 2011.9. (**Session chair**)

2. Shiraiwa, M., The role of long-lived reactive oxygen intermediates in the reaction of ozone with aerosol particles, 5th Biennial Meeting of Society for Free Radical Research-Asia (SFRR-Asia), 8th Conference of Asian Society for Mitochondrial Research and Medicine (ASMRM), and 11th Conference of Japanese Society of Mitochondrial Research and Medicine (J-mit), Kagoshima, 2011.8.31 (**Invited lecture**).

3. Shiraiwa, M., Y. Sosedova, A. Rouvière, M. Ammann, and U. Pöschl, Heterogeneous reaction kinetics and mechanism of the nitration of aerosolized protein by O_3 and NO_2, International Aerosol Conference, 1D4, Helsinki, 2010.08.30. (**Session chair**)

4. Shiraiwa, M., C. Pfrang and U. Pöschl, Kinetic multi-layer model of aerosol surface and bulk chemistry (KM-SUB): the influence of interfacial transport and bulk diffusion on the oxidation of oleic acid by ozone, European Geophysical Union, EGU2010-1902, Vienna, 2010.05.05.

5. Shiraiwa, M., Y. Kondo, N. Moteki, N. Takegawa, L. K. Sahu, A. Takami, and S. Hatakeyama, Mixing state of black carbon aerosol in Asian outflow, 10th International Global Atmospheric Conference, Annecy (France), 2008.09.12.

Poster Presentations.

1. Shiraiwa, M., M. Ammann, T. Koop and U. Pöschl, Gas uptake and chemical aging of amorphous semi-solid aerosol particles, European Aerosol Conference, Manchester, UK, 2011.9.
2. Shiraiwa, M., Y. Sosedova, A. Rouviere, H. Yang, Y. Zhang, J.P.D. Abbatt, M. Ammann, U. Pöschl, The role of long-lived reactive oxygen intermediates in the reaction of ozone with aerosol particles, European Geophysical Union, EGU2011-5621, Vienna, 2011.4.7.
3. Shiraiwa, M., M. Ammann, T. Koop and U. Pöschl, Gas uptake and chemical aging of amorphous semi-solid aerosol particles, European Geophysical Union, Vienna, 2011.4.7.
4. Shiraiwa, M., C. Pfrang, R. Garland, and U. Pöschl, Kinetic models of aerosol surface and bulk chemistry, American Geophysical Union, A11G-0172, San Francisco, 2010.12.13.
5. Shiraiwa, M., C. Pfrang, R. Garland, and U. Pöschl, Kinetic models of aerosol surface and bulk chemistry, 2010 EUCAARI annual conference, Helsinki, 2010.11.24.
6. Shiraiwa, M., C. Pfrang and U. Pöschl, Kinetic multi-layer model of aerosol surface and bulk chemistry (KM-SUB): the influence of interfacial transport and bulk diffusion on the oxidation of oleic acid by ozone, European Geophysical Union, Vienna, 2010.05.05.
7. Shiraiwa, M., Y. Sosedova, A. Rouvière, M. Ammann, and U. Pöschl, Heterogeneous reaction kinetics and mechanism of the nitration of aerosolized protein by O_3 and NO_2, European Geophysical Union, EGU2010-1915, Vienna, 2010.05.05.
8. Shiraiwa, M., R. Garland and U. Pöschl, Kinetic double-layer model of aerosol surface chemistry and gas-particle interactions (K2-SURF): Degradation of polycyclic aromatic hydrocarbons exposed to O_3, NO_2, H_2O, OH and NO_3, European Geophysical Union, EGU2010-1907, Vienna, 2010.05.05.
9. Shiraiwa, M., R. Garland and U. Pöschl, Kinetic double-layer model of aerosol surface chemistry and gas-particle interactions (K2-SURF): Degradation of polycyclic aromatic hydrocarbons exposed to O_3, NO_2, H_2O, OH and NO_3, 2009 EUCAARI Annual Conference, Helsinki, 2009.11.14.
10. Shiraiwa, M., R. Garland and U. Pöschl, Modeling aerosol surface chemistry and gas-particle interaction kinetics with a kinetic double-layer model: PAH oxidation by ozone, nitrogen dioxide, and water vapor, European Aerosol Conference, T027A01, Karlsruhe (Germany), 2009.09.09 (Received ***Best Poster Award***).
11. Shiraiwa, M., R. Garland and U. Pöschl, Modeling aerosol surface chemistry and gas-particle interaction kinetics with K2-SURF: PAH oxidation, European Geophysical Union, EGU2009-636,

Vienna, 2010.04.21.

12. Shiraiwa, M., R. Garland, and U. Pöschl, Modeling aerosol surface chemistry and gas-particle interaction kinetics with K2-SURF: PAH oxidation, 2008 EUCAARI Annual Conference, Helsinki, 2008.11.20.
13. Shiraiwa, M., Y. Kondo, N. Moteki, and N. Takegawa, Transport of Asian pollution to the western Pacific: possible influence on regional climate, Alliance for Global Sustainability, MIT, Boston, 2008.01.29.

Appendix B. Selected Publications

1. Shiraiwa, M., R. M. Garland and U. Pöschl (2009). Kinetic double-layer model of aerosol surface chemistry and gas-particle interactions (K2-SURF): Degradation of polycyclic aromatic hydrocarbons exposed to O_3, NO_2, H_2O, OH and NO_3. ***Atmospheric Chemistry and Physics*** 9(24): 9571-9586.

2. Pfrang, C., M. Shiraiwa and U. Pöschl (2010). Coupling aerosol surface and bulk chemistry with a kinetic double layer model (K2–SUB): an exemplary study of the oxidation of oleic acid by ozone. ***Atmospheric Chemistry and Physics*** 10: 4357-4557.

3. Shiraiwa, M., C. Pfrang and U. Pöschl (2010). Kinetic multi-layer model of aerosol surface and bulk chemistry (KM-SUB): the influence of interfacial transport and bulk diffusion on the oxidation of oleic acid by ozone. ***Atmospheric Chemistry and Physics*** 10(8): 3673-3691.

4. Shiraiwa, M., Y. Sosedova, A. Rouviere, H. Yang, Y. Zhang, J. P. D. Abbatt, M. Ammann and U. Pöschl (2011). The role of long-lived reactive oxygen intermediates in the reaction of ozone with aerosol particles. ***Nature Chemistry*** 3(4): 291-295. DOI: 10.1038/nchem.988.

5. Shiraiwa, M., M. Ammann, T. Koop and U. Pöschl (2011), Gas uptake and chemical aging of semi-solid organic aerosol particles. ***Proceedings of the National Academy of Sciences of the United States of America***, 108, 11003-1100.

6. Pfrang, C., M. Shiraiwa and U. Pöschl (2011). Chemical ageing and transformation of diffusivity in semi-solid multi-component organic aerosol particles. ***Atmospheric Chemistry and Physics*** 11, 7343-7354.

7. Shiraiwa, M., K. Selzle, Y. Hong, Y. Sosedova, M. Ammann, and U. Pöschl. Reaction kinetics and mechanism of the nitration of aerosolized protein by O_3 and NO_2. *to be submitted*.

B1) Shiraiwa et al., Atmos. Chem. Phys., 2009

Kinetic double-layer model of aerosol surface chemistry and gas-particle interactions (K2-SURF): Degradation of polycyclic aromatic hydrocarbons exposed to O_3, NO_2, H_2O, OH and NO_3

Manabu Shiraiwa, Rebecca M Garland and Ulrich Pöschl

Max Planck Institute for Chemistry, Department of Biogeochemistry
J.J. Becherweg 27/29, D55128, Mainz, Germany

Atmospheric Chemistry and Physics 9(24): 9571-9586, 2009.

Authors contributions.

UP and RG designed research. MS and RG analyzed data and performed kinetic modeling. MS and UP discussed the results and wrote the paper.

Atmos. Chem. Phys., 9, 9571–9586, 2009
www.atmos-chem-phys.net/9/9571/2009/

Atmospheric Chemistry and Physics

Kinetic double-layer model of aerosol surface chemistry and gas-particle interactions (K2-SURF): Degradation of polycyclic aromatic hydrocarbons exposed to O_3, NO_2, H_2O, OH and NO_3

M. Shiraiwa, R. M. Garland, and U. Pöschl

Max Planck Institute for Chemistry, Biogeochemistry Department, P.O. Box 3060, 55128 Mainz, Germany

Received: 7 August 2009 – Published in Atmos. Chem. Phys. Discuss.: 1 September 2009
Revised: 7 December 2009 – Accepted: 8 December 2009 – Published: 21 December 2009

Abstract. We present a kinetic double-layer surface model (K2-SURF) that describes the degradation of polycyclic aromatic hydrocarbons (PAHs) on aerosol particles exposed to ozone, nitrogen dioxide, water vapor, hydroxyl and nitrate radicals. The model is based on multiple experimental studies of PAH degradation and on the PRA framework (Pöschl-Rudich-Ammann, 2007) for aerosol and cloud surface chemistry and gas-particle interactions.

For a wide range of substrates, including solid and liquid organic and inorganic substances (soot, silica, sodium chloride, octanol/decanol, organic acids, etc.), the concentration- and time-dependence of the heterogeneous reaction between PAHs and O_3 can be efficiently described with a Langmuir-Hinshelwood-type mechanism. Depending on the substrate material, the Langmuir adsorption constants for O_3 vary over three orders of magnitude ($K_{\mathrm{ads,O3}} \approx 10^{-15}$–$10^{-13}\,\mathrm{cm}^3$), and the second-order rate coefficients for the surface layer reaction of O_3 with different PAH vary over two orders of magnitude ($k_{\mathrm{SLR,PAH,O3}} \approx 10^{-18}$–$10^{-17}\,\mathrm{cm}^2\,\mathrm{s}^{-1}$). The available data indicate that the Langmuir adsorption constants for NO_2 are similar to those of O_3, while those of H_2O are several orders of magnitude smaller ($K_{\mathrm{ads,H2O}} \approx 10^{-18}$–$10^{-17}\,\mathrm{cm}^3$). The desorption lifetimes and adsorption enthalpies inferred from the Langmuir adsorption constants suggest chemisorption of NO_2 and O_3 and physisorption of H_2O. Note, however, that the exact reaction mechanisms, rate limiting steps and possible intermediates still remain to be resolved (e.g., surface diffusion and formation of O atoms or O_3^- ions at the surface).

The K2-SURF model enables the calculation of ozone uptake coefficients, γ_{O3}, and of PAH concentrations in the quasi-static particle surface layer. Competitive adsorption and chemical transformation of the surface (aging) lead to a strong non-linear dependence of γ_{O3} on time and gas phase composition, with different characteristics under dilute atmospheric and concentrated laboratory conditions. Under typical ambient conditions, γ_{O3} of PAH-coated aerosol particles are expected to be in the range of 10^{-6}–10^{-5}.

At ambient temperatures, NO_2 alone does not efficiently degrade PAHs, but it was found to accelerate the degradation of PAHs exposed to O_3. The accelerating effect can be attributed to highly reactive NO_3 radicals formed in the gas phase or on the surface. Estimated second-order rate coefficients for O_3-NO_2 and PAH-NO_3 surface layer reactions are in the range of 10^{-17}–$10^{-16}\,\mathrm{cm}^2\,\mathrm{s}^{-1}$ and 10^{-15}–$10^{-12}\,\mathrm{cm}^2\,\mathrm{s}^{-1}$, respectively.

The chemical half-life of PAHs is expected to range from a few minutes on the surface of soot to multiple hours on organic and inorganic solid particles and days on liquid particles. On soot, the degradation of particle-bound PAHs in the atmosphere appears to be dominated by a surface layer reaction with adsorbed ozone. On other substrates, it is likely dominated by gas-surface reactions with OH or NO_3 radicals (Eley-Rideal-type mechanism).

To our knowledge, K2-SURF is the first atmospheric process model describing multiple types of parallel and sequential surface reactions between multiple gaseous and particle-bound chemical species. It illustrates how the general equations of the PRA framework can be simplified and adapted for specific reaction systems, and we suggest that it may serve as a basis for the development of a general master mechanism of aerosol and cloud surface chemistry.

Correspondence to: M. Shiraiwa
(m.shiraiwa@mpic.de)

Published by Copernicus Publications on behalf of the European Geosciences Union.

1 Introduction

Aerosols are ubiquitous in the atmosphere and have strong effects on climate and public health. Depending on chemical composition and surface properties, aerosol particles can act as condensation nuclei for cloud droplets and ice crystals, and they can influence trace gas concentrations through heterogeneous chemical reactions (Seinfeld and Pandis, 1998; Pöschl, 2005; Fuzzi et al., 2006; Andreae and Rosenfeld, 2008; Hallquist et al., 2009). Polycyclic aromatic hydrocarbons (PAHs) are one of the most prominent groups of toxic air pollutants. They originate from biomass burning and fossil fuel combustion, and they reside to a large extent in fine air particulate matter that can penetrate deep into human lungs (Finlayson-Pitts and Pitts, 2000; Pöschl, 2002; Schauer et al., 2003). Chemical degradation and transformation (oxidation or nitration) can change the surface properties of aerosol particles and the toxicity of PAH (Pitts, 1983; Atkinson and Arey, 1994; Pöschl, 2002; Schauer et al., 2004; Pöschl et al., 2007).

Moreover, PAH as well as its oxygenated or nitrated derivatives are well defined model substances for the molecular structure of soot, which is the black solid product of incomplete combustion or pyrolysis of organic matter (Homann, 1998; Messerer et al., 2005; Pöschl, 2005; Sadezky et al., 2005). Soot contributes to regional and global climate change because of its role in direct, indirect and semi-direct radiative forcing (Hansen et al., 1997; Ackerman et al., 2000; Jacobson, 2000). Upon emission from combustion sources, fresh soot is initially hydrophobic and mostly externally mixed with non-refractory compounds (Shiraiwa et al., 2007; Schwarz et al., 2008). However, condensation of semi-volatile compounds and chemical processing by ozone and other oxidants can make soot particles hydrophilic (Mikhailov et al., 2006) and influence their ability to act as cloud condensation nuclei (Kuwata et al., 2007). Furthermore, chemical reactions with atmospheric photo-oxidants can lead to substantial degradation, short-term and seasonal variations, and measurement artefacts in the determination of PAHs (Schauer et al., 2003, 2004; Marchand et al., 2004; Liu et al., 2006; Lee and Kim, 2007; Lammel et al., 2009).

As detailed below (Sect. 3), several laboratory studies have investigated the heterogeneous reaction of PAHs on various substrates with ozone, nitrogen dioxide, water vapour, hydroxyl and nitrate radicals. So far, however, the experimental results had not yet been compiled in a form that enables efficient modelling of PAH degradation in different types of reaction systems and direct comparison of relevant physicochemical parameters (accommodation, uptake, and reaction rate coefficients; adsorption constants; etc.).

Recently, Springmann et al. (2009) have demonstrated the applicability and usefulness of the PRA framework (Ammann and Pöschl, 2007; Pöschl et al., 2007) for atmospheric modeling of the degradation of benzo[a]pyrene on soot by ozone and nitrogen dioxide. In this study we show that the PRA model approach can be efficiently extended to other PAHs and photo-oxidants. Within the European integrated project on aerosol, cloud, climate and air quality interactions (EUCAARI, Kulmala et al., 2009), we have reviewed and synthesized available literature data to develop a reaction mechanism describing the degradation of PAHs exposed to O_3, NO_2, H_2O, OH and NO_3 radicals in a kinetic double-layer surface model (K2-SURF). PAH degradation and related ozone uptake are simulated over a wide range of conditions, and the atmospheric implications are discussed.

2 Model description

The K2-SURF model is based on the PRA framework for aerosol and cloud surface chemistry and gas-particle interactions (Pöschl, Rudich and Ammann 2007; Ammann and Pöschl 2007). This framework describes the gas-particle interface by several model compartments and molecular layers in which volatile, semi-volatile and non-volatile species can undergo mass transport and chemical reactions: gas phase, near-surface gas phase, sorption layer, quasi-static surface layer, and (near-surface) bulk of the particle.

As illustrated in Fig. 1, the K2-SURF model does not consider semi-volatile species and processes in the particle bulk, which is just regarded as a substrate that may influence the properties of the quasi-static surface layer.

In describing the degradation of particle-bound polycyclic aromatic hydrocarbons (PAHs) exposed to O_3, H_2O, NO_2, OH, and NO_3, the focus was on the gas phase diffusion, gas-surface mass transport, surface layer reactions, and gas-surface reactions, which are discussed in following sections. We assumed that the effects of surface-bulk mass transport and chemical reactions in the bulk are negligible compared to gas-surface mass transport and chemical reactions at the surface. Nevertheless, the chemical species in the quasi-static surface layer (PAH) can interact with the near-surface particle bulk (substrate), which may influence the effective physicochemical properties of the quasi-static surface layer and related kinetic parameters such as surface accommodation coefficients, desorption lifetimes, and surface reaction rate coefficients (Pöschl et al. 2007).

2.1 Gas phase diffusion and gas-surface mass transport

Based on kinetic theory, the gas kinetic flux of X_i colliding with the surface $J_{\mathrm{coll,X}i}$ can be expressed as

$$J_{\mathrm{coll,X}i} = [\mathrm{X}_i]_{\mathrm{gs}} \omega_{\mathrm{X}i}/4 \quad (1)$$

where $[X_i]_{gs}$ is near-surface gas phase concentration of X_i and ω_{Xi} is mean thermal velocity given by $\omega_{\mathrm{X}i} = (8RT/(\pi M_{\mathrm{X}i}))^{1/2}$, where M_{Xi} is the molar mass of X_i, R is the gas constant, and T is the absolute temperature. Here we assume that the gas phase concentrations of O_3, H_2O, and NO_2 are homogeneous throughout gas phase

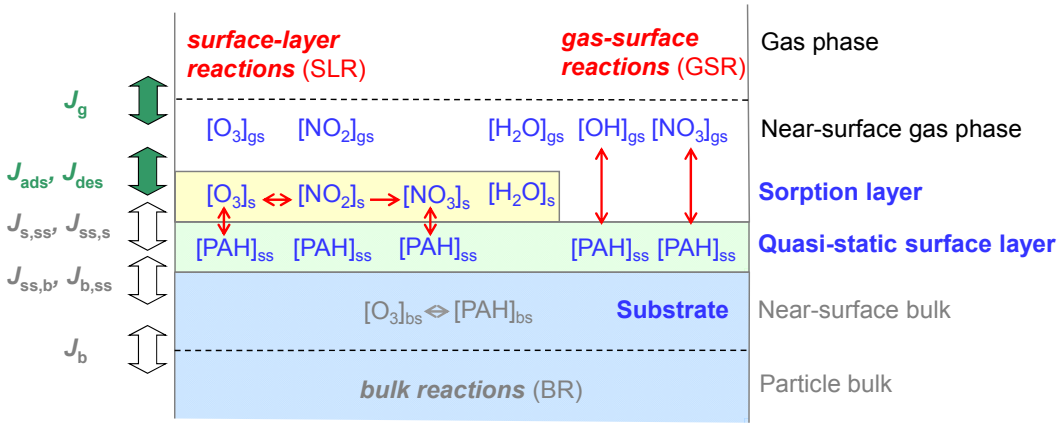

Fig. 1. Schematic illustration of the kinetic double-layer surface model (K2-SURF). Compartments, transport fluxes (thick green arrows), and chemical reactions (thin red arrows) of volatile species (O_3, H_2O, NO_2, OH and NO_3) and non-volatile species (PAHs).

and near-surface gas phase ($[X_i]_{gs} = [X_i]_g$). This assumption is well justified when uptake coefficients are below 10^{-3} (Ammann and Pöschl, 2007).

On the other hand, uptake of OH and NO_3 by PAH is reported to be high (>0.1) (Bertram et al., 2001; Gross and Bertram, 2008), therefore, the significant net uptake of OH and NO_3 will lead to local depletion of concentration at near-surface gas phase ($[X_i]_{gs} < [X_i]_g$) and gas phase diffusion will influence further uptake. In this case near-surface gas phase concentration should be corrected using a gas phase diffusion correction factor $C_{g,Xi}$.

$$[X_i]_{gs} = C_{g,Xi}[X_i]_g \tag{2}$$

$C_{g,Xi}$ can be described as follows based on PRA framework (Pöschl et al., 2007).

$$C_{g,X_i} = \frac{1}{1+\gamma_{X_i}\frac{0.75 + 0.28\ Kn_{X_i}}{Kn_{X_i}(1 + Kn_{X_i})}} \tag{3}$$

Kn_{Xi} is Knudsen number which can be approximated by gas phase diffusion coefficient $D_{g,Xi}$ and particle diameter d_p.

$$Kn_{X_i} = \frac{6\ D_{g,X_i}}{\omega_{X_i} d_p} \tag{4}$$

We calculated $C_{g,OH}$ and $C_{g,NO3}$ using the reported values of $D_{g,OH}$ = 217 hPa cm^2 s^{-1} (Ivanov et al., 2007), γ_{OH} = 0.32 (Bertram et al., 2001), $D_{g,NO3}$ = 107 hPa cm^2 s^{-1} (Rudich et al., 1996) and γ_{NO3}=0.13 (Gross and Bertram, 2008). Figure 2 illustrates the decrease of $C_{g,OH}$ and $C_{g,NO3}$ with increasing d_p, i.e., how the effect of gas diffusion increases with increasing particle diameter.

The flux of adsorption of gas molecules on the quasi-static particle surface can be expressed as

$$J_{ads,Xi} = \alpha_{s,Xi} J_{coll,Xi} = k_{a,Xi}[X_i]_{gs} \tag{5}$$

where $\alpha_{s,Xi}$ is surface accommodation coefficient and $k_{a,Xi}$ (= $\alpha_{s,Xi}\omega_{Xi}/4$) is a first-order adsorption rate coefficient. In Langmuir adsorption model, $\alpha_{s,Xi}$ is determined by the surface accommodation coefficient on an adsorbate-free surface $\alpha_{s,0,Xi}$ and the sorption layer coverage θ_s, which is given by the sum of the fractional surface coverage of all competing adsorbate species (i.e. O_3, H_2O, and NO_2) $\theta_{s,Xp}$.

$$\alpha_{s,Xi} = \alpha_{s,0,Xi}(1 - \theta_s) = \alpha_{s,0,Xi}(1 - \sum \theta_{s,Xp}) \tag{6}$$

$\theta_{s,Xp}$ is the ratio between the actual and the maximum surface concentration value of X_p: $\theta_{s,Xp} = [X_p]_s/[X_p]_{s,max} = \sigma_{s,Xp}[X_p]_s$, where $\sigma_{s,Xp}$ is the effective molecular cross section of X_p. In this study, we assume that the effective molecular cross section is the same for all co-adsorbed species unless mentioned otherwise. Accordingly, the inverse molecular cross section can be regarded as the overall concentration of non-interfering sorption sites on the quasi-static surface layer (Pöschl et al., 2007): $[SS]_{ss} = \sigma_{s,Xp}^{-1}$.

The adsorbed molecules can thermally desorb back to the gas phase. Desorption, the inverse of adsorption, can be described by a first-order rate coefficient $k_{d,Xi}$, which is assumed to be independent on $\theta_{s,Xi}$. The flux of desorption of gas molecules on the quasi-static particle surface can be expressed as

$$J_{des,Xi} = k_{d,Xi}\ [X_i]_s = \tau_{d,Xi}^{-1}\ [X_i]_s \tag{7}$$

The desorption lifetime $\tau_{d,Xi}$ is the mean residence time on the surface in the absence of surface reaction and surface-bulk transport. Since molecules are desorbed thermally, $k_{d,Xi}$ depends strongly on temperature. This can be described by an Arrhenius equation as described below.

$$k_{d,Xi} = A\ \exp(\Delta H_{ads,Xi}/RT) \tag{8}$$

A pre-exponential factor A is typically $\sim 10^{14}$ s^{-1} for chemisorbed species, which is approximately the vibrational

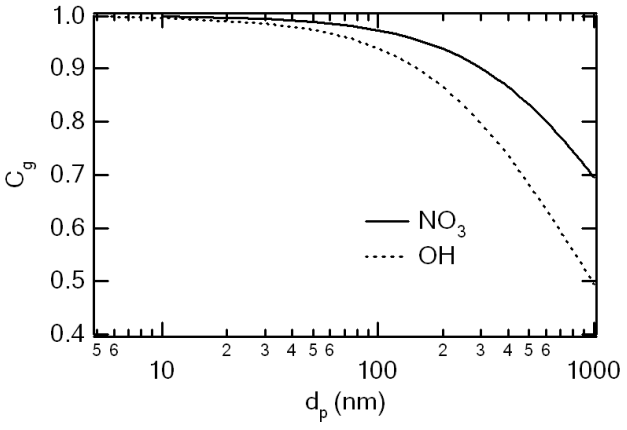

Fig. 2. Gas phase diffusion correction factor (C_g) for OH and NO_3 plotted against particle diameter (d_p).

frequency of a molecule bound to the surface. For physisorbed species, A is typically $\sim 10^{12}\,s^{-1}$. Adsorption enthalpy of gaseous X_i, $\Delta H_{ads,Xi}$ can be estimated roughly by assuming A.

The uptake coefficient of gas species X_i can be expressed as a ratio between the net fluxes of X_i from the gas phase to the condensed phase $J_{net,Xi}$, and $J_{coll,Xi}$.

$$\gamma_{Xi} = \frac{J_{net,Xi}}{J_{coll,Xi}} = \frac{J_{ads,Xi} - J_{des,Xi}}{J_{coll,Xi}} \quad (9)$$

2.2 Surface layer reactions (Langmuir-Hinshelwood-type mechanism)

The surface layer reactions (SLRs) occur within the surface double layer and involve only adsorbed species or components of the quasi-static layer. In this study the PAH-O_3 system is considered to follow a Langmuir-Hinshelwood-type mechanism, in which ozone first adsorbs to the surface and then reacts with PAH in a quasi-static surface layer (Pöschl et al., 2001; Ammann et al., 2003; Ammann and Pöschl, 2007; Pöschl et al., 2007). Note, however, that traditionally the term "Langmuir-Hinshelwood mechanism" is used for surface catalytic reactions between adsorbed gas species and not to describe reactions that transform the surface (Masel, 1996; IUPAC, 1997). Here we consider three SLRs:

$$PAH(ss) + O_3(s) \rightarrow O1-PAH(ss) \quad (SLR1)$$

$$O_3(s) + NO_2(s) \rightarrow NO_3(s) \quad (SLR2)$$

$$PAH(ss) + NO_3(s) \rightarrow O2-PAH(ss) \quad (SLR3)$$

The products of SLR1 and SLR3, O1-PAH and O2-PAH, are oxidized non-volatile PAHs. The surface reaction of O_3 and NO_2 produces the highly reactive NO_3 radical, which can react with PAH immediately. The degradation rate of PAH ($L_{SLR,PAH}$) can be described using the second-order rate coefficients $k_{SLR,PAH,O3}$ and $k_{SLR,PAH,NO3}$,

$$L_{SLR,PAH} = k_{SLR,PAH,O_3}[PAH]_{ss}[O_3]_s + k_{SLR,PAH,NO_3}[PAH]_{ss}[NO_3]_s = k_{s,PAH}[PAH]_{ss} \quad (10)$$

where $k_{s,PAH}$ ($= k_{SLR,PAH,O3}[O_3]_s + k_{SLR,PAH,NO3}[NO_3]_s$) is an apparent first-order PAH decay rate coefficient.

The loss rate of ozone by SLR1-SLR2 ($L_{SLR,O3}$) can be described as

$$L_{SLR,O_3} = k_{SLR,PAH,O_3}[PAH]_{ss}[O_3]_s + k_{SLR,O_3,NO_2}[O_3]_s[NO_2]_s = k_{s,O_3}[O_3]_s \quad (11)$$

where $k_{s,O3}$ ($=k_{SLR,PAH,O3}[PAH]_{ss}+k_{SLR,O3,NO3}[NO_2]_s$) is an apparent first-order ozone loss rate coefficient.

The production rate of NO_3 on the surface, $P_{SLR,NO3}$, can be described as

$$P_{SLR,NO_3} = k_{SLR,O_3,NO_2}[O_3]_s[NO_2]_s - k_{SLR,PAH,NO_3}[PAH]_{ss}[NO_3]_s \quad (12)$$

2.3 Gas-surface reaction (Eley-Rideal-type mechanism)

The gas-surface reaction is a single kinetic step of collision and reaction between gaseous species and surface molecules, which can be regarded as an Eley-Rideal-type mechanism (Ammann and Pöschl, 2007; Pöschl et al., 2007). Note that traditionally the term "Eley-Rideal mechanism" (also named Rideal-Eley or Langmuir-Rideal mechanism) is used for surface catalytic reaction between adsorbed gas species rather than for reactions that transform the surface (Masel, 1996; IUPAC, 1997). Here we consider two GSRs.

$$PAH(ss) + OH(gs) \rightarrow O3-PAH(ss) \quad (GSR1)$$

$$PAH(ss) + NO_3(gs) \rightarrow O4-PAH(ss) \quad (GSR2)$$

Heterogeneous loss of PAH on the surface ($L_{GSR,PAH}$) can be described by the following equation (Pöschl et al., 2007).

$$L_{GSR,PAH} = \sum_{X_i} \gamma_{GSR,X_i,PAH}\,\theta_{ss,PAH}\,(1-\theta_s)\,J_{coll,X_i} \quad (13)$$

Here $\gamma_{GSR,Xi,PAH}$ is defined as the elementary surface reaction probability that X_i (OH or NO_3) undergoes gas-surface reaction when colliding with PAH on the surface. $\theta_{ss,PAH}$ is the surface coverage of PAH.

2.4 Steady-state conditions

The surface mass balance and rate equations can be described as below in summary (Pöschl et al., 2007).

$$d[O_3]_s/dt = J_{ads,O3} - J_{des,O3} - L_{SLR,O3} \quad (14)$$

$$d[H_2O]_s/dt = J_{ads,H2O} - J_{des,H2O} \quad (15)$$

$$d[NO_2]_s/dt = J_{ads,NO2} - J_{des,NO2} - L_{SLR,NO2} \quad (16)$$

$$d[PAH]_{ss}/dt = -L_{SLR,PAH} - L_{GSR,PAH} \quad (17)$$

$$d[NO_3]_s/dt = P_{SLR,NO3} - J_{des,NO3} \quad (18)$$

Steady-state conditions are characterized by $d[X_i]_s/dt=0$ (X_i=O_3, H_2O, and NO_2). The effective Langmuir adsorption equilibrium constant $K'_{ads,Xi}$ can be described as below should be follows.

$$K'_{ads,X_i}[X_i]_{gs} = \frac{\theta_{s,X_i}}{1-\theta_s} \quad (19)$$

$$K'_{ads,X_i} = \sigma_{s,X_i}\frac{k_{a,0,X_i}}{k_{d,X_i}+k_{s,X_i}} \quad (20)$$

If surface reactions are much slower than desorption ($k_{d,Xi} \gg k_{s,Xi}$), then $K'_{ads,Xi}$ is equal to a Langmuir adsorption equilibrium constant $K_{ads,Xi}$ ($=\sigma_{s,Xi}k_{a,0,Xi}/k_{d,Xi}$). Under these conditions the desorption lifetime $\tau_{d,Xi}$ and first-order rate coefficient $k_{d,Xi}$ are given by

$$k_{d,X_i} = \frac{1}{\tau_{d,X_i}} \approx \sigma_{s,X_i}\frac{k_{a,0,X_i}}{K'_{ads,X_i}} = \frac{\alpha_{s,0,X_i}\omega_{X_i}\sigma_{s,X_i}}{4\,K'_{ads,X_i}} \quad (21)$$

The surface concentration of X_i can be expressed as

$$[X_i]_s = \sigma_{s,X_i}^{-1}\theta_{s,X_i} = \sigma_{s,X_i}^{-1}\frac{K'_{ads,X_i}[X_i]_{gs}}{1+\sum K'_{ads,X_i}[X_i]_{gs}} \quad (22)$$

An apparent first order rate coefficient $k_{s,PAH}$ can be described as

$$k_{s,PAH} = k_{s,PAH,max}\frac{K'_{ads,X_i}[X_i]_{gs}}{1+\sum_p K'_{ads,X_p}[X_p]_{gs}} \quad (23)$$

where $k_{s,PAH,max}$ is a maximum pseudo-first order rate coefficient of PAH.

The uptake coefficient of ozone (γ_{O3}) can be calculated as

$$\gamma_{O_3} = \frac{L_{SLR,O_3}}{J_{coll,O_3}} = \frac{4\,k_{s,PAH}}{\sigma_{PAH}\,\omega_{O_3}[O_3]_{gs}} \quad (24)$$

The initial concentration of PAH is considered to be the inverse of the effective molecular cross section σ_{PAH} and is estimated assuming one aromatic ring has 0.2 nm^2. For example, σ_{BaP} is assumed to be 1 nm^2 because BaP consists of five aromatic rings (Pöschl et al., 2001).

3 Experimental data analysis and steady-state conditions

3.1 PAH-O_3-H_2O system

The kinetics of the heterogeneous reaction between gaseous ozone and PAHs bound on various substrates have been investigated in several laboratory studies (Wu et al., 1984; Alebic-Juretic et al., 1990; Pöschl et al., 2001; Ammann et al., 2003; Mmereki and Donaldson, 2003; Kwamena et al., 2004; Mmereki et al., 2004; Donaldson et al., 2005; Kahan et al., 2006; Kwamena et al., 2006, 2007). The investigated PAHs comprise benzo[a]pyrene (BaP), anthracene, naphthalene, pyrene, phenanthrene, benzo[a]anthracene (BaA), perylene, and fluoranthene. The substrates include soot, azelaic acid, phenylsiloxane, glass, ZnSe, non-activated silica gel, fused silica, octanol, decanol, stearic acid, octanoic acid, and hexanoic acid and water. As specified in Table 1, the PAHs were deposited on aerosol particles, solid or liquid substrates, or on organic thin films on water. Self-assembled monolayers (SAM) of alkenes and cypermethrin were also analyzed for comparison (Dubowski et al., 2004; Segal-Rosenheimer and Dubowski, 2008), as they follow similar reaction mechanisms and kinetics.

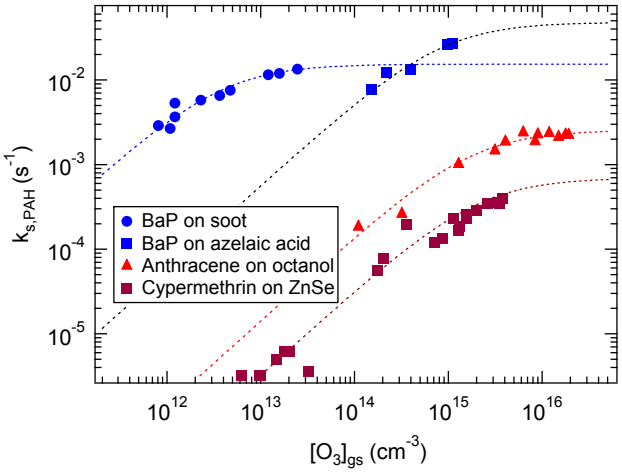

Fig. 3. Pseudo-first-order PAH decay rate coefficients ($k_{s,PAH}$) as a function of gas phase ozone concentration ($[O_3]_{gs}$) under dry conditions: BaP on soot aerosol (Pöschl et al., 2001), BaP on azelaic acid aerosol (Kwamena et al., 2004), Anthracene on octanol (Kahan et al., 2006), and cypermethrin on ZnSe (Segal-Rosenheimer and Dubowski, 2008).

3.1.1 Basic physicochemical parameters

As illustrated in Fig. 3, the pseudo-first order PAH decay rate coefficients ($k_{s,PAH}$) typically exhibit a nonlinear dependence on gas phase ozone concentration, which is consistent with a Langmuir-Hinshelwood-type mechanism. In contrast, an Eley-Rideal-type mechanism would lead to a linear dependence of $k_{s,PAH}$ on gas phase ozone concentration. In the PAH-O_3-H_2O system Eq. (23) can be simplified to

$$k_{s,PAH} = \frac{k_{s,PAH,max}K'_{ads,O_3}[O_3]_{gs}}{1+K'_{ads,O_3}[O_3]_{gs}+K'_{ads,H_2O}[H_2O]_{gs}} \quad (25)$$

The parameters of $k_{s,PAH,max}$ and $K'_{ads,O3}$ were obtained by a non-linear least-squares fit of Eq. (25) to the experimental data pairs of $k_{s,PAH}$ and $[O_3]_{gs}$ for each PAH and substrate

Table 1. Basic physicochemical parameters of O_3 in the PAH-O_3-H_2O system with different PAHs and substrates. The upper part is kinetics data of PAHs on solid substrates, the middle part is that of PAHs on liquid substrates, and the bottom part is that of non-PAH.

PAH	Substrate	RH (%)	$K_{ads,O3}$ (10^{-15} cm^3)	$k_{s,PAH,max}$ (s^{-1})	$k_{SLR,PAH,O3}$ (10^{-17} cm^2 s^{-1})	$k_{d,O3}$ (s^{-1})	$\tau_{d,O3}$ (s)	$\Delta H_{ads,O3}$ (kJ mol^{-1})	Reference
BaP	soot aerosol	25	255	0.0155	3.37	0.08	13.0	−86	Pöschl et al. (2001)
BaP	azelaic acid aerosol	72	4.39	0.0600	10.4	3.56	0.28	−76	Kwamena et al. (2004)
BaP	soot aerosol	0	255	0.0154	2.66	0.06	16.3	−86	Pöschl et al. (2001)
BaP	azelaic acid aerosol	0	1.18	0.0480	8.30	13.2	0.08	−73	Kwamena et al. (2004)
BaP	NaCl aerosol	0	0.12	0.0320	5.54	130	0.01	−67	Kwamena et al. (2004)
BaP	fused silica	0	27.1	0.0325	5.62	0.58	1.74	−81	Wu et al. (1984)
BaP	silica gel	0	9.4	0.0325	5.62	1.67	0.60	−78	Alebic-Juretic et al. (1990)
Anthracene	glass	0	2.85	0.0060	1.04	5.48	0.18	−75	Kwamena et al. (2006)
Anthracene	azelaic acid aerosol	0	2.24	0.0550	9.52	6.97	0.14	−75	Kwamena et al. (2007)
BaA	silica gel	0	38.6	0.004	0.69	0.40	2.47	−82	Alebic-Juretic et al. (1990)
Pyrene	silica gel	0	86.0	0.001	0.17	0.18	5.51	−84	Alebic-Juretic et al. (1990)
Perylene	silica gel	0	67.9	0.004	0.69	0.23	4.35	−83	Alebic-Juretic et al. (1990)
Perylene	fused silica	0	4.4	0.004	0.69	3.55	0.28	−76	Wu et al. (1984)
Fluoranthene	silica gel	0	65.0	0.0001	0.02	0.24	4.17	−83	Alebic-Juretic et al. (1990)
BaP	octanol	0	0.35	0.0055	0.94	45.0	0.02	−70	Kahan et al. (2006)
Anthracene	phenylsiloxane oil aerosol	0	104	0.0100	1.73	0.15	6.66	−84	Kwamena et al. (2007)
Anthracene	octanol/decanol	0	0.56	0.0026	0.44	28.0	0.04	−71	Kahan et al. (2006)
Anthracene	octanol on water	0	1.83	0.0026	0.45	8.53	0.12	−74	Mmereki and Donaldson (2003)
Anthracene	water	0	0.45	0.0026	0.45	34.7	0.03	−71	Mmereki and Donaldson (2003)
Anthracene	stearic acid on water	0	0.47	0.0024	0.41	33.4	0.03	−71	Mmereki et al. (2004)
Anthracene	octanoic acid on water	0	0.94	0.0013	0.22	16.7	0.06	−72	Mmereki et al. (2004)
Anthracene	hexanoic acid on water	0	1.2	0.0004	0.07	13.0	0.08	−73	Mmereki et al. (2004)
Naphthalene	octanol	0	0.97	0.0009	0.15	16.1	0.06	−72	Kahan et al. (2006)
Pyrene	octanol	0	0.32	0.0007	0.12	48.8	0.02	−70	Kahan et al. (2006)
Pyrene	water	0	0.86	0.0012	0.20	18.2	0.06	−72	Donaldson et al. (2005)
Pyrene	octanol on water	0	1.66	0.0015	0.26	9.41	0.11	−74	Donaldson et al. (2005)
Phenanthrene	octanol	0	0.16	0.0006	0.10	97.6	0.01	−68	Kahan et al. (2006)
SAM C3&C8	ZnSe	0	25	0.0060	1.04	0.62	1.60	−80	Dubowski et al. (2004)
Cypermethrin	ZnSe	0	0.47	0.0007	0.12	33.2	0.03	−71	Segal-Rosenheimer and Dubowski (2007)

(IGOR software). The experimental data were taken from the referenced studies, and the fit results are summarized in Table 1.

Pöschl et al. (2001) also measured the surface concentration of ozone, $[O_3]_s$, as a function of gas phase ozone concentration, which can be described by the following equation:

$$[O_3]_s = \frac{\sigma_{s,X_i}^{-1} K'_{ads,O_3}[O_3]_{gs}}{1+K'_{ads,O_3}[O_3]_{gs}+K'_{ads,H_2O}[H_2O]_{gs}} \quad (26)$$

A non-linear least squares fit yielded $\sigma_{s,O3}$=0.17 nm^2 ($[SS]_{ss}$=5.8×10^{14} cm^{-2}). We assumed this value for the other studies as well, because Pöschl et al. (2001) is the only study that reported $[O_3]_s$. Second-order rate coefficients ($k_{SLR,PAH,O3}$) were calculated using the relation $k_{s,PAH,max}$=$k_{SLR,PAH,O3}\sigma_{s,O3}^{-1}$. Ozone desorption lifetimes ($\tau_{d,O3}$) and the corresponding desorption rate coefficients ($k_{d,O3}$) were estimated using Eq. (21), assuming a surface accommodation coefficient of $\alpha_{s,0,O3}$=1.0×10^{-3} (Rogaski et al., 1997) for the adsorbate-free surface.

The obtained $\tau_{d,O3}$ values are in the range of 10 ms–10 s depending on the substrate (Table 1). The relatively long desorption lifetimes suggest chemisorption of O_3^- possibly in the form of O atoms. Thus, the $\tau_{d,O3}$ values should be regarded as apparent desorption lifetimes that may effectively include the dissociation of ozone or other intermediate steps of chemical interaction at the surface as will be discussed below.

From $k_{d,O3} = \tau_{d,O3}^{-1}$ approximate adsorption enthalpies $\Delta H_{ads,O3}$ were estimated using Eq. (8) and assuming a pre-exponential factor of $A = 10^{14}$ s^{-1} (Pöschl et al., 2001). Test calculations with $A = 10^{12}$–10^{15} s^{-1} gave an uncertainty range of ± 6 kJ mol^{-1} in $\Delta H_{ads,O3}$. $K'_{ads,O3}$ is approximated to $K_{ads,O3}$, as $k_{d,O3}$ is one to three orders of magnitude larger than $k_{s,O3}$. The $K_{ads,O3}$ values are one to three orders of magnitude larger for solid substrates compared to liquid substrates. This corresponds to longer desorption lifetimes and larger negative adsorption enthalpy values for solid substrates ($\Delta H_{ads,O3} \approx -(70–90)$ kJ mol^{-1}). Additionally, $k_{s,PAH,max}$ and $k_{SLR,PAH,O3}$ are by an order of magnitude larger on solid substrates. Self-assembled monolayers of alkenes show similar adsorption and reaction rate coefficients as PAHs on solid substrates, whereas the parameters for cypermethrin are similar to PAHs on liquid substrates.

Most studies were performed under dry conditions (RH ≈ 0%), but Pöschl et al. (2001) and Kwamena et al. (2004) also reported results for humid conditions. The $K_{ads,H2O}$ values obtained from these data are of the order of 10^{-17} cm^{-3} (Table 2), i.e., 2–4 orders of magnitude smaller than $K_{ads,O3}$. Assuming $\alpha_{s,0,H2O}$ = 6.0 × 10^{-4}

Table 2. Basic physicochemical parameters of H_2O in the BaP-O_3-NO_2-H_2O system on soot and azelaic acid.

Substrate	RH (%)	NO_2 (ppb)	$K_{ads,H2O}$ (10^{-17} cm^3)	$[SS]_{ss}$ (10^{14} cm^{-2})	$\tau_{d,H2O}$ (s)	$k_{d,H2O}$ (s^{-1})	$\Delta H_{ads,H2O}$ (kJ mol^{-1})	Reference	Data set
soot	25	0	0.17	4.60	1.33×10^{-4}	7.54×10^{3}	-35 ± 9	Pöschl et al. (2001)	$[O_3]_s$ vs. $[O_3]_{gs}$
soot	25	1000	0.15	2.24	5.69×10^{-5}	1.76×10^{4}	-33 ± 9	Schauer (2004)	$[O_3]_s$ vs. $[O_3]_{gs}$
soot	25	0	1.02	–	7.95×10^{-4}	1.26×10^{3}	-39 ± 9	Pöschl et al. (2001)	$k_{s,BaP}$ vs. $[O_3]_{gs}$
soot	25	1000	1.18	–	4.48×10^{-4}	2.23×10^{3}	-38 ± 9	Schauer (2004)	$k_{s,BaP}$ vs. $[O_3]_{gs}$
azelaic acid	72	0	0.10	–	9.80×10^{-5}	1.02×10^{4}	-34 ± 9	Kwamena et al. (2004)	$k_{s,BaP}$ vs. $[O_3]_{gs}$

(Rogaski et al., 1997) we obtained H_2O desorption lifetimes of the order of 0.1 ms, indicating physisorption of H_2O. The adsorption enthalpy $\Delta H_{ads,H2O}$ was estimated to be $-36(\pm 9)$ kJ mol^{-1} assuming a pre-exponential factor in the range of 10^8–10^{12} s^{-1} (Pöschl et al., 2001).

Kwamena et al. (2007) pointed out that the substrate influences the partitioning of ozone to the surface irrespective of the PAH adsorbed to it. They also suggested that different experimental approaches can yield different results. In particular, they found that PAHs may dissolve into the substrate of thin film experiments, thereby affecting the reaction kinetics and partitioning of O_3 as will be discussed below.

According to molecular dynamics (MD) simulations the desorption lifetime of ozone on at the interface of pure water and air should be only 36 ps (Vieceli et al., 2005) which is much shorter than the values listed in Table 1. Possible explanations for the differences are: (1) The surfaces considered in our study are covered by PAH molecules and thus likely to interact differently with ozone. (2) The desorption lifetimes calculated from measurement-derived adsorption constants depend inversely on the assumed surface accommodation coefficients ($\alpha_{s,0}$) and might thus be up to three orders of magnitude shorter if $\alpha_{s,0}$ were close to unity. (3) The chemical species actually residing at the surface might be O atoms rather than ozone molecules, and thus additional processes such as a dissociation reaction or other intermediate steps of chemical interactions at the surface might have to be considered for full mechanistic understanding. (4) Surface-bulk exchange as well as mass transport and chemical reactions might also play a role for liquid substrates. Further investigations will be needed to resolve these issues, and we are planning to pursue such investigations using K2-SURF as well as kinetic double- and multi-layer models that resolves also diffusion and reaction in the bulk of the particle or substrate, respectively (K2-SUB, Pfrang et al., 2009; KM-SUB, Shiraiwa et al., 2009).

3.1.2 Uptake of ozone

Ozone uptake coefficients for the PAH-O_3-H_2O system were calculated using Eq. (24) and are shown in Fig. 4. The γ_{O3} values exhibt a strong dependence on the gas phase concentration of ozone ($[O_3]_{gs} \approx 10^{11}$–$10^{16}$ cm^{-3} corresponding to 10–10^6 ppb under dry standard conditions at 1013 hPa and 298 K). The symbols represent literature data (Table 1), and the curves represent three characteristic K2-SURF model scenarios: (1) a soot surface with $\tau_{d,O3}$=10 s and $k_{SLR,PAH,O3} = 2.7 \times 10^{-17}$ (red solid line); (2) a solid organic surface with $\tau_{d,O3}$=1 s and $k_{SLR,PAH,O3} = 2.7 \times 10^{-17}$ (red dotted line); (3) a liquid organic surface with $\tau_{d,O3}$=0.1 s and $k_{SLR,PAH,O3} = 5.0 \times 10^{-18}$ (black solid line).

Systems on a solid substrate such as soot, glass and solid organic substrate are well described by the red lines in Fig. 4, covering over five orders of magnitude in both γ_{O3} and $[O_3]_{gs}$. Most experimental data were obtained at high $[O_3]_{gs}$, but along the model lines γ_{O3} can be extrapolated to atmospheric conditions ($[O_3]_{gs}$<150 ppb). There γ_{O3} is estimated to be $\sim10^{-5}$ for PAHs on a soot surface and $\sim10^{-6}$ on a solid organic surface.

On liquid substrates γ_{O3} is substantially lower ($\approx 10^{-8}$). A possible explanation is that some PAH may be dissolved in the liquid substrate (Kwamena et al., 2007), leading to a reduction of the actual PAH concentration on the surface and to a decrease of γ_{O3} according to Eq. (24). Transport of PAH from the quasi-static layer to the bulk can be modelled by surface-bulk exchange fluxes ($J_{ss,b}$, $J_{b,ss}$) which goes beyond the present study. Still, these data are well fitted by the black solid line suggesting γ_{O3} values of the order of 10^{-8} under atmospheric conditions.

McCabe and Abbatt (2009) have already pointed out a remarkable similarity of γ_{O3} on a variety of surfaces (soot, 1-hexadecene, metal oxides, atmospheric mineral dust, PAHs coated to soot, organic, and water substrates) both in their absolute magnitude and in their partial pressure dependence, especially given the very different experimental techniques (Knudsen cells, aerosol flow tubes, etc.). Possible explanations and rate limiting steps discussed in their and earlier studies are: surface diffusion of adsorbed ozone molecules (Kwamena et al., 2007) and/or multiple steps of chemical reaction involving possible intermediates like O_3^- ions (Nelander and Nord, 1979) or O atoms (Stephens et al., 1986; Pöschl et al., 2001; Sullivan et al., 2004).

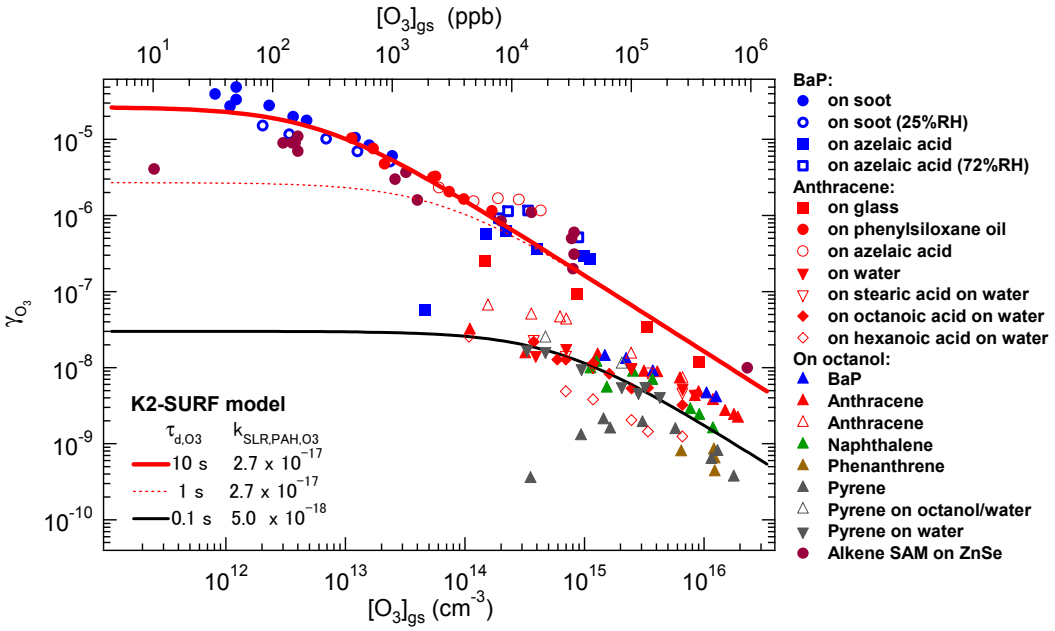

Fig. 4. Ozone uptake coefficients (γ_{O3}) for different PAHs and substrates. Symbols represent literature data (Table 1). Lines show model results assuming the following parameters: (1) $\tau_{d,O3}$ = 10 s and $k_{SLR,PAH,O3}$ = 2.7 × 10^{-17} for soot surfaces (red solid line), (2) $\tau_{d,O3}$ = 1 s and $k_{SLR,PAH,O3}$ = 2.7 × 10^{-17} for solid organic surfaces (red dotted line), (3) $\tau_{d,O3}$ = 0.1 s and $k_{SLR,PAH,O3}$ = 5.0 × 10^{-18} for liquid surfaces (black solid line).

3.2 PAH-O_3-H_2O-NO_2 system

The oxidation of the PAH benzo[a]pyrene upon interaction with O_3, H_2O and NO_2 was investigated using data from Schauer (2004). As illustrated in Fig. 5, the pseudo-first order PAH decay rate coefficients ($k_{s,PAH}$) exhibit a nonlinear dependence on gas phase ozone concentration, which is consistent with a Langmuir-Hinshelwood-type reaction mechanism and can be described by the following equations.

$$[O_3]_s = \frac{\sigma_{s,O_3}^{-1} K'_{ads,O_3}[O_3]_{gs}}{1+K'_{ads,O_3}[O_3]_{gs}+K'_{ads,H_2O}[H_2O]_{gs}+K'_{ads,NO_2}[NO_2]_{gs}} \quad (27)$$

$$k_{s,PAH} = \frac{k_{s,PAH,max} K'_{ads,O_3}[O_3]_{gs}}{1+K'_{ads,O_3}[O_3]_{gs}+K'_{ads,H_2O}[H_2O]_{gs}+K'_{ads,NO_2}[NO_2]_{gs}} \quad (28)$$

Non-linear least squares fits yielded the effective NO_2 adsorption constants summarized in Table 3 (assuming $K_{ads,NO2} \approx K'_{ads,NO2}$). They are of the order of 10^{-14} cm^3, which is similar to the ozone adsorption constants. Assuming $\alpha_{s,0,NO2}$ = 0.064 (Tabor et al., 1994) we obtained NO_2 desorption lifetime estimates of about $\tau_{d,NO2} \approx$ 50 ms, indicating chemisorption of NO_2. The adsorption enthalpy $\Delta H_{ads,NO2}$ was estimated to be $-67(\pm 6)$ kJ mol^{-1} assuming a range of pre-exponential factors ($A \approx 10^{12}$–10^{14} s^{-1}).

Table 4 shows the basic physicochemical parameters of O_3 in this system. The apparent overall concentration of sorption sites $[SS]_{ss}$ decreases systematically as the NO_2 concentration increases, which implies that the effective molecular cross section of adsorbed ozone is smaller than that of NO_2. This finding suggests that ozone may indeed be adsorbed in the form of O atoms, because molecular O_3 is not expected to be smaller than NO_2. Alternatively or in addition, other intermediates might also be involved in the co-adsorption of O_3 and NO_2 (e.g., NO_3 or N_2O_5 formed by reaction of NO_2 with O_3 or O). Further investigations will be needed to elucidate the actual mechanism of interaction between different co-adsorbed species, and additional processes could be flexibly included in K2-SURF. Nevertheless, the simple Langmuir-Hinshelwood-type formalisms applied in this study appear to sufficient for efficient description of multi-component systems as illustrated in Figs. 4 and 5.

Apparent second-order surface reaction rate coefficients $k_{SLR,PAH,O3}$ were derived assuming $k_{SLR,O3,NO2}$ = 0, because no PAH degradation was observed upon exposure to NO_2 without O_3 (Pöschl, 2002; Schauer, 2004; Schauer et al., 2004). Interestingly, however, the measured and derived rate coefficients $k_{s,PAH,max}$ and $k_{SLR,PAH,O3}$ exhibit a systematic increase with increasing NO_2 concentration. For example, $k_{SLR,PAH,O3}$ increases by a factor of ~2 from 2.66 × 10^{-17} cm^2 s^{-1} in the absence of NO_2 to

Table 3. Basic physicochemical parameters of NO_2 in the BaP-O_3-NO_2-H_2O system on soot (Schauer, 2004).

RH (%)	NO_2 (ppb)	$K_{ads,NO2}$ (10^{-15} cm^3)	$[SS]_{ss}$ (10^{14} cm^{-2})	$k_{d,NO2}$ (s^{-1})	$\tau_{d,NO2}$ (s)	$\Delta H_{ads,NO2}$ (kJ mol^{-1})	Data set
0	100	82	4.50	16.0	0.062	−70	$[O_3]_s$ vs. $[O_3]_{gs}$
0	500	34	3.50	49.6	0.020	−67	$[O_3]_s$ vs. $[O_3]_{gs}$
0	1000	53	3.00	37.1	0.027	−68	$[O_3]_s$ vs. $[O_3]_{gs}$
25	1000	10	2.24	263	0.004	−63	$[O_3]_s$ vs. $[O_3]_{gs}$
0	100	69	–	19.0	0.053	−69	$k_{s,BaP}$ vs. $[O_3]_{gs}$
0	250	54	–	27.3	0.037	−68	$k_{s,BaP}$ vs. $[O_3]_{gs}$
25	250	86	–	17.2	0.058	−70	$k_{s,BaP}$ vs. $[O_3]_{gs}$
0	500	71	–	23.8	0.042	−69	$k_{s,BaP}$ vs. $[O_3]_{gs}$
0	750	17	–	99.2	0.010	−65	$k_{s,BaP}$ vs. $[O_3]_{gs}$

Table 4. Basic physicochemical parameters of O_3 in the BaP-O_3-NO_2-H_2O system on soot (Schauer, 2004).

RH (%)	NO_2 (ppb)	$K_{ads,O3}$ (10^{-15} cm^3)	$k_{s,PAH,max}$ (s^{-1})	$[SS]_{ss}$ (10^{14} cm^{-2})	$k_{SLR,PAH,O3}$ (10^{-17} cm^2 s^{-1})	$k_{d,O3}$ (s^{-1})	$\tau_{d,O3}$ (s)	$\Delta H_{ads,O3}$ (kJ mol^{-1})
0	0	255	0.015	5.80	2.66	0.06	16.3	−86
0	100	331	0.013	4.50	2.89	0.06	16.5	−86
0	250	369	0.015	*4.00**	3.75	0.06	16.4	−86
25	250	332	0.021	*4.00**	5.25	0.07	14.7	−86
0	500	347	0.020	3.50	5.71	0.07	13.5	−86
0	750	296	0.020	*3.25**	6.15	0.09	10.7	−85
0	1000	513	–	3.00	–	0.06	17.1	−86
25	1000	474	–	2.24	–	0.09	11.8	−85

* Values in italic are interpolated.

5.70×10^{-17} cm^2 s^{-1} at 500 ppb NO_2. The accelerating effect of NO_2 can be attributed to the formation of highly reactive NO_3 radicals in the gas phase or on the surface. Other reactive nitrogen species like N_2O_5 or HNO_3 are unlikely to play a major role because the uptake coefficients reported for them are $<10^{-5}$ (Gross and Bertram, 2008).

4 Numerical modeling of transient conditions

Here we simulate the temporal evolution of surface composition and uptake coefficients of ozone over timescales from microseconds to days under standard conditions (298 K, 1013 hPa). The model calculations were performed by solving the rate equations (Eq. 14–18) numerically with Matlab software (ode23s solver). No steady-state assumptions were applied in the numerical simulations.

The initial PAH surface concentration is set to 1×10^{14} cm^{-2}, and the initial surface concentration of gas species (X_i = O_3, H_2O, NO_2, and NO_3) is set to zero. In the exemplary simulations, we consider soot and solid organic surfaces. The required basic physicochemical parameters are listed in Table 5. The $\alpha_{s,0}$ values were taken from earlier studies (Tabor et al., 1994; Rogaski et al., 1997). The τ_d and $k_{SLR,PAH,O3}$ values were taken from Sect. 3. The gas phase ozone concentration is set to 100 ppb, which is typical for polluted air masses. The chemical half-life of the PAH ($t_{1/2}$) is defined as the time when the PAH concentration reaches half of the initial concentration.

4.1 PAH-O_3-H_2O system

Here we simulate PAH degradation upon interaction with O_3 and H_2O. Fig. 6 shows the surface concentrations of all involved chemical species and the uptake coefficient of O_3 (γ_{O3}). Figure 6a displays the model results for a soot surface at 25% RH. The initial plateau of γ_{O3} is equal to $\alpha_{s,0,O3}$ (=10^{-3}) up to 1 s, which can be explained by adsorption of O_3 onto a nearly adsorbate-free surface. The second plateau of γ_{O3} at $\sim 10^{-5}$ is due to chemical reaction of O_3 with PAH. Under dry conditions the model results are similar (not shown in figure), but due to the absence of competitively adsorbing H_2O the surface coverage of O_3 increases and the PAH chemical half-life decreases 188 s (25% RH) to 168 s (dry).

Table 5. Basic physicochemical parameters of O_3, H_2O, and NO_2 used in the numerical simulations of transient conditions.

X_i	Substrate	K_{ads,X_i} (10^{-15} cm^3)	$k_{SLR,PAH,O3}$ (10^{-17} cm^2 s^{-1})	$\tau_{d,Xi}$ (s)	$\alpha_{s,0,Xi}$	ω_{Xi} (cm s^{-1})
O_3	soot	160	2.7	10	10^{-3}	3.60×10^4
	solid organic	1.6–16	2.7	0.1–1	10^{-3}	3.60×10^4
	liquid	0.16–1.6	0.5	0.01–0.1	10^{-3}	3.60×10^4
H_2O		10^{-3}	–	10^{-4}	4.0×10^{-4}	5.90×10^4
NO_2		50	–	0.05	0.064	3.69×10^4

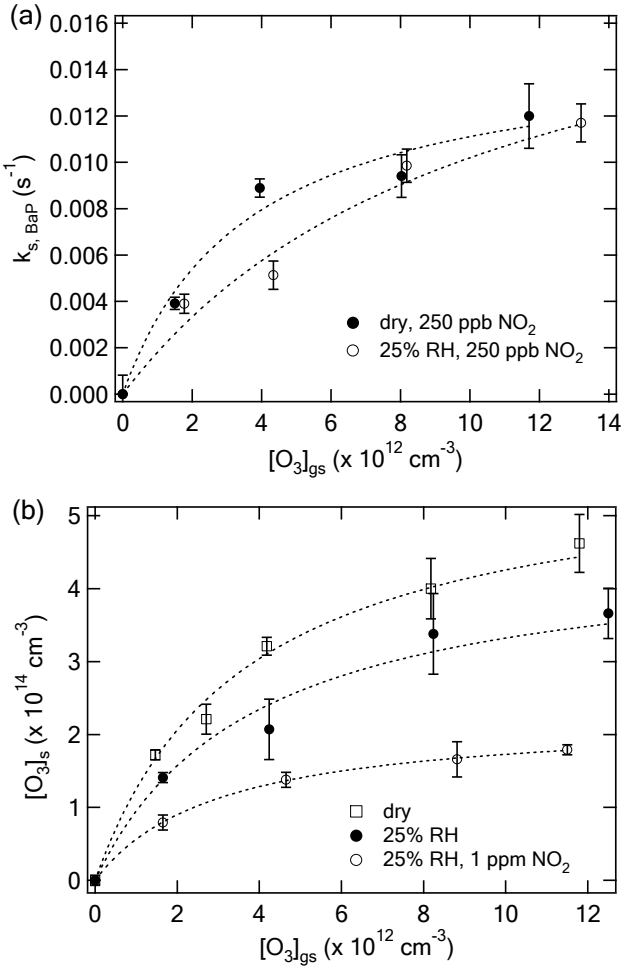

Fig. 5. Experimental data and fit lines for the BaP-O_3-NO_2-H_2O system (Schauer, 2004). **(a)** Pseudo-first-order BaP decay coefficients ($k_{s,BaP}$) as a function of gas phase ozone concentration ($[O_3]_{gs}$) under dry and wet (25% RH) conditions with 250 ppb NO_2. **(b)** The surface concentration of ozone ($[O_3]_s$) as a function of $[O_3]_{gs}$. The data were measured under dry, wet (25% RH), and wet (25% RH) and NO_2 (1 ppm) conditions. Fit curves assume a Langmuir-Hinshelwood-type mechanism.

Fig. 6b displays the model results for a solid organic surface at 25% RH. Under these conditions the dominant species on the surface is H_2O, and the O_3 surface concentration is much lower than on soot. Consequently, the PAH degradation proceeds slower and the second plateau of γ_{O3} is longer ($\sim10^4$ s) and lower ($\gamma_{O3} = \times10^{-7}$).

The differences of PAH degradation on soot and on the solid organic surface are mainly caused by the different desorption lifetimes of ozone as derived and discussed in Sect. 3 ($\sim$10 s vs. $\sim$0.1 s). We speculate that the longer apparent desorption lifetime on soot may reflect stronger electron donor-acceptor interactions between the graphene layers (aromatic rings) and the adsorbed ozone molecules or oxygen atoms, respectively.

4.2 PAH-O_3-H_2O-OH system

Here we simulate PAH degradation by O_3, H_2O, and OH radicals for which we assume an elementary surface reaction probability of $\gamma_{GSR,OH,PAH} = 0.32$ (Bertram et al., 2001). The two dotted lines in Fig. 6a and 6b correspond to different OH concentration levels: an estimated global average value of $[OH]_g = 10^6$ cm^{-3}) (Prinn et al., 1992) and an approximate upper limit value of $[OH]_g = 10^7$ cm^{-3}. The near-surface gas phase concentration $[OH]_{gs}$ was calculated from Eqs. (2) and (3) assuming a particle diameter of 200 nm ($C_{g,OH} = 0.87$).

Figure 6a indicates that OH does not significantly affect PAH degradation on soot, where ozone is strongly adsorbed and plays a dominant role. On the solid organic surface, however, where ozone is less efficiently adsorbed, OH strongly accelerates PAH degradation as shown in Fig. 6b. Consequently, the PAH decay proceeds faster and the length of the second plateau of γ_{O3} decreases with increasing OH concentration.

4.2.1 PAH chemical half-life on the surface and atmospheric implications

Here we simulate the chemical half-life of PAH ($t_{1/2}$) on soot, organic and liquid surfaces, when exposed to ambient concentrations of O_3 and OH at 25% RH.

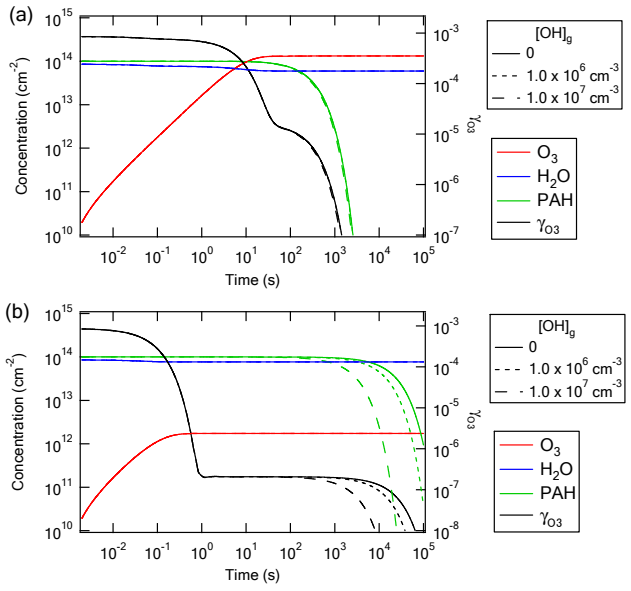

Fig. 6. Temporal evolution of the surface concentration of the volatile species (O_3 and H_2O), of PAH in the quasi-static surface layer, and of the ozone uptake coefficient (γ_{O3}) at 100 ppb O_3 and 25% RH assuming OH concentration of 0 (solid line), 1.0×10^6 cm^{-3} (dotted line) and 1.0×10^6 cm^{-3} (dashed line). PAHs are either **(a)** on soot or **(b)** on a solid organic surface.

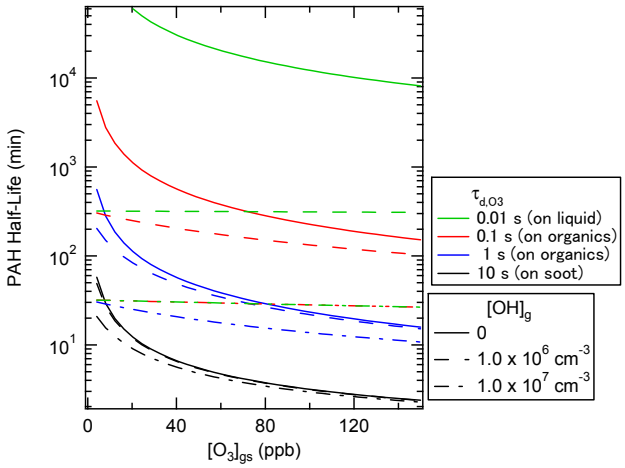

Fig. 7. Chemical half-life of PAHs on different substrates (soot, solid organic, liquid) as a function of gas phase ozone concentration at 25% RH assuming OH concentrations of 0 (solid lines), 1.0×10^6 cm^{-3} (dashed lines), and 1.0×10^7 cm^{-3} (dotted lines). The desorption lifetime of O_3 ($\tau_{d,O3}$) was set to 10 s (soot), 1 or 0.1 s (solid organic), and 0.01 s (liquid), respectively.

Figure 7 displays the results of calculations. The black line is the $t_{1/2}$ of PAH on a soot surface, which showed $t_{1/2}$ of ~10 min at typical atmospheric O_3 concentration of 30 ppb. We calculated $t_{1/2}$ under dry conditions as well, which resulted in a $t_{1/2}$ value of ~5 min at 30 ppb O_3. Therefore, the competitive adsorption of O_3 and H_2O leads to a significant increase in $t_{1/2}$. However, the $t_{1/2}$ values showed only a slight change with increasing $[OH]_g$. This is because PAH degradation on soot is dominated by the surface layer reaction of PAH with O_3.

The $t_{1/2}$ values on a solid organic surface (red and blue line) are estimated to 2–15 h at 30 ppb O_3 when $[OH]_g$ is 0. The $t_{1/2}$ value on a liquid surface like octanol and water (green line) is estimated to a few days. As shown in Fig. 7, $\tau_{d,O3}$ is a critical factor in estimating the chemical half-life of PAH on the surface. OH plays a critical role in these cases. It accelerates the PAH degradation by one to two orders of magnitude depending on OH concentration.

In summary, the PAH chemical half-life on the surface ($t_{1/2}$) ranges from ~10 min on soot, to 1–5 h on solid organics and 6 h on liquid particles under typical ambient conditions (30 ppb O_3, 25% RH, 10^6 cm^{-3} OH). Therefore, the relative importance of PAH degradation by O_3 and OH depends on the substrate of PAH.

4.3 PAH-O_3-H_2O-NO_2-NO_3 system

Here we simulate PAH degradation on soot upon interactions with O_3, H_2O, NO_2, and NO_3. As shown in Table 4, NO_2 could accelerate PAH degradation. For example, the apparent $k_{SLR,PAH,O3}$ is increased from 2.7×10^{-17} cm^2 s^{-1} to 5.7×10^{-17} cm^2 s^{-1} under 500 ppb NO_2, leading to a reduction of $t_{1/2}$ from 188 s to 170 s at 100 ppb O_3 and 25% RH. Here we consider two possible explanations for the acceleration of PAH degradation by NO_2: (1) surface reaction of O_3 with NO_2 (Langmuir-Hinshelwood-type mechanism) and (2) gas-surface reaction between PAH and gas phase NO_3 radical (Eley-Rideal-type mechanism).

4.3.1 Surface reaction of O_3 with NO_2

Here we simulate degradation of PAH on soot upon interactions with O_3, NO_2 and H_2O considering a surface reaction of O_3 with NO_2 (SLR2) and the subsequent reaction of NO_3 with PAH (SLR3). We tested $k_{SLR,O3,NO2}$ and $k_{SLR,PAH,NO3}$ values in the range of 10^{-18}–10^{-11} cm^2 s^{-1}. The desorption lifetime of NO_3 ($\tau_{d,NO3}$) was assumed to be 10 and 0.01 s. The concentration of NO_2 at 25% RH is set to 500 ppb. The resulting PAH chemical half-lifes ($t_{1/2}$) are summarized in Table 6.

The $t_{1/2}$ value should be ~170 s considering the acceleration of PAH degradation as discussed above. Moreover, the fact that the PAH-O_3-H_2O-NO_2 system is well described by Langmuir-Hinshelwood-type mechanism (Fig. 5) indicates $L_{SLR,O3} \ll J_{des,O3}$, leading to $k_{s,O3}$ ($=k_{SLR,PAH,O3}[PAH]_{ss}+k_{SLR,O3,NO2}[NO_2]_s$) $\ll k_{d,O3}$.

Table 6. Chemical half-life of PAHs in the PAH-O_3-NO_2-H_2O system assuming different values for the O_3-NO_2 and PAH-NO_3 surface layer reaction rate coefficients ($k_{SLR,O3,NO2}$, $k_{SLR,PAH,NO3}$).

$\tau_{d,NO3}$=10 s	$t_{1/2}$ (s)	$k_{SLR,PAH,NO3}$($cm^2\ s^{-1}$)			
		10^{-17}	10^{-16}	10^{-14}	10^{-11}
$k_{SLR,O3,NO2}$ ($cm^2\ s^{-1}$)	10^{-18}	263	262	245	242
	10^{-17}	265	253	154	145
	10^{-16}	287	197	41	36

$\tau_{d,NO3}$=0.01 s	$t_{1/2}$ (s)	$k_{SLR,PAH,NO3}$ ($cm^2\ s^{-1}$)			
		10^{-17}	10^{-16}	10^{-14}	10^{-11}
$k_{SLR,O3,NO2}$ ($cm^2\ s^{-1}$)	10^{-18}	263	263	263	244
	10^{-17}	266	266	264	153
	10^{-16}	297	297	280	40

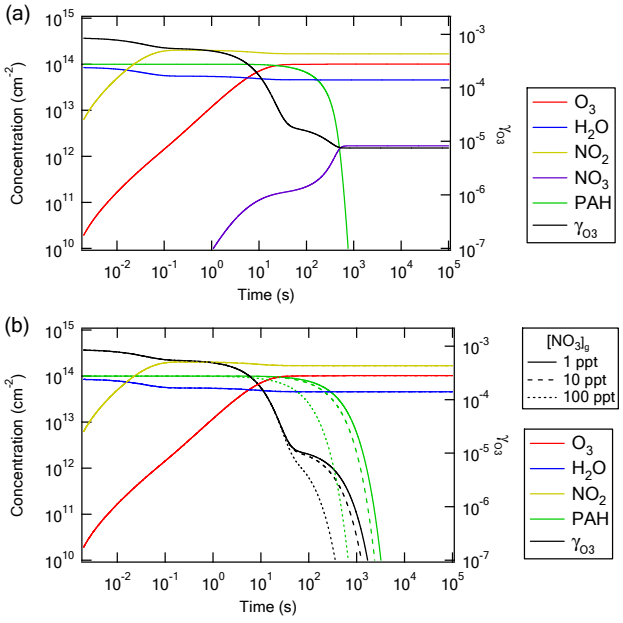

Fig. 8. Temporal evolution of the surface concentrations of PAHs and volatile species (O_3 and H_2O) on soot, and of the ozone uptake coefficient (γ_{O3}) at 100 ppb O_3, 500 ppb NO_2 and 25% RH. **(a)** PAH-O_3-H_2O-NO_2 system considering surface reaction of O_3 with NO_2. **(b)** PAH-O_3-H_2O-NO_2-NO_3 system assuming NO_3 concentrations of 1 ppt (solid line), 10 ppt (dashed line) and 100 ppt (dotted line), respectively.

Considering $k_{d,O3}$ is $\sim 10^{-1}$ and $[NO_2]_s$ and $[PAH]_{ss}$ is $\sim 10^{14}$, then $k_{SLR,O3,NO2}$ should be $<10^{-16}$.

Based on these criteria, $k_{SLR,O3,NO2}$ should be of the order of 10^{-17}–10^{-16} $cm^2\ s^{-1}$, whereas $k_{SLR,PAH,NO3}$ is of the order of 10^{-15}–10^{-12} $cm^2\ s^{-1}$. This is reasonable because $k_{SLR,O3,NO2}$ is on the same order of $k_{SLR,PAH,O3}$ and the NO_3 radical is expected to have high reactivity. The possible combination of rate coefficients are (1) $\tau_{d,NO3}$=10 s, $k_{SLR,O3,NO2}$=10^{-17}–10^{-16} $cm^2\ s^{-1}$, $k_{SLR,PAH,NO3}$=10^{-15}–10^{-14} $cm^2\ s^{-1}$ and (2) $\tau_{d,NO3}$=0.01 s, $k_{SLR,O3,NO2}$=10^{-17}–10^{-16} $cm^2\ s^{-1}$, $k_{SLR,PAH,NO3}$=10^{-13}–10^{-12} $cm^2\ s^{-1}$.

Figure 8a shows the exemplary simulation of this system using $\tau_{d,NO3}$=10 s, $k_{SLR,O3,NO2}$=10^{-17} $cm^2\ s^{-1}$, and $k_{SLR,PAH,NO3}$=10^{-14} $cm^2\ s^{-1}$. Temporal evolution is similar to Fig. 6a, but the PAH degradation was accelerated by formation of NO_3 radical, whose concentration reaches $\sim 10^{12}$ cm^{-2}. The uptake coefficient of O_3 (γ_{O3}) stayed 10^{-5} because of continuous surface reaction of O_3 with NO_2. γ_{NO2} was also calculated and it was 0.064 initially up to 10^{-2} s, which is equal to $\alpha_{s,0,NO2}$. As it is shown by $[NO_2]_s$ which reached steady-state condition quickly, γ_{NO2} decreased away after 0.1 s.

4.3.2 Gas-surface reaction with NO_3

Gas-surface reaction between gas phase NO_3 radicals and PAH is another possible explanation for the acceleration of PAH degradation. This system corresponds to a possible nighttime chemistry of PAH degradation, as NO_3 is the dominant oxidant at nighttime.

Here we simulate PAH degradation by O_3, H_2O, NO_2, and gas phase NO_3 radicals for which we assume an elementary surface reaction probability of $\gamma_{GSR,OH,PAH}$=0.13 (Rudich et al., 1996). Note that the surface reaction of O_3 with NO_2 is not considered in this simulation. The near-surface gas phase concentration $[NO_3]_{gs}$ was calculated from Eqs. (2) and (3) assuming a particle diameter of 200 nm ($C_{g,NO3}$=0.94). The NO_2 concentration at 25% RH is set to 500 ppb. Four NO_3 concentrations that cover the range of ambient concentrations (1, 10, 20, and 100 ppt) are assumed (Finlayson-Pitts and Pitts, 2000).

Figure 8b indicates that the presence of NO_3 does not impact the degradation of PAHs significantly when $[NO_3]_g$=1 ppt,, but rather ozone plays a dominant role in PAH degradation. The NO_3 radicals compensate the competitive adsorption of NO_2 when $[NO_3]_g$=10 ppt with $t_{1/2}$ of 186 s. The $t_{1/2}$ is 144 s when $[NO_3]_g$=20 ppt. And for $[NO_3]_g$=100 ppt, the $t_{1/2}$ is calculated to 38 s, indicating PAH degradation is dominated by the NO_3 radical at this condition.

4.3.3 PAH chemical half-life on the surface and atmospheric implications

Here we simulate the chemical half-life of PAH ($t_{1/2}$) on soot, organic and liquid surfaces, when exposed to O_3, H_2O, NO_2, and NO_3 at typical ambient concentration level at night time (<150 ppb O_3, 60% RH, 100 ppb NO_2, 1–10 ppt NO_3). Note that at higher RH water vapor may undergo multilayer adsorption and its effect may thus not be well described

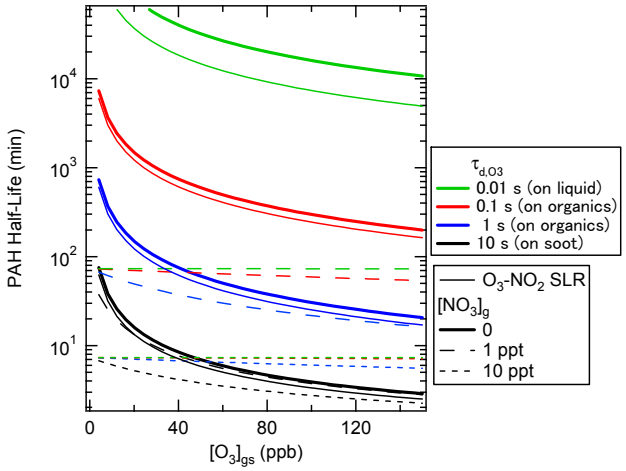

Fig. 9. Chemical half-life of PAHs on different substrates (soot, solid organic, liquid) as a function of gas phase ozone concentration at 100 ppb NO_2 and 60% RH. The desorption lifetime of O_3 ($\tau_{d,O3}$) is set to 10 s (soot), 1 or 0.1 s (solid organic), and 0.01 s (liquid), respectively. The assumed NO_3 gas phase concentrations are 0 (thick solid lines), 1 ppt (dashed lines), and 10 ppt (dotted lines), respectively. Thin solid lines indicate that O_3-NO_2 surface layer reactions are taken into account assuming $[NO_3]_g$=0.

by a Langmuir adsorption isotherm (Thomas et al., 1999; Mikhailov et al., 2009). Figure 9 displays the results of calculations. Neither the surface reaction of O_3 with NO_2 nor gas-surface reaction of NO_3 was considered for the thick solid line. NO_3 accelerates the PAH degradation by one to three orders of magnitude depending on NO_3 concentration (dotted and dashed line). The surface reaction of O_3 and NO_2 decreases the $t_{1/2}$ by ca. 40% on every surface (solid line).

In summary, under typical ambient conditions at night time (i.e. 30 ppb O_3, 100 ppb NO_2, 60% RH, 1 ppt NO_3), $t_{1/2}$ ranges from ∼10 min on soot, to 30–60 min on solid organics and liquid particles.

5 Conclusions

We have developed and applied a kinetic double-layer surface model (K2-SURF) and chemical reaction mechanism to describe the degradation of polycyclic aromatic hydrocarbons (PAHs) on aerosol particles interacting with ozone, nitrogen dioxide, water vapor, hydroxyl and nitrate radicals. Basic physicochemical parameters have been derived from experimental data and used to simulate PAH degradation and ozone uptake by aerosol particles under a wide range of conditions. The main conclusions are:

(1) The heterogeneous reaction between particle-bound PAHs and ozone can be well described by Langmuir-Hinshelwood-type mechanism and rate equations with effective Langmuir adsorption constants and surface reaction rate coefficients depending on the substrate material. Note, however, that the exact reaction mechanisms, rate limiting steps and possible intermediates still remain to be resolved (e.g., surface diffusion and formation of O atoms or O_3^- ions at the surface).

(2) Competitive and reversible adsorption and chemical transformation of the surface (aging) lead to a strong non-linear dependence of the ozone uptake coefficients on time and gas phase composition with different characteristic features under dilute atmospheric and concentrated laboratory conditions. Under typical ambient conditions the ozone uptake coefficients of PAH-coated aerosol particles are likely in the range of 10^{-6}–10^{-5}.

(3) Nitrogen dioxide undergoes competitive co-adsorption with ozone. At ambient temperatures NO_2 alone does not efficiently degrade PAHs, but it can accelerate PAH degradation by ozone. The accelerating effect of NO_2 can be explained by the formation of highly reactive NO_3 radicals in the gas phase and on the surface.

(4) The chemical half-life of PAH is expected to range from a few minutes on the surface of soot, to multiple hours on solid organics and days on liquid particles. On soot, PAH degradation appears to be dominated by a surface layer reaction with adsorbed O_3 (Langmuir-Hinshelwood-type mechanism). On other substrates, it seems to be dominated by gas-surface reaction with OH and NO_3 radicals (Eley-Rideal-type mechanism).

Table A1. Frequently used symbols.

Symbol	Meaning
γ_{Xi}	uptake coefficient of X_i
$\tau_{d,Xi}$	desorption lifetime of X_i
ω_{Xi}	mean thermal velocity of X_i in the gas phase
$C_{g,Xi}$	gas phase diffusion correction factor of X_i
d_p	particle diameter
$k_{d,Xi}$	first-order desorption rate coefficient of X_i
$k_{SLRv,Xp,Xq}$, $k_{SLRv,Xp,Yq}$	second-order rate coefficients for surface layer reactions of X_p with X_q, X_p with Y_q, respectively
$K_{ads,Xi}$	adsorption equilibrium constant of X_i
$K'_{ads,Xi}$	effective adsorption equilibrium constant of X_i
$\alpha_{s,0,Xi}$	surface accommodation coefficient of X_i on an adsorbate-free surface
$t_{1/2}$	chemical half-life of PAHs on the surface
$[SS]_{ss}$	sorption site surface concentration
$[X_i]_g$	gas phase concentration of X_i
$[X_i]_{gs}$	near-surface gas phase concentration of X_i
$[X_i]_s$	surface concentration of X_i (sorption layer)
$[Y_j]_{ss}$	surface concentration of Y_j (quasi-static layer)

(5) To our knowledge, K2-SURF is the first atmospheric process model describing multiple types of parallel and sequential surface reactions between multiple gaseous and particle-bound chemical species. We propose that K2-SURF may be used to design, analyze, and interpret experiments for better understanding of heterogeneous reaction systems. For example, systematic sensitivity studies can help to determine the range of experimental conditions (reactant concentrations, reaction time, etc.) that are likely to provide most information and direct insight into possible reaction mechanisms and the underlying physicochemical parameters (e.g., Langmuir-Hinselwood-type vs. Eley-Rideal-type mechanisms, physisorption vs. chemisorption, adsorption/desorption vs. chemical reaction rate coefficients, etc.). Moreover, we suggest that K2-SURF may serve as a basis for the development of a general master mechanism of aerosol and cloud surface chemistry.

Acknowledgements. This work was funded by the Max Planck Society (MPG) and the European integrated project on cloud climate and air quality interactions (No 036833-2, EUCAARI). MS is supported by the Max Planck Graduate Center – Johannes Gutenberg University Mainz (MPGC-JOGU), and the Ministry of Education, Culture, Sports, Science and Technology – Japan (MEXT). We thank N. Kwamena, J. P. D. Abbatt, T. Kahan and J. Donaldson for providing experimental data; J. Crowley, M. Ammann, N. Donahue, M. Rossi, T. Mentel, Y. Dubowski, Y. Iinuma, C. Pfrang, N. Kwamena and two anonymous referees for stimulating comments and discussions; and H. Su for support in model development.

The service charges for this open access publication have been covered by the Max Planck Society.

Edited by: V.-M. Kerminen

References

Ackerman, A. S., Toon, O. B., Stevens, D. E., Heymsfield, A. J., Ramanathan, V., and Welton, E. J.: Reduction of tropical cloudiness by soot, Science, 288, 1042–1047, 2000.

Alebic-Juretic, A., Cvitas, T. and Klasinc, L.: Heterogeneous polycyclic aromatic hydrocarbon degradation with ozone on silica-gel carrier, Environ. Sci. Technol., 24, 62–66, 1990.

Ammann, M. and Pöschl, U.: Kinetic model framework for aerosol and cloud surface chemistry and gas-particle interactions - Part 2: Exemplary practical applications and numerical simulations, Atmos. Chem. Phys., 7, 6025–6045, 2007, http://www.atmos-chem-phys.net/7/6025/2007/.

Ammann, M., Pöschl, U., and Rudich, Y.: Effects of reversible adsorption and Langmuir-Hinshelwood surface reactions on gas uptake by atmospheric particles, Phys. Chem. Chem. Phys., 5, 351–356, 2003.

Andreae, M. O. and Rosenfeld, D.: Aerosol-cloud-precipitation interactions. Part 1, The nature and sources of cloud-active aerosols, Earth-Sci. Rev., 89, 13–41, 2008.

Atkinson, R. and Arey, J.: Atmospheric chemistry of gas-phase polycyclic aromatic-hydrocarbons – Formation of atmospheric mutagens, Environ. Health Persp., 102, 117–126, 1994.

Bertram, A. K., Ivanov, A. V., Hunter, M., Molina, L. T., and Molina, M. J.: The reaction probability of OH on organic surfaces of tropospheric interest, J. Phys. Chem. A, 105, 9415–9421, 2001.

Donaldson, D. J., Mmereki, B. T., Chaudhuri, S. R., Handley, S., and Oh, M.: Uptake and reaction of atmospheric organic vapours on organic films, Faraday Discuss., 130, 227–239, 2005.

Dubowski, Y., Vieceli, J., Tobias, D. J., Gomez, A., Lin, A., Nizkorodov, S. A., McIntire, T. M., and Finlayson-Pitts, B. J.: Interaction of gas-phase ozone at 296 K with unsaturated self-assembled monolayers: A new look at an old system, J. Phys. Chem. A, 108, 10473–10485, 2004.

Finlayson-Pitts, B. J. and Pitts, J. N.: Chemistry of the upper and lower atmosphere, Academic Press, 2000.

Fuzzi, S., Andreae, M. O., Huebert, B. J., Kulmala, M., Bond, T. C., Boy, M., Doherty, S. J., Guenther, A., Kanakidou, M., Kawamura, K., Kerminen, V.-M., Lohmann, U., Russell, L. M., and Pöschl, U.: Critical assessment of the current state of scientific knowledge, terminology, and research needs concerning the role of organic aerosols in the atmosphere, climate, and global change, Atmos. Chem. Phys., 6, 2017–2038, 2006, http://www.atmos-chem-phys.net/6/2017/2006/.

Gross, S. and Bertram, A. K.: Reactive Uptake of NO_3, N_2O_5, NO_2, HNO_3, and O_3 on Three Types of Polycyclic Aromatic Hydrocarbon Surfaces, J. Phys. Chem. A, 112, 3104–3113, 2008.

Hallquist, M., Wenger, J. C., Baltensperger, U., Rudich, Y., Simpson, D., Claeys, M., Dommen, J., Donahue, N. M., George, C., Goldstein, A. H., Hamilton, J. F., Herrmann, H., Hoffmann, T., Iinuma, Y., Jang, M., Jenkin, M. E., Jimenez, J. L., Kiendler-Scharr, A., Maenhaut, W., McFiggans, G., Mentel, Th. F., Monod, A., Prévôt, A. S. H., Seinfeld, J. H., Surratt, J. D., Szmigielski, R., and Wildt, J.: The formation, properties and impact of secondary organic aerosol: current and emerging issues, Atmos. Chem. Phys., 9, 5155–5235, 2009, http://www.atmos-chem-phys.net/9/5155/2009/.

Hansen, J., Sato, M., and Ruedy, R.: Radiative forcing and climate response, J. Geophys. Res.-Atmos., 102, 6831–6864, 1997.

Homann, K. H.: Fullerenes and soot formation – New pathways to large particles in flames, Angew. Chem. Int. Edit., 37, 2435–2451, 1998.

IUPAC: Compendium of Chemical Terminology, 2nd edition (the "Gold Book"), edited by: Wilkinson, A. D. M. A. A., Blackwell Scientific Publications, Oxford, 1997.

Ivanov, A. V., Trakhtenberg, S., Bertram, A. K., Gershenzon, Y. M., and Molina, M. J.: OH, HO_2, and ozone gaseous diffusion coefficients, J. Phys. Chem. A, 111, 1632–1637, 2007.

Jacobson, M. Z.: A physically-based treatment of elemental carbon optics: Implications for global direct forcing of aerosols, Geophys. Res. Lett., 27, 217–220, 2000.

Kahan, T. F., Kwamena, N. O. A., and Donaldson, D. J.: Heterogeneous ozonation kinetics of polycyclic aromatic hydrocarbons on organic films, Atmos. Environ., 40, 3448–3459, 2006.

Kulmala, M., Asmi, A., Lappalainen, H. K., Carslaw, K. S., Pöschl, U., Baltensperger, U., Hov, Ø., Brenquier, J.-L., Pandis, S. N., Facchini, M. C., Hansson, H.-C., Wiedensohler, A., and O'Dowd, C. D.: Introduction: European Integrated Project on

Aerosol Cloud Climate and Air Quality interactions (EUCAARI) - integrating aerosol research from nano to global scales, Atmos. Chem. Phys., 9, 2825–2841, 2009, http://www.atmos-chem-phys.net/9/2825/2009/.

Kuwata, M., Kondo, Y., Mochida, M., Takegawa, N., and Kawamura, K.: Dependence of CCN activity of less volatile particles on the amount of coating observed in Tokyo, J. Geophys. Res., 112, D11207, doi:10.1029/2006JD007758, 2007.

Kwamena, N. O. A., Earp, M. E., Young, C. J., and Abbatt, J. P. D.: Kinetic and product yield study of the heterogeneous gas-surface reaction of anthracene and ozone, J. Phys. Chem. A, 110, 3638–3646, 2006.

Kwamena, N. O. A., Staikova, M. G., Donaldson, D. J., George, I. J., and Abbatt, J. P. D.: Role of the aerosol substrate in the heterogeneous ozonation reactions of surface-bound PAHs, J. Phys. Chem. A, 111, 11050–11058, 2007.

Kwamena, N. O. A., Thornton, J. A., and Abbatt, J. P. D.: Kinetics of surface-bound benzo[a]pyrene and ozone on solid organic and salt aerosols, J. Phys. Chem. A, 108, 11626–11634, 2004.

Lammel, G., Sehili, A. M., Bond, T. C., Feichter, J., and Grassl, H.: Gas/particle partitioning and global distribution of polycyclic aromatic hydrocarbons – A modelling approach, Chemosphere, 76, 98–106, 2009.

Lee, J. Y. and Kim, Y. P.: Source apportionment of the particulate PAHs at Seoul, Korea: impact of long range transport to a megacity, Atmos. Chem. Phys., 7, 3587–3596, 2007, http://www.atmos-chem-phys.net/7/3587/2007/.

Liu, Y., Sklorz, M., Schnelle-Kreis, J., Orasche, J., Ferge, T., Kettrup, A., and Zimmermann, R.: Oxidant denuder sampling for analysis of polycyclic aromatic hydrocarbons and their oxygenated derivates in ambient aerosol: Evaluation of sampling artefact, Chemosphere, 62, 1889–1898, 2006.

Marchand, N., Besombes, J. L., Chevron, N., Masclet, P., Aymoz, G., and Jaffrezo, J. L.: Polycyclic aromatic hydrocarbons (PAHs) in the atmospheres of two French alpine valleys: sources and temporal patterns, Atmos. Chem. Phys., 4, 1167–1181, 2004, http://www.atmos-chem-phys.net/4/1167/2004/.

Masel, R. I.: Principles of adsorption and reaction on solid surfaces, John Wiley & Sons, 1996.

McCabe, J. and Abbatt, J. P. D.: Heterogeneous Loss of Gas-Phase Ozone on n-Hexane Soot Surfaces: Similar Kinetics to Loss on Other Chemically Unsaturated Solid Surfaces, J. Phys. Chem. C, 113, 2120–2127, 2009.

Messerer, A., Rothe, D., Niessner, R., and Pöschl, U.: Kinetic observations and model calculations on continuous regeneration of NFZ diesel carbon particle precipitation systems, Chem.-Ing.-Tech., 77, 881–886, 2005.

Mikhailov, E., Vlasenko, S., Martin, S. T., Koop, T., and Pöschl, U.: Amorphous and crystalline aerosol particles interacting with water vapor - Part 1: Microstructure, phase transitions, hygroscopic growth and kinetic limitations, Atmos. Chem. Phys. Discuss., 9, 7333–7412, 2009, http://www.atmos-chem-phys-discuss.net/9/7333/2009/.

Mikhailov, E. F., Vlasenko, S. S., Podgorny, I. A. and Ramanathan, V.: Optical properties of soot-water drop agglomerates: An experimental study, J. Geophys. Res.-Atmos., 111, 16, 2006.

Mmereki, B. T. and Donaldson, D. J.: Direct observation of the kinetics of an atmospherically important reaction at the air-aqueous interface, J. Phys. Chem. A, 107, 11038–11042, 2003.

Mmereki, B. T., Donaldson, D. J., Gilman, J. B., Eliason, T. L., and Vaida, V.: Kinetics and products of the reaction of gas-phase ozone with anthracene adsorbed at the air-aqueous interface, Atmos. Environ., 38, 6091–6103, 2004.

Nelander, B. and Nord, L.: Do ozone-olefin complexes really exist, J. Am. Chem. Soc., 101, 3769–3770, 1979.

Pfrang, C., Shiraiwa, M., and Pöschl, U.: Coupling aerosol surface and bulk chemistry with a kinetic double layer model (K2-SUB): oxidation of oleic acid by ozone, Atmos. Chem. Phys. Discuss., 9, 26969–27019, 2009, http://www.atmos-chem-phys-discuss.net/9/26969/2009/.

Pitts, J. N.: Formation and fate of gaseous and particulate mutagens and carcinogens in real and simulated atmospheres, Environ. Health Persp., 47, 115–140, 1983.

Pöschl, U.: Formation and decomposition of hazardous chemical components contained in atmospheric aerosol particles, J. Aerosol Med., 15, 203–212, 2002.

Pöschl, U.: Atmospheric aerosols: Composition, transformation, climate and health effects, Angew. Chem. Int. Edit., 44, 7520–7540, 2005.

Pöschl, U., Letzel, T., Schauer, C., and Niessner, R.: Interaction of ozone and water vapor with spark discharge soot aerosol particles coated with benzo[a]pyrene: O_3 and H_2O adsorption, benzo[a]pyrene degradation, and atmospheric implications, J. Phys. Chem. A, 105, 4029–4041, 2001.

Pöschl, U., Rudich, Y., and Ammann, M.: Kinetic model framework for aerosol and cloud surface chemistry and gas-particle interactions - Part 1: General equations, parameters, and terminology, Atmos. Chem. Phys., 7, 5989–6023, 2007, http://www.atmos-chem-phys.net/7/5989/2007/.

Prinn, R., Cunnold, D., Simmonds, P., Alyea, F., Boldi, R., Crawford, A., Fraser, P., Gutzler, D., Hartley, D., Rosen, R., and Rasmussen, R.: Global average concentration and trend for hydroxyl radicals deduced from ALE/GAGE trichloroethane (methyl chloroform) data for 1978–1990, J. Geophys. Res.-Atmos., 97, 2445–2461, 1992.

Rogaski, C. A., Golden, D. M., and Williams, L. R.: Reactive uptake and hydration experiments on amorphous carbon treated with NO_2, SO_2, O_3, HNO_3, and H_2SO_4, Geophys. Res. Lett., 24, 381–384, 1997.

Rudich, Y., Talukdar, R. K., Imamura, T., Fox, R. W., and Ravishankara, A. R.: Uptake of NO_3 on KI solutions: rate coefficient for the NO_3+I-reaction and gas-phase diffusion coefficients for NO3, Chem. Phys. Lett., 261, 467–473, 1996.

Sadezky, A., Muckenhuber, H., Grothe, H., Niessner, R., and Pöschl, U.: Raman microspectroscopy of soot and related carbonaceous materials: Spectral analysis and structural information, Carbon, 43, 1731–1742, 2005.

Schauer, C.: Analysis and reactivity of polycyclic aromatic hydrocarbon in aerosol, Technical University of Munich, 2004.

Schauer, C., Niessner, R., and Pöschl, U.: Polycyclic aromatic hydrocarbons in urban air particulate matter: Decadal and seasonal trends, chemical degradation, and sampling artifacts, Environ. Sci. Technol., 37, 2861–2868, 2003.

Schauer, C., Niessner, R., and Pöschl, U.: Analysis of nitrated polycyclic aromatic hydrocarbons by liquid chromatography with fluorescence and mass spectrometry detection: air particulate matter, soot, and reaction product studies, Anal. Bioanal. Chem., 378, 725–736, 2004.

Schwarz, J. P., Gao, R. S., Spackman, J. R., Watts, L. A., Thomson, D. S., Fahey, D. W., Ryerson, T. B., Peischl, J., Holloway, J. S., Trainer, M., Frost, G. J., Baynard, T., Lack, D. A., de Gouw, J. A., Warneke, C., and Del Negro, L. A.: Measurement of the mixing state, mass, and optical size of individual black carbon particles in urban and biomass burning emissions, Geophys. Res. Lett., 35, L13810, doi:10.1029/2008gl033968, 2008.

Segal-Rosenheimer, M. and Dubowski, Y.: Photolysis of thin films of cypermethrin using in situ FTIR monitoring: Products, rates and quantum yields, J. Photochem Photobio A, 200, 262–269, 2008.

Seinfeld, J. H. and Pandis, S. N.: Atmospheric chemistry and physics – From air pollution to climate change, John Wiley & Sons, Inc., 1998.

Shiraiwa, M., Kondo, Y., Moteki, N., Takegawa, N., Miyazaki, Y., and Blake, D. R.: Evolution of mixing state of black carbon in polluted air from Tokyo, Geophys. Res. Lett., 34, L16803, doi:10.1029/2007gl029819, 2007.

Shiraiwa, M., Pfrang, C., and Pöschl, U.: Kinetic multi-layer model of aerosol surface and bulk chemistry (KM-SUB): the influence of interfacial transport and bulk diffusion on the oxidation of oleic acid by ozone, submitted, 2009.

Springmann, M., Knopf, D. A., and Riemer, N.: Detailed heterogeneous chemistry in an urban plume box model: reversible co-adsorption of O_3, NO_2, and H_2O on soot coated with benzo[a]pyrene, Atmos. Chem. Phys., 9, 7461–7479, 2009, http://www.atmos-chem-phys.net/9/7461/2009/.

Stephens, S., Rossi, M. J., and Golden, D. M.: The heterogeneous reaction of ozone on carbonaceous surfaces, Int. J. Chem. Kinet., 18, 1133–1149, 1986.

Sullivan, R. C., Thornberry, T., and Abbatt, J. P. D.: Ozone decomposition kinetics on alumina: effects of ozone partial pressure, relative humidity and repeated oxidation cycles, Atmos. Chem. Phys., 4, 1301–1310, 2004, http://www.atmos-chem-phys.net/4/1301/2004/.

Tabor, K., Gutzwiller, L., and Rossi, M. J.: Heterogeneous chemical-kinetics of NO_2 on amorphous-carbon at ambient temperature, J. Phys. Chem., 98, 6172–6186, 1994.

Thomas, E., Rudich, Y., Trakhtenberg, S., and Ussyshkin, R.: Water adsorption by hydrophobic organic surfaces: Experimental evidence and implications to the atmospheric properties of organic aerosols, J. Geophys. Res.-Atmos., 104, 16053–16059, 1999.

Vieceli, J., Roeselova, M., Potter, N., Dang, L. X., Garrett, B. C., and Tobias, D. J.: Molecular dynamics simulations of atmospheric oxidants at the air-water interface: Solvation and accommodation of OH and O_3, J. Phys. Chem. B, 109, 15876–15892, 2005.

Wu, C. H., Salmeen, I., and Niki, H.: Fluorescence spectroscopic study of reactions between gaseous ozone and surface-adsorbed polycyclic aromatic-hydrocarbons, Environ. Sci. Technol., 18, 603–607, 1984.

B2) Pfrang et al., Atmos. Chem. Phys., 2010

Coupling aerosol surface and bulk chemistry with a kinetic double layer model (K2–SUB): an exemplary study of the oxidation of oleic acid by ozone

Christian Pfrang[1,2], Manabu Shiraiwa[2], and Ulrich Pöschl[2]

1. University of Reading, Department of Chemistry, P. O. BOX 224, Whiteknights, Reading RG6 6AD, UK
2. Max Planck Institute for Chemistry, Department of Biogeochemistry
J.J. Becherweg 27/29, D55128, Mainz, Germany

Atmospheric Chemistry and Physics 10: 4357-4557, 2010.

Authors contributions.

CP and UP designed research. CP analyzed data and performed kinetic modeling. MS contributed to kinetic modeling. CP, MS, and UP discussed the results. CP wrote the paper.

Atmos. Chem. Phys., 10, 4537–4557, 2010
www.atmos-chem-phys.net/10/4537/2010/
doi:10.5194/acp-10-4537-2010

Atmospheric Chemistry and Physics

Coupling aerosol surface and bulk chemistry with a kinetic double layer model (K2-SUB): oxidation of oleic acid by ozone

C. Pfrang[1,2], **M. Shiraiwa**[2], **and U. Pöschl**[2]

[1]University of Reading, Department of Chemistry, P. O. BOX 224, Whiteknights, Reading RG6 6AD, UK
[2]Max Planck Institute for Chemistry, Biogeochemistry Department, 55128 Mainz, Germany

Received: 28 October 2009 – Published in Atmos. Chem. Phys. Discuss.: 15 December 2009
Revised: 12 April 2010 – Accepted: 25 April 2010 – Published: 18 May 2010

Abstract. We present a kinetic double layer model coupling aerosol surface and bulk chemistry (K2-SUB) based on the PRA framework of gas-particle interactions (Pöschl-Rudich-Ammann, 2007). K2-SUB is applied to a popular model system of atmospheric heterogeneous chemistry: the interaction of ozone with oleic acid. We show that our modelling approach allows de-convoluting surface and bulk processes, which has been a controversial topic and remains an important challenge for the understanding and description of atmospheric aerosol transformation. In particular, we demonstrate how a detailed treatment of adsorption and reaction at the surface can be coupled to a description of bulk reaction and transport that is consistent with traditional resistor model formulations.

From literature data we have derived a consistent set of kinetic parameters that characterise mass transport and chemical reaction of ozone at the surface and in the bulk of oleic acid droplets. Due to the wide range of rate coefficients reported from different experimental studies, the exact proportions between surface and bulk reaction rates remain uncertain. Nevertheless, the model results suggest an important role of chemical reaction in the bulk and an approximate upper limit of $\sim 10^{-11}$ cm^2 s^{-1} for the surface reaction rate coefficient. Sensitivity studies show that the surface accommodation coefficient of the gas-phase reactant has a strong non-linear influence on both surface and bulk chemical reactions. We suggest that K2-SUB may be used to design, interpret and analyse future experiments for better discrimination between surface and bulk processes in the oleic acid-ozone system as well as in other heterogeneous reaction systems of atmospheric relevance.

Correspondence to: C. Pfrang
(c.pfrang@reading.ac.uk)

1 Introduction

Atmospheric aerosols are highly variable components of the Earth system that have a substantial impact on the hydrological cycle and climate (Rosenfeld, 2000; Charlson et al., 2001; Ramanathan et al., 2001; Breon et al., 2002; Penner et al., 2004, Andreae et al., 2004; Pöschl, 2005; Fuzzi et al., 2006; Bergstrom et al., 2007, Choularton et al., 2008; Andreae and Rosenfeld, 2008). Thus, full understanding of the properties and transformation of aerosol particles is of key importance for atmospheric science.

The oxidation of organic substances in the atmosphere is predominantly initiated by hydroxyl radicals (OH), nitrate radicals (NO_3) and ozone (O_3) (Wayne, 2000). While atmospheric lifetimes of volatile organic compounds are largely determined by the rate coefficients of the chemical reactions with OH, NO_3, and O_3 (e.g. King et al., 1999; Pfrang et al., 2006a, b, 2007 and 2008), mass transport parameters are important additional factors for organic aerosol components. Chemical reactions can occur at the surface and in the bulk of aerosol particles, and the rates and relative proportions of surface and bulk reactions are hardly known.

Experimental studies are often rationalised with traditional "resistor" modelling formulations (e.g. Worsnop et al., 2002; Smith et al., 2002; Hearn et al., 2005; Knopf et al., 2005; Grimm et al., 2006; Gonzalez-Labrada et al., 2007; King et al., 2008, 2009; Gross et al., 2009), but the applicability and

usefulness of this approach is limited with regard to multi-component systems and transient conditions.

To overcome these limitations, Pöschl et al. (2007) have developed a kinetic flux modelling approach (PRA framework) which enables a consistent and flexible treatment of aerosol chemistry and gas-particle interactions, including mass transport and chemical reactions in multiphase and multi-component systems. Springmann et al. (2009) demonstrated the applicability and usefulness of the PRA framework in an urban plume box model of the degradation of benzo[a]pyrene on soot by ozone and nitrogen dioxide. Shiraiwa et al. (2009) showed that the PRA approach can be efficiently applied to other polycyclic aromatic hydrocarbons (PAHs) and photo-oxidants (O_3, NO_2, OH and NO_3) with multiple types of parallel and sequential surface reactions using a kinetic double-layer model (K2-SURF).

De-convolution of competing surface and bulk processes is essential for a detailed understanding of aerosol transformation and ageing. A well studied model system for atmospherically relevant heterogeneous reactions is the interaction of oleic acid with atmospheric trace gases, in particular O_3 (e.g. Smith et al., 2002; Hearn et al., 2005; Grimm et al., 2006; Reynolds et al., 2006; Hung and Ariya, 2007; Gonzalez-Labrada et al., 2007; Hearn and Smith, 2007; Lee and Chan, 2007; Voss et al., 2007; Zahardis and Petrucci, 2007; King et al., 2008, 2009, 2010; Vesna et al., 2008a, b, 2009; Sage et al., 2009; Last et al., 2009).

Despite intense research efforts to fully understand the oleic acid–ozone system, there remain large uncertainties documented in the wide range of reported uptake coefficients varying by nearly four orders of magnitude (see Table 1). There is also controversy on the relative importance of bulk and surface processes (compare e.g. Hearn et al., 2005). Here we demonstrate how the competing surface and bulk processes can be de-convoluted with a kinetic double layer model coupling surface and bulk chemistry (K2-SUB).

2 Modelling approach

Our kinetic double-layer model coupling aerosol surface and bulk chemistry (K2-SUB) builds on the PRA framework (Pöschl et al., 2007) and uses the same terminology. For definitions and detailed explanation of symbols see Appendices A and B as well as Pöschl et al. (2007). The mass balance for a reactive liquid-phase species Y (e.g. oleic acid) can be expressed as

$$\frac{dN_y}{dt} = \frac{dN_{y,ss}}{dt} + \frac{dN_{y,b}}{dt} = \frac{d[Y]_{ss}}{dt} \times A_{ss} + \frac{d[Y]_b}{dt} \times V_b \quad (1)$$

with N_y being the total number of Y molecules; $N_{y,ss}$ and $N_{y,b}$ are the numbers of molecules in surface and bulk; $[Y]_{ss}$ and $[Y]_b$ the surface and bulk concentrations of Y; and A_{ss} and V_b being surface area and bulk volume of the particle.

Expressed in fluxes:

$$\frac{d[Y]_{ss}}{dt} = J_{b,ss,Y} - J_{ss,b,Y} - L_{ss,Y} \quad (2)$$

and

$$\frac{d[Y]_b}{dt} = \left(J_{ss,b,Y} - J_{b,ss,Y}\right) \times \frac{A_{ss}}{V_b} + L_{b,Y} \quad (3)$$

with the terms $L_{ss,Y}$ and $L_{b,Y}$ representing the chemical loss of Y in surface and bulk; $J_{b,ss,Y} = k_{b,ss,Y} \times [Y]_b$ and $J_{ss,b,Y} = k_{ss,b,Y} \times [Y]_{ss}$ are the fluxes of bulk-surface and surface-bulk mass transport, respectively.

The uptake coefficient of a gas-phase species X (e.g. O_3), γ_x, is defined by

$$\gamma_x = \frac{J_{ads,X} - J_{des,X}}{J_{coll,X}} \quad (4)$$

where $J_{ads,X}$ and $J_{des,X}$ are fluxes of adsorption and desorption of X and $J_{coll,X}$ corresponds to the gas kinetic flux of X molecules colliding with the surface

$$J_{coll,X} = \frac{[X]_{gs}\omega_X}{4}. \quad (5)$$

$[X]_{gs}$ is the gas phase concentration of X near the surface. For low values of γ_x and small particles (high Knudsen number, $Kn_x = \lambda_x r_p^{-1}$ with λ_x corresponding to the mean free path of X and r_p being the particle radius), $[X]_{gs}$ equals the average gas phase concentration $[X]_g$. In case of high uptake and large particles, the rate of gas uptake can be limited by gas-phase diffusion. Differences between $[X]_{gs}$ and $[X]_g$ can be described by a diffusion correction factor ($C_{g,X}$) as detailed by Pöschl et al. (2007). Figure 1 illustrates the structure of the kinetic double-layer model (K2-SUB) presented here.

Assuming steady-state we obtain the following mass balance equation for X at the surface:

$$J_{ads,X} - J_{des,X} - J_{s,b,X} + J_{b,s,X} - L_{s,X} = 0 \quad (6)$$

Assuming near-planar geometry of the surface, the flux of chemical loss of X in the sorption layer, $L_{s,X}$, can be equated to the chemical loss of Y in the surface, $L_{ss,Y}$:

$$L_{s,X} = k_{SLR,X,Y}[X]_s[Y]_{ss} = k_{s,X} \times [X]_s = L_{ss,Y}. \quad (7)$$

$k_{SLR,X,Y}$ is the second-order rate coefficient for the surface layer reactions between X and Y and $k_{s,X}$ is the corresponding pseudo-first order reaction rate coefficient. For very small particles where the surface curvature is strong on molecular scales, Eq. (7) could be corrected by the ratio of sorption layer and quasi-static surface areas. The concentration of X at the surface, $[X]_s$, is given by (terms are defined in Appendices A and B):

$$[X]_s = [SS]_{ss}\frac{K'_{ads,X}[X]_{gs}}{1 + K'_{ads,X}[X]_{gs}}. \quad (8)$$

Table 1. Experimental conditions and results of laboratory studies investigating the reactive uptake of ozone by oleic acid (compare Tables 1 and 2 in Zahardis and Petrucci, 2007; Gonzalez-Labrada et al., 2007 and King et al., 2009).

Method/ detection[a]	r_p/ µm	$[O_3]$/ cm^{-3}	Timescale/ s	$k_{SLR,X,Y}$/ $cm^2\ s^{-1}$	γ_X	Reference
AFT/ CIMS	0.3–0.5	2.5×10^{15}	4		$(7.5\pm1.2)\times10^{-4}$	Hearn and Smith (2004)
AFT/ AMS	0.1–0.3	2.5×10^{14}	7		$(1.6\pm0.2)\times10^{-3}$	Morris et al. (2002)
AFT/ Single particle MS	0.7–2.5	3.4×10^{15}	8		(0.99 ± 0.09) – $(7.3\pm1.5)\times10^{-3}$[b] $(5.8–9.8)\times10^{-3}$[c]	Smith et al. (2002)
AFT/ CIMS	0.3–0.6	$2.5–25\times10^{14}$	4		$(1.38\pm0.06)\times10^{-3}$ $(8.8\pm0.5)\times10^{-4}$[d]	Hearn et al. (2005)
EC/ TDPBMS	0.2	7×10^{13}	∼15		$(6.1\pm5)\times10^{-4}$	Ziemann (2005)
AFT/ AMS	1–15	2.5×10^{14}			$(1.25\pm0.2)\times10^{-3}$	Katrib et al. (2005)
CFT/ CIMS (O_3^-)	N/A	$2–4\times10^{12}$			$(0.64\pm0.05)\times10^{-4}$[e] $(7.9\pm0.3)\times10^{-4}$[f]	Knopf et al. (2005)
CFT/ CIMS (O_3^-)	500	1.0×10^{14}	0.1		$(5.2\pm0.1)\times10^{-5}$[e] $(8.3\pm0.02)\times10^{-4}$[f]	Moise and Rudich (2002)
CFT/ CIMS (O_3^-)	25	$10^{11}-10^{12}$	>0.1		$(8.0\pm1.0)\times10^{-4}$	Thornberry and Abbatt (2004)
Monolayer on pendant drop/ ST	N/A	$7–615\times10^{12}$	∼500	4.9×10^{-11}	$(2.6\pm0.1)\times10^{-6}$	Gonzalez-Labrada et al., 2007
Deuterated monolayer on Langmuir trough/ NR	N/A	$4.2–12\times10^{12}$	∼6000	$(7.3\pm0.9)\times10^{-11}$ and $(2.1\pm2.7)\times10^{-12}$[g]	$\sim4\times10^{-6}$	King et al., 2009

[a] AFT: aerosol flow tube; CIMS: chemical ionisation mass spectrometry; CFT: coated flow tube; AMS: aerosol mass spectrometry; EC: environmental chamber; TDPBMS: thermal desorption particle beam mass spectrometry; MS: mass spectrometry; ST: surface tension measurement; NR: neutron reflectometry.
[b] This corresponds to a radii range of monodisperse particles respectively from 2.45 µm to 680 nm with other values for different diameter particles given in the original work.
[c] These are the corrected values when accounting for the diffusion of oleic acid; see original work for more details.
[d] This is a corrected value accounting for oleic acid loss via secondary chemistry; see the original work for more details.
[e] This value is for solid-phase oleic acid; see the original work for more details.
[f] This value is liquid-phase oleic acid; see the original work for more details.
[g] Two branches have been reported with the the dominating branch (branching ratio 0.86) being the faster reaction which leads to formation of surface active products (see King et al., 2009 for more details).

Under steady-state conditions, the reacto-diffusive flux of X in the particle bulk ($J_{b,rd,X}$) can be related to the flux of bulk-surface and surface-bulk transfer of X in the sorption layer ($J_{b,s,X}$ and $J_{s,b,X}$) by the following equation

$$J_{b,rd,X} = J_{s,b,X} - J_{b,s,X}. \quad (9)$$

$J_{b,rd,X}$ can be re-written as

$$J_{b,rd,X} = C_{b,rd,X}\sqrt{k_{b,X}D_{b,X}}[X]_{bs}. \quad (10)$$

Provided that the interfacial mass transfer proceeds faster than the chemical loss of X, the near-surface bulk concentration $[X]_{bs}$ can be approximated by

$$[X]_{bs} = K_{sol,cp,X}RT[X]_{gs}. \quad (11)$$

The pseudo-first order loss rate coefficient $k_{b,X}$ is given by

$$k_{b,X} = k_{BR,X,Y}\times[Y]_b \quad (12)$$

with $k_{BR,X,Y}$ corresponding to the second-order bulk reaction rate coefficient (the other parameters from Eq. (10) are defined in Appendices A and B). $J_{b,rd,X}$ thus represents both diffusion and reactive loss of X in the particle bulk.

Assuming that the chemical loss of X equals the chemical loss of Y (stoichiometric coefficients of unity) we can write

$$L_{b,Y} = J_{b,rd,X}\times\frac{A_{ss}}{V_b}. \quad (13)$$

Note that Eq. (13) could be flexibly modified to account for stoichiometric coefficients deviating from unity. Recently, Sage et al. (2009) suggested that the stoichiometric ratio between oleic acid and ozone can vary and might be as high as 3.75 under certain conditions. Nevertheless, the uncertainties in reaction stoichiometry appear to be lower than the uncertainties of reaction rate coefficients as discussed

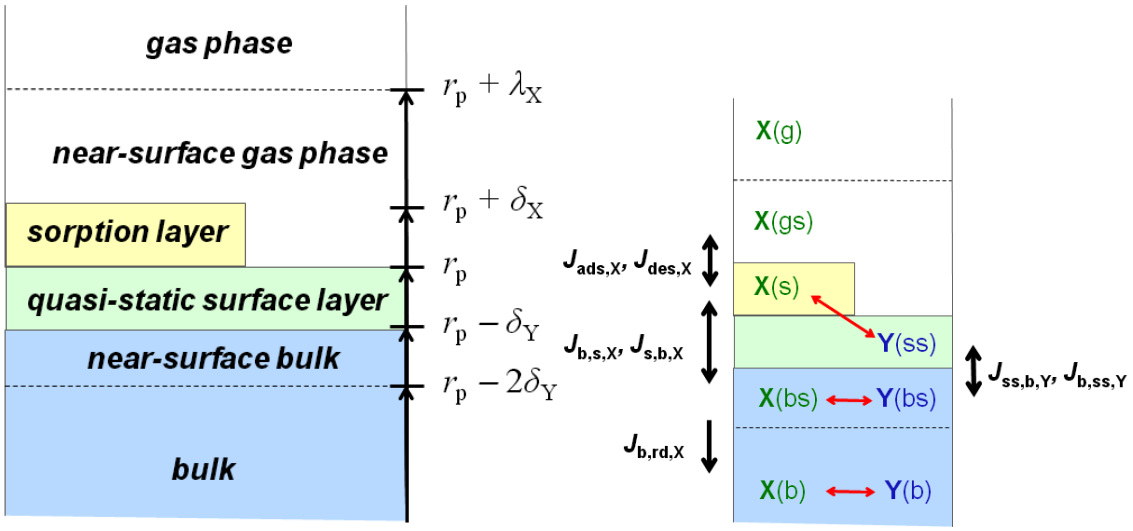

Fig. 1. Kinetic double-layer surface model (K2-SUB): **(a)** model compartments and distances from the particle centre; **(b)** model species, transport fluxes (black arrows) and chemical reactions (red arrows). r_p is the particle radius, δ_X and δ_Y are the effective molecular diameters and molecular layer thicknesses for volatile species X and non-volatile species Y, respectively; λ_x is the mean free path of X in the gas phase.

above (Sect. 1, Table 1). Thus, we do not explore this aspect in the present study.

By inserting Eqs. (7), (10) and (13) into Eqs. (1), (2) and (3) we obtain

$$\frac{dN_{y,ss}}{dt} = \frac{d[Y]_{ss}}{dt} \times A_{ss} = \{ k_{b,ss,Y} \times [Y]_b - k_{ss,b,Y} \times [Y]_{ss} - k_{SLR,X,Y}[X]_s[Y]_{ss} \} \times A_{ss} \quad (14)$$

and

$$\frac{dN_{y,b}}{dt} = \frac{d[Y]_b}{dt} \times V_b = \{ k_{ss,b,Y} \times [Y]_{ss} - k_{b,ss,Y} \times [Y]_b - C_{b,rd,X}\sqrt{k_{b,X}D_{b,X}}[X]_{bs} \} \times A_{ss}. \quad (15)$$

Thus

$$\frac{d[Y]_b}{dt} = \{ k_{ss,b,Y} \times [Y]_{ss} - k_{b,ss,Y} \times [Y]_b - C_{b,rd,X}\sqrt{k_{b,X}D_{b,X}}[X]_{bs} \} \times \frac{A_{ss}}{V_b}, \quad (16)$$

and for a spherical particle with a radius much larger than the effective molecular diameter of Y ($r_p \gg \delta_Y$)

$$\frac{d[Y]_b}{dt} = \{ k_{ss,b,Y} \times [Y]_{ss} - k_{b,ss,Y} \times [Y]_b - C_{b,rd,X}\sqrt{k_{b,X}D_{b,X}}[X]_{bs} \} \times \frac{3}{r_p} \quad (17)$$

Under steady-state conditions, using Eqs. (4), (6) and (9) the uptake coefficient can be described as

$$\gamma_X = \frac{J_{b,rd,X} + L_{s,X}}{J_{coll,X}}. \quad (18)$$

This expression can be re-formulated in the popular resistor model approach (compare Pöschl et al., 2007; Eqs. 105–124) as sum of resistance terms

$$\frac{1}{\gamma_X} = \frac{1}{\alpha_{s,X}} + \frac{1}{\alpha_{s,X}\frac{k_{s,X}}{k_{d,X}} + \frac{1}{\frac{1}{\alpha_{s,X}\frac{k_{s,b,X}}{k_{d,X}}} + \frac{1}{\alpha_{s,X}\frac{k_{s,b,X}}{k_{d,X}}\frac{C_{b,X}\sqrt{k_{b,X}D_{b,X}}}{k_{b,s,X}}}}} \quad (19)$$

or by inserting inverse resistance (conductance) terms

$$\frac{1}{\gamma_X} = \frac{1}{\alpha_{s,X}} + \frac{1}{\Gamma_{s,X} + \frac{1}{\frac{1}{\Gamma_{s,b,X}} + \frac{1}{\Gamma_{b,X}}}} \quad (20)$$

with conductance terms for surface reaction of X,

$$\Gamma_{s,X} = \frac{4k_{a,X}k_{s,X}}{k_{d,X}\omega_X}, \quad (21)$$

for surface-bulk transfer of X

$$\Gamma_{s,b,X} = \alpha_{s,X}\frac{k_{s,b,X}}{k_{d,X}}, \quad (22)$$

and for particle bulk diffusion and reaction of X

$$\Gamma_{b,X} = \frac{4}{\omega_x}K_{sol,cp,X}RTC_{b,rd,X}\sqrt{k_{b,X}D_{b,X}}. \quad (23)$$

Our modelling approach is designed to be compatible with resistor-model formulations (e.g. Worsnop et al., 2002; Smith et al., 2002; King et al., 2008, 2009), as derived in

detail in Appendix C. Please note that the advantage of the K2-SUB approach is that we are not limited to special cases, i.e. we can describe any combination of surface and bulk reactions and transport at any reactivity ratio. K2-SUB provides a general set of equations that describe all physicochemical processes involved. It enables free variation of all relevant parameters in particular mass transfer and reaction rate coefficients. It thus can describe limiting cases as well as any state in between depending on the investigated reaction systems, conditions and rate parameters. The added flexibility compared to previous approaches also facilitates description of Langmuir-Hinshelwood- and Eley-Rideal-type reaction mechanisms.

3 Derivation of kinetic parameters for the oxidation of oleic acid particles by ozone

In this study we have focused on the simulation of experimental data from Ziemann (2005), who reported time-resolved concentration data of oleic acid in fine droplets (r_p = 0.2 µm) interacting with ozone at a fixed gas-phase concentration level ($[X]_{gs}$ = 6.95×10^{13} cm^{-3} corresponding to 2.8 ppm). Unfortunately, many other studies have reported changes in concentration only as a function of ozone exposure (product of ozone concentration and time), which is less suitable for detailed process modelling. For consistent description and comparison of surface, bulk and total amounts of oleic acid in the investigated particles, we have multiplied the volume concentrations reported by Ziemann (2005) with the particle volume ($V_p = 4/3\pi r_p^3$) to obtain the absolute number of molecules.

For the initial concentration of pure oleic acid we took $[Y]_{b,0}$ = 1.21×10^{21} cm^{-3} corresponding to 3.15 mol L^{-1} as reported by Ziemann (2005). From the concentration of the pure substance we derived an approximate value for the effective molecular diameter of oleic acid, δ_Y:

$$[Y]_{b,0} \approx \frac{1}{\delta_Y^3}. \quad (24)$$

From $\delta_Y \approx 0.8$ nm we obtained an approximate value for the effective molecular cross-section $\sigma_y \approx \delta_Y^2 \approx 0.064$ nm^2. The initial surface concentration of oleic acid ($[Y]_{ss,0}$) was obtained from the relation

$$[Y]_{ss,0} = \delta_Y \times [Y]_{b,0}. \quad (25)$$

Values for $k_{b,ss,Y}$ and $k_{ss,b,Y}$ are derived by considering the average distance travelled by molecules diffusing in one direction (Atkins, 1998):

$$\sqrt{x^2} = \sqrt{\frac{4D_b t}{\pi}}, \quad (26)$$

with x corresponding to a distance the molecule needs to travel (this equals δ_Y, in our case 0.8 nm) and D_b being the diffusion coefficient (for oleic acid $D_{b,Y}$ is assumed to be 10^{-10} cm^2 s^{-1}; this corresponds to the lowest value assumed by Smith et al. (2003) when testing possible effects of slow diffusion in pure oleic acid droplets). For a droplet of 200 nm there is no oleic acid concentration gradient to be expected in the droplet since the small droplets can be assumed to be well mixed (Smith et al., 2002). For larger droplets a diffusion correction has been suggested (Smith et al., 2003), and this aspect is further explored in a follow-up study (Shiraiwa et al., 2010). An oleic acid molecule would take approximately 50 µs to travel the distance of δ_Y, so that we obtain a "transport velocity" ($k_{b,ss,Y}$) of 1.6×10^{-3} cm s^{-1}. This transport velocity can be related to $k_{ss,b,Y}$ by

$$k_{b,ss,Y} \times [Y]_{b,max} = k_{ss,b,Y} \times [Y]_{ss,max}. \quad (27)$$

The surface concentration is assumed to be limited by the number of surface sites with

$$[Y]_{ss,max} = \frac{1}{\delta_Y^2} = 1.56\times10^{14}\text{cm}^{-2} \quad (28)$$

and

$$[Y]_{b,max} = \frac{1}{\delta_Y^3} = 1.95\times10^{21}\text{cm}^{-3}. \quad (29)$$

We thus obtain a value for $k_{ss,b,Y}$ of 1.99×10^4s^{-1}.

The same line of thought presented for the oleic acid transport velocity ($k_{b,ss,Y}$) was followed to derive the transport velocity for ozone ($k_{b,s,X}$). Using a diffusion coefficient for ozone ($D_{b,X}$) in organic solvents of 10^{-5} cm^2 s^{-1} (Smith et al., 2002, 2003) and δ_X for ozone of 0.4 nm (derived from Eq. (28) with a value for surface sites for ozone of 5.7×10^{14} cm^{-2} reported by Pöschl et al., 2001; compare also a computational study by Vieceli et al., 2004), we obtain from Eq. (26) that $k_{b,s,X}$ is 318 cm s^{-1}.

$k_{s,b,X}$ however can be expected to be substantially different from $k_{ss,b,Y}$. As opposed to $k_{b,s,X}$, $k_{b,ss,Y}$ and $k_{ss,b,Y}$, $k_{s,b,X}$ is not isotropic and the ozone molecules will experience forces significantly different from those experienced by the oleic acid molecules. We thus derived $k_{s,b,X}$ by fitting the value of $K_{sol,cp,X}$ to match the literature value of Henry's law coefficient ($H_{cp,X}$ = 4.8×10^{-4} mol cm^{-3} atm^{-1}; e.g. Smith et al., 2002; King et al., 2009). The two other parameters affecting $K_{sol,cp,X}$ in our treatment have been varied within the ranges $k_{d,X}$ = 1–10^3 s^{-1} and $\alpha_{s,0,X}$ = 4×10^{-4}–1 (compare experimental values summarised in Shiraiwa et al., 2009: $k_{d,X}$ = 0.1–10^2 s^{-1} and $\alpha_{s,0,X} \approx 10^{-3}$ for O_3). The experimental data (Ziemann, 2005) can be matched for $k_{d,X}$ = 10^2 s^{-1} and $\alpha_{s,0,X}$ = 4.2×10^{-4}, i.e. for the minimum value for $k_{s,b,X}$ of 9.8×10^4 s^{-1} (base case 1, BC1). Please note that $\alpha_{s,0,X}$ is a critical parameter with a highly nonlinear impact on chemical losses in both surface and bulk (as shown in the sensitivity study in Sect. 4). For reasonable reaction rate coefficients and $k_{d,X}$ values similar to those used in Shiraiwa et al. (2009), experimental data ($H_{cp,X}$ and the temporal evolution of the oleic acid concentration measured

by Ziemann, 2005) can be matched for $\alpha_{s,0,X} \approx 4\times10^{-4}$–$10^{-3}$. However, it should be noted that the experimental data can also be reproduced with other combinations of $\alpha_{s,0,X}$ and $k_{d,X}$, that are closer to predictions from molecular dynamic simulations for related systems (e.g. $\alpha_{s,0,X} \approx 10^{-2}$ and $k_{d,X} \approx 10^9$ s; compare Vieceli et al. (2005) for a computational study of ozone at the air–water interface). These aspects will be further investigated in follow-up studies. For BC1 we chose the lower value for $\alpha_{s,0,X}$ to be able to match the reported bulk reaction rate coefficient, while the higher value for $\alpha_{s,0,X}$ was employed in base case 2 (BC2) with a reduced bulk reactivity (for BC2 we used $\alpha_{s,0,X} = 8.5\times10^{-4}$, $k_{d,X} = 10^3\ s^{-1}$ and $k_{s,b} = 4.85\times10^5\ s^{-1}$).

In analogy to Eq. (27) we can estimate $[X]_{s,max}$

$$k_{b,s,X} \times [X]_{b,max} = k_{s,b,X} \times [X]_{s,max}. \quad (30)$$

The surface reactivity has been estimated considering experimental values from King et al. (2009) and Gonzalez-Labrada et al. (2007) for monolayers of oleic acid on an aqueous sub phase: two branches have been found by King et al. (2009) with second-order rate coefficients of $k_1 = 7.3\times10^{-11}\ cm^2\ s^{-1}$ and $k_2 = 2.1\times10^{-12}\ cm^2\ s^{-1}$ and branching ratios (for deuterated oleic acid) of k_1/k_2 = 0.86/0.14. Gonzalez-Labrada et al. (2007) reported a rate coefficient of $4.9\times10^{-11}\ cm^2\ s^{-1}$. Rosen et al. (2008) reported first-order rate coefficients for reactions of O_3 with oleic acid on silica and polystyrene latex core particles of 0.64–2.2 s^{-1} suggesting a much smaller surface rate coefficient of $\sim$1–5$\times10^{-15}\ cm^2\ s^{-1}$ (when assuming saturation of the surface sorption sites). We used $k_{SLR,X,Y} = 6\times10^{-12}\ cm^2\ s^{-1}$ for the surface reaction on a droplet of pure oleic acid which is approximately one order of magnitude below the experimental values reported for oleic acid monolayers on aqueous sub phases. A surface reaction of a pure oleic acid droplet slower than that of a monolayer of oleic acid on an aqueous sub phase can be rationalised since an aqueous sub phase will lead to a reasonably well aligned hydrophobic (but bent) tail of oleic acid containing the reactive site (double bond) sticking out of the liquid phase which is likely to facilitate attack by ozone. In pure oleic acid we would expect a random orientation of oleic acid molecules on the surface and thus a somewhat reduced reactivity. The chosen value for $k_{SLR,X,Y}$ is substantially above the estimated rate coefficient derived from work by Rosen et al. (2008) since SEM images in Rosen et al.'s paper indicate that oleic acid was present in small islands on the particle surface rather than in a layer, so that the number of surface sorption sites is likely to be substantially reduced leading to a higher (but undetermined) rate coefficient.

The bulk reaction rate coefficient for reaction of ozone with oleic acid has been measured by Razumovskii et al. (1972) and confirmed using a "Double Bond Analyser" by Titov et al. (2005) for oleic acid dissolved in CCl_4 to be $k_{BR,X,Y} = 1.7\times10^{-15}\ cm^3\ s^{-1}$ (corresponding to the reported value of $1\times10^6\ L\ mol^{-1}\ s^{-1}$). This rate coefficient has been used in many previous studies (e.g. Smith et al., 2002 or King et al., 2009).

In view of the large uncertainty and the lack of experimental data on surface reactivity for droplets of pure oleic acid we chose two base cases for our model validation: in base case 1 (BC1) we employ Titov et al.'s value for $k_{BR,X,Y}$ (together with $k_{d,X} = 100\ s^{-1}$, $\alpha_{s,0,X} = 4.2\times10^{-4}$ and $k_{s,b,X} = 9.8\times10^4\ s^{-1}$) for the droplet of pure oleic acid to fit the experimental data by Ziemann (2005) and $H_{cp,X}$; base case 2 (BC2) uses conditions where bulk and surface reactions are of similar importance assuming $\sim$30 times lower $k_{BR,X,Y}$ of $5\times10^{-17}\ cm^3\ s^{-1}$ (together with $k_{d,X} = 1000\ s^{-1}$, $\alpha_{s,0,X} = 8.5\times10^{-4}$ and $k_{s,b,X} = 4.85\times10^5\ s^{-1}$). Further input parameters are detailed in Appendix D.

4 Simulation results and discussion

K2-SUB was applied to illustrate the relative importance of surface and bulk losses of the liquid-phase species in different regimes. We simulated experimental data (Ziemann, 2005) in two base cases and then performed detailed sensitivity studies: base case 1 (BC1) assumes fast bulk reaction (using Titov et al.'s value for bulk reactivity) while base case 2 (BC2) illustrates the importance of surface processes in the oleic acid-ozone system at reduced bulk reactivity. Selected results are presented here, while the complete set of data is tabulated in Table 2 and presented in the electronic supplement (see http://www.atmos-chem-phys.net/10/4537/2010/acp-10-4537-2010-supplement.zip).

4.1 Base case 1 (BC1): fast bulk reaction

In base case 1 the experimental results are matched for $k_{SLR,X,Y} = 6\times10^{-12}\ cm^2\ s^{-1}$ and $k_{BR,X,Y} = 1.7\times10^{-15}\ cm^3\ s^{-1}$ as illustrated in Fig. 2a–c. Figure 2a shows the time evolution of the uptake coefficient and the total number of oleic acid molecules as a function of time. The experimental data (presented as black symbols; Ziemann, 2005) is matched by the simulated decay (red line) and the uptake coefficient (black line) shows an initial plateau before dropping off after ca. 30 s. Figure 2b illustrates the changes in concentrations of ozone and oleic acid at the surface (red lines) and in the droplet bulk (blue lines). Initially, there is no ozone in the droplet and ozone is taken up into the particle as oleic acid reacts away. Figure 2c shows the relative importance of bulk and surface processes for the turnover in the droplet. The dashed lines indicate the change in the numbers of oleic acid molecules at the surface (red line) and in the bulk (blue line) as a function of time. For the 0.2 µm droplet of pure oleic acid there are obviously many more molecules in the bulk than at the particle surface.

For direct comparison of the rates of conversion at the surface and in the bulk of the particle, we define absolute loss rates (solid lines in Fig. 2c) as the products of

Table 2. Physico-chemical parameters investigated in the model simulations (base cases and sensitivity studies; the complete set of data is presented in the electronic supplement, see http://www.atmos-chem-phys.net/10/4537/2010/acp-10-4537-2010-supplement.zip).

Model scenario	Run	r_p/ 10^{-5} m	$\alpha_{s,0,X}$/ 10^{-4}	$k_{d,X}$/ 10^2 s^{-1}	$D_{b,X}$/ 10^{-5}c m^2 s^{-1}	$D_{b,Y}$/ 10^{-10} cm^2 s^{-1}	$k_{s,b,X}$/ 10^4 s^{-1}	$k_{SLR,X,Y}$/ 10^{-12} cm^2 s^{-1}	$k_{BR,X,Y}$/ 10^{-16} cm^3 s^{-1}
Base case 1 (BC1)	1	2	4.2	1	1	1	9.8	6	17
Bulk reaction only	2	2	4.2	1	1	1	9.8	0	17
Surface reaction only	3	2	4.2	1	1	1	9.8	6	0
$k_{SLR,X,Y}$/ 10	4	2	4.2	1	1	1	9.8	0.6	17
$k_{SLR,X,Y}\times$ 10	5	2	4.2	1	1	1	9.8	60	17
$k_{BR,X,Y}\times$ 10	6	2	4.2	1	1	1	9.8	6	170
$k_{BR,X,Y}$/ 10	7	2	4.2	1	1	1	9.8	6	1.7
$H_{cp,X}$/ 10	8	2	4.2	1	1	1	9.8	6	17
$H_{cp,X}\times$ 8	9	2	4.2	1	1	1	9.8	6	17
$[X]_{gs}$/ 10	10	2	4.2	1	1	1	9.8	6	17
$[X]_{gs}\times$ 10	11	2	4.2	1	1	1	9.8	6	17
$D_{b,X}$/ 10	12	2	4.2	1	0.1	1	9.8	6	17
$D_{b,X}\times$ 10	13	2	4.2	1	10	1	9.8	6	17
$D_{b,Y}\times 10^3$	14	2	4.2	1	1	1000	9.8	6	17
$r_p\times$ 5	15	10	4.2	1	1	1	9.8	6	17
r_p/ 2	16	1	4.2	1	1	1	9.8	6	17
r_p/ 4	17	0.5	4.2	1	1	1	9.8	6	17
$k_{d,X}$/ 2; $\alpha_{s,0,X}$/ 2	18	2	2.1	0.5	1	1	9.8	6	17
$k_{d,X}\times$ 2; $\alpha_{s,0,X}\times$ 2	19	2	8.4	2	1	1	9.8	6	17
$k_{s,b,X}$/ 2; $\alpha_{s,0,X}\times$ 2	20	2	8.4	1	1	1	4.9	6	17
$k_{s,b,X}\times$ 2; $\alpha_{s,0,X}$/ 2	21	2	2.1	1	1	1	19.6	6	17
Surface reaction only to match experiment	22	2	4.2	1	1	1	9.8	10	0
Bulk reaction only to match experiment	23	2	4.2	1	1	1	9.8	0	18
Base case 2 (BC2)	24	2	8.5	10	1	1	48.5	6	0.5
Bulk reaction only	25	2	8.5	10	1	1	48.5	0	0.5
Surface reaction only	26	2	8.5	10	1	1	48.5	6	0
$k_{SLR,X,Y}$/ 10	27	2	8.5	10	1	1	48.5	0.6	0.5
$k_{SLR,X,Y}\times$ 10	28	2	8.5	10	1	1	48.5	60	0.5
$k_{BR,X,Y}\times$ 10	29	2	8.5	10	1	1	48.5	6	5
$k_{BR,X,Y}$/ 10	30	2	8.5	10	1	1	48.5	6	0.05
$H_{cp,X}$/ 10	31	2	8.5	10	1	1	48.5	6	0.5
$H_{cp,X}\times$ 8	32	2	8.5	10	1	1	48.5	6	0.5
$[X]_{gs}$/ 10	33	2	8.5	10	1	1	48.5	6	0.5
$[X]_{gs}\times$ 10	34	2	8.5	10	1	1	48.5	6	0.5
$D_{b,X}$/ 10	35	2	8.5	10	0.1	1	48.5	6	0.5
$D_{b,X}\times$ 10	36	2	8.5	10	10	1	48.5	6	0.5
$D_{b,Y}\times 10^3$	37	2	8.5	10	1	1000	48.5	6	0.5
$r_p\times$ 5	38	10	8.5	10	1	1	48.5	6	0.5
r_p/ 2	39	1	8.5	10	1	1	48.5	6	0.5
r_p/ 4	40	0.5	8.5	10	1	1	48.5	6	0.5
$k_{d,X}$/ 2; $\alpha_{s,0,X}$/ 2	41	2	4.25	5	1	1	48.5	6	0.5
$k_{d,X}\times$ 2; $\alpha_{s,0,X}\times$ 2	42	2	17	20	1	1	48.5	6	0.5
$k_{s,b,X}$/ 2; $\alpha_{s,0,X}\times$ 2	43	2	17	10	1	1	24.3	6	0.5
$k_{s,b,X}\times$ 2; $\alpha_{s,0,X}$/ 2	44	2	4.25	10	1	1	97	6	0.5
Surface reaction only to match experiment	45	2	8.5	10	1	1	48.5	10	0
Bulk reaction only to match experiment	46	2	8.5	10	1	1	48.5	0	1.2

concentration-based chemical loss rates with the surface area and bulk volume, respectively: $L^*_{ss,Y} = L_{ss,Y} \times A_{ss}$ and $L^*_{b,Y} = L_{b,Y} \times V_b$. Figure 2c shows the relative importance of surface and bulk loss: during the first 30 s initial period ca. twice as many molecules are lost in the bulk than at the surface, and the absolute bulk loss rate remains dominant throughout the model run.

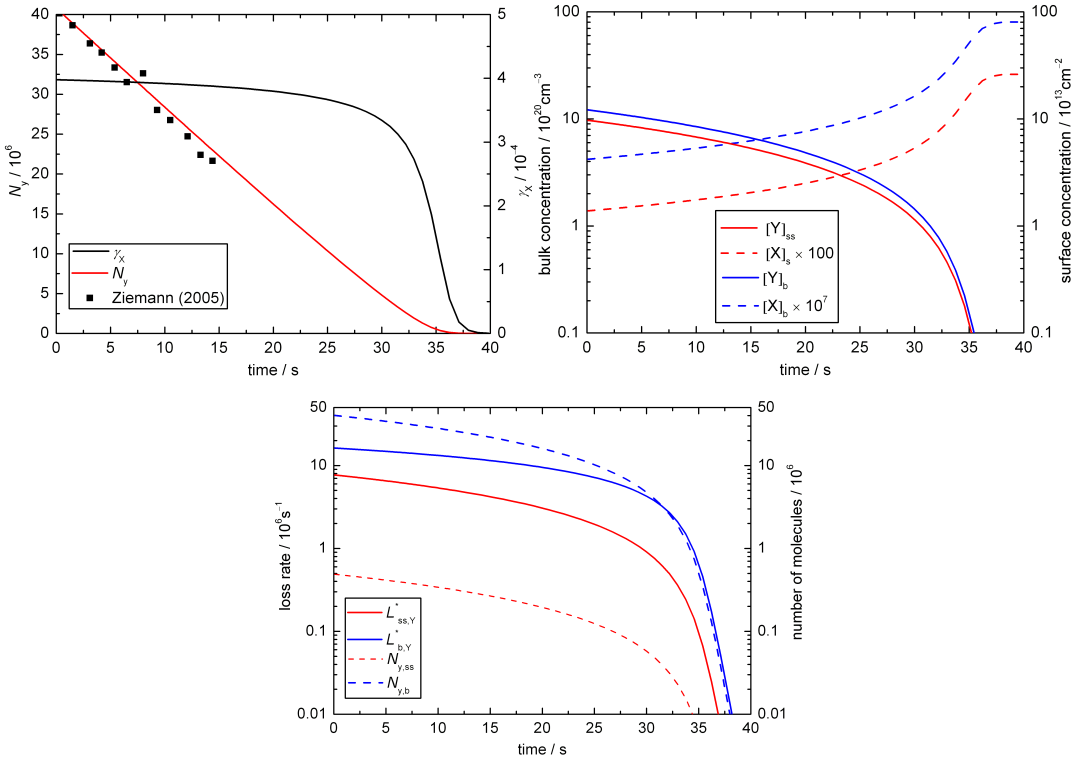

Fig. 2. Temporal evolution of aerosol particle composition and kinetic parameters in base case 1 (BC1; X = O_3, Y = oleic acid): **(a)** ozone uptake coefficient (γ_X) and total number of oleic acid molecules (N_Y; symbols indicate experimental data from Ziemann, 2005); **(b)** surface and bulk concentrations (square brackets); **(c)** numbers of oleic acid molecules at the surface and in the bulk of the particle ($N_{y,ss}$, $N_{y,b}$) and corresponding absolute loss rates ($L^*_{ss,Y} = L_{ss,Y} \times A_{ss}$, $L^*_{b,Y} = L_{b,Y} \times V_b$).

BC1 sensitivity study

In order to establish the dependencies of our results on the chosen set of kinetic input parameters for our base model BC1 (justified in Sect. 3 and detailed in Appendix D) we varied all parameters and the complete set of results of these sensitivity studies are presented in the electronic supplement (a summary of the model conditions is given in Table 2). Initially we varied $k_{SLR,X,Y}$, $k_{BR,X,Y}$, $K_{sol,cp,X}$, and $[X]_{gs}$.

Solubility

Assuming ~one order of magnitude difference in the Henry's law coefficients (see Fig. 3a and b) leads to substantial deviations from the experimental data with a higher coefficient showing dramatically faster decay of oleic acid ($K_{sol,cp,X}$ could only be increased eight fold, since higher values cause problems for the Matlab solver for long reaction times). This strong dependence on $K_{sol,cp,X}$ demonstrates that $K_{sol,cp,X}$ has a larger influence on the decay behaviour than variations in the reaction parameters.

Diffusivity

We also varied the diffusion coefficients: $D_{b,X}$ was altered by one order of magnitude (see Fig. 4a and b) and we increased $D_{b,Y}$ by three orders of magnitude (corresponding to the largest oleic acid diffusion coefficient chosen by Smith et al., 2003). A change of $D_{b,X}$ leads to a deviation from the experimental data (compare Fig. 4a and b with Fig. 2c), i.e. ozone diffusion has an impact on the turnover in the droplet. Fig. 4b illustrates how for slow diffusion of X the surface loss initially dominates the total loss of Y, while the bulk loss becomes dominant after ~20 s. The figure also suggests that even during the initial surface-dominated decay most molecules that are being lost originate from the bulk, i.e. bulk-to-surface transport of oleic acid is relatively fast and the chemical reaction at the surface is the rate-determining step. The system is not sensitive even to a three orders of magnitude change of $D_{b,Y}$, so that oleic acid diffusion is clearly not limiting the loss of reactants (see run 14 tabulated in Table 2 and illustrated in the electronic supplement, see http://www.atmos-chem-phys.net/10/4537/2010/acp-10-4537-2010-supplement.zip).

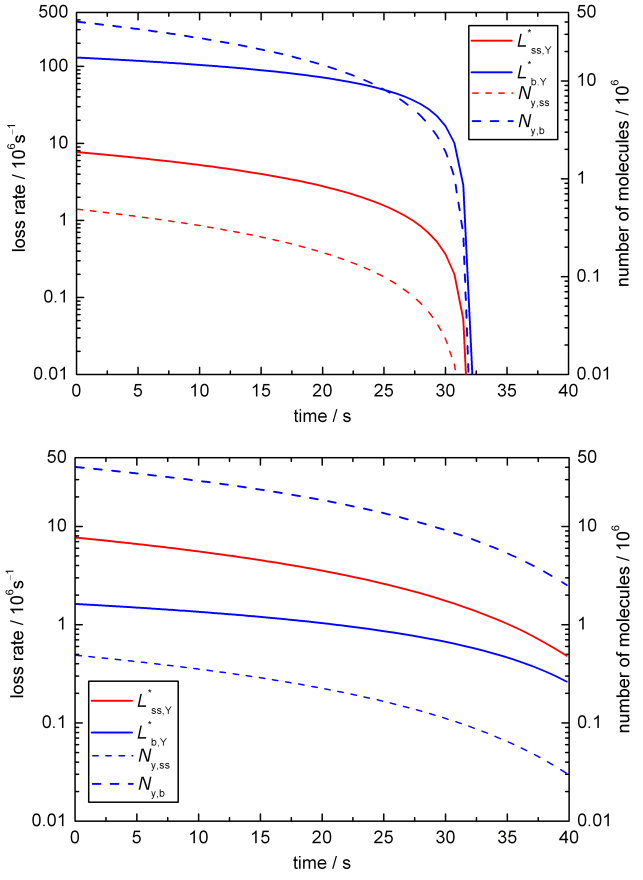

Fig. 3. Temporal evolution of aerosol particle composition and kinetic parameters in sensitivity studies for BC1 with $K_{\mathrm{sol,cp,X}}$ **(a)** eight fold above the literature value and **(b)** ten fold below. Plots are analogous to Fig. 2c.

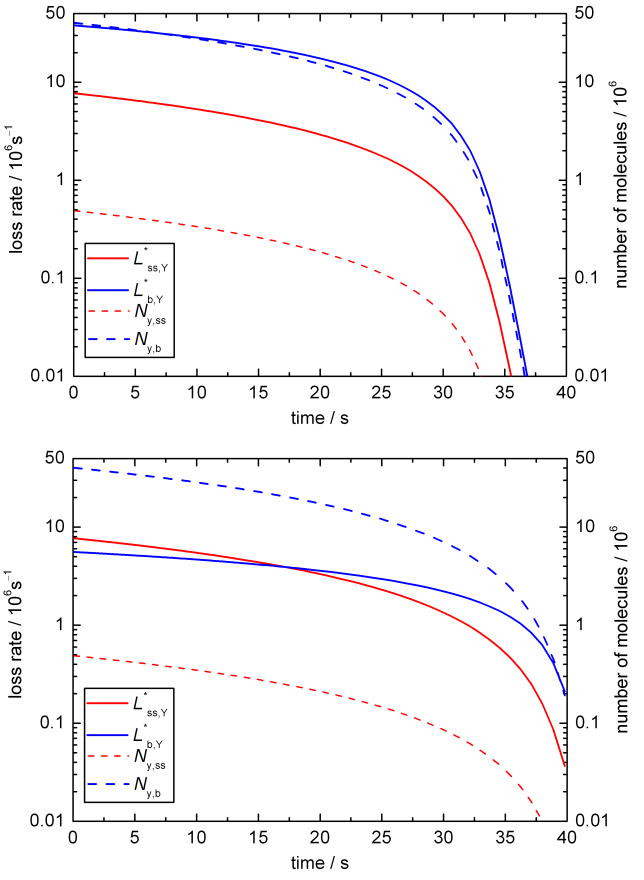

Fig. 4. Temporal evolution of aerosol particle composition and kinetic parameters in sensitivity studies for BC1 with $D_{\mathrm{b,X}}$ **(a)** ten fold above the literature value and **(b)** ten fold below. Plots are analogous to Fig. 2c.

Particle size

We tested the model for a range of droplet radii of 1000, 100 and 50 nm as shown in Fig. 5a–c. Unsurprisingly larger particles require longer reaction times. Due to the change in surface to volume ratio the relative contribution from the surface reaction becomes more important for smaller particles.

Surface accommodation

For BC1 the model is relatively insensitive to changes in the rate coefficients for chemical reaction. Under these conditions the reactive decay is limited by transport of ozone into the bulk. The sensitivity studies illustrate that the surface accommodation coefficient ($\alpha_{\mathrm{s,0,X}}$) is particularly important in this regime: massive deviations are seen when varying $\alpha_{\mathrm{s,0,X}}$ (see Fig. 6a and b).

Exclusive surface or bulk reaction

As illustrated in Fig. 7, we can also match the experimental results fairly well in sensitivity studies where we assumed that chemical reactions proceed either only at the surface ($k_{\mathrm{SLR,X,Y}} = 1\times10^{-11}$ cm^2 s^{-1}) or only in the bulk (with $k_{\mathrm{BR,X,Y}} = 1.8\times10^{-15}$ cm^3 s^{-1}). Up to 30 s the temporal evolution of the observable parameters N_{y} and γ_{x} in both scenarios is similar to each other and to BC1, but at the end of the model run (after 40 s) the surface reaction would still be going on whereas practically all oleic acid would have been consumed in the bulk reaction ($N_{\mathrm{y}} \approx 0$ and $\gamma_{\mathrm{x}} \approx 0$). Thus we suggest that future experimental studies should aim at covering longer reaction times to allow for better discrimination of surface and bulk processes.

4.2 Base case 2 (BC2): slow bulk reaction

Details of the model and input parameters for base case 2 (BC2) are justified in Sect. 3 and given in Appendix D. Selected results of the calculations are presented

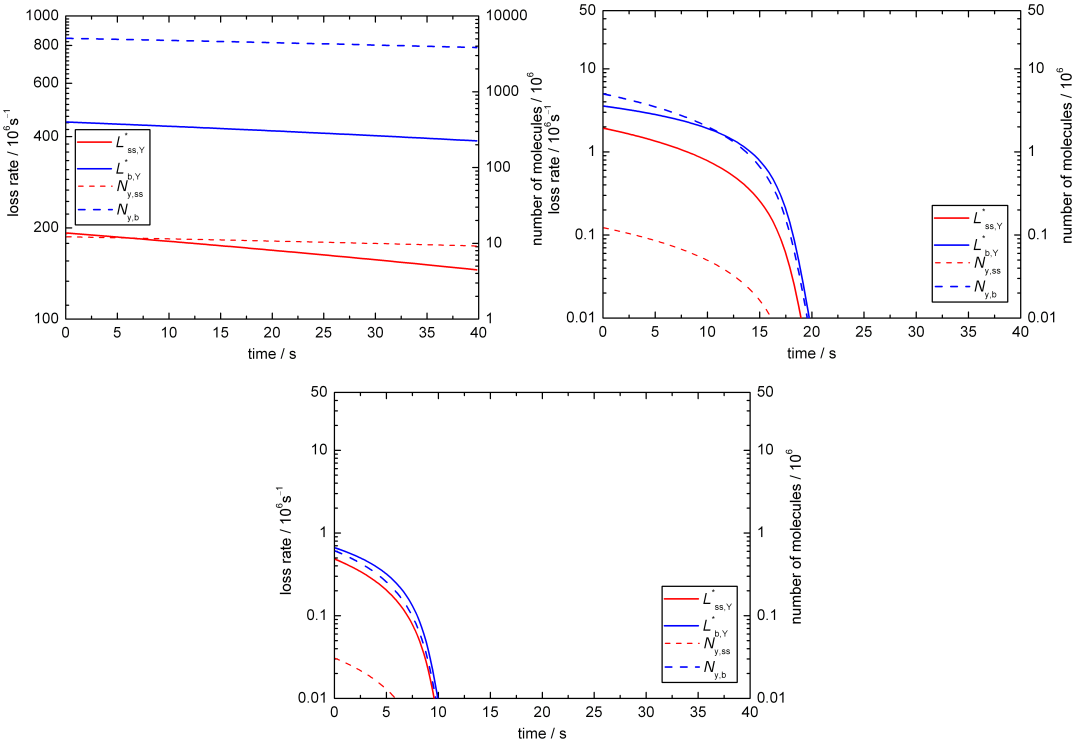

Fig. 5. Temporal evolution of aerosol particle composition and kinetic parameters in sensitivity studies for BC1 with a range of droplet radii: **(a)** 1000 nm, **(b)** 100 nm and **(c)** 50 nm. Plots are analogous to Fig. 2c.

here (the full data set is presented in the electronic supplement and tabulated in Table 2). Figure 8a–c shows that experimental results are matched for the chosen conditions for $k_{\mathrm{SLR,X,Y}} = 6\times10^{-12}\,\mathrm{cm^2\,s^{-1}}$ and $k_{\mathrm{BR,X,Y}} = 5\times10^{-17}\,\mathrm{cm^3\,s^{-1}}$. These conditions lead to very similar proportions of absolute bulk and surface loss rates (see solid lines in Fig. 8c).

A general feature of BC2 compared to BC1 is the fact that after ∼30 s the decay of oleic acid proceeds much slower (compare e.g. Figs. 2a and 8a). This behaviour can be explained by the different bulk reaction rate coefficients and the temporal evolution of the reacto-diffusive length ($l_{\mathrm{rd,X}} = \sqrt{D_{\mathrm{b,X}}/k_{\mathrm{b,X}}}$), which can be regarded as the distance from the surface up to which the chemical reaction proceeds effectively (Finlayson-Pitts and Pitts, 2000; Pöschl et al., 2007).

In BC1 the bulk reaction rate coefficient is high ($k_{\mathrm{BR,X,Y}} = 1.7\times10^{-15}\,\mathrm{cm^3\,s^{-1}}$) but the initial value of $l_{\mathrm{rd,X}}$ is as small as ∼20 nm, indicating that the reaction proceeds fast but only close to the surface. After ∼30 s, $l_{\mathrm{rd,X}}$ increases steeply and oleic acid is quickly depleted throughout the bulk of the particle.

In BC2 the bulk reaction rate coefficient is by a factor of ∼30 lower ($k_{\mathrm{BR,X,Y}} = 5\times10^{-17}\,\mathrm{cm^3\,s^{-1}}$) and the initial value of $l_{\mathrm{rd,X}}$ is as large as ∼130 nm, indicating that the reaction proceeds slow and throughout the bulk of the particle. Due to the low value of $k_{\mathrm{BR,X,Y}}$ the depletion of oleic acid continues to proceed slowly also after ∼30 s. Further details and effects of bulk reactivity, concentration gradients and diffusion are explored and discussed in a follow-up study (Shiraiwa et al., 2010).

BC2 sensitivity study

In order to establish the dependencies of our results on the chosen set of kinetic input parameters for BC2 we varied all parameters and detailed results of this sensitivity study are presented in the electronic supplement together with those for BC1.

First we varied $k_{\mathrm{SLR,X,Y}}$, $k_{\mathrm{BR,X,Y}}$, $K_{\mathrm{sol,cp,X}}$, and $[\mathrm{X}]_{\mathrm{gs}}$. The model is clearly sensitive to small changes in the reactivity both on the surface and in the bulk of the droplet (much more so than BC1: compare runs 4–7 with runs 27–30 tabulated in Table 2 and illustrated in the electronic supplement, see http://www.atmos-chem-phys.net/10/4537/2010/acp-10-4537-2010-supplement.zip), so that the model results deviate substantially for the low and high rate coefficients tested.

Solubility

The effect of changing the Henry's law coefficients by ∼one order of magnitude is even stronger than that for BC1

which can be attributed to the fact that the reaction proceeds throughout the bulk of the particle and is not limited by the reacto-diffusive length ($l_{rd,X}$) as discussed above (Sect. 4.2.).

Diffusivity

A reduction of the diffusion coefficient $D_{b,X}$ does show a small deviation from the experimental data, while an increase results in no significant deviation, i.e. ozone diffusion has a small impact on the turnover in the droplet. The system is not sensitive even to three orders of magnitude larger $D_{b,Y}$, so that oleic acid diffusion is again not limiting the loss of reactants.

Particle size

We also tested the model for a range of droplet radii of 1000, 100 and 50 nm showing a similar picture to BC1 (compare runs 38–40).

Surface accommodation

In base case 2 surface and bulk reaction rate coefficients become both much more important than in BC1. The turnover in the droplet is thus not limited by transport, but by chemical reaction. Nevertheless, the assumed value for $\alpha_{s,0,X}$ remains important.

Our study underlines the strong influence of $\alpha_{s,X}$ in all conditions which becomes apparent when inspecting Eq. (19): $\alpha_{s,X}$ appears in all terms and our modelling results demonstrate its highly non-linear impact on reactive losses in atmospheric particles. More experimental data are needed to better pin down $\alpha_{s,0,X}$. Our analysis also demonstrates that it is vital to use a model when designing an experimental study to be able to choose the most insightful experimental conditions: BC1 and BC2 show substantial deviations for reaction times above ∼30 s, but experimental data are only available for the first 15 s, so that both base cases fit the experiment. BC1 accommodates the fast bulk reaction rate coefficient reported by Titov et al. (2005), while BC2 is compatible with the experimental data only for substantially slower bulk reaction.

Exclusive surface or bulk reaction

The experimental results, i.e. the first 15 s of oleic acid decay, can also be matched when assuming exclusive surface or bulk reaction (see Fig. 9a and b) with $k_{SLR,X,Y} = 1\times10^{-11}$ cm^2 s^{-1} or $k_{BR,X,Y} = 1.2\times10^{-16}$ cm^3 s^{-1}, respectively. These results indicate for both base cases (BC1 and BC2) that the surface reaction of a pure oleic acid droplet is slower than that of a monolayer of oleic acid on an aqueous sub phase (compare Gonzalez-Labrada et al., 2007 and King et al., 2009) which can be rationalised by the lack of alignment of oleic acid molecules in organic rather than aqueous solution. This different orientation is likely to reduce the surface reactivity (compare discussion in Sect. 3). Overall, the results suggest an upper limit for the surface reaction of $\sim1\times10^{-11}$ cm^2 s^{-1} for the chosen set of input parameters. However, it should be noted that the upper limit for the surface rate coefficient would be ∼one order of magnitude higher if the desorption lifetime of ozone at the interface would be as short as nano- to pico-seconds (compare Vieceli et al., 2005 for a study of ozone at the air–water interface). Vieceli et al. (2004) found that the collision rate between ozone and a double bond is sensitive to several factors, including the extent of localization of the double bonds in the system and the distance that ozone diffuses into the organic phase. These aspects will be further investigated in follow-up studies.

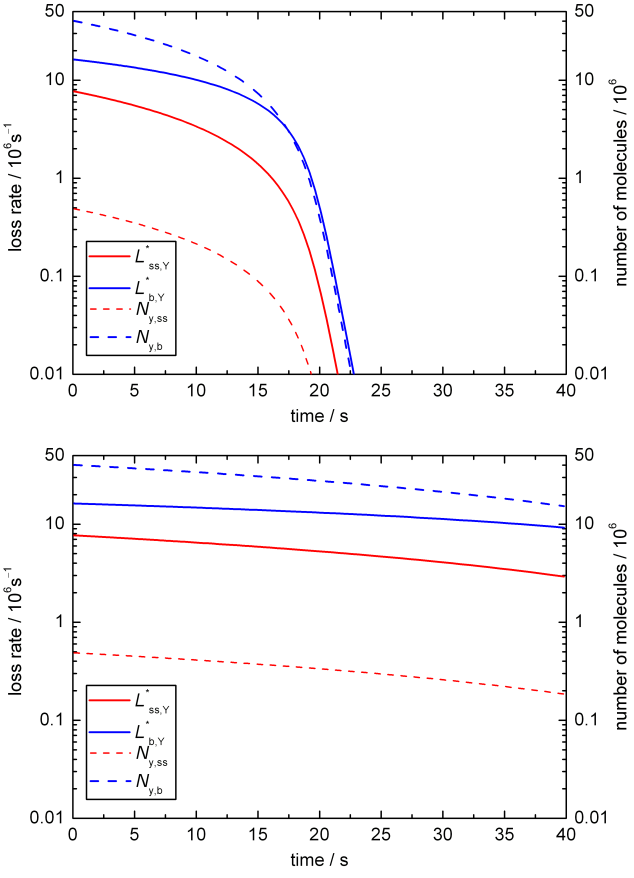

Fig. 6. Temporal evolution of aerosol particle composition and kinetic parameters in sensitivity studies for BC1 for **(a)** doubling and **(b)** halving $\alpha_{s,0,X}$ (while compensating with $k_{d,X}$ to maintain agreement with the experimental Henry's law coefficient $H_{cp,X}$). Plots are analogous to Fig. 2c.

4.3 Comparison with literature: surface vs. bulk reactivity and secondary chemistry

Hearn et al. (2005) studied the reaction of polydisperse oleic acid particles (mean radii ∼400 nm) with ozone in an aerosol

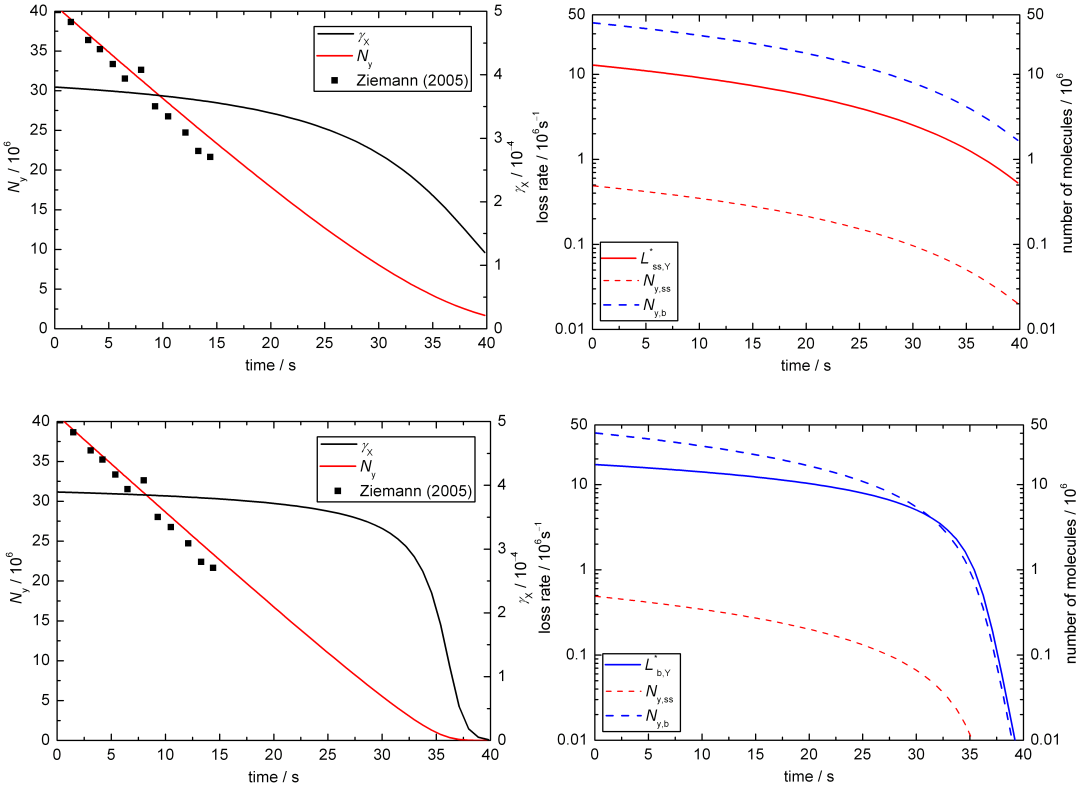

Fig. 7. Temporal evolution of aerosol particle composition and kinetic parameters in sensitivity studies for BC1 with chemical reaction occurring only at the surface **(a–b)** or only in the bulk **(c–d)**. Plots are analogous to Fig. 2a and Fig. 2c.

chemical ionisation mass spectrometer. The reaction was found to occur at the particle surface although previous measurements suggested bulk reactivity (Moise and Rudich, 2002; Morris et al., 2002; Smith et al., 2002; Thornberry and Abbatt, 2004; Vieceli et al., 2004). Hearn et al. attribute this discrepancy to a reduced rate of ozone diffusion into the bulk caused by pure oleic acid behaving like a solid rather than a disordered liquid. This would result in a surface-dominated reaction between ozone and the double bond of oleic acid. Hearn et al. (2005) suggest that most of the reactions occur in the first monolayer. Knopf et al. (2005) studied O_3 uptake by multi-component mixtures containing oleic acid and found that physical state and microstructure of these mixtures are of key importance. Low fractions of added solid components decreased the uptake by one order of magnitude compared to liquid mixtures. Furthermore, solid-liquid mixtures showed an increased uptake with increasing film age. McNeill et al. (2007) studied the reaction of ozone with internally mixed submicron aqueous droplets containing sodium oleate. They found evidence for a surface process and suggest that a Langmuir-Hinshelwood model may be applied with ozone first adsorbing to the surface before the reaction takes place. The measured rate coefficient was found to reach a plateau for high $[O_3]$. McNeill et al. (2007) suggest that oleate predominantly reacts in a monolayer on the aqueous sub-phase with reactive sites residing in a liquid-like film with ozone diffusing through the film and out again while the surface to which ozone adsorbs might be changing over the course of the reaction. Other studies also suggest that changes in ozone diffusion or solubility might occur during reaction (e.g. Moise and Rudich, 2000; Hearn et al., 2005). More importantly, a disruption of the order of the oleic acid dimers by surface-active reaction products might lead to a transition from surface-dominated reaction to bulk reaction (Hearn et al., 2005). Experimental evidence in support of this suggestion has recently been provided by King et al. (2009): a monolayer of oleic acid on an aqueous subphase is replaced by a new monolayer during O_3-initiated oxidation. Intriguingly, no product film has been found in studies of the ozonolysis of the methyl ester of oleic acid (Pfrang et al., 2010). Grimm et al. (2006) studied 1–2 mm droplets and found that ozone may penetrate up to 10 µm into these particles suggesting a bulk-phase process for atmospherically relevant aerosol droplets.

McNeill et al. (2008) investigated the heterogeneous OH oxidation of palmitic acid as a function of the particle size. Their experimental results are consistent with a model considering surface-only reactions with volatilisation of products, surface renewal and secondary chemistry between palmitic acid and the oxidation products. This study suggests that heterogeneous oxidation rates of organic aerosol are fastest for materials present at the particle surface, rather

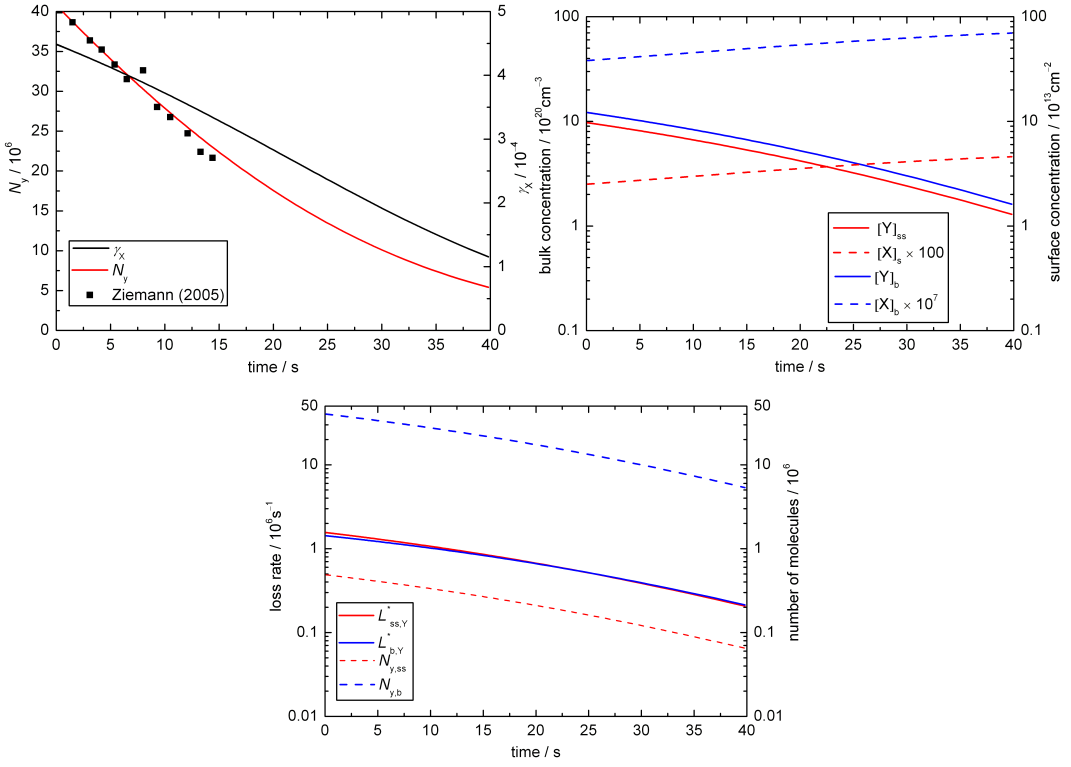

Fig. 8. Temporal evolution of aerosol particle composition and kinetic parameters in base case 2 (BC2; X = O_3, Y = oleic acid): **(a)** ozone uptake coefficient (γ_X) and total number of oleic acid molecules (N_Y; symbols indicate experimental data from Ziemann, 2005); **(b)** surface and bulk concentrations (square brackets); **(c)** numbers of oleic acid molecules at the surface and in the bulk of the particle ($N_{y,ss}$, $N_{y,b}$) and corresponding absolute loss rates ($L^*_{ss,Y} = L_{ss,Y} \times A_{ss}$, $L^*_{b,Y} = L_{b,Y} \times V_b$).

than in the bulk. The gradient in oxidation rates is steepest for solid particles such as palmitic acid. Liquid particles – such as the oleic acid droplets considered in our study – show more shallow gradients between surface and bulk rates (McNeill et al., 2008). Our model analysis demonstrates indeed that bulk reactivity is of key importance at least for oleic acid particles with radii of 200 nm or larger. There is evidence for the occurrence of surface renewal in our model system: the comparison of the absolute loss rates to the number of molecules at the particle surface and in the bulk (see e.g. Fig. 8c) suggests significant bulk-surface transport (bulk transport will be considered explicitly in the KM–SUB model).

Criegee intermediates are suggested to lead to a significant additional loss of oleic acid, e.g. 36% of the oleic acid molecules were attributed to reaction of oleic acid with a Criegee intermediate rather than with ozone (Hearn et al., 2005) confirming an earlier study by Hearn and Smith (2004). Interference of secondary reactions by Criegee intermediates was also found by Hung and Ariya (2007). Recently, Sage et al. (2009) not only confirmed the occurrence of secondary reactions of Criegee intermediates with the organic acid, but also found evidence for additional, previously unrecognised secondary chemistry that might involve the carbon backbone. Secondary chemistry is not currently considered in our model, but could be implemented if kinetic parameters for secondary reactions in the ozone–oleic acid system would become available (Hearn et al., 2005 quantified the loss due to secondary reaction by comparing methyl oleate and oleic acid reactivities, but could not measure the rate coefficient for the secondary process). Secondary chemistry would suggest an even slower initial reaction, so that the upper limit determined for the surface reaction in our model study would remain valid.

The chemical composition of the particle will obviously change over the course of the reaction and the extent of the deviation from initial particle composition will become increasingly significant for longer reaction timescales. Dominant initial products from the ozonolysis of oleic acid are known to be nonanal, which is likely to evaporate, as well as 9-oxononanoic, nonanoic, and azelaic acids in the liquid phase (e.g. Rudich et al., 2007; Vesna et al., 2009). We expect first-generation products other than nonanal to remain in the particle. Renewal of the surface layer by evaporation is thus unlikely to accelerate the oxidation process substantially. The evaporation of products from particle to gas phase is not considered in the current model, but we are planning to incorporate evaporation and condensation in follow-up

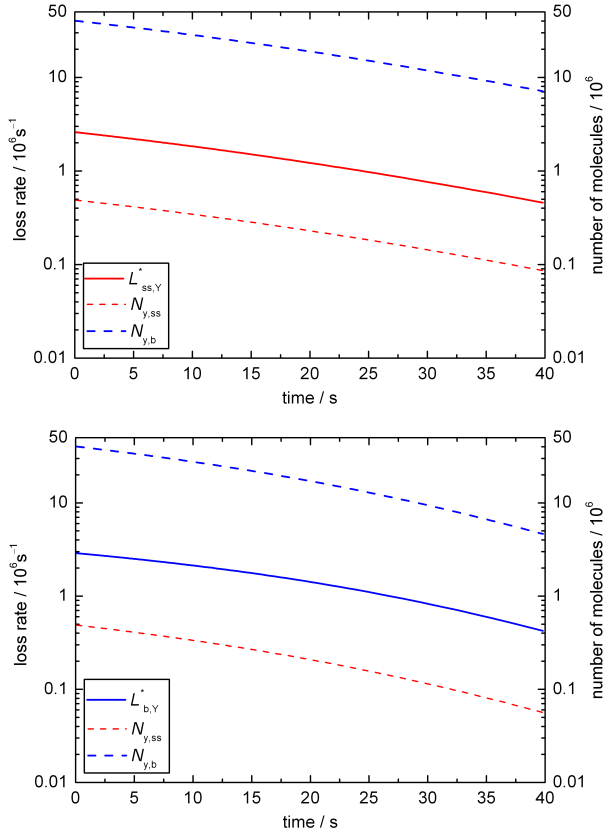

Fig. 9. Temporal evolution of aerosol particle composition and kinetic parameters in sensitivity studies for BC2 with chemical reaction occurring **(a)** only at the surface or **(b)** only in the bulk. Plots are analogous to Fig. 2c.

studies. The influence of the changing chemical composition of the particle surface on adsorbate-surface interactions i.e. on the surface accommodation coefficient can be taken into account by describing $\alpha_{s,0,X}$ as a linear combination of the initial surface accommodation coefficients that would be observed on pure substrates made up by the different surface components Y_p weighted by their fractional surface area θ_{ss,Y_p} (Pöschl et al., 2007; discussed in detail in Shiraiwa et al., 2010):

$$\alpha_{s,0,X} = \sum_p \alpha_{s,0,X,Y_p} \theta_{ss,Y_p}. \quad (31)$$

In a similar way, the influence of changing chemical composition of the particle bulk on the bulk diffusion coefficient can be taken into account by describing $D_{b,X}$ as a linear combination of the initial bulk diffusion coefficients that would be observed in pure bulk:

$$D_{b,X} = \sum_p D_{b,X,Y_p} \Phi_{b,Y_p}. \quad (32)$$

$\Phi_{b,Yp}$ refers to the fraction of Y_p in the bulk. For the base cases presented in this paper, $\alpha_{s,0,X}$ and $D_{b,X}$ are assumed to be constant for simplicity. Bulk diffusion of the liquid phase species can be corrected in analogy to Eq. (32) for the gas-phase compound (see Shiraiwa et al., 2010). However, the diffusion of oleic acid is not resolved in K2-SUB to maintain compatibility with resistor model formulations. Bulk diffusion of oleic acid is explicitly included in the KM-SUB model (Shiraiwa et al., 2010) and corrections for the changing chemical composition in the liquid phase could efficiently be implemented in KM-SUB. For long reaction times, the increasing proportion of products in the particle will also introduce additional uncertainties in the calculations since branching ratios and molecular properties are less well known in particular for second- and third-generation products.

It is apparent that discrepancies remain between the large number of studies of the O_3-oleic acid system. K2-SUB can be used to design, interpret and analyse future experimental investigations to allow choosing most insightful experimental conditions and de-convoluting surface and bulk processes.

While our modelling approach maintains compatibility with previous resistor-model formulations (e.g. Worsnop et al., 2002; Smith et al., 2002; King et al., 2008, 2009) K2-SUB enables free variation of all relevant parameters and thus can describe not only limiting cases, but also any state in between those. The testing and application of different sets of equations for different limiting cases used previously is adequate for the analysis of certain laboratory data, but it appears not to be well suited for efficient modelling of different types of clouds and aerosols under varying atmospheric conditions. Simulations for various multi-component and multi-phase reaction systems that are much more realistic models for atmospheric aerosol can be performed in future, incremental developments of K2-SUB. Such extensions would not be straight forward – if at all possible – for resistor-based models. Many experimental and nearly all atmospheric systems do not adhere to ideal limiting-case behaviour, so that K2-SUB is a potentially powerful tool to help improving our understanding of interfacial oxidation processes of atmospheric importance.

5 Conclusions

1. We demonstrate how a detailed treatment of adsorption and reaction at the surface can be coupled to a description of bulk reaction and transport that is consistent with traditional resistor model formulations. To our knowledge, K2-SUB is the first model in which this coupling has been realised.

2. From literature data we have derived a set of kinetic parameters that enable detailed description of mass transport and chemical reaction on the surface and in the bulk of oleic acid particles.

3. The available reaction rate coefficients support that chemical reaction in the bulk plays an important role. Due to the wide range of rate coefficients reported from the different experimental studies, however, the exact proportion between surface and bulk reaction remains uncertain. Our model runs suggest for the chosen set of input parameters that the surface reaction rate coefficient is not significantly above 1×10^{-11} cm^2 s^{-1} for droplets of pure oleic acid.

4. Test calculations showed that the surface accommodation coefficient of the gas-phase reactant has a strong non-linear influence on the surface and bulk reactions. Our two base cases demonstrate how slight variations in $\alpha_{s,0,X}$ lead to either transport-limited (BC1) or reaction-limited (BC2) systems.

5. Further experimental data are required to establish the relative contributions of surface and bulk processes to the loss of oleic acid and other organic species in atmospheric aerosols.

6. We propose that K2-SUB may be used to design, interpret and analyse experiments for better discrimination between surface and bulk processes in the oleic acid-ozone system as well as in other heterogeneous reaction systems. For example, the model results suggest that longer reaction times than investigated in earlier studies ($>$30 s for 200 nm particles at 2.8 ppm [O_3]) are needed to unravel the proportions between surface and bulk reaction. Many experimental and nearly all atmospheric reaction systems do not adhere to ideal limiting-case behaviour tailor-made for traditional resistor model formulations, so that K2-SUB is a potentially powerful tool to help improving our understanding of interfacial oxidation processes of atmospheric importance.

6 Supplementary material

The complete set of results of the model runs tabulated in Table 2 is presented in the electronic supplement (see http://www.atmos-chem-phys.net/10/4537/2010/acp-10-4537-2010-supplement.zip) as 138 gif image files (three plots per model run equivalent to those exemplified in Fig. 2a, b and c).

Appendix A

List of symbols

Symbol	Meaning	SI Unit
$\alpha_{s,0,X}$	initial surface accommodation coefficient of X	
$\alpha_{s,X}$	surface accommodation coefficient of X	
γ_x	uptake coefficient of X (normalized by gas kinetic flux of surface collisions)	
$\gamma_{b,X}$	resistor model conductance of particle bulk diffusion and reaction of X	
$\gamma_{g,X}$	resistor model conductance of gas phase diffusion of X	
$\gamma_{s,X}$	resistor model conductance of surface reaction of X	
$\gamma_{s,b,X}$	resistor model conductance of surface-bulk transfer of X	
δ_X	effective molecular diameter of X	m
δ_Y	effective molecular diameter of Y	m
$\sigma_{s,X}$	molecular cross section of X in the sorption layer	m^2
$\sigma_{ss,Y}$	molecular cross section of Y in the quasi-static layer	m^2
$\tau_{d,X}$	desorption lifetime of X	s
Φ_{b,Y_p}	fraction of Y_p in the bulk	
ω_x	mean thermal velocity of X in the gas phase	m s^{-1}
A_{ss}	Particle surface area ($A_{ss} = 4\pi r_p^2$)	m^2
$C_{b,rd,X}$	reacto-diffusive geometry correction factor of X	
$C_{g,X}$	gas phase diffusion correction factor of X	
$D_{b,X}$	particle bulk diffusion coefficient of X	m^2 s^{-1}
$D_{g,X}$	gas phase diffusion coefficient of X	m^2 s^{-1}
$H_{cp,X}$	Henry's law coefficient of X (concentration/pressure)	mol m^{-3} Pa^{-1}
$J_{ads,X}$, $J_{des,X}$	flux of adsorption and desorption of X	m^{-2} s^{-1}
$J_{b,rd,X}$	reacto-diffusive flux of X in the particle bulk	m^{-2} s^{-1}
$J_{b,s,X}$, $J_{s,b,X}$	flux of bulk-surface and surface-bulk transfer of X (sorption layer)	m^{-2} s^{-1}
$J_{b,ss,Y}$, $J_{ss,b,Y}$	flux of bulk-surface and surface-bulk transfer of Y (quasi-static layer)	m^{-2} s^{-1}
$J_{coll,X}$	gas kinetic flux of X colliding with the surface	m^{-2} s^{-1}
$J_{s,b,net,X}$	net flux of surface-bulk transfer of X	m^{-2} s^{-1}
$k_{a,X}$	first-order adsorption rate coefficient of X	m s^{-1}
$k_{a,0,X}$	first-order adsorption rate coefficient of X on an adsorbate-free surface	m s^{-1}
$k_{b,X}$	pseudo-first-order rate coefficient for chemical loss of X in the particle bulk	s^{-1}
$k_{b,s,X}$	first-order rate coefficient for bulk-to-surface transfer of X	m s^{-1}
$k_{b,ss,Y}$	first-order rate coefficient for bulk-to-surface transfer of Y	m s^{-1}

$k_{d,X}$	first-order desorption rate coefficient of X	s^{-1}
$k_{BR,X,Y}$	second order bulk reaction rate coefficient	$m^3\ s^{-1}$
$k_{s,X}$	pseudo-first-order rate coefficient for chemical loss of X in the sorption layer	s^{-1}
$k_{s,b,X}$	first-order rate coefficient for surface-to-bulk transfer of X	s^{-1}
$k_{s,b,net,X}$	pseudo-first-order rate coefficient for net surface-to-bulk transfer of X	s^{-1}
$k_{ss,Y}$	pseudo-first-order rate coefficient for chemical loss of Yin the quasi-static surface layer	s^{-1}
$k_{ss,b,Y}$	first-order rate coefficients for surface-bulk transfer of Y	s^{-1}
$k_{SLR,X,Y}$	second-order rate coefficient for surface layer reactions of X with Y	$m^2\ s^{-1}$
$K'_{ads,X}$	effective adsorption equilibrium constant of X	m^3
$K_{sol,cp,X}$	solubility or gas-particle partitioning coefficient of X	$mol\ m^{-3}\ Pa^{-1}$
$K_{sol,cc,X}$	dimensionless solubility or gas-particle partitioning coefficient of X	
$L_{b,Y}$	chemical loss rate (concentration-based) of Y in the bulk	$m^{-3}\ s^{-1}$
$L^*_{b,Y}$	absolute chemical loss rate of Y in the bulk	s^{-1}
$l_{rd,X}$	reacto-diffusive length for X in the particle bulk	m
$L_{s,X}$	chemical loss rate (concentration-based) of X on the surface	$m^{-2}\ s^{-1}$
$L_{ss,Y}$	chemical loss rate (concentration-based) of Y on the surface	$m^{-2}\ s^{-1}$
$L^*_{ss,Y}$	absolute chemical loss rate of Y in the bulk	s^{-1}
R	gas constant	$J\ K^{-1}\ mol^{-1}$
r_p	particle radius	m
$[SS]_{ss}$	sorption site surface concentration	m^{-2}
T	absolute temperature	K
V_b	volume of the particle bulk ($V_b = 4/3\pi(r_p-\delta_Y)^3$)	m^3
V_p	total particle volume ($V_p = 4/3\pi r_p^3$)	m^3
X	volatile molecular species	
$[X]_b$	particle bulk number concentration of X	m^{-3}
$[X]_{bs}$	near-surface particle bulk number concentration of X	m^{-3}
$[X]_{b,max}$	maximum particle bulk number concentration of X	m^{-3}
$[X]_g$	gas phase number concentration of X	m^{-3}
$[X]_{gs}$	near-surface gas phase number concentration of X	m^{-3}
$[X]_s$	surface number concentration of X (sorption layer)	m^{-2}
$[X]_{s,max}$	maximum surface number concentration of X (sorption layer)	m^{-2}
Y	non-volatile molecular species	
$[Y]_{ss}$	surface number concentration of Y (quasi-static layer)	m^{-2}
$[Y]_{ss,0}$	initial surface number concentration of Y (quasi-static layer)	m^{-2}
$[Y]_{ss,max}$	max. surface number concentration of Y (quasi-static layer)	m^{-2}
$[Y]_b$	average concentration of Y across the whole particle bulk (including near-surface bulk)	m^{-2}
$[Y]_{b,0}$	initial concentration of Y across the whole particle bulk (including near-surface bulk)	m^{-2}
$[Y]_{b,max}$	max. concentration of Y across the whole particle bulk (including near-surface bulk)	m^{-2}

Appendix B

Relevant equations from PRA framework (Pöschl et al., 2007)

$$\gamma_X = \alpha_{s,X}\frac{k_{s,X}+k_{s,b,net,X}}{k_{s,X}+k_{s,b,net,X}+k_{d,X}} \quad \text{(B1)}$$

with

$$k_{s,b,net,X} = k_{s,b,X}\left(1+\frac{k_{b,s,X}}{C_{b,rd,X}\sqrt{k_{b,X}D_{b,X}}}\right)^{-1}, \quad \text{(B2)}$$

and the reacto-diffusive geometry correction factor (conversion from planar to spherical geometry; determined by the particle radius, r_p, and the reacto-diffusive length for species X: $l_{rd,X} = \sqrt{D_{b,X}/k_{b,X}}$):

$$C_{b,rd,X} = \coth\left(\frac{r_p}{l_{rd,X}}\right) - \frac{l_{rd,X}}{r_p}. \quad \text{(B3)}$$

$K_{sol,cp,X}$ is the solubility or gas-particle partitioning coefficient for X and describes the partitioning of a volatile species between gas phase and particle bulk (at infinite dilution, it equals Henry's law coefficient; $K_{sol,cp,X}RT = K_{sol,cc,X}$ giving the ratio of condensed phase and gas phase concentrations)

$$K_{sol,cc,X} = K_{sol,cp,X}RT = \frac{k_{s,b,X}}{k_{b,s,X}}\frac{k_{a,X}}{k_{d,X}} = \frac{k_{s,b,X}}{k_{b,s,X}}\frac{\alpha_{s,X}\omega_X}{4k_{d,X}} \quad \text{(B4)}$$

$$k_{a,0,X} = \alpha_{s,0,X}\frac{\omega_X}{4} \quad \text{(B5)}$$

$$\alpha_{s,X} = \alpha_{s,0,X}\left(1-\theta_{s,X}\right) \quad \text{(B6)}$$

$$K'_{ads,X} = \frac{\sigma_X k_{a,0,X}}{k_{d,X}+k_{s,X}+k_{s,b,net,X}} \quad \text{(B7)}$$

$$\frac{[X]_{bs}}{[X]_s} = \frac{k_{s,b,X}}{k_{b,s,X}+C_{b,rd,X}\sqrt{k_{b,X}D_{b,X}}} \quad \text{(B8)}$$

Appendix C

Resistor model formulations and the PRA framework

The description of heterogeneous reactions is often achieved by resistor model formulations (e.g. Worsnop et al., 2002; Smith et al., 2002; King et al, 2008, 2009; Gross et al., 2009) which are valid under certain assumptions and consistent with the PRA framework as described under Special Case B in Pöschl et al. (2007). Uptake coefficients (γ) generally refer to a gas-phase species X. A sorption layer uptake coefficient can be defined under steady state condition by Eq. (B1) (compare Pöschl et al., 2007, Eq. 115). Resistor model formulation of Special Case B in Pöschl et al. (2007) is obtained from inversion of Eq. (B1):

$$\frac{1}{\gamma_X} = \frac{1}{\alpha_{s,X}} + \frac{1}{\Gamma_{s,X}+\frac{1}{\frac{1}{\Gamma_{s,b,X}}+\frac{1}{\Gamma_{b,X}}}} \quad \text{(C1)}$$

with resistor model conductance terms for surface reaction ($\Gamma_{s,X}$) for surface-bulk transfer ($\Gamma_{s,b,X}$) and for particle bulk diffusion and reaction ($\Gamma_{b,X}$) (as defined in Eqs. 21, 22 and 23)

$$\Gamma_{b,X} = \frac{4}{\omega_x}K_{sol,cp,X}RTC_{b,rd,X}\sqrt{k_{b,X}D_{b,X}} \quad \text{(C2)}$$

Equation (C2) is equivalent to resistor model formulations, exemplified here by the treatment used by Smith et al. (2002; Eq. 4):

$$\Gamma_{rxn} = \frac{4HRTD}{\bar{c}l}[\coth(a/l-l/a)] \quad \text{(C3)}$$

$$\begin{aligned} k_{b,X} &= k_2[\text{Oleic}] \\ l_{rd,X} &= l \\ \omega_X &= \bar{c} \\ \text{with } r_p &= a \\ K_{sol,cp,X} &= H \\ D_{b,X} &= D \\ \gamma_{rxn} &= \Gamma_{b,X} \\ \text{and } C_{b,rd,X} &= \coth\left(\tfrac{a}{l}\right)-\tfrac{l}{a}\text{; compare Eq. (B3).} \end{aligned}$$

C1 For reaction of ozone near the particle surface

Case 1b in Smith et al., 2002; for $l_{rd,X} < r_p/20$; diffusion-limited case. The uptake is given by (Smith et al., 2002, Eqs. 9 and C2)

$$\gamma = \frac{4HRT}{\bar{c}}\sqrt{Dk_2}\sqrt{[\text{Oleic}]} \cong \frac{4}{\omega_x}K_{sol,cp,X}RT\sqrt{k_{b,X}D_{b,X}} \quad \text{(C4)}$$

with $1 \le C_{b,rd,X} \ge 0.95 \approx 1$.

Derivation:

Limiting case for $l_{rd,X} = r_p/20$ in Eq. (C2) with $C_{b,rd,X}$ as defined in Eq. (B3) and $\coth\left(20r_p/r_p\right) = \frac{e^{40}+1}{e^{40}-1} \approx 1$, thus $C_{b,rd,X} = 1-\frac{1}{20} = 0.95$, and for $l_{rd,X} < r_p/20$:$C_{b,rd,X} \approx 1$.

C2 For fast diffusion of ozone through the particle

Case 1a in Smith et al., 2002; for $l_{rd,X} > r_p$; reaction not limited by diffusion) the uptake is given by

$$\gamma = \frac{4HRT}{\bar{c}}\frac{a}{3}k_2[\text{Oleic}] \cong \frac{4}{3\omega_x}K_{sol,cp,X}RTr_pk_{b,X}. \quad \text{(C5)}$$

Derivation:

$\coth x = \cosh x/\sin hx$; Taylor series: $\coth x \cong 1/x + x/3 - x^3/45\ldots$

Using Taylor and neglecting all terms higher than power 1 in x:

$$C_{b,rd,X} = \coth\left(\frac{r_p}{l_{rd,X}}\right)-\frac{l_{rd,X}}{r_p} \approx \left(\frac{l_{rd,X}}{r_p}+\frac{r_p}{3l_{rd,X}}\right) - \frac{l_{rd,X}}{r_p} = \frac{r_p}{3l_{rd,X}}. \quad \text{(C6)}$$

Equation (C2) thus becomes:

$$\Gamma_{b,X} = \frac{4}{\omega_x}K_{sol,cp,X}RT\frac{r_p}{3l_{rd,X}}\sqrt{k_{b,X}D_{b,X}}. \quad \text{(C7)}$$

Using Eq. (C4):

$$\Gamma_{b,X} = \frac{4}{\omega_x}K_{sol,cp,X}RT\frac{r_p\sqrt{k_{b,X}D_{b,X}}}{3D_{b,X}}\sqrt{k_{b,X}D_{b,X}} = \frac{4}{3\omega_x}K_{sol,cp,X}RTr_pk_{b,X}. \quad \text{(C8)}$$

C3 For the reactive uptake being dominated by reaction at the surface

Case 2 in Smith et al., 2002; bulk reaction and conductance term are assumed to be negligible, i.e. uptake is assumed to

be equal to surface conductance term

$$\gamma = \Gamma_{s,X} = \frac{k_2^{surf}[O_3]_{surf}[Oleic]_{surf}}{\text{normalised by gas} - \text{collision rate}}$$
$$= \frac{k_2^{surf}\left(P_{O_3} H \delta_X\right)[Oleic]\delta_X}{P_{O_3}/4RT}$$
$$= \frac{4HRT}{\bar{c}}\delta_X^2 k_2^{surf}[Oleic] \cong \frac{4k_{a,X}}{\omega_X}\frac{k_{s,X}}{k_{d,X}}. \quad \text{(C9)}$$

Derivation:

- $k_{s,X} = k_2^{surf}[Oleic]\delta_X$;
- $HRT\delta_X = K_{sol,cp,X}RT\delta_X = K_{sol,cc,X}\delta_X = \frac{k_{s,b,X}}{k_{b,s,X}}\frac{k_{a,X}}{k_{d,X}}\delta_X$ and $\frac{k_{b,s,X}}{k_{s,b,X}} = \delta_X$ so that $HRT\delta_X = \frac{k_{a,X}}{k_{d,X}}$ (compare Eqs. B4, 21 and 30).

Appendix D

Model input parameters

K2-SUB model input parameters for the investigated chemical species (X = O_3 and Y = oleic acid) based on experimental data from Ziemann (2005), Smith et al. (2002), Gonzalez-Labrada et al. (2007), King et al. (2008, 2009) and Pöschl et al. (2001).

r_p = 0.2 µm (Ziemann, 2005)

$D_{b,X}$ = 1×10^{-5} cm^2 s^{-1} (estimated based on diffusion of O_2 in range of organic solvents; Smith et al., 2002; King et al., 2008)

$D_{b,Y}$ = 10^{-7}–10^{-10} cm^2 s^{-1} (compare Smith et al., 2003)

ω_X = 3.6×10^4 cm s^{-1} (Smith et al., 2002; Pöschl et al., 2001; Ammann and Pöschl, 2007; King et al., 2009)

$H_{cp,X}$ = 4.8×10^{-4} mol cm^{-3} atm^{-1} (Smith et al., 2002; Morris et al., 2002; King et al., 2008, 2009)

$\alpha_{s,0,X}$ = 4.2×10^{-4} (BC1) and 8.5×10^{-4} (BC2) (compare Pöschl et al., 2001; Ammann and Pöschl, 2007; Shiraiwa et al., 2009)

$k_{d,X}$ = 100 s^{-1} (BC1) and 1000 s^{-1} (BC2) ($k_{d,X}$ = 0.1–10^2 s^{-1} for ozone; Shiraiwa et al., 2009)

$k_{SLR,X,Y}$ = 6×10^{-12} cm^2 s^{-1}; compare 7.3×10^{-11} cm^2 s^{-1} and 2.1×10^{-12} cm^2 s^{-1} (King et al., 2009); 4.9×10^{-11} cm^2 s^{-1} (Gonzalez-Labrada et al., 2007)

$[X]_{gs}$ = 6.95×10^{13}cm^{-3} corresponding to 2.8 ppm (Ziemann, 2005)

$k_{b,X}$ = $k_{BR,X,Y}\times[Y]$ with $k_{BR,X,Y} = 1.7\times10^{-15}$ cm^3 s^{-1} corresponding to a literature value of 1×10^6 L mol^{-1} s^{-1} (Razumovskii et al., 1972, Lisitsyn et al., 2004 and Titov et al., 2005; used in BC1; reduced to 5×10^{-17} cm^3 s^{-1} in BC2) and $[Y]_0 = 1.21\times10^{21}$ cm^{-3} corresponding to 3.15 mol L^{-1} (Ziemann, 2005)

T = 296 K

$k_{b,s,X}$ = 318 cm s^{-1}

$k_{b,ss,Y}$ = 1.6×10^{-3} cm s^{-1}

$k_{ss,b,Y}$ = 1.99×10^4 s^{-1}

$k_{s,b,X}$ = 9.8×10^4 s^{-1} (BC1) and 4.85×10^5 s^{-1} (BC2)

σ_X = 1.8×10^{-15} cm^2 (Pöschl et al., 2001; Ammann and Pöschl, 2007) and thus δ_X = 0.4 nm (compare computational study by Vieceli et al., 2004)

δ_Y = 0.8 nm (compare work by Iwahashi, 1991)

Acknowledgements. CP wishes to thank the Royal Society (grant VO080001), the Research Endowment Trust Fund (University of Reading) and the NERC (grant NE/G000883/1). UP and MS acknowledge support from the European integrated project on cloud climate and air quality interactions (No. 036833-2 EUCAARI), the Max Planck Graduate Centre (MPGC), and the Ministry of Education, Culture, Sports, Science and Technology – Japan (MEXT).

The service charges for this open access publication have been covered by the Max Planck Society.

Edited by: M. Kulmala

References

Ammann, M., Pöschl, U., and Rudich, Y.: Effects of reversible adsorption and Langmuir-Hinshelwood surface reactions on gas uptake by atmospheric particles, Phys. Chem. Chem. Phys., 5, 351–356, 2003.

Ammann, M. and Pöschl, U.: Kinetic model framework for aerosol and cloud surface chemistry and gas-particle interactions – Part 2: Exemplary practical applications and numerical simulations, Atmos. Chem. Phys., 7, 6025–6045, 2007, http://www.atmos-chem-phys.net/7/6025/2007/.

Andreae, M. O., Rosenfeld, D., Artaxo, P., Costa, A. A., Frank, G. P., Longo, K. M., and Silva-Dias, M. A. F.: Smoking rain clouds over the Amazon, Science, 303, 1337–1342, 2004.

Andreae, M. O. and Rosenfeld, D.: Aerosol-cloud-precipitation interactions. Part 1. The nature and sources of cloud-active aerosols, Earth-Sci. Rev., 89, 13–41, doi:10.1016/j.earscirev.2008.03.001, 2008.

Atkins, P. W.: Physical Chemistry, Oxford University Press, 1998.

Bergstrom, R. W., Pilewskie, P., Russell, P. B., Redemann, J., Bond, T. C., Quinn, P. K., and Sierau, B.: Spectral absorption properties of atmospheric aerosols, Atmos. Chem. Phys., 7, 5937–5943, 2007, http://www.atmos-chem-phys.net/7/5937/2007/.

Breon, F. M., Tanre, D., and Generoso, S.: Aerosol effect on cloud droplet size monitored from satellite, Science, 295, 834–838, 2002.

Charlson, R. J., Seinfeld, J. H., Nenes, A., Kulmala, M., Laaksonen, A., and Facchini, M. C.: Atmospheric science - Reshaping the theory of cloud formation, Science, 292, 2025–2026, 2001.

Choularton, T. W., Bower, K. N., Weingartner, E., Crawford, I., Coe, H., Gallagher, M. W., Flynn, M., Crosier, J., Connolly, P., Targino, A., Alfarra, M. R., Baltensperger, U., Sjogren, S., Verheggen, B., Cozic, J., and Gysel, M.: The influence of small aerosol particles on the properties of water and ice clouds, Faraday Discuss., 137, 205–222, 2008.

Fuzzi, S., Andreae, M. O., Huebert, B. J., Kulmala, M., Bond, T. C., Boy, M., Doherty, S. J., Guenther, A., Kanakidou, M., Kawamura, K., Kerminen, V.-M., Lohmann, U., Russell, L. M., and Pöschl, U.: Critical assessment of the current state of scientific knowledge, terminology, and research needs concerning the role of organic aerosols in the atmosphere, climate, and global change, Atmos. Chem. Phys., 6, 2017–2038, 2006, http://www.atmos-chem-phys.net/6/2017/2006/.

Gonzalez-Labrada, E., Schmidt, R., and DeWolf, C. E.: Kinetic analysis of the ozone processing of an unsaturated organic monolayer as a model of an aerosol surface, Phys. Chem. Chem. Phys., 9, 5814–5821, 2007.

Grimm, R. L., Hodyss, R., and Beauchamp, J. L.: Probing interfacial chemistry of single droplets with field-induced droplet ionization mass spectrometry: Physical adsorption of polycyclic aromatic hydrocarbons and ozonolysis of oleic acid and related compounds, Anal. Chem., 78, 3800–3806, 2006.

Gross, S., Iannone, R., Xiao, S., and Bertram, A. K.: Reactive uptake studies of NO_3 and N_2O_5 on alkenoic acid, alkanoate, and polyalcohol substrates to probe nighttime aerosol chemistry, Phys. Chem. Chem. Phys., 11, 7792–7803, 2009.

Hearn, J. D. and Smith, G. D.: Kinetics and product studies for ozonolysis reactions of organic particles using aerosol CIMS, J. Phys. Chem. A, 108, 10019–10029, 2004.

Hearn, J. D., Lovett, A. J., and Smith, G. D:; Ozonolysis of oleic acid particles: evidence for a surface reaction and secondary reactions involving Criegee intermediates, Phys. Chem. Chem. Phys., 7, 501–511, 2005.

Hearn, J. D. and Smith, G. A.: Ozonolysis of mixed oleic acid/n-docosane particles: The roles of phase, morphology, and metastable states, J. Phys. Chem. A, 111, 11059–11065, 2007.

Hung, H. M. and Ariya, P.: Oxidation of oleic acid and oleic acid/sodium chloride(aq) mixture droplets with ozone: Changes of hygroscopicity and role of secondary reactions, J. Phys. Chem. A, 111, 620–632, 2007.

Iwahashi, M., Yamaguchi, Y., Kato, T., Horiuchi, T., Sakurai, I., and Suzuki, M.: Temperature-dependence of molecular conformation and liquid structure of cis-9-octadecanoic acid, J. Phys. Chem., 95, 445–451, 1991.

Katrib, Y., Biskos, G., Buseck, P. R., Davidovits, P., Jayne, J. T., Mochida, M., Wise, M. E., Worsnop, D. R., and Martin, S. T.: Ozonolysis of mixed oleic-acid/stearic-acid particles: Reaction kinetics and chemical morphology, J. Phys. Chem. A, 109, 10910–10919, 2005.

King, M. D., Canosa-Mas, C. E., and Wayne, R. P.: Frontier molecular orbital correlations for predicting rate constants between alkenes and the tropospheric oxidants NO_3, OH and O_3, Phys. Chem. Chem. Phys., 1, 2231–2238, 1999.

King, M. D., Thompson, K. C., Ward, A. D., Pfrang, C., and Hughes, B. R.: Oxidation of biogenic and water-soluble compounds in aqueous and organic aerosol droplets by ozone: a kinetic and product analysis approach using laser Raman tweezers, Faraday Discuss., 137, 173–192, 2008.

King, M. D., Rennie, A. R., Thompson, K. C., Fisher, F. N., Dong, C. C., Thomas, R. K., Pfrang, C., and Hughes, A. V.: Oxidation of oleic acid at the air-water interface and its potential effects on cloud critical supersaturations, Phys. Chem. Chem. Phys., 11, 7699–7707, 2009.

King, M. D., Rennie, A. R., Pfrang, C., Hughes, A. V., Thomas, R. K., Dong, C. C., and Thompson, K. C.: Interaction of nitrogen oxide with a monolayer of oleic acid at the air-water interface: a simple proxy for atmospheric aerosol, Atmos. Environ., 44, 1822–1825, 2010.

Knopf, D. A., Anthony, L. M., and Bertram, A. K.: Reactive uptake of O_3 by multicomponent and multiphase mixtures containing oleic acid, J. Phys. Chem. A, 109, 5579–5589, 2005.

Last, D. J., Najera, J. J., Percival, C. J., and Horn, A. B.: A comparison of infrared spectroscopic methods for the study of heterogeneous reactions occurring on atmospheric aerosol proxies, Phys. Chem. Chem. Phys., 11, 8214–8225, 2009.

Lee, A. K. Y. and Chan, C. K.: Single particle Raman spectroscopy for investigating atmospheric heterogeneous reactions of organic aerosols, Atmos. Environ., 41, 4611–4621, 2007.

Lisitsyn, D. M., Razumovskii, S. D., Tishenin, M. A., and Titov, V. N.: Kinetic parameters of oxidation of individual fatty acids with ozone, Bull. Exp. Biol. Med., 138, 457–459, 2004.

Moise, T. and Rudich, Y.: Reactive uptake of ozone by proxies for organic aerosols: Surface versus bulk processes, J. Geophys. Res.-Atmos., 105, 14667–14676, 2000.

Moise, T. and Rudich, Y.: Reactive uptake of ozone by aerosol-associated unsaturated fatty acids: Kinetics, mechanism, and products, J. Phys. Chem. A, 106, 6469–6476, 2002.

Morris, J. W., Davidovits, P., Jayne, J. T., Jimenez, J. L., Shi, Q., Kolb, C. E., Worsnop, D. R., Barney, W. S., and Cass, G.: Kinetics of submicron oleic acid aerosols with ozone: a novel aerosol mass spectrometric technique, Geophys. Res. Lett., 29, 1357, doi:10.1029/2002GL014692, 2002.

McNeill, V. F., Wolfe G. M., and Thornton, J. A.: The Oxidation of Oleate in Submicron Aqueous Salt Aerosols: Evidence of a Surface Process, J. Phys. Chem. A, 111, 1073–1083, 2007.

McNeill, V. F., Yatavelli, R. L. N., Thornton, J. A., Stipe, C. B., and Landgrebe, O.: Heterogeneous OH oxidation of palmitic acid in single component and internally mixed aerosol particles: vaporization and the role of particle phase, Atmos. Chem. Phys., 8, 5465–5476, 2008, http://www.atmos-chem-phys.net/8/5465/2008/.

Penner, J. E., Dong, X. Q., and Chen, Y.: Observational evidence of a change in radiative forcing due to the indirect aerosol effect, Nature, 427, 231–234, 2004.

Pfrang, C., King, M. D., Canosa-Mas, C. E., and Wayne, R. P.: Correlations for gas-phase reactions of NO_3, OH and O_3 with alkenes: An update, Atmos. Environ., 40, 1170–1179, 2006a.

Pfrang, C., King, M. D., Canosa-Mas, C. E., and Wayne, R. P.: Structure-activity relations (SARs) for gas-phase reactions of NO_3, OH and O_3 with alkenes: An update, Atmos. Environ., 40, 1180–1186, 2006b.

Pfrang, C., King, M. D., Canosa-Mas, C. E., Flugge, M., and Wayne, R. P.: Gas-phase rate coefficients for the reactions of NO_3, OH and O_3 with α,β-unsaturated esters and ketones: structure-activity relations (SARs), Atmos. Environ., 41, 1792–1802, 2007.

Pfrang, C., King, M. D., Braeckevelt, M., Canosa-Mas, C. E., and Wayne, R. P.: Gas-phase rate coefficients for reactions of NO_3, OH, O_3 and $O(^3P)$ with unsaturated alcohols and ethers: Correlations and structure-activity relations (SARs), Atmos. Environ., 42, 3018–3034, 2008.

Pfrang, C., King, M. D., Lucas, C. O. M., Rennie, A. R., Hoare, I. D., Brown, G. D., and Campbell, R. A.: Establishing the fate of organic films on atmospheric aerosol: the reaction of ozone with a monolayer of d-methyl oleate studied by fast neutron reflectometry, in preparation, 2010.

Pöschl, U., Letzel, T., Schauer, C., and Niessner, R.: Interaction of ozone and water vapor with spark discharge soot aerosol particles coated with benzo[a]pyrene: O_3 and H_2O adsorption, benzo[a]pyrene degradation, and atmospheric implications, J. Phys. Chem. A, 105, 4029–4041, 2001.

Pöschl, U.: Atmospheric aerosols: Composition, transformation, climate and health effects, Angew. Chem.-Int. Edit., 44, 7520–7540, 2005.

Pöschl, U., Rudich, Y., and Ammann, M.: Kinetic model framework for aerosol and cloud surface chemistry and gas-particle interactions – Part 1: General equations, parameters, and terminology, Atmos. Chem. Phys., 7, 5989–6023, 2007, http://www.atmos-chem-phys.net/7/5989/2007/.

Ramanathan, V., Crutzen, P. J., Kiehl, J. T., and Rosenfeld, D.: Atmosphere – Aerosols, climate, and the hydrological cycle, Science, 294, 2119–2124, 2001.

Razumovskii, S. D. and Zaikov, G. E.: Bull. Acad. Sci. USSR Div. Geologic, 616–620, 1971.

Reynolds, J. C., Last, D. J., McGillen, M., Nijs, A., Horn, A. B., Percival, C., Carpenter, L. J., and Lewis, A. C.: Structural analysis of oligomeric molecules formed from the reaction products of oleic acid ozonolysis, Environ. Sci. Technol., 40, 6674–6681, 2006.

Rosen, E. P., Garland, E. R., and Baer, T.: Ozonolysis of Oleic Acid Adsorbed to Polar and Nonpolar Aerosol Particles, J. Phys. Chem. A, 112, 10315–10324, 2008.

Rosenfeld, D.: Suppression of rain and snow by urban and industrial air pollution, Science, 287, 1793–1796, 2000.

Rudich, Y., Donahue, N. M., and Mentel, T. F.: Aging of organic aerosol: Bridging the gap between laboratory and field studies, Annu. Rev. Phys. Chem., 58, 321–352, 2007.

Sage, A. M., Weitkamp, E. A., Robinson, A. L., and Donahue, N. M.: Reactivity of oleic acid in organic particles: changes in oxidant uptake and reaction stoichiometry with particle oxidation, Phys. Chem. Chem. Phys., 11, 7951–7962, 2009.

Shiraiwa, M., Garland, R. M., and Pöschl, U.: Kinetic double-layer model of aerosol surface chemistry and gas-particle interactions (K2-SURF): Degradation of polycyclic aromatic hydrocarbons exposed to O_3, NO_2, H_2O, OH and NO_3, Atmos. Chem. Phys., 9, 9571–9586, 2009, http://www.atmos-chem-phys.net/9/9571/2009/.

Shiraiwa, M., Pfrang, C., and Pöschl, U.: Kinetic multi-layer model of aerosol surface and bulk chemistry (KM-SUB): the influence of interfacial transport and bulk diffusion on the oxidation of oleic acid by ozone, Atmos. Chem. Phys., 10, 3673–3691, 2010, http://www.atmos-chem-phys.net/10/3673/2010/.

Smith, G. D., Woods, E., DeForest, C. L., Baer, T., and Miller, R. E.: Reactive uptake of ozone by oleic acid aerosol particles: Application of single-particle mass spectrometry to heterogeneous reaction kinetics, J. Phys. Chem. A, 106, 8085–8095, 2002.

Smith, G. D., Woods, E., Baer, T., and Miller, R. E.: Aerosol uptake described by numerical solution of the diffusion – Reaction equations in the particle, J. Phys. Chem. A, 107, 9582–9587, 2003.

Springmann, M., Knopf, D. A., and Riemer, N.: Detailed heterogeneous chemistry in an urban plume box model: reversible co-adsorption of O_3, NO_2, and H_2O on soot coated with benzo[a]pyrene, Atmos. Chem. Phys., 9, 7461–7479, 2009, http://www.atmos-chem-phys.net/9/7461/2009/.

Thornberry, T. and Abbatt, J. P. D.: Heterogeneous reaction of ozone with liquid unsaturated fatty acids: detailed kinetics and gas-phase product studies, Phys. Chem. Chem. Phys., 6, 84–93, 2004.

Titov, V. N., Konovalova, G. G., Lisitsyn, D. M., Razumovskii, S. D., Nezhdanova, I. B., and Kukharchuk, V. V.: Kinetics of fatty acid oxidation in low density lipoproteins evaluated by registration of the oxidizer consumption and reaction product yield, Bull. Exp. Biol. Med., 140, 38–40, 2005.

Vesna, O., Kalberer, M., and Ammann, M.: Formation of hydrogen peroxide in the ozonolysis of mixed oleic acid – NaCl aerosol particles under humid conditions. Abstracts of Papers, 235th ACS National Meeting, New Orleans, LA, United States, 6–10 April, 2008a.

Vesna, O., Sjogren, S., Weingartner, E., Samburova, V., Kalberer, M., Gäggeler, H. W., and Ammann, M.: Changes of fatty acid aerosol hygroscopicity induced by ozonolysis under humid conditions, Atmos. Chem. Phys., 8, 4683–4690, 2008b, http://www.atmos-chem-phys.net/8/4683/2008/.

Vesna, O., Sax, M., Kalberer, M., Gaschen, A., Ammann, M.: Product study of oleic acid ozonolysis as function of humidity, Atmos. Environ., 43, 3662–3669, 2009.

Vieceli, J., Ma, O. L., and Tobias, D. J.: Uptake and Collision Dynamics of Gas Phase Ozone at Unsaturated Organic Interfaces, J. Phys. Chem. A, 108, 5806–5814, 2004.

Vieceli, J., Roeselova, M., Potter, N., Dang, L. X., Garrett, B. C., and Tobias, D. J.: Molecular dynamics simulations of atmospheric oxidants at the air-water interface: Solvation and accommodation of OH and O_3, J. Phys. Chem. B, 109, 15876–15892, 2005.

Voss, L. F., Bazerbashi, M. F., Beekman, C. P., Hadad, C. M., and Allen, H. C.: Oxidation of oleic acid at air/liquid interfaces, J. Geophys. Res.-Atmos., 112(D6), D06209/1–D06209/9, doi:10.1029/2006JD007677, 2007.

Wayne, R. P.: Chemistry of Atmospheres, third ed., Oxford University Press, Oxford, 2000.

Worsnop, D. R., Morris, J. W., Shi, Q., Davidovits, P., and Kolb., C. E.: A chemical kinetic model for reactive transfor-

mations of aerosol particles, Geophys. Res. Lett., 29, 1996, doi:10.1029/2002GL015542, 2002.

Zahardis, J. and Petrucci, G. A.: The oleic acid-ozone heterogeneous reaction system: products, kinetics, secondary chemistry, and atmospheric implications of a model system – a review, Atmos. Chem. Phys., 7, 1237–1274, 2007, http://www.atmos-chem-phys.net/7/1237/2007/.

Ziemann, P. J.: Aerosol products, mechanisms, and kinetics of heterogeneous reactions of ozone with oleic acid in pure and mixed particles, Faraday Discuss., 130, 469–490, 2005.

B3) Shiraiwa et al., Atmos. Chem. Phys., 2010

Kinetic multi-layer model of aerosol surface and bulk chemistry (KM-SUB): the influence of interfacial transport and bulk diffusion on the oxidation of oleic acid by ozone

Manabu Shiraiwa[1], Christian Pfrang[1,2], and Ulrich Pöschl[1]

1. Max Planck Institute for Chemistry, Department of Biogeochemistry
J.J. Becherweg 27/29, D55128, Mainz, Germany
2. University of Reading, Department of Chemistry, P. O. BOX 224, Whiteknights, Reading RG6 6AD, UK

Atmospheric Chemistry and Physics 10(8): 3673-3691, 2010.

Authors contributions.

MS and UP designed research. MS performed kinetic modeling. CP contributed analyzing data. MS and UP wrote the paper.

Atmos. Chem. Phys., 10, 3673–3691, 2010
www.atmos-chem-phys.net/10/3673/2010/

Atmospheric Chemistry and Physics

Kinetic multi-layer model of aerosol surface and bulk chemistry (KM-SUB): the influence of interfacial transport and bulk diffusion on the oxidation of oleic acid by ozone

M. Shiraiwa[1], **C. Pfrang**[1,2], **and U. Pöschl**[1]

[1]Max Planck Institute for Chemistry, Biogeochemistry Department, P.O. Box 3060, 55128 Mainz, Germany
[2]University of Reading, Department of Chemistry, P.O. Box 224, Whiteknights, Reading RG6 6AD, UK

Received: 17 December 2009 – Published in Atmos. Chem. Phys. Discuss.: 8 January 2010
Revised: 8 April 2010 – Accepted: 9 April 2010 – Published: 20 April 2010

Abstract. We present a novel kinetic multi-layer model that explicitly resolves mass transport and chemical reaction at the surface and in the bulk of aerosol particles (KM-SUB). The model is based on the PRA framework of gas-particle interactions (Pöschl-Rudich-Ammann, 2007), and it includes reversible adsorption, surface reactions and surface-bulk exchange as well as bulk diffusion and reaction. Unlike earlier models, KM-SUB does not require simplifying assumptions about steady-state conditions and radial mixing. The temporal evolution and concentration profiles of volatile and non-volatile species at the gas-particle interface and in the particle bulk can be modeled along with surface concentrations and gas uptake coefficients.

In this study we explore and exemplify the effects of bulk diffusion on the rate of reactive gas uptake for a simple reference system, the ozonolysis of oleic acid particles, in comparison to experimental data and earlier model studies. We demonstrate how KM-SUB can be used to interpret and analyze experimental data from laboratory studies, and how the results can be extrapolated to atmospheric conditions. In particular, we show how interfacial and bulk transport, i.e., surface accommodation, bulk accommodation and bulk diffusion, influence the kinetics of the chemical reaction. Sensitivity studies suggest that in fine air particulate matter oleic acid and compounds with similar reactivity against ozone (carbon-carbon double bonds) can reach chemical lifetimes of many hours only if they are embedded in a (semi-)solid matrix with very low diffusion coefficients ($\leq 10^{-10}$ cm^2 s^{-1}).

Depending on the complexity of the investigated system, unlimited numbers of volatile and non-volatile species and chemical reactions can be flexibly added and treated with KM-SUB. We propose and intend to pursue the application of KM-SUB as a basis for the development of a detailed master mechanism of aerosol chemistry as well as for the derivation of simplified but realistic parameterizations for large-scale atmospheric and climate models.

Correspondence to: U. Pöschl
(u.poschl@mpic.de)

1 Introduction

Aerosols are ubiquitous in the atmosphere and have strong effects on climate and public health (Seinfeld and Pandis, 1998; Finlayson-Pitts and Pitts, 2000; Pöschl, 2005). Depending on chemical composition and surface properties, aerosol particles can act as condensation nuclei for cloud droplets and ice crystals, and they can affect the abundance of trace gases through heterogeneous chemical reactions (Ammann et al., 1998; Pöschl, 2005; Fuzzi et al., 2006; Andreae and Rosenfeld, 2008; Hallquist et al., 2009). Gas-particle interactions can also significantly change the physical and chemical properties of aerosols such as toxicity, reactivity, hygroscopicity and radiative properties (Pöschl, 2002; Rudich, 2003; Kanakidou et al., 2005; Rincon et al., 2009; Wiedensohler et al., 2009). Chemical reactions and mass transport lead to continuous transformation and changes in the composition of atmospheric aerosols ("chemical aging") (Schwartz and Freiberg, 1981; Hanson, 1997; Smith et al., 2003; Ammann and Pöschl, 2007).

Atmospheric particles consist of a wide variety of organic and inorganic chemical compounds which can exist in different liquid or (semi-)solid states (crystalline, amorphous,

glassy, ultraviscous, gel-like) (Seinfeld and Pandis, 1998; Finlayson-Pitts and Pitts, 2000; Mikhailov et al., 2009). Chemical reactions can occur both at the surface and in the bulk of liquid and (semi-)solid particles. It is often difficult to discriminate surface and bulk reactions, and the relative importance of surface and bulk processes is not well understood (e.g., Moise and Rudich, 2000; Hearn et al., 2005; Pfrang et al., 2009). Resistor model formulations are widely used to describe and investigate heterogeneous reactions and multiphase processes in laboratory, field and model studies of atmospheric chemistry (Hanson, 1997; Finlayson-Pitts and Pitts, 2000; Worsnop et al., 2002; Anttila et al., 2006; King et al., 2008, 2009; and references therein). The traditional resistor models, however, are usually based on simplifying assumptions such as steady-state conditions, homogeneous mixing, and limited numbers of non-interacting species and processes.

In order to overcome these limitations, Pöschl, Rudich and Ammann have developed a kinetic model framework (PRA framework) with a double-layer surface concept and universally applicable rate equations and parameters for mass transport and chemical reactions at the gas-particle interface of aerosols and clouds (Pöschl et al., 2007). Ammann and Pöschl (2007) provided first examples on how the PRA framework can be applied to describe various physicochemical processes in aerosols and clouds such as reactive gas uptake on solid particles and solubility saturation of liquid droplets under transient or steady-state conditions. Springmann et al. (2009) demonstrated the applicability and usefulness of the PRA framework in an urban plume box model of the degradation of benzo[a]pyrene on soot by ozone and nitrogen dioxide. Shiraiwa et al. (2009) presented a kinetic double-layer surface model (K2-SURF) and master mechanism for the degradation of a wide range of polycyclic aromatic hydrocarbons (PAHs) by multiple photo-oxidants (O_3, NO_2, OH and NO_3) through different types of parallel and sequential surface reactions. Pfrang et al. (2009) developed a kinetic double-layer model coupling aerosol surface and bulk chemistry (K2-SUB), in which mass transport and chemical reactions in the particle are not explicitly resolved but represented by a reacto-diffusive flux (Danckwerts, 1951; Hanson, 1997).

Here we present a kinetic multi-layer model of aerosol surface and bulk chemistry (KM-SUB) that explicitly treats all steps of mass transport and chemical reaction from the gas-particle interface to the particle core, resolving concentration gradients and diffusion throughout the particle bulk. We demonstrate the applicability of KM-SUB for a common model system of organic aerosol chemistry, the ozonolysis of oleic acid droplets (e.g., Moise and Rudich, 2002; Katrib et al., 2004, 2005; King et al., 2004, 2009; Knopf et al., 2005; Ziemann, 2005; Hearn and Smith, 2007; Pfrang et al., 2009; Sage et al., 2009; Vesna et al., 2009), and we compare the results of our numerical simulations with the results of earlier experimental and theoretical studies of this system.

2 Model description

The kinetic multi-layer model of aerosol surface and bulk chemistry (KM-SUB) builds on the formalism and terminology of the PRA framework (Ammann and Pöschl, 2007; Pöschl et al., 2007). A list of symbols is given in Appendix A.

As illustrated in Fig. 1, KM-SUB consists of multiple model compartments and layers, respectively: gas phase, near-surface gas phase, sorption layer, quasi-static surface layer, near-surface bulk, and a number of n bulk layers. The quasi-static surface layer has a monolayer thickness that corresponds to the (average) effective molecular diameter of non-volatile species Y_j (δ_{Y_j}). The thickness of bulk layers (δ) follows from the number of layers (n) and particle radius (r_p) : $\delta = (r_p - \delta_{Y_j})/n$.

The following processes are considered in KM-SUB: gas phase diffusion, gas-surface transport (reversible adsorption), surface layer reactions, surface-bulk transport, bulk diffusion, and bulk reactions. As outlined in the PRA framework, the following differential equations can be used to describe the mass balance of volatile species X_i and non-volatile species Y_j for each model layer:

$$\mathrm{d}[X_i]_s/\mathrm{d}t = J_{ads,X_i} - J_{des,X_i} + P_{s,X_i} - L_{s,X_i} - J_{s,b,X_i} + J_{b,s,X_i} \quad (1)$$

$$\mathrm{d}[Y_j]_{ss}/\mathrm{d}t = J_{b,ss,Y_j} - J_{ss,b,Y_j} + P_{ss,Y_j} - L_{ss,Y_j} \quad (2)$$

$$\mathrm{d}[X_i]_{b1}/\mathrm{d}t = (J_{s,b,X_i} - J_{b,s,X_i})A(1)/V(1) - (J_{b1,b2,X_i} - J_{b2,b1,X_i})A(2)/V(1) + P_{b1,X_i} - L_{b1,X_i} \quad (3)$$

$$\mathrm{d}[Y_j]_{b1}/\mathrm{d}t = (J_{ss,b,Y_j} - J_{b,ss,Y_j})A(1)/V(1) - (J_{b1,b2,Y_j} - J_{b2,b1,Y_j})A(2)/V(1) + P_{b1,Y_j} - L_{b1,Y_j} \quad (4)$$

$$\mathrm{d}[X_i]_{bk}/\mathrm{d}t = (J_{bk-1,bk,X_i} - J_{bk,bk-1,X_i})A(k)/V(k) - (J_{bk,bk+1,X_i} - J_{bk+1,bk,X_i})A(k+1)/V(k) + P_{bk,X_i} - L_{bk,X_i} \quad (k = 2,...,n-1) \quad (5)$$

$$\mathrm{d}[Y_j]_{bk}/\mathrm{d}t = (J_{bk-1,bk,Y_j} - J_{bk,bk-1,Y_j})A(k)/V(k) - (J_{bk,bk+1,Y_j} - J_{bk+1,bk,Y_j})A(k+1)/V(k) + P_{bk,Y_j} - L_{bk,Y_j} \quad (k = 2,...,n-1) \quad (6)$$

$$\mathrm{d}[X_i]_{bn}/\mathrm{d}t = (J_{bn-1,bn,X_i} - J_{bn,bn-1,X_i})A(n)/V(n) + P_{bn,X_i} - L_{bn,X_i} \quad (7)$$

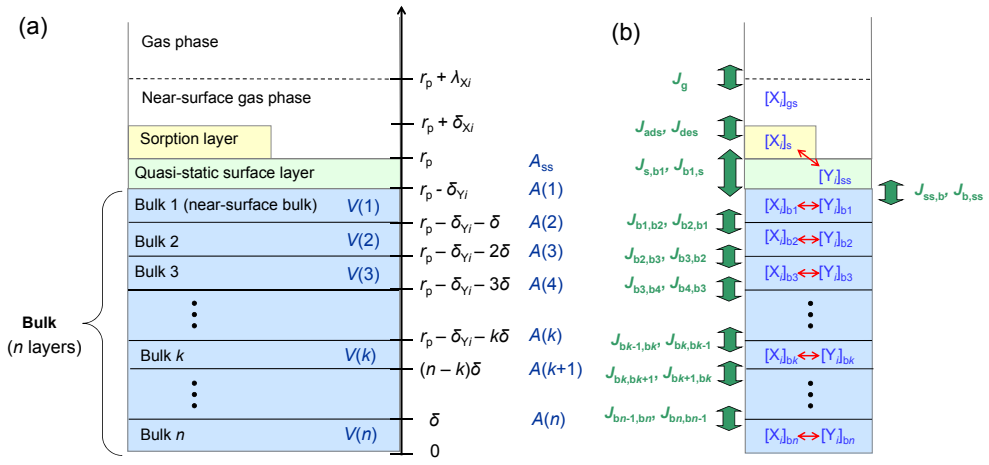

Fig. 1. Kinetic multi-layer model (KM-SUB): **(a)** Model compartments and layers with corresponding distances from particle center ($r_p \pm x$), surface areas (A) and volumes (V); λ_{X_i} is the mean free path of X_i in the gas phase; δ_{X_i} and δ_{Y_j} are the thicknesses of sorption and quasi-static bulk layers; δ is the bulk layer thickness. **(b)** Transport fluxes (green arrows) and chemical reactions (red arrows).

$$d[Y_j]_{bn}/dt = (J_{bn-1,bn,Y_j} - J_{bn,bn-1,Y_j})A(n)/V(n) + P_{bn,Y_j} - L_{bn,Y_j} \quad (8)$$

The various types of mass transport fluxes (J) and rates of chemical production and loss (P, L) are defined in the list of symbols (Table A1). $A(k)$ and $V(k)$ are the outer surface area and the volume of the bulk layer k, respectively (Fig. 1). For spherical particles, $A(k)$ and $V(k)$ can be calculated from the particle bulk radius ($r_b = r_p - \delta_{Y_j}$), bulk layer thickness (δ) and layer index number k as follows.

$$V(k) = \frac{4}{3}\pi\left[(r_b - (k-1)\delta)^3 - (r_b - k\delta)^3\right] \quad (9)$$

$$A(k) = 4\pi\,(r_b - (k-1)\delta)^2 \quad (10)$$

For planar geometry (thin films), the surface-to-volume ratio is constant:

$$A(k)/V(k) = 1/\delta \quad (11)$$

The surface-to-volume ratios of the layers play an important role in accounting for particle geometry. The absolute number of non-volatile molecules Y_j in the particle (N_{Y_j}) can be calculated as follows:

$$N_{Y_j} = [Y_j]_{ss}A_{ss} + \sum_{k=1}^{n}[Y_j]_{bk}V(k) \quad (12)$$

where A_{ss} is the surface area of the particle. In the following sub-sections we specify the formalisms used to describe and calculate fluxes or rates of gas-surface interactions, surface-bulk transport, bulk diffusion and bulk reactions.

2.1 Gas-surface interactions and surface layer reactions

The principles and details of gas-phase and gas-surface transport (J_{ads}, J_{des}) and surface layer reactions (L_s, L_{ss} P_s, P_{ss}) have been discussed and illustrated in the PRA framework (Pöschl et al., 2007; Ammann and Pöschl, 2007) and in the K2-SURF study of aerosol surface chemistry (Shiraiwa et al., 2009). Here we just briefly summarize the key aspects and equations. The fluxes of surface collisions, adsorption and desorption of a volatile species X_i (J_{coll,X_i}, J_{ads,X_i} and J_{des,X_i}) are given by:

$$J_{coll,X_i} = [X_i]_{gs}\omega_{X_i}/4 \quad (13)$$

$$J_{ads,X_i} = \alpha_{s,X_i}J_{coll,X_i} \quad (14)$$

$$J_{des,X_i} = k_{d,X_i}[X_i]_s \quad (15)$$

$$\alpha_{s,X_i} = \alpha_{s,0,X_i}(1-\theta_s) \quad (16)$$

$$\theta_s = \sum_i \sigma_{s,X_i}[X_i]_s \quad (17)$$

$[X_i]_{gs}$ is the near-surface gas phase concentration of X_i, ω_{X_i} is the mean thermal velocity, α_{s,X_i} is the surface accommodation coefficient, and k_{d,X_i} is the desorption rate coefficient or inverse desorption lifetime, respectively ($k_{d,X_i} = \tau_{d,X_i}^{-1}$). $\alpha_{s,0,X_i}$ is the surface accommodation coefficient on an adsorbate-free surface, σ_{s,X_i} is the effective molecular cross section of X_i in the sorption layer, and θ_s is the surface coverage by adsorbed species.

The influence of changing chemical composition of the quasi-static particle surface on adsorbate-surface interactions (reversible adsorption) can be taken into account by describing $\alpha_{s,0,X_i}$ and τ_{d,X_i} as a linear combination of the parameter values $\alpha_{s,0,X_i,Y_j}$ and τ_{d,X_i,Y_j} that would be observed on pure

substrates made up by the different surface components Y_j weighted by their fractional surface area θ_{ss,Y_j} (Pöschl et al., 2007):

$$\alpha_{s,0,X_i} = \sum_j \alpha_{s,0,X_i,Y_j} \theta_{ss,Y_j} \quad (18)$$

$$\tau_{d,X_i} = \sum_j \tau_{d,X_i,Y_j} \theta_{ss,Y_j} \quad (19)$$

For slow gas uptake and in the gas kinetic-regime (small uptake coefficient, large Knudsen number), $[X_i]_{gs}$ is practically the same as the average gas phase concentration of X_i in the investigated system, $[X_i]_g$. For rapid gas uptake in the continuum or transition regime (large uptake coefficient, small Knudsen number), the gas phase diffusion correction factor C_{g,X_i} can be used to calculate $[X_i]_{gs}$ from $[X_i]_g : [X_i]_{gs} = C_{g,X_i}[X_i]_g$ (Pöschl et al., 2007; Shiraiwa et al., 2009). The uptake coefficient (γ_{X_i}) for X_i is given by:

$$\gamma_{X_i} = \frac{J_{ads,X_i} - J_{des,X_i}}{J_{coll,X_i}} + \gamma_{gsr,X_i} \quad (20)$$

γ_{gsr,X_i} is the reaction probability for elementary gas-surface reactions (potentially relevant for free radicals but assumed to be zero in the remainder of this study).

General rate equations of chemical production and loss by surface layer reactions (P_{s,X_i}, P_{ss,Y_i}, L_{s,X_i}, L_{ss,Y_i}) are specified in the PRA framework (Sect. 3.3, Pöschl et al., 2007). Different types of surface layer reactions can proceed within the sorption layer ($P_{s,s,X_i} - L_{s,s,X_i}$), within the quasi-static surface layer ($P_{ss,ss,Y_j} - L_{ss,ss,Y_j}$), and between sorption layer and quasi-static layer ($P_{s,ss,X_i} - L_{s,ss,X_i}$, $P_{ss,s,Y_j} - L_{ss,s,Y_j}$). The generalized rate equations for reactions between volatile species X_i in the sorption layer and non-volatile species Y_j in the quasi-static layer are given by:

$$P_{s,ss,X_i} - L_{s,ss,X_i} = \sum_v \sum_p \sum_q c_{SLRv,s,X_i} k_{SLRv,X_p,Y_q} [X_p]_s [Y_q]_{ss} \quad (21)$$

$$P_{ss,ss,Y_j} - L_{ss,ss,Y_j} = \sum_v \sum_p \sum_q c_{SLRv,ss,Y_j} k_{SLRv,X_p,Y_q} [X_p]_s [Y_q]_{ss} \quad (22)$$

Here c_{SLRv,s,X_i} and c_{SLRv,ss,Y_j} stand for the stoichiometric coefficients (negative for starting materials and positive for reaction products) of species X_i and Y_j in reaction SLRv; v=1, …, v_{max} in a system with a total number of v_{max} (photo-)chemical reactions occurring on the surface of the investigated aerosol particles. $k_{SLRv,Xp,Yq}$ is a second-order reaction rate coefficient. In the exemplary simulations of the ozonolysis of oleic acid performed in this study and presented in Sect. 3, we consider only chemical loss and a second-order surface layer reaction between O_3 (X) and oleic acid (Y) with the following rate equation:

$$L_{s,X} = L_{ss,Y} = k_{SLR,X,Y} [X]_s [Y]_{ss} \quad (23)$$

2.2 Surface-bulk transport

The surface-bulk transport of volatile species X_i (J_{s,b,X_i} and J_{b,s,X_i}) is defined as exchange between sorption layer and near-surface bulk, and the surface-bulk transport of non-volatile species Y_j (J_{ss,b,Y_j} and J_{b,ss,Y_j}) is defined as exchange between quasi-static surface layer and near-surface bulk. Based on the PRA framework, surface to bulk transport can be described by:

$$J_{s,b,X_i} = k_{s,b,X_i} [X_i]_s \quad (24)$$

$$J_{ss,b,Y_j} = k_{ss,b,Y_j} [Y_j]_{ss} \quad (25)$$

k_{s,b,X_i} and k_{ss,b,Y_j} are first-order transport rate coefficients (s^{-1}) of X_i and Y_j, respectively. In the same way, bulk to surface transport (J_{b,s,X_i} and J_{b,ss,Y_j}) can be described as follows:

$$J_{b,s,X_i} = k_{b,s,X_i} [X_i]_{b1} \quad (26)$$

$$J_{b,ss,Y_j} = k_{b,ss,Y_j} [Y_j]_{b1} \quad (27)$$

k_{b,s,X_i} and k_{b,ss,Y_j} (cm s^{-1}) are transport rate coefficients, which can be regarded as effective transport velocities. Estimates for these effective transport velocities can be derived from the corresponding bulk diffusion coefficients D_{b,X_i} and D_{b,Y_j} ($cm^2\ s^{-1}$) by considering the average distance traveled by molecules diffusing in one direction: $x = (4D_b t/\pi)^{1/2}$ (Atkins, 1998; Pfrang et al., 2009), On average, a molecule Y_j in the near-surface bulk layer ($k = 1$) needs to travel a distance of $x \approx (\delta + \delta_{Y_j})/2$ to move into the quasi-static surface layer. The average time required to travel over this distance by diffusion is $t = (\delta + \delta_{Y_j})^2 \pi / (16 D_{b,Y_j})$. By division of travel distance over travel time we obtain the following estimate for the effective transport velocity:

$$k_{b,ss,Y_j} \approx 8 D_{b,Y_j} / ((\delta + \delta_{Y_j})\pi) \quad (28)$$

Under equilibrium conditions, mass conservation implies $k_{b,ss,Y_j}[Y_j]_{b1} = k_{ss,b,Y_j}[Y_j]_{ss}$, and for pure Y_j the surface and bulk concentrations are given by the inverse of the effective molecular cross section and of the effective molecular volume, respectively: $[Y_j]_{ss} = \delta_{Y_j}^{-2}$ and $[Y_j]_{b1} = \delta_{Y_j}^{-3}$. Thus, we obtain

$$k_{ss,b,Y_j} \approx k_{b,ss,Y_j} / \delta_{Y_j} \approx 8 D_{b,Y_j} / ((\delta + \delta_{Y_j}) \delta_{Y_j} \pi) \quad (29)$$

In analogy, the bulk-to-surface transport velocity of X_i can be calculated for an average travel distance of $x \approx (\delta + \delta_{X_i} + 2\delta_{Y_j})/2$ from the near-surface bulk layer into the sorption layer:

$$k_{b,s,X_i} \approx 8 D_{b,X_i} / ((\delta + \delta_{X_i} + 2\delta_{Y_j})\pi) \quad (30)$$

An estimate for k_{s,b,X_i} can be determined by matching the rate coefficients for gas-surface and surface-bulk transport

with a literature value or estimate for the gas-particle equilibrium partitioning coefficient ($K_{\mathrm{sol,cc,X}_i}$) or Henry's law coefficient, respectively (Pöschl et al., 2007):

$$k_{\mathrm{s,b,X}_i} = \frac{4k_{\mathrm{b,s,X}_i} K_{\mathrm{sol,cc,X}_i} k_{\mathrm{d,X}_i}}{\alpha_{\mathrm{s,X}_i} \omega_{\mathrm{X}_i}} \quad (31)$$

where $k_{\mathrm{d,X}_i}$ is the first-order rate coefficient of desorption. From the fluxes and rates of gas-surface transport, surface-bulk transport and surface reaction follows the bulk accomodation coefficient of X_i:

$$\alpha_{\mathrm{b,X}_i} = \alpha_{\mathrm{s,X}_i} \frac{J_{\mathrm{s,b,X}_i}}{J_{\mathrm{des,X}_i} + J_{\mathrm{s,b,X}_i} + L_{\mathrm{s,X}_i}} \quad (32)$$

2.3 Bulk diffusion

Bulk diffusion is explicitly treated in the KM-SUB model as the mass transport ($J_{\mathrm{b}k,\mathrm{b}k\pm1}$) from one bulk layer (bulk k) to the next (bulk $k \pm 1$). In analogy to surface–bulk mass transport, we describe the mass transport fluxes between different layers of the bulk by first-order rate equations:

$$J_{\mathrm{b}k,\mathrm{b}k\pm1,\mathrm{X}_i} = k_{\mathrm{b,b,X}_i}[\mathrm{X}_i]_{\mathrm{b}k} \quad (33)$$

$$J_{\mathrm{b}k,\mathrm{b}k\pm1,\mathrm{Y}_j} = k_{\mathrm{b,b,Y}_j}[\mathrm{Y}_j]_{\mathrm{b}k} \quad (34)$$

Estimates for the transport rate coefficients or effective velocities of X_i and Y_j, $k_{\mathrm{b,b,X}_i}$ and $k_{\mathrm{b,b,Y}_j}$ ($\mathrm{cm\,s^{-1}}$), can be calculated from the corresponding diffusion coefficients. For this purpose we assume that each layer is homogeneously mixed (no concentration gradient within a layer) and that the average travel distance for molecules moving from one layer to the next is the layer thickness δ:

$$k_{\mathrm{b,b,X}_i} = 4D_{\mathrm{b,X}_i}/(\pi\delta) \quad (35)$$

$$k_{\mathrm{b,b,Y}_j} = 4D_{\mathrm{b,Y}_j}/(\pi\delta) \quad (36)$$

This treatment of bulk diffusion yields practically the same results (concentration profiles) as the solving of partial differential equations (Smith et al., 2003), but it is more flexible and requires no assumptions about interfacial transport. As detailed in Appendix B, the ozone concentrations calculated for the near-surface bulk indicate that the assumption of Henry's law equilibrium is not a realistic boundary layer condition for the PDE method when applied to reactive systems.

The influence of changing chemical composition of the particle bulk on diffusion can be taken into account by describing $D_{\mathrm{b,X}_i}$ or $D_{\mathrm{b,Y}_j}$ as a linear combination of the parameter values that would be observed in pure bulk Y_p:

$$D_{\mathrm{b,X}_i} = \sum_p D_{\mathrm{b,X}_i,\mathrm{Y}_p} \Phi_{\mathrm{b,Y}_p} \quad (37)$$

$$D_{\mathrm{b,Y}_j} = \sum_p D_{\mathrm{b,Y}_j,\mathrm{Y}_p} \Phi_{\mathrm{b,Y}_p} \quad (38)$$

The weighting factor $\Phi_{\mathrm{b,Y}_p}$ could be the mole, mass, or volume fraction of Y_p in the bulk (Pöschl et al., 2007).

2.4 Bulk reaction

Chemical reactions proceeding within the bulk of a particle are defined as bulk reactions (BR). For simplicity, we assume that all relevant bulk reactions proceed via quasi-elementary steps with straightforward first- or second-order rate dependences on the concentrations within each bulk layer. The following generalized expressions can be used to describe net chemical production (i.e. production minus loss) of bulk species X_i or Y_j within the bulk layer k.

$$P_{\mathrm{b}k,\mathrm{X}_i} - L_{\mathrm{b}k,\mathrm{X}_i} = \sum_v \sum_p c_{\mathrm{BR}v,\mathrm{X}_i} [\mathrm{X}_p]_{\mathrm{b}k} \left(k_{\mathrm{BR}v,\mathrm{X}_p} + \sum_q k_{\mathrm{BR}v,\mathrm{X}_p,\mathrm{X}_q} [\mathrm{X}_q]_{\mathrm{b}k} + \sum_r k_{\mathrm{BR}v,\mathrm{X}_p,\mathrm{Y}_r} [\mathrm{Y}_r]_{\mathrm{b}k} \right) \quad (39)$$

$$P_{\mathrm{b}k,\mathrm{Y}_j} - L_{\mathrm{b}k,\mathrm{Y}_j} = \sum_v \sum_p c_{\mathrm{BR}v,\mathrm{Y}_j} [\mathrm{Y}_p]_{\mathrm{b}k} \left(k_{\mathrm{BR}v,\mathrm{Y}_p} + \sum_q k_{\mathrm{BR}v,\mathrm{Y}_p,\mathrm{Y}_q} [\mathrm{Y}_q]_{\mathrm{b}k} + \sum_r k_{\mathrm{BR}v,\mathrm{X}_r,\mathrm{Y}_p} [\mathrm{X}_r]_{\mathrm{b}k} \right) \quad (40)$$

Here $c_{\mathrm{BR}v,\mathrm{X}_i}$ and $c_{\mathrm{BR}v,\mathrm{Y}_j}$ stand for the stoichiometric coefficients (negative for starting materials and positive for reaction products) of species X_i and Y_j in reaction BRv; v=1, …, $v_{\max}$ in a system with a total number of $v_{\max}$ chemical reactions occurring in the bulk layer k. $k_{\mathrm{BR}v,\mathrm{X}p}$ and $k_{\mathrm{BR}v,\mathrm{Y}p}$ are first-order reaction rate coefficients and $k_{\mathrm{BR}v,\mathrm{X}p,\mathrm{X}q}$, $k_{\mathrm{BR}v,\mathrm{X}p,\mathrm{Y}r}$, $k_{\mathrm{BR}v,\mathrm{Y}p,\mathrm{Y}q}$ and $k_{\mathrm{BR}v,\mathrm{X}r,\mathrm{Y}p}$ are second-order bulk reaction rate coefficients between X_p and X_q, X_p and Y_r, Y_p and Y_q, and X_r and Y_p respectively, in the condensed phase bulk of a system with multiple volatile species which can react with each other. In principle, higher-order reactions might also occur in real systems and could be flexibly included in the model. In the exemplary simulations of the ozonolysis of oleic acid performed in this study and presented in Sect. 3, we consider only chemical loss and a second-order bulk reaction between $\mathrm{O_3}$ (X) and oleic acid (Y) with the following rate equation:

$$L_{\mathrm{b}k,\mathrm{X}} = L_{\mathrm{b}k,\mathrm{Y}} = k_{\mathrm{BR,X,Y}}[\mathrm{X}]_{\mathrm{b}k}[\mathrm{Y}]_{\mathrm{b}k} \quad (41)$$

3 Model application: oxidation of oleic acid by ozone

To test and demonstrate the applicability of the KM-SUB model, we simulated the oxidation of oleic acid particles by ozone in comparison to experimental data from Ziemann (2005). The same data set has recently been used by Pfrang et al. (2009) for simulations with a kinetic double-layer model (K2-SUB; Appendix C). The gas phase ozone concentration was set to $[\mathrm{X}]_{\mathrm{g}} = [\mathrm{X}]_{\mathrm{gs}} = 7.0 \times 10^{13}\,\mathrm{cm^{-3}}$ (corresponding to 2.8 ppm at 1013 hPa and 298 K). The initial surface and bulk concentrations of ozone (X) were set to

Table 1. Kinetic parameters for the interaction of ozone (X) and oleic acid (Y) in different model scenarios (base cases 1–3).

Parameter	Base case 1	Base case 2	Base case 3
$\alpha_{s,0,X}$	4.2×10^{-4}	8.5×10^{-4}	4.2×10^{-4}
$\tau_{d,X}$ (s)	0.01	0.001	0.01
$D_{b,X}$ ($cm^2\,s^{-1}$)	10^{-5}	10^{-5}	10^{-10}
$D_{b,Y}$ ($cm^2\,s^{-1}$)	10^{-10}	10^{-10}	10^{-15}
$k_{SLR,X,Y}$ ($cm^2\,s^{-1}$)	6.0×10^{-12}	6.0×10^{-12}	6.0×10^{-12}
$k_{BR,X,Y}$ ($cm^3\,s^{-1}$)	1.7×10^{-15}	5.0×10^{-17}	1.7×10^{-15}

$[X]_{s,0} = [X]_{bk,0} = 0$, and the initial surface and bulk concentrations of oleic acid (Y) were set to $[Y]_{ss,0}$=9.7×10^{13} cm^{-2} and $[Y]_{ss,0}$=1.2×10^{21} cm^{-3}, respectively. Accordingly, the initial value of the total number of oleic acid molecules in particles with a radius of 0.2 µm was $N_{Y,0} = 4.1\times10^7$.

We modeled the temporal evolution of the particle surface and bulk composition and of the ozone uptake coefficient by numerically solving the differential equations of mass balance for each model compartment with Matlab software (ode23tb solver with 999 time steps). The rate equations describing the ozone – oleic acid reaction system are listed in Appendix D. The kinetic parameters required for the model simulations are summarized in Table 1: the surface accommodation coefficient of ozone ($\alpha_{s,0,X}$), the desorption lifetime of ozone ($\tau_{d,X}$), the bulk diffusion coefficients of ozone and oleic acid ($D_{b,X}$, $D_{b,Y}$), the second-order surface layer reaction rate coefficient ($k_{SLR,X,Y}$), and the second-order bulk reaction rate coefficient ($k_{BR,X,Y}$). Additional input parameters were the mean thermal velocity of ozone ($\omega_X = 3.6\times10^4\,cm\,s^{-1}$), the Henry's law coefficient ($K_{sol,cc,X} = 4.8\times10^{-4}\,mol\,cm^{-3}\,atm^{-1}$), and the molecular diameters of oleic acid ($\delta_Y = 0.8$ nm) and ozone ($\delta_X = 0.4$ nm) (Pfrang et al., 2009). The model simulations were performed with $n = 100$ layers corresponding to a layer thickness of $\delta = 1.99$ nm for r_p =0.2 µm, unless mentioned otherwise. For simplicity the physico-chemical parameters were assumed to be constant throughout each model run.

The first-generation products of oleic acid oxidation by ozone are mainly 1-nonanal, 9-oxononanoic acid, nonanoic acid, and azelaic acid (Moise and Rudich, 2002; Katrib et al., 2004; Thornberry and Abbatt, 2004; Vesna et al., 2009). 1-Nonanal is highly volatile and likely to evaporate from the particle (Sage et al., 2009). The other products, however, have higher molecular masses and are more polar, less volatile and likely to remain in the condensed phase (Jimenez et al., 2009). Moreover, they may undergo recombination reactions forming second-generation products of higher molecular mass such as dimers or oligomers in the bulk (Rudich et al., 2007, and references therein). These effects go beyond the scope of the present study, but the gas-particle partitioning of (semi-)volatile species and the effects of chemical transformation on particle size and properties shall be incorporated in follow-up studies.

Here we focus on three model scenarios (base cases) characterizing the influence of different parameters and conditions on the uptake of ozone and the decay of oleic acid. The derivation and choice of kinetic parameters were discussed in detail by Pfrang et al. (2009). In view of the uncertainties and limited availability of experimental data we compare three cases covering a range of plausible parameter variations.

In base case 1 (BC1, kinetic limitation by interfacial transport) we assumed fast bulk reaction with a literature-derived rate coefficient of $k_{BR,X,Y} = 1.7\times10^{-15}\,cm^3\,s^{-1}$ (equivalent to $10^6\,L\,mol^{-1}\,s^{-1}$) (Titov et al., 2005). The surface reaction rate coefficient $k_{SLR,X,Y} = 6\times10^{-12}\,cm^2\,s^{-1}$ was adopted from Pfrang et al. (2009). Note that this value is an order of magnitude lower than reported value by other studies (Gonzalez-Labrada et al., 2007; King et al., 2009). Bulk diffusion coefficients were adopted from earlier studies ($D_{b,X} = 10^{-5}\,cm^2\,s^{-1}$, $D_{b,Y} = 10^{-10}\,cm^2\,s^{-1}$) (Smith et al., 2002, 2003), and the parameters of reversible adsorption were adjusted to match the experimental data of oleic acid decay ($\alpha_{s,0,X} = 4.2\times10^{-4}$ and $\tau_{d,X} = 0.01$ s).

In base case 2 (BC2, kinetic limitation by bulk reaction) we assumed slow bulk reaction with a rate coefficient ~30 times lower than in BC1 ($k_{BR,X,Y} = 5\times10^{-17}\,cm^3\,s^{-1}$). The adsorption parameters were re-adjusted to match the experimental data ($\alpha_{s,0,X} = 8.5\times10^{-4}$, $\tau_{d,X} = 0.001$ s), and all other parameters were kept equal to BC1. Note that in BC1 and BC2 the results can be reproduced with different combinations of $\alpha_{s,0,X}$ and $\tau_{d,X}$, that are closer to prediction of molecular dynamic simulations (e.g., $\alpha_{s,0,X} \approx 10^{-2}$ and $\tau_{d,X} \approx 10^{-9}$ s) (Vieceli et al., 2005; Shiraiwa et al., 2009). These aspects will be further investigated in follow-up studies.

In base case 3 (BC3, kinetic limitation by bulk diffusion) we assumed slow mass transport in the bulk with diffusion coefficients that are characteristic for amorphous (semi-)solid matrices (Bird et al., 2007; Swallen et al., 2007; Mikhailov et al., 2009) and five orders of magnitude lower than in BC1 and BC2 ($D_{b,X} = 10^{-10}\,cm^2\,s^{-1}$ and $D_{b,Y} = 10^{-15}\,cm^2\,s^{-1}$).

3.1 Base case 1: kinetic limitation by interfacial transport

Figure 2 illustrates the model results of KM-SUB in base case 1 with the kinetic parameters specified in Table 1. As shown in Fig. 2a, the simulated decay of oleic acid is in very good agreement with the experimentally observed decay. Throughout the experimental time scale of 1–15 s, the simulated ozone uptake coefficient is nearly constant and identical to the surface and bulk accommodation coefficients ($\gamma_X \approx \alpha_{b,X} \approx \alpha_{s,X} \approx \alpha_{s,0,X} \approx 4\times10^{-4}$), indicating that the gas uptake is limited by interfacial mass transport, i.e., by the process of bulk accommodation which is in turn

limited by the process of surface accommodation. After ~30 s the ozone uptake coefficient rapidly drops off when reaction partner oleic acid is used up by the rapid bulk reaction ($\gamma_X/\gamma_{X,0} \approx N_Y/N_{Y,0} < 1\%$ after ~37 s).

As shown in Fig. 2b, the surface concentration of oleic acid also decreases gradually over the first ~30 s and drops off rapidly afterwards. In contrast, the surface concentration of ozone exhibits a rapid initial increase from zero to a plateau level of $[X]_s \approx 10^{11}$ cm^{-2}, which is reached within less than a second (~20 ms) and determined by the combination of reversible adsorption, surface reaction, and surface-to-bulk transport driven by the chemical reaction in the bulk. Over the first 30 s, $[X]_s$ gradually increases with the decay of oleic acid and the related decrease of chemical loss. As the chemical loss by reaction with oleic acid rapidly drops off after ~30 s, $[X]_s$ swiftly increases by an order of magnitude to a steady-state level of ~10^{12} cm^{-2}, which is governed by reversible adsorption.

To test how the number of model layers in the particle bulk affects the simulation results, we have run the model with $n = 1$, 5 and 100 layers corresponding to layer thicknesses of $\delta = 199.2$, 39.8 and 1.99 nm, respectively. The results obtained with $n = 100$ and 5 were practically identical, demonstrating the robustness of the multi-layer model approach with transport rate coefficients (velocities) scaled by the layer thickness (Eqs. 28–31). As shown in Fig. 2, the deviations obtained with $n = 1$ were relatively minor, but they indicate that the particle bulk cannot be regarded as well mixed under the conditions of base case 1. Similar deviations were obtained with the kinetic double-layer model K2-SUB, in which the bulk processes are not explicitly resolved but represented by a reacto-diffusive flux (Appendix C, Pfrang et al., 2009).

The KM-SUB model results for the bulk concentration profiles of ozone and oleic acid were also essentially the same with $n = 100$ and 5. For high resolution and to avoid congestion of the plot, however, only the profiles obtained 100 layers are shown in Fig. 3. The y-axis indicates the radial distance from the particle center (r) normalized by the particle radius (r_p), ranging from the particle core ($\delta/r_p \approx 0$) to the near-surface bulk ($(r_p - \delta)/r_p \approx 1$).

As shown in Fig. 3a, ozone rapidly diffuses into the particle bulk. A gradient between the near-surface bulk and the core is established within less than a second (~20 ms), and the concentration profile is determined by the interplay of interfacial mass transport (surface and bulk accommodation) with bulk diffusion and chemical reaction. During the first few seconds, the ozone concentration in the particle core is about a factor of ~50 lower than in the near surface bulk. Up to ~30 s, the ozone concentration gradient decreases gradually with the decay of oleic acid and the related decrease of chemical loss. As the chemical loss by reaction with oleic acid rapidly drops off after ~30 s, the ozone concentration gradient swiftly relaxes, and after ~37 s ozone is well mixed throughout the particle bulk at the concentration level of solubility saturation ($[X]_{b,sat} = 8 \times 10^{14}$ cm^{-3} $= K_{sol,CC,X}[X]_{gs}$ with $K_{sol,CC,X} = 4.8 \times 10^{-4}$ mol cm^{-3} atm^{-1}).

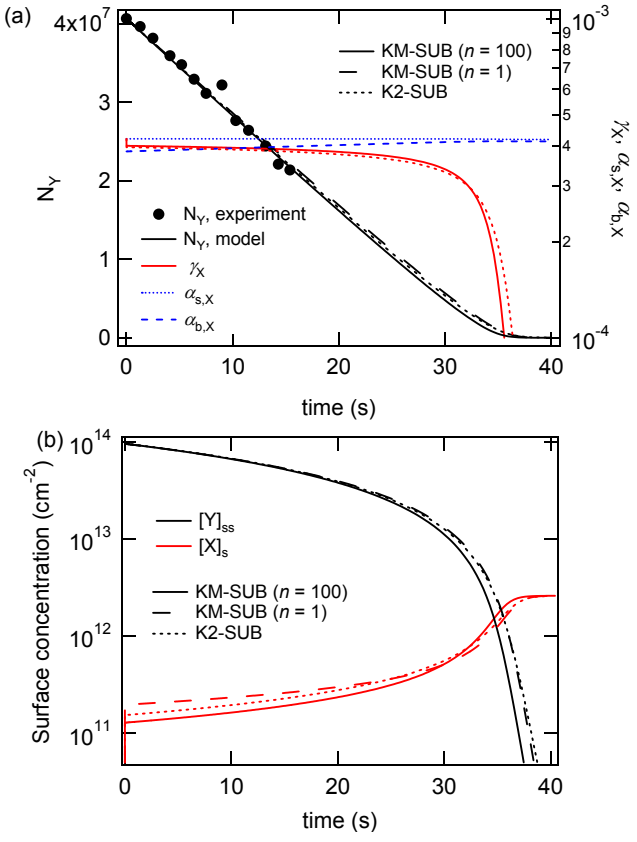

Fig. 2. Temporal evolution of model base case 1 in KM-SUB with $n = 1$ (dashed lines) and $n = 100$ (solid lines) and in K2-SUB (dotted lines). **(a)** Experimental data (black symbols; Ziemann, 2005) and model results for the total number of oleic acid molecules (N_Y, black line) and for the uptake coefficient of ozone (γ_{X_i}, red line), surface accommodation coefficient ($\alpha_{s,X}$, blue dotted line), and bulk accommodation coefficient ($\alpha_{b,X}$, blue dashed line). **(b)** Surface concentrations of oleic acid (black line) and ozone (red line).

As shown in Fig. 3b, the ozone gradient and the ozonolysis of oleic acid cause a reverse gradient in the bulk concentration of oleic acid. Because the concentration of oleic acid is several orders of magnitude larger than that of ozone, however, the strong gradient of ozone induces only a small gradient in oleic acid. During the first few seconds, the oleic acid concentration in the near-surface bulk is ~5% lower than in the particle core. As the ozone gradient relaxes after ~30 s, the small oleic acid gradient also disappears. Thus, oleic acid can effectively be regarded as well-mixed.

Figure 4a shows the loss rate of oleic acid and ozone by chemical reaction in the particle bulk (L_b) as calculated with KM-SUB for different model layers and with KM-SUB and K2-SUB effectively averaged over the whole bulk volume. The averaged values of L_b calculated by K2-SUB and KM-SUB are almost identical, demonstrating consistency

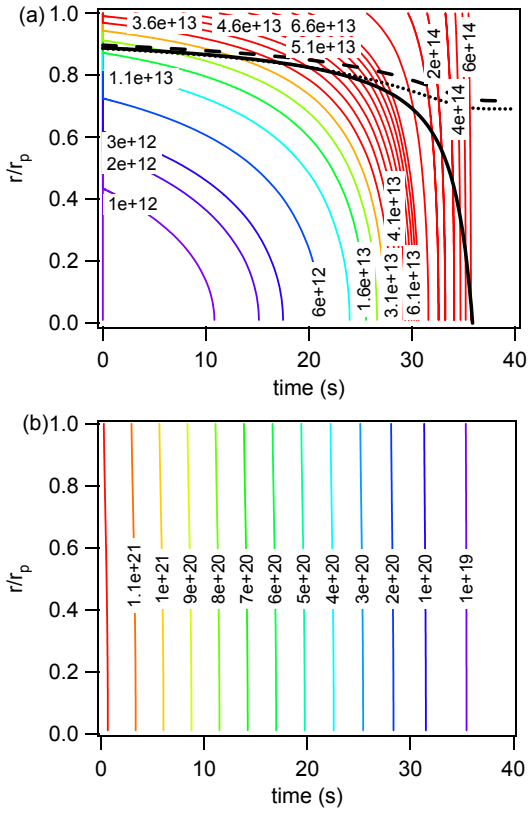

Fig. 3. Temporal evolution of bulk concentration profiles for model base case 1 for **(a)** ozone and **(b)** oleic acid (KM-SUB with $n = 100$). The y-axis indicates the radial distance from the particle center (r) normalized by the particle radius, ranging from the particle core ($r/r_p = \delta/r_p \approx 0$) to the near-surface bulk ($r/r_p = 1$). The colored lines are isopleths of bulk concentration with labeled in units of cm^{-3} (blue=low, red=high). The black solid line represents the reacto-diffusive length for ozone normalized by the particle radius ($1 - l_{rd,X}/r_p$). The black dotted line represents the 50% isoline for the concentration difference between the particle core and the near-surface bulk, and the black dashed line shows 63% isoline of L_b^*.

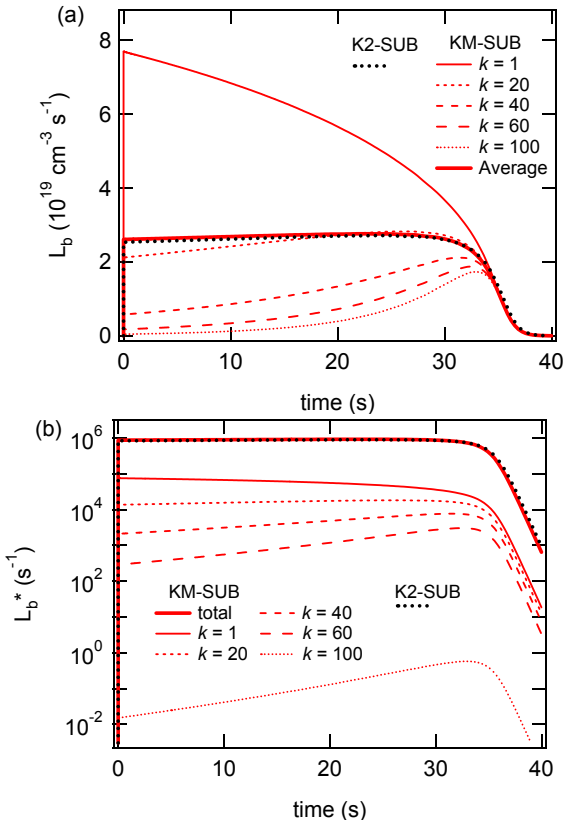

Fig. 4. (a) Loss rate (L_b) and **(b)** absolute loss rate (L_{bk}^*) of oleic acid in the bulk calculated by KM-SUB for bulk layers 1 (near-surface bulk), 20, 40, 60, and 100 (core) in BC1. L_b calculated by K2-SUB and volume average $L_b (= L_b^*/V_b)$ calculated by KM-SUB are shown in panel (a). Total absolute los rate (L_b^*) calculated by KM-SUB and K2-SUB are also shown in panel (b).

of KM-SUB with K2-SUB and with the underlying resistor model formulation of the reacto-diffusive flux $J_{b,rd}$. Due to the overall kinetic limitation by interfacial transport, the volume-average loss rate L_b remains near-constant up to ~30 s. During the first few seconds, the loss rate in the near-surface bulk (L_{b1}, $r/r_p \approx 1$) is more than a factor of 2 higher than the volume-average loss rate, while the loss rates in layers around the particle core (L_{b40} to L_{b100}, $r/r_p < 0.6$) are more than a factor of 2 lower. L_{b1} continually decreases due to progressing consumption of oleic acid, whereas L_{b40} to L_{b100} exhibit a pronounced increase up to ~35 s due to the penetration of ozone to the particle core (see also Fig. 3a). After ~35 s all loss rates drop off rapidly and approach zero after ~37 s as oleic acid is essentially used up.

Up to ~30 s, the strong radial gradient of loss rates L_b and the approximate coincidence of L_{b20} ($r/r_p \approx 0.8$) with L_b indicate that the overall rate of conversion or absolute loss rate of oleic acid and ozone molecules in the particle is strongly dominated by the outer bulk layers at $r/r_p > 0.8$. Due to the spherical geometry the outer layers also have much larger volumes, which further enhances their relative importance with regard to the absolute loss rate of molecules in each layer ($L_{bk}^* = L_{bk} V_{bk}$) and in the entire particle ($L_b^* = L_b V_b$). Figure 4b illustrates this by displaying the values of L_{bk}^* and L_b^* corresponding to the values of L_{bk} and L_b displayed in Fig. 4a (note the linear scaling of Fig. 4a and the logarithmic scaling of Fig. 4b). L_b^* calculated by KM-SUB and K2-SUB are almost identical.

The black solid line in Fig. 3a represents the reacto-diffusive length for ozone normalized by the particle radius ($1 - l_{rd,X}/r_p$), which can be regarded as the distance from the surface up to which the chemical reaction proceeds effectively (Finlayson-Pitts and Pitts, 2000; Pöschl et al., 2007). The initial value of $l_{rd,X} \approx 20$ nm is consistent with the values reported by Smith et al. (2003) and Katrib et al. (2004). Over the first ~30 s of the model run $l_{rd,X}$ remains fairly constant,

and the reacto-diffusive line (black solid) coincides with the 50% isoline for the concentration difference between the particle core and the near-surface bulk (black dotted), and with the 63% (=1−1/e) isoline of L_b^* (black dashed). During this time 63% of L_b^*, i.e., 63% of the overall rate of conversion of oleic acid ozonolysis, occur in the outermost 10 bulk layers, i.e. at $r/r_p > 0.9$ (corresponding to ∼30% of the particle bulk volume). After ∼30 s, $l_{rd,X}$ increases steeply as oleic acid is depleted and ozone can freely penetrate throughout the bulk of the particle.

3.2 Base case 2: kinetic limitation by bulk reaction

In base case 2 the second-order bulk reaction rate coefficient was by a factor of ∼30 smaller than in BC1, while the surface accommodation coefficient was by a factor of ∼2 higher (Table 1). As shown in Fig. 5a, the simulation results of BC2 are also in very good agreement with the observed decay of oleic acid. The calculated ozone uptake coefficient behaves very differently than in BC1. The initial value of γ_X in BC2 is by a factor of ∼2 higher than in BC1. It reflects rapid uptake into the initially ozone-free particle bulk, which is limited by the kinetics of interfacial transport, i.e., bulk accommodation and surface accommodation, respectively. After less than one second (∼20 ms), however, γ_X steeply drops off to a level that is reaction-limited ($\gamma_X \approx 10^{-4} < \alpha_{b,X} \approx 8 \times 10^{-4}$) and continues to decrease gradually with decreasing abundance of the reaction partner oleic acid.

After a rapid initial increase (∼20 ms), the ozone surface concentration reaches a plateau level which increases only slightly until the end of the simulation, while the oleic acid surface concentration decreases gradually. In contrast to BC1, none of the compositional and kinetic parameters exhibit abrupt changes after ∼30 s. Instead, they all undergo a gradual evolution reflecting the kinetics of the rate-limiting bulk reaction.

The results of multi-layer model KM-SUB with both $n = 100$ and 1 were practically identical to the results of the double-layer model K2-SUB, indicating that the particle bulk can be regarded as well mixed under the conditions of BC2.

Due to faster interfacial transport and slower chemical reaction, the ozone concentration in the bulk increases much faster than in BC1 (Fig. 6a vs. Fig. 3a). After less than one second (∼20 ms), the ozone concentration in the core of the particle is only ∼30% lower than in the near-surface bulk, and the gradient continues to decrease with decreasing abundance of oleic acid. Due to the slow decay of oleic acid, however, a small ozone gradient persists until the end of the simulation (Fig. 6a) and thus longer than in BC1, where the initially very strong gradient essentially disappears after ∼37 s when practically all oleic acid (>99%) has been consumed by the rapid bulk reaction (Fig. 3a). As illustrated in Fig. 6b, oleic acid can be regarded as well-mixed (concentration differences <1%).

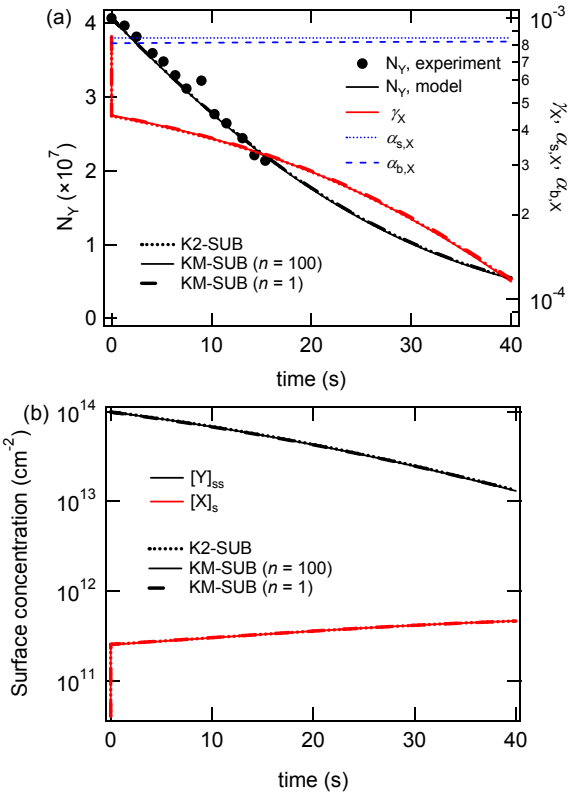

Fig. 5. Temporal evolution of model base case 2 in KM-SUB with $n = 1$ (dashed lines) and $n = 100$ (solid lines) and in K2-SUB (dotted lines). **(a)** Experimental data (black symbols; Ziemann, 2005) and model results for the total number of oleic acid molecules (N_Y, black line) and for the uptake coefficient of ozone (γ_X, red line), surface accommodation coefficient ($\alpha_{s,X}$, blue dotted line), and bulk accommodation coefficient ($\alpha_{b,X}$, blue dashed line). **(b)** Surface concentrations of oleic acid (black line) and ozone (red line).

Figure 7a shows the loss rate of oleic acid and ozone by chemical reaction in the particle bulk (L_b) as calculated with KM-SUB for different model layers and with KM-SUB and K2-SUB effectively averaged over the whole bulk volume. The average values of L_b calculated by K2-SUB and KM-SUB are almost identical. Due to the kinetic limitation by bulk reaction, the volume-average loss rate L_b decreases continuously due to consumption of oleic acid. Initially, L_b in the near-surface bulk (L_{b1}, $r/r_p \approx 1$) is ∼40% higher than that in the core (L_{b100}) corresponding to the concentration gradient of O_3 in the bulk. They become almost same in 20 s as concentration gradient becomes smaller. Figure 7b illustrates $L_{bk}^* (= L_{bk} V_{bk})$ and $L_b^* (= L_b V_b)$ corresponding to the values of L_{bk} and L_b displayed in Fig. 7a (note the linear scaling of Fig. 7a and the logarithmic scaling of Fig. 7b). L_b^* calculated by KM-SUB and K2-SUB are almost identical.

The black solid line in Fig. 6a represents again the reacto-diffusive length for ozone normalized by the particle radius ($1 - l_{rd,X}/r_p$). Due to the lower reaction rate coefficient, the initial value of $l_{rd,X} \approx 120$ nm is by a factor of ∼6 larger

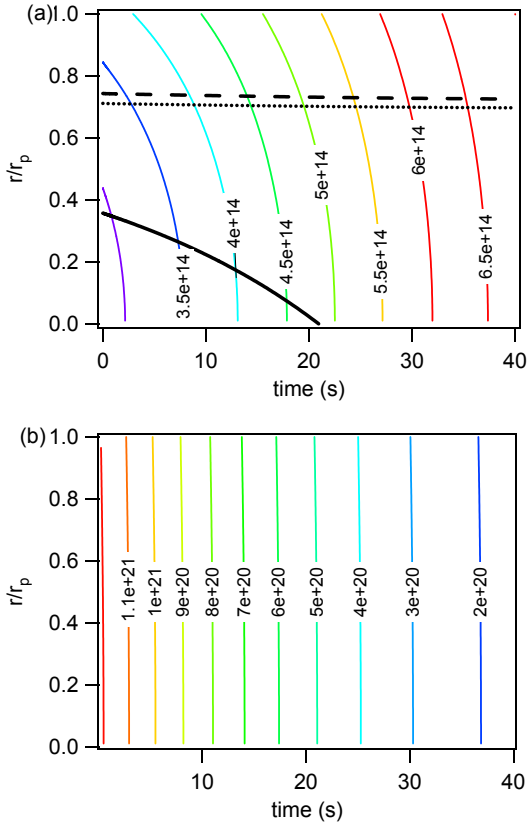

Fig. 6. Temporal evolution of bulk concentration profiles for model base case 1 for **(a)** ozone and **(b)** oleic acid (KM-SUB with $n = 100$). The y-axis indicates the radial distance from the particle center (r) normalized by the particle radius, ranging from the particle core ($r/r_p = \delta/r_p \approx 0$) to the near-surface bulk ($r/r_p = 1$). The colored lines are isopleths of bulk concentration with labeled in units of cm^{-3} (blue=low, red=high). The black solid line represents the reacto-diffusive length for ozone normalized by the particle radius ($1 - l_{rd,X}/r_p$). The black dotted line represents the 50% isoline for the concentration difference between the particle core and the near-surface bulk, and the black dashed line shows 63% isoline of L_b^*.

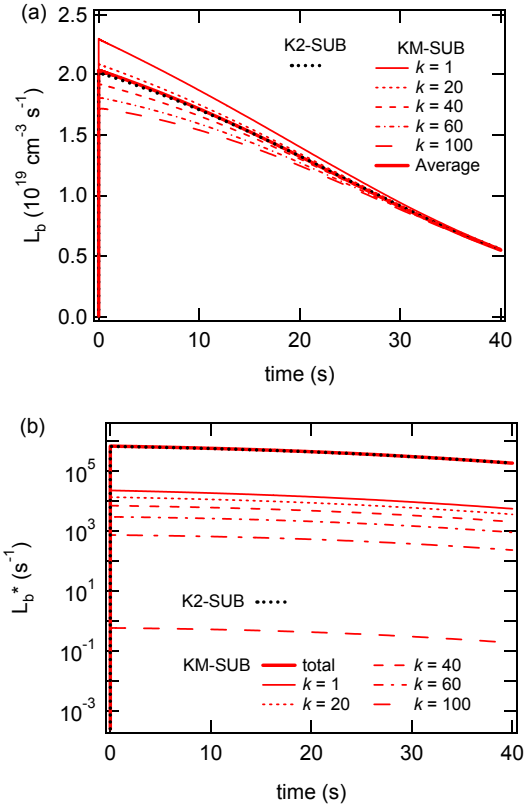

Fig. 7. (a) Loss rate (L_b) and **(b)** absolute loss rate (L_{bk}^*) of oleic acid in the bulk calculated by KM-SUB for bulk layers 1 (near-surface bulk), 20, 40, 60, and 100 (core) in BC2. L_b calculated by K2-SUB and volume average $L_b (= L_b^*/V_b)$ calculated by KM-SUB are shown in panel (a). Total absolute los rate (L_b^*) calculated by KM-SUB and K2-SUB are also shown in panel (b).

than in BC1, and after ~20 s it is already larger than the particle radius (200 nm), indicating that the reaction effectively proceeds throughout the whole bulk. The 50% isoline (black dotted) for the ozone concentration difference between the particle core and the near-surface bulk and the 63% ($= 1-1/e$) isoline of L_b^* (black dashed) remain near-constant throughout the simulation. They are from the beginning at the same level reached at the end of BC1, which reflects that both ozone and oleic can be regarded as well mixed in BC2 due to slow reaction and rapid diffusion.

BC1 may be regarded as more realistic, because it uses the only reported value of the bulk reaction rate coefficient of ozone with oleic acid, whereas BC2 assumes a ~30 times lower value. Nevertheless, both model cases are in good agreement with the available experimental data. Thus, further experiments covering a wider range of reaction times and conditions are needed to elucidate the actual reaction mechanism (see Pfrang et al., 2009).

3.3 Base case 3: kinetic limitation by bulk diffusion

Base case 3 is based on base case 1 but the bulk diffusion coefficients are lower by five orders of magnitude ($D_{b,X} = 10^{-10}\,cm^2\,s^{-1}$, $D_{b,Y} = 10^{-15}\,cm^2\,s^{-1}$, Table 1), corresponding to characteristic diffusivities of amorphous (semi-)solid matrices (Bird et al., 2007; Swallen et al., 2007; Mikhailov et al., 2009).

As illustrated in Fig. 8a, the decay of oleic acid is very slow in BC3 because the low diffusivity effectively protects oleic acid in the particle bulk from oxidation. Within ~1 s the calculated ozone uptake coefficient drops from the initial value of $\sim 4\times10^{-3}$ to $\sim 2\times10^{-5}$, which is due to a rapid decrease of the oleic acid surface concentration from $\sim 10^{14}\,cm^{-2}$ to $\sim 10^{12}\,cm^{-2}$. After ~1 s the ozone surface concentration remains practically constant at $\sim 10^{12}\,cm^{-2}$ (adsorption equilibrium). The low levels of ozone uptake

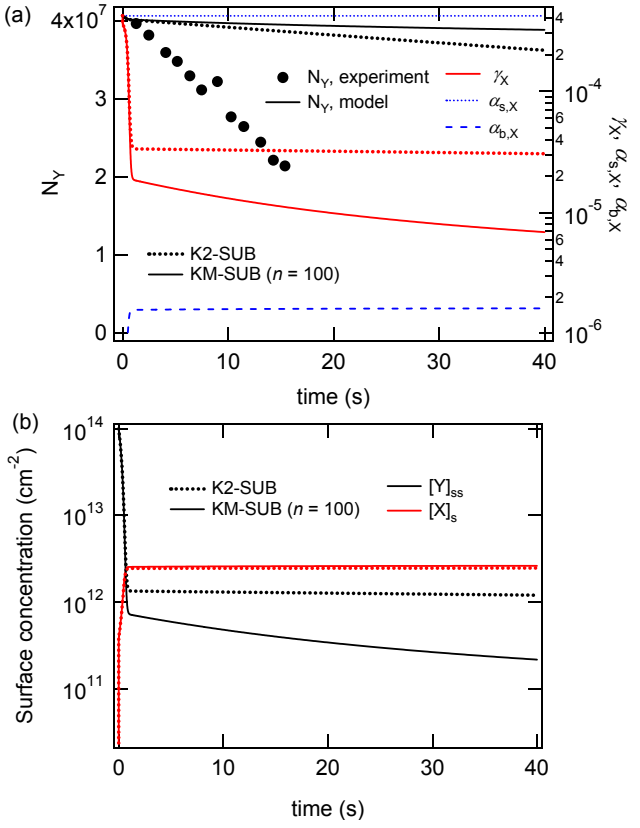

Fig. 8. Temporal evolution of model base case 3 with KM-SUB ($n = 100$). **(a)** Experimental data (black symbols; Ziemann, 2005) and model results for the total number of oleic acid molecules (N_Y, black line) and for the uptake coefficient of ozone (γ_X, red line), surface accommodation coefficient ($\alpha_{s,X}$, blue dotted line), and bulk accommodation coefficient ($\alpha_{b,X}$, blue dashed line). **(b)** Surface concentrations of oleic acid (black line) and ozone (red line).

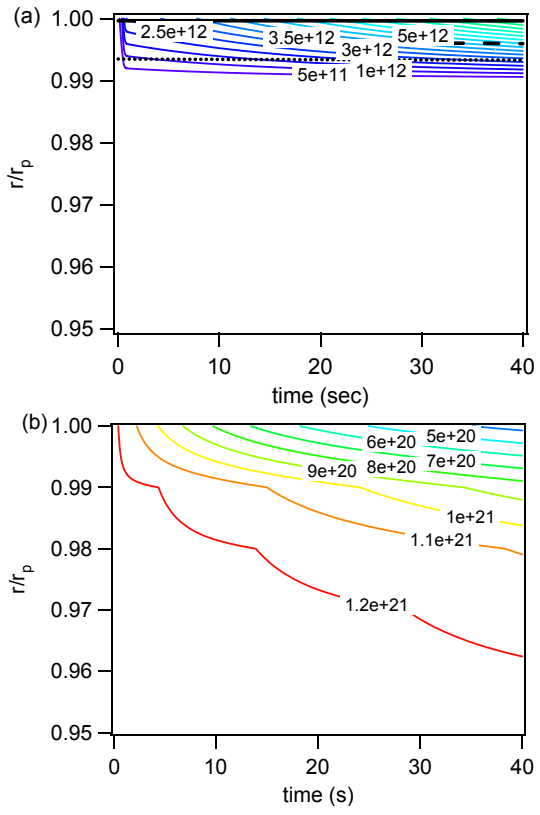

Fig. 9. Temporal evolution of bulk concentration profiles for model base case 3 for **(a)** ozone and **(b)** oleic acid (KM-SUB with $n = 100$). The y-axis indicates the radial distance from the particle center (r) normalized by the particle radius, ranging from $r/r_p = 0.95$ to the near-surface bulk ($r/r_p = 1$). The colored lines are isopleths of bulk concentration with labeled in units of cm^{-3} (blue=low, red=high). The black solid line represents the reacto-diffusive length for ozone normalized by the particle radius ($1 - l_{rd,X}/r_p$). The black dotted line represents the 50% isoline for the concentration difference between the particle core and the near-surface bulk, and the black dashed line shows 63% isoline of L_b^*.

coefficient and oleic acid surface concentration are maintained by surface bulk exchange and decrease slowly as ozone increases and oleic acid decreases also in the near-surface bulk. In contrast to BC1, the bulk accommodation coefficient α_b, X($\approx 2 \times 10^{-6}$) is much smaller than $\alpha_{s,X}$ and γ_X, reflecting the slow uptake of ozone into the particle bulk, which is limited by the kinetics of surface-bulk exchange and bulk diffusion.

Due to fast reaction and slow diffusion, both ozone and oleic acid exhibit steep concentration gradients near the surface, whereas the inner particle bulk remains nearly unchanged (Fig. 9). During the simulation period ozone penetrates only into the near-surface bulk, and thus the chemical consumption of oleic acid is also restricted to the near-surface bulk ($r/r_p > 0.99$). Accordingly, the reacto-diffusive length is very small (~0.1 nm; black solid line in Fig. 9a), and the 50% isoline (black dotted) for the ozone concentration difference between particle core and near-surface bulk as well as the 63% ($= 1-1/e$) isoline of L_b^* (black dashed) remain restricted to the near surface bulk ($r/r_p > 0.99$). This is also reflected in Fig. 10, showing that the values of L_b and L_b^* are essentially zero except for $k = 1$ (near-surface bulk layer).

Compared to KM-SUB, the simulated decay of oleic acid and ozone uptake are faster in K2-SUB. At the end of the model run (40 s), the total amount of oleic acid (N_Y) is lower by ~10% while the surface concentration of oleic acid ($[Y]_{ss}$) and the ozone uptake coefficient (γ_X) are higher by a factor of ~5. This is because K2-SUB assumes that oleic acid is radially well-mixed and does not resolve its concentration profile. In fact, the diffusion coefficient of oleic acid ($D_{b,Y}$) does not appear in the equation for the reacto-diffusive flux (Eq. C1), which represents the effects of all bulk processes in the traditional resistor model approach. In case of kinetic limitation by bulk diffusion, however, the

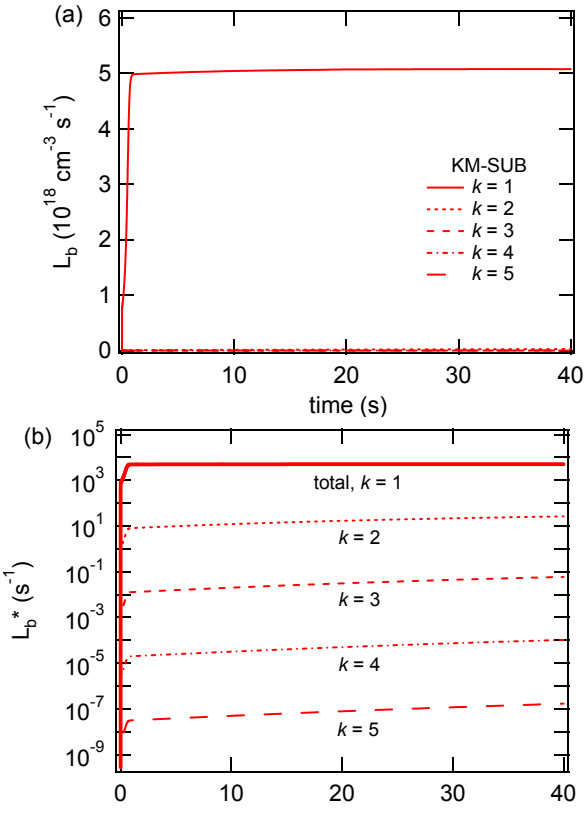

Fig. 10. (a) Loss rate (L_b) and **(b)** absolute loss rate (L^*_{bk}) of oleic acid in the bulk calculated by KM-SUB for bulk layers 1 (near-surface bulk), 2, 3, 4, and 5 in BC3. Total absolute loss rate (L^*_b) are also shown.

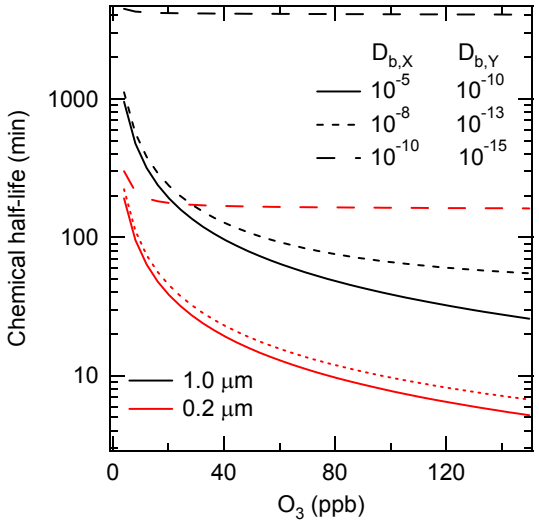

Fig. 11. Chemical half-life (min) of pure oleic acid particles with particle radius of 1.0 (black) and 0.2 μm (red) as a function of gas phase O_3 mixing ratio. The diffusion coefficients are $D_{b,X} = 10^{-5}$ cm^2 s^{-1}, $D_{b,Y} = 10^{-10}$ cm^2 s^{-1} (solid line, BC1), $D_{b,X} = 10^{-8}$ cm^2 s^{-1}, $D_{b,Y} = 10^{-13}$ cm^2 s^{-1} (dotted line), and $D_{b,X} = 10^{-10}$ cm^2 s^{-1}, $D_{b,Y} = 10^{-15}$ cm^2 s^{-1} (dashed line, BC3).

reaction rates are influenced by the mass transport of both volatile and non-volatile reactants in the particle bulk.

3.4 Chemical half-life of oleic acid and atmospheric implications

In the preceding sections we showed how the KM-SUB model can be used to interpret and analyze experimental data from laboratory studies, which are often carried out with high O_3 concentration to observe measurable effects on short experimental time scales. Here we demonstrate how the results can be extrapolated to dilute atmospheric conditions.

We estimated the chemical half-life ($t_{1/2}$) of pure oleic acid particles, when exposed to ozone at average ambient mixing ratios (<150 ppb). The radii of oleic acid particles (r_p) were set to be 0.2 and 1.0 μm. The chemical half-life was defined as the time when number of oleic acid molecules was degraded to half of its initial value. The solid lines of Fig. 11 show the results of such calculations with BC1. At typical atmospheric O_3 mixing ratios of 30 ppb, $t_{1/2}$ was ∼25 min for r_p =0.2 μm and ∼130 min for r_p =1.0 μm. The chemical half-life depended strongly on particle radius (i.e. number of oleic acid molecules contained in the particle). In the typical polluted air with 100 ppb O_3, $t_{1/2}$ was shortened to ∼8 min for $r_p = 0.2$ μm and ∼40 min for $r_p = 1.0$ μm. The calculations were also made in BC2, which gave almost the same results for $r_p = 0.2$ μm and gave ∼20% smaller value for $r_p = 1.0$ μm compared to BC1.

The ozonolysis of oleic acid leads to an increase of oxygen content and hygroscopicity (Asad et al., 2004), and it can convert CCN-inactive particles into CCN (King et al., 2009). Our model results suggest that the transformation of oleic acid particles will occur on a timescale of ∼1 h depending on atmospheric O_3 concentration and particle size. This is in good agreement with the characteristic time of 1.3 h reported by King et al. (2009).

In spite of the short lifetimes found in laboratory experiments, however, oleic acid is detected also in aged atmospheric aerosol particles (Rogge et al., 1991; Morris et al., 2002). Possible explanations include reduced concentrations of O_3 (and other photo-oxidants) in the particle bulk due to the following effects: (a) chemical reaction with other reactive species, self-reaction or catalytic decomposition; (b) competitive co-adsorption and surface reaction of multiple species such as water vapor and nitrogen oxides (Shiraiwa et al., 2009; Springmann et al., 2009); (c) slow mass transport because of low diffusion coefficients in solid or semi-solid phases (crystalline, glassy, rubbery, gel-like or ultra-viscous: Mikhailov et al., 2009). The formation of semi-solid amorphous phases is generally favored by low temperature and low relative humidity (Zobrist et al., 2008), and it can occur in the core of atmospheric particles as well as

in coatings formed by condensation of secondary particulate matter. For example, oligomerisation reactions may lead to high molecular mass, low hygroscopicity and low diffusivity of secondary organic coatings, effectively shutting off further ozonolysis and oxidation of oleic acid and other organic compounds in the bulk of coated particles.

The potential importance of the phase state of aerosol particles (solid, semi-solids, or liquid) for the ozonolysis of oleic acid was already pointed out by Knopf et al. (2005) and Zahardis and Petrucci (2007). To explore and quantify the effects and of kinetic limitation by bulk diffusion, we performed sensitivity studies with low diffusion coefficients that are characteristic for mass transport in highly viscous or semi-solid matrices (Bird et al., 2007; Swallen et al., 2007; Mikhailov et al., 2009).

The dotted lines in Fig. 11 show the effect of reducing the diffusion coefficients of O_3 and oleic acid by three orders of magnitude ($D_{b,X} = 10^{-8}\,cm^2\,s^{-1}$, $D_{b,Y} = 10^{-13}\,cm^2\,s^{-1}$). It increased $t_{1/2}$ by up to ~100%, depending on ozone concentration and particle diameter. The dashed lines shows the effect of reducing the diffusion coefficients to the same level as in the base case 3 presented and discussed above ($D_{b,X} = 10^{-10}\,cm^2\,s^{-1}$, $D_{b,Y} = 10^{-15}\,cm^2\,s^{-1}$). In this case the chemical lifetimes increase by up to a factor of ~100 and become nearly independent of ozone concentration: ~3 h for $r_p = 0.2\,\mu m$ and ~3 days for $r_p = 1.0\,\mu m$. The results confirm mass transport can have strong non-linear effects on the chemical aging of atmospheric aerosols, and that (semi-)solid matrices with low diffusion coefficients can effectively shield reactive organic compounds from degradation by atmospheric photo-oxidants.

4 Conclusions

We presented a novel kinetic multi-layer model (KM-SUB) that explicitly resolves all steps of mass transport and chemical reaction at the surface and in the bulk of aerosol particles. It includes adsorption and desorption, surface reactions and surface-bulk exchange as well as bulk diffusion and reaction.Unlike earlier models of aerosol chemistry (e.g., resistor model), the KM-SUB model approach does not require any simplifying assumptions about steady-state and mixing conditions. The temporal evolution of concentration profiles of volatile and non-volatile species in the particle bulk can be modeled along with surface concentrations and uptake coefficients.

The effects of bulk diffusion on the rate of gas uptake and particle transformation were explored for a popular reference system, the ozonolysis of oleic acid particles, assuming different diameters and different sets of kinetic parameters (surface accommodation coefficients, diffusion coefficients, etc.).

Under conditions where the reaction system was kinetically limited by interfacial transport or chemical reaction, the multi-layer model (KM-SUB) was in good agreement with a double-layer model (K2-SUB) using traditional resistor formulations for bulk processes. In case of kinetic limitation by bulk diffusion, however, the K2-SUB model overestimated the rates of gas uptake and oleic acid degradation, because it does not resolve and account for the concentration profile of oleic acid. Comparison with a partial differential equation (PDE) model confirmed the ability of KM-SUB to resolve diffusion and concentration profiles in the particle bulk.

We demonstrated and discussed how the KM-SUB model can be used to interpret and analyze experimental data from laboratory studies, and how the results can be extrapolated to atmospheric conditions. For liquid oleic acid particles, the chemical half-life of oleic acid molecules with regard to oxidation by ozone was estimated to of the order of one hour. In (semi-)solid particles with low bulk diffusivity, however, the chemical half-life can increase dramatically (up to multiple hours and days). The results of sensitivity studies with different bulk diffusion coefficients confirmed that the phase state of atmospheric particles is highly relevant for chemical transformation and aging (Knopf et al., 2005; McNeill et al., 2007, 2008; Zahardis and Petrucci, 2007; Griffiths et al., 2009; Mikhailov et al., 2009).

Depending on the complexity of the investigated system, unlimited numbers of volatile and non-volatile species and chemical reactions can be added flexibly. Thus, the KM-SUB approach may serve as a basis for the development of a detailed master mechanism of aerosol chemistry and for the derivation of simplified but realistic parameterizations for large-scale atmospheric and climate models.

Appendix A

List of Symbols

Symbol	Meaning	Unit
α_{b,X_i}	bulk accommodation coefficient of X_i	
α_{s,X_i}	surface accommodation coefficient of X_i	
$\alpha_{s,0,X_i}$	surface accommodation coefficient of X_i on an adsorbate-free surface	
$\alpha_{s,0,X_i,Y_j}$	surface accommodation coefficient of X_i on an adsorbate-free surface composed of Y_j	
δ	thickness of bulk layers	cm
δ_{X_i}, δ_{Y_j}	effective molecular diameter of X_i and Y_j	cm
λ_{X_i}	mean free path of X_i in the gas phase	cm

Symbol	Meaning	Unit
θ_s	sorption layer surface coverage	
θ_{ss}	quasi-static layer surface coverage	
σ_{s,X_i}	effective molecular cross section of X_i in the sorption layer	cm^2
γ_{X_i}	uptake coefficient of X_i (normalized by gas kinetic flux of surface collisions)	
γ_{gsr,X_i}	reaction probability for elementary gas-surface reactions	
τ_{d,X_i}	desorption lifetime of X_i	s
τ_{d,X_i,Y_j}	desorption lifetime of X_i on a surface composed of Y_j	s
$\Phi_{b,Yp}$	weighting factor (mole, mass, or volume fraction of Y_p in the bulk)	
ω_{X_i}	mean thermal velocity of X_i in the gas phase	$cm\,s^{-1}$
$A(k)$	outer surface area of bulk layer k	cm^2
A_{ss}	surface area of particle (quasi-static layer)	
c_{SLRv,s,X_i}, c_{SLRv,ss,Y_j}	stoichiometric coefficients of species X_i and Y_j in surface layer reaction SLRv	
c_{BRv,X_i}, c_{BRv,Y_j}	stoichiometric coefficients of species X_i and Y_j in bulk reaction BRv	
C_{b,rd,X_i}	reacto-diffusive geometry correction factor for X_i	
C_{g,X_i}	gas phase diffusion correction factor for X_i	
D_{b,X_i}, D_{b,Y_j}	bulk diffusion coefficient of X_i and Y_j	$cm^2\,s^{-1}$
J_{ads,X_i}, J_{des,X_i}	flux of adsorption and desorption of X_i	$cm^{-2}\,s^{-1}$
J_{coll,X_i}	flux of surface collisions of X_i	$cm^{-2}\,s^{-1}$
J_{b,rd,X_i}	reacto-diffusive flux of X_i	$cm^{-2}\,s^{-1}$
J_{b,s,X_i}, J_{b,ss,Y_j}	flux of bulk-to-surface transport of X_i (sorption layer) and Y_j (quasi-static layer)	$cm^{-2}\,s^{-1}$
J_{s,b,X_i}, J_{ss,b,Y_j}	flux of surface-to-bulktransport of X_i (sorption layer) and Y_j(quasi-static layer)	$cm^{-1}\,s^{-1}$

Symbol	Meaning	Unit
$J_{bk,bk-1,X_i}$, $J_{bk,bk-1,Y_j}$	flux of transport from bulk layer k to bulk layer k-1 for X_i and Y_j	$cm^{-2}\,s^{-1}$
k_{b,b,X_i}, k_{b,b,Y_j}	rate coefficient (velocity) of bulk transport of X_i and Y_j	$cm\,s^{-1}$
k_{b,s,X_i}	rate coefficient (velocity) of bulk-to-surface transport of X_i	$cm\,s^{-1}$
k_{BR,X_i,Y_j}	second-order rate coefficients for bulk reactions of X_i with Y_j	$cm^3\,s^{-1}$
k_{b,ss,Y_i}	rate coefficient (velocity) of bulk-to-surface transport of Y_j	$cm\,s^{-1}$
k_{d,X_i}	first-order desorption rate coefficient of X_i	s^{-1}
k_{s,b,X_i}	first-order rate coefficient for surface-to-bulk transport of X_i	s^{-1}
k_{ss,b,Y_j}	first-order rate coefficients for surface-bulk transport of Y_j	s^{-1}
$k_{SLR,Xp,Yq}$	second-order rate coefficients for surface layer reactions of X_p with Y_q	$cm^2\,s^{-1}$
K_{sol,cc,X_i}	gas-particle partitioning coefficient of X_i	
l_{rd,X_i}	reacto-diffusive length of X_i and Y_j	$cm^{-3}\,s^{-1}$
L_{b,X_i}, L_{b,Y_j}	loss rate of X_i and Y_j by reaction in the particle bulk	$cm^{-3}\,s^{-1}$
L_{bk,X_i}, L_{bk,Y_j}	loss rate of X_i and Y_j by reaction in bulk layer k	$cm^{-3}\,s^{-1}$
L_{s,X_i}, L_{ss,Y_j}	loss rate of X_i and Y_j by surface layer reaction	$cm^{-2}\,s^{-1}$
L^*_{b,X_i}, L^*_{b,Y_j}	absolute loss rate of X_i and Y_j by reaction in the particle bulk	s^{-1}
L^*_{bk,X_i}, L^*_{bk,Y_j}	absolute loss rate of X_i and Y_j by reaction in bulk layer k	s^{-1}
L^*_{s,X_i}, L^*_{ss,Y_j}	absolute loss rate of X_i and Y_j by surface layer reaction	s^{-1}
n	number of bulk layers	
N_Y	total number of Y molecules	
P_{b,X_i}, P_{b,Y_j}	production rate of X_i and Y_j by reaction in the particle bulk	$cm^{-3}\,s^{-1}$
P_{bk,X_i}, P_{bk,Y_j}	production rate of X_i and Y_j by reaction in bulk layer k	$cm^{-3}\,s^{-1}$
P_{s,X_i}, P_{ss,Y_j}	production rate of X_i and Y_j by surface layer reaction	$cm^{-2}\,s^{-1}$
r_b	particle bulk radius	cm
r_p	particle radius	cm

Symbol	Meaning	Unit
$[X_i]_g$	gas phase number concentration of X_i	cm^{-3}
$[X_i]_{gs}$	Near-surface gas phase number concentration of X_i	cm^{-3}
$[X_i]_s$	surface number concentration of X_i (sorption layer)	cm^{-2}
$[Y_j]_{ss}$	surface number concentration of Y_j (quasi-static layer)	cm^{-2}
$[X_i]_{bk}, [Y_j]_{bk}$	Bulk number concentration of X_i and Y_j in the bulk layer k	cm^{-3}
V_b	volume of particle bulk	
$V(k)$	volume of bulk layer k	cm^{-3}

Appendix B

Partial differential equation model (PDE)

Smith et al. (2003) demonstrated that the diffusion and reaction in the bulk can be described by the following partial differential equations:

$$\frac{\partial [X]_b}{\partial t} = \frac{D_{b,X}}{r^2}\frac{\partial}{\partial r}\left(r^2\frac{\partial [X]_b}{\partial r}\right) - k_{BR,X,Y}[X]_b[Y]_b \quad \text{(B1)}$$

$$\frac{\partial [Y]_b}{\partial t} = \frac{D_{b,Y}}{r^2}\frac{\partial}{\partial r}\left(r^2\frac{\partial [Y]_b}{\partial r}\right) - k_{BR,X,Y}[X]_b[Y]_b \quad \text{(B2)}$$

where X=O_3 and Y=oleic acid. The first term describes diffusion based on the Fick's law and the second term describes chemical reaction in the bulk. Note that this partial differential equation (PDE) method can only simulate the processes in the bulk and not coupled with surface processes. In solving these PDE equations, several assumptions are required as boundary conditions (Smith et al., 2003): (1) The concentration of the near-surface bulk is fixed over time, (2) the flux of X at the core is zero ($\partial[X]_b/\partial r|_{r=0} = 0$), (3) the flux of Y at both near-surface bulk and core is zero ($\partial[X]_b/\partial r|_{r=r_p} = \partial[X]_b/\partial r|_{r=0} = 0$). PDE model simulations were performed by numerically solving the partial differential equations with Matlab software (PDEPE solver).

We investigate large particles with a radius of 1.0 µm as investigated by Smith et al. (2003), and we compare the KM-SUB results ($n = 200$) to the results of the PDE model. The gas phase ozone concentration was set to $[X]_g = [X]_{gs} = 7.0 \times 10^{13}\,cm^{-3}$ (corresponding to 2.8 ppm at 1013 hPa and 298 K). The initial surface and bulk concentrations of ozone (X) were set to $[X]_{s,0} = [X]_{bk,0} = 0$, and the initial surface and bulk concentrations of oleic acid (Y) were set to $[Y]_{ss,0} = 9.7 \times 10^{13}\,cm^{-2}$ and $[Y]_{ss,0} = 1.2 \times 10^{21}\,cm^{-3}$, respectively. The kinetic parameters used are based on base case 1 summarized in Table 1 with the second-order surface reaction rate coefficient ($k_{SLR,X,Y}$) of zero. Unlike KM-SUB, the PDE model depends on the assumption of a fixed ozone concentration in the near surface bulk. Smith et al. (2003) had assumed solubility saturation according to Henry's law. In case of fast reaction, however, chemical loss leads to a substantial decrease and lower value of the actual ozone concentration. For comparability, the concentration of ozone in the near-surface bulk of the PDE model was set to a value of $5.0 \times 10^{13}\,cm^{-3}$, which is similar to the value calculated by KM-SUB.

Figure A1 shows the concentration profiles of ozone (top) and oleic acid (bottom) obtained by simulations with KM-SUB (left) and with the PDE model (right). The diffusion of O_3 into the bulk was very slow due to the large particle diameter, so that there was a large concentration gradient of O_3. The concentration of O_3 at the core remains small ($<10^3\,cm^{-3}$) over the reaction time considered. Oleic acid showed also a concentration gradient, which was due to the O_3 concentration gradient and a slow diffusion coefficient of oleic acid ($D_{b,Y} = 10^{-10}\,cm^2\,s^{-1}$). If a larger $D_{b,Y}$ of $10^{-7}\,cm^2\,s^{-1}$ was used in the simulation, the concentration of oleic acid was homogeneous throughout the bulk, which was consistent with the results reported by Smith et al. (2003).

The KM-SUB and PDE methods yield very similar results, but the concentration gradients for both O_3 and oleic acid were slightly steeper in the PDE model. A possible reason for the difference may be that the PDE model requires the assumption of a fixed ozone concentration in the near surface bulk and zero flux values at the surface and at center of the particles as specified above (boundary conditions). Another possible reason for deviations is the estimation of bulk transport velocities ($k_{b,b}$). If we assume $k_{b,b} = D_b/\delta$ instead of Eqs. (35) and (36), the KM-SUB results become nearly identical to the PDE results. Note that varying the number of layers in the KM-SUB model made practically no difference.

Appendix C

Kinetic double-layer model (K2-SUB)

A kinetic double-layer of surface and bulk chemistry (K2-SUB) was developed by Pfrang et al. (2009). K2-SUB uses one layer for bulk, therefore concentration profiles in the bulk is not obtained. The diffusion and reaction in the bulk is considered by the reacto-diffusive flux ($J_{b,rd}$) (Danckwerts, 1951; Hanson, 1997; Pöschl et al., 2007). The loss rate of oleic acid in the bulk can be described as follows (Pfrang et al., 2009), which is based on the resistor model formulation (Hanson, 1997):

$$L_{b,Y} = J_{b,rd,X}\frac{A_{ss}}{V_b}$$
$$= C_{b,rd,X}\sqrt{k_{BR,X,Y}[Y]_b D_{b,X}}[X]_{bs}\frac{A_{ss}}{V_b} \quad \text{(C1)}$$

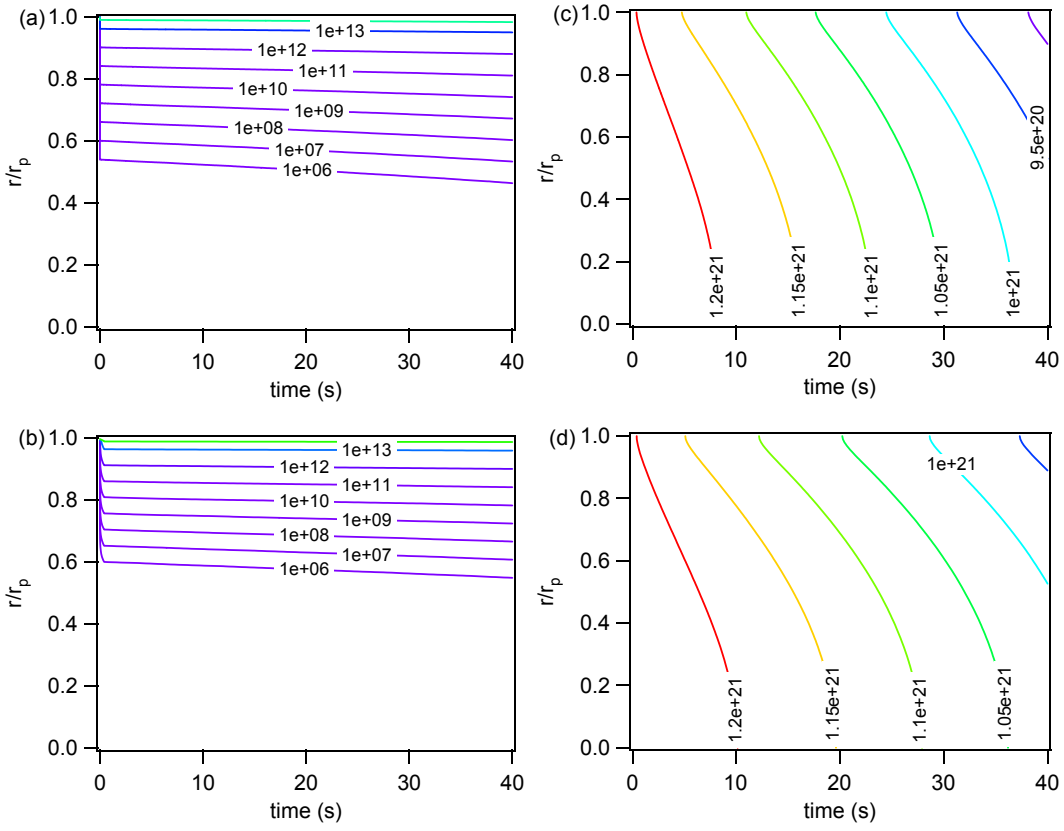

Fig. A1. Temporal evolution of bulk concentration profiles for ozone by **(a)** KM-SUB and **(b)** PDE method and for oleic acid by **(c)** KM-SUB and **(d)** PDE method. The y-axis indicates the radial distance from the particle center (r) normalized by the particle radius, ranging from the particle core ($r/r_p \approx 0$) to the near-surface bulk ($r/r_p = 1$). The colored lines are isopleths of bulk concentration with labeled in units of cm^{-3} (blue = low, red = high).

where A_{ss} and V_b is the surface area and volume of bulk particle. $C_{b,rd,X}$ is the reacto-diffusive geometry correction factor (conversion from planar to spherical geometry) (Pöschl et al., 2007). $C_{b,rd,X}$ is a function of particle radius (r_p) and the reacto-diffusive length $l_{rd,X}$, which can be regarded as the distance from the surface up to which the chemical reaction proceeds effectively (Finlayson-Pitts and Pitts, 2000; Pöschl et al., 2007):

$$C_{b,rd,X} = \coth\left(\frac{r_p}{l_{rd,X}}\right) - \frac{l_{rd,X}}{r_p} \quad \text{(C2)}$$

$$l_{rd,X} = \sqrt{D_{b,X}/(k_{BR,X,Y}[Y]_b)} \quad \text{(C3)}$$

K2-SUB presented by Pfrang et al. (2009) assumed the steady-state condition of O_3 in surface and bulk. K2-SUB was modified by removing these assumptions by including the gas-surface interaction fluxes (adsorption ($J_{ads,X}$), desorption ($J_{des,X}$) and surface layer reaction ($L_{s,X}$ and $L_{ss,X}$)) in the differential equations (X=O_3, Y=oleic acid). The differential equations below can be solved using Matlab solver.

$$d[X]_s/dt = J_{ads,X} - J_{des,X} - L_{s,X} - J_{s,b,X} + J_{b,s,X} \quad \text{(C4)}$$

$$d[Y]_{ss}/dt = J_{b,ss,Y} - J_{ss,b,Y} - L_{ss,Y} \quad \text{(C5)}$$

$$d[X]_b/dt = (J_{s,b,X} - J_{b,s,X} - J_{b,rd,X})A_{ss}/V_b \quad \text{(C6)}$$

$$d[Y]_b/dt = (J_{ss,b,Y} - J_{b,ss,Y} - J_{b,rd,X})A_{ss}/V_b \quad \text{(C7)}$$

Appendix D

KM-SUB rate equations for the ozone – oleic acid model system

The general rate equations outlined in the main text of this manuscript can be applied to any system with multiple chemical components and reactions. The equations actually needed to model the simple two-component system of ozone (X) and oleic acid (Y) investigated in this study are more compact as specified below:

$$d[X]_s/dt = \alpha_{s,0,X}(1-\theta_s)[X]_{gs}\omega_X/4 - \tau_{d,X}^{-1}[X]_s - k_{SLR,X,Y}[X]_s[Y]_{ss} - k_{s,b,X}[X]_s + k_{b,s,X}[X]_{b1} \quad \text{(D1)}$$

$$d[Y]_{ss}/dt = k_{b,ss,Y}[Y]_{b1} - k_{ss,b,Y}[Y]_{ss} - k_{SLR,X,Y}[X]_s[Y]_{ss} \quad \text{(D2)}$$

$$d[X]_{b1}/dt = (k_{s,b,X}[X]_s - k_{b,s,X}[X]_{b1})A(1)/V(1) - (k_{b,b,X}[X]_{b1} - k_{b,b,X}[X]_{b2})A(2)/V(1) - k_{BR,X,Y}[X]_{b1}[Y]_{b1} \quad \text{(D3)}$$

$$d[Y]_{b1}/dt = (k_{ss,b,Y}[Y]_{ss} - k_{b,ss,Y}[Y]_{b1})A(1)/V(1) - (k_{b,b,Y}[Y]_{b1} - k_{b,b,Y}[Y]_{b2})A(2)/V(1) - k_{BR,X,Y}[X]_{b1}[Y]_{b1} \quad \text{(D4)}$$

$$d[X]_{bk}/dt = (k_{b,b,X}[X]_{bk-1} - k_{b,b,X}[X]_{bk})A(k)/V(k) - (k_{b,b,X}[X]_{bk} - k_{b,b,X}[X]_{bk+1})A(k+1)/V(k) - k_{BR,X,Y}[X]_{bk}[Y]_{bk} \quad (k = 2, ..., n-1) \quad \text{(D5)}$$

$$d[Y]_{bk}/dt = (k_{b,b,Y}[Y]_{bk-1} - k_{b,b,Y}[Y]_{bk})A(k)/V(k) - (k_{b,b,Y}[Y]_{bk} - k_{b,b,Y}[Y]_{bk+1})A(k+1)/V(k) - k_{BR,X,Y}[X]_{bk}[Y]_{bk} \quad (k = 2, ..., n-1) \quad \text{(D6)}$$

$$d[X]_{bn}/dt = (k_{b,b,X}[X]_{bn-1} - k_{b,b,X}[X]_{bn})A(n)/V(n) - k_{BR,X,Y}[X]_{bn}[Y]_{bn} \quad \text{(D7)}$$

$$d[Y]_{bn}/dt = (k_{b,b,Y}[Y]_{bn-1} - k_{b,b,Y}[Y]_{bn})A(n)/V(n) - k_{BR,X,Y}[X]_{bn}[Y]_{bn} \quad \text{(D8)}$$

Acknowledgements. This work was funded by the Max Planck Society (MPG) and the European integrated project on cloud climate and air quality interactions (No 036833-2 EUCAARI). MS is supported by the Max Planck Graduate Center (MPGC) and the Ministry of Education, Culture, Sports, Science and Technology – Japan (MEXT). CP wishes to thank the Royal Society (grant VO080001) and the NERC (grant NE/G000883/1). We acknowledge M. Ammann for stimulating discussions and two anonymous referees for constructive comments and suggestions.

The service charges for this open access publication have been covered by the Max Planck Society.

Edited by: V.-M. Kerminen

References

Ammann, M., Kalberer, M., Jost, D. T., Tobler, L., Rossler, E., Piguet, D., Gäggeler, H. W., and Baltensperger, U.: Heterogeneous production of nitrous acid on soot in polluted air masses, Nature, 395, 157–160, 1998.

Ammann, M. and Pöschl, U.: Kinetic model framework for aerosol and cloud surface chemistry and gas-particle interactions – Part 2: Exemplary practical applications and numerical simulations, Atmos. Chem. Phys., 7, 6025–6045, 2007, http://www.atmos-chem-phys.net/7/6025/2007/.

Andreae, M. O. and Rosenfeld, D.: Aerosol-cloud-precipitation interactions, Part 1. The nature and sources of cloud-active aerosols, Earth-Sci. Rev., 89, 13–41, 2008.

Anttila, T., Kiendler-Scharr, A., Tillmann, R., and Mentel, T. F.: On the reactive uptake of gaseous compounds by organic-coated aqueous aerosols: Theoretical analysis and application to the heterogeneous hydrolysis of N_2O_5, J. Phys. Chem. A., 110, 10435–10443, 2006.

Asad, A., Mmereki, B. T., and Donaldson, D. J.: Enhanced uptake of water by oxidatively processed oleic acid, Atmos. Chem. Phys., 4, 2083–2089, 2004, http://www.atmos-chem-phys.net/4/2083/2004/.

Atkins, P. W.: Physical Chemistry, Oxford University Press, Oxford, 1998.

Bird, R. B., Stewart, W. E., and Lightfoot, E. N.: Transport Phenomena (2nd Ed.), John Wiley & Sons, Inc., New York, 2007.

Danckwerts, P. V.: Absorption by simultaneous diffusion and chemical reaction into particles of various shapes and into falling drops, Transactions of the Faraday Society, 47, 1014–1023, 1951.

Finlayson-Pitts, B. J. and Pitts, J. N.: Chemistry of the upper and lower atmosphere, San Diego, California, Academic Pres, 2000.

Fuzzi, S., Andreae, M. O., Huebert, B. J., Kulmala, M., Bond, T. C., Boy, M., Doherty, S. J., Guenther, A., Kanakidou, M., Kawamura, K., Kerminen, V.-M., Lohmann, U., Russell, L. M., and Pöschl, U.: Critical assessment of the current state of scientific knowledge, terminology, and research needs concerning the role of organic aerosols in the atmosphere, climate, and global change, Atmos. Chem. Phys., 6, 2017–2038, 2006, http://www.atmos-chem-phys.net/6/2017/2006/.

Gonzalez-Labrada, E., Schmidt, R., and DeWolf, C. E.: Kinetic analysis of the ozone processing of an unsaturated organic monolayer as a model of an aerosol surface, Phys. Chem. Chem. Phys., 9, 5814–5821, 2007.

Griffiths, P. T., Badger, C. L., Cox, R. A., Folkers, M., Henk, H. H., and Mentel, T. F.: Reactive Uptake of N_2O_5 by Aerosols Containing Dicarboxylic Acids. Effect of Particle Phase, Composition, and Nitrate Content, J. Phys. Chem. A., 113, 5082–5090, 2009.

Hallquist, M., Wenger, J. C., Baltensperger, U., Rudich, Y., Simpson, D., Claeys, M., Dommen, J., Donahue, N. M., George, C., Goldstein, A. H., Hamilton, J. F., Herrmann, H., Hoffmann, T., Iinuma, Y., Jang, M., Jenkin, M. E., Jimenez, J. L., Kiendler-Scharr, A., Maenhaut, W., McFiggans, G., Mentel, Th. F., Monod, A., Prévôt, A. S. H., Seinfeld, J. H., Surratt, J. D., Szmigielski, R., and Wildt, J.: The formation, properties and impact of secondary organic aerosol: current and emerging issues, Atmos. Chem. Phys., 9, 5155–5236, 2009, http://www.atmos-chem-phys.net/9/5155/2009/.

Hanson, D. R.: Surface-specific reactions on liquids, J. Phys. Chem. B., 101, 4998–5001, 1997.

Hearn, J. D., Lovett, A. J., and Smith, G. D.: Ozonolysis of oleic acid particles: evidence for a surface reaction and secondary reactions involving Criegee intermediates, Phys. Chem. Chem. Phys., 7, 501–511, 2005.

Hearn, J. D. and Smith, G. A.: Ozonolysis of mixed oleic acid/n-docosane particles: The roles of phase, morphology, and metastable states, J. Phys. Chem. A., 111, 11059–11065, 2007.

Jimenez, J. L., Canagaratna, M. R., Donahue, N. M., Prevot, A. S. H., Zhang, Q., Kroll, J. H., DeCarlo, P. F., Allan, J. D., Coe, H., Ng, N. L., Aiken, A. C., Docherty, K. S., Ulbrich, I. M., Grieshop, A. P., Robinson, A. L., Duplissy, J., Smith, J. D., Wilson, K. R., Lanz, V. A., Hueglin, C., Sun, Y. L., Tian, J., Laaksonen, A., Raatikainen, T., Rautiainen, J., Vaattovaara, P., Ehn, M., Kulmala, M., Tomlinson, J. M., Collins, D. R., Cubison, M. J., Dunlea, E. J., Huffman, J. A., Onasch, T. B., Alfarra, M. R., Williams, P. I., Bower, K., Kondo, Y., Schneider, J., Drewnick, F., Borrmann, S., Weimer, S., Demerjian, K., Salcedo, D., Cottrell, L., Griffin, R., Takami, A., Miyoshi, T., Hatakeyama, S., Shimono, A., Sun, J. Y., Zhang, Y. M., Dzepina, K., Kimmel, J. R., Sueper, D., Jayne, J. T., Herndon, S. C., Trimborn, A. M., Williams, L. R., Wood, E. C., Middlebrook, A. M., Kolb, C. E., Baltensperger, U., and Worsnop, D. R.: Evolution of Organic Aerosols in the Atmosphere, Science, 326, 1525–1529, 2009.

Kanakidou, M., Seinfeld, J. H., Pandis, S. N., Barnes, I., Dentener, F. J., Facchini, M. C., Van Dingenen, R., Ervens, B., Nenes, A., Nielsen, C. J., Swietlicki, E., Putaud, J. P., Balkanski, Y., Fuzzi, S., Horth, J., Moortgat, G. K., Winterhalter, R., Myhre, C. E. L., Tsigaridis, K., Vignati, E., Stephanou, E. G., and Wilson, J.: Organic aerosol and global climate modelling: a review, Atmos. Chem. Phys., 5, 1053–1123, 2005, http://www.atmos-chem-phys.net/5/1053/2005/.

Katrib, Y., Martin, S. T., Hung, H. M., Rudich, Y., Zhang, H. Z., Slowik, J. G., Davidovits, P., Jayne, J. T., and Worsnop, D. R.: Products and mechanisms of ozone reactions with oleic acid for aerosol particles having core-shell morphologies, J. Phys. Chem. A., 108, 6686–6695, 2004.

Katrib, Y., Biskos, G., Buseck, P. R., Davidovits, P., Jayne, J. T., Mochida, M., Wise, M. E., Worsnop, D. R., and Martin, S. T.: Ozonolysis of mixed oleic-acid/stearic-acid particles: Reaction kinetics and chemical morphology, J. Phys. Chem. A., 109, 10910–10919, 2005.

King, M. D., Thompson, K. C., and Ward, A. D.: Laser tweezers Raman study of optically trapped aerosol droplets of Seawater and oleic acid reacting with ozone: Implications for cloud-droplet properties J. Am. Chem. Soc., 126, 16710–16711, 2004.

King, M. D., Thompson, K. C., Ward, A. D., Pfrang, C., and Hughes, B. R.: Oxidation of biogenic and water-soluble compounds in aqueous and organic aerosol droplets by ozone: a kinetic and product analysis approach using laser Raman tweezers, Faraday Discuss., 137, 173–192, 2008.

King, M. D., Rennie, A. R., Thompson, K. C., Fisher, F. N., Dong, C. C., Thomas, R. K., Pfrang, C., and Hughes, A. V.: Oxidation of oleic acid at the air-water interface and its potential effects on cloud critical supersaturations, Phys. Chem. Chem. Phys., 11, 7699–7707, 2009.

Knopf, D. A., Anthony, L. M., and Bertram, A. K.: Reactive uptake of O_3 by multicomponent and multiphase mixtures containing oleic acid, J. Phys. Chem. A., 109, 5579–5589, 2005.

McNeill, V. F., Wolfe, G. M., and Thornton, J. A.: The oxidation of oleate in submicron aqueous salt aerosols: Evidence of a surface process, J. Phys. Chem. A., 111, 1073–1083, 2007.

McNeill, V. F., Yatavelli, R. L. N., Thornton, J. A., Stipe, C. B., and Landgrebe, O.: Heterogeneous OH oxidation of palmitic acid in single component and internally mixed aerosol particles: vaporization and the role of particle phase, Atmos. Chem. Phys., 8, 5465–5476, 2008, http://www.atmos-chem-phys.net/8/5465/2008/.

Mikhailov, E., Vlasenko, S., Martin, S. T., Koop, T., and Pöschl, U.: Amorphous and crystalline aerosol particles interacting with water vapor: conceptual framework and experimental evidence for restructuring, phase transitions and kinetic limitations, Atmos. Chem. Phys., 9, 9491–9522, 2009, http://www.atmos-chem-phys.net/9/9491/2009/.

Moise, T. and Rudich, Y.: Reactive uptake of ozone by proxies for organic aerosols: Surface versus bulk processes, J. Geophys. Res.-Atmos., 105, 14667–14676, 2000.

Moise, T. and Rudich, Y.: Reactive uptake of ozone by aerosol-associated unsaturated fatty acids: Kinetics, mechanism, and products, J. Phys. Chem. A., 106, 6469–6476, 2002.

Morris, J. W., Davidovits, P., Jayne, J. T., Jimenez, J. L., Shi, Q., Kolb, C. E., Worsnop, D. R., Barney, W. S., and Cass, G.: Kinetics of submicron oleic acid aerosols with ozone: a novel aerosol mass spectrometric technique, Geophys. Res. Lett., 29, 1357, doi:10.1029/2002gl014692, 2002.

Pfrang, C., Shiraiwa, M., and Pöschl, U.: Coupling aerosol surface and bulk chemistry with a kinetic double layer model (K2-SUB): oxidation of oleic acid by ozone, Atmos. Chem. Phys. Discuss., 9, 26969–27019, 2009, http://www.atmos-chem-phys-discuss.net/9/26969/2009/.

Pöschl, U.: Formation and decomposition of hazardous chemical components contained in atmospheric aerosol particles, Journal of Aerosol Medicine-Deposition Clearance and Effects in the Lung, 15, 203–212, 2002.

Pöschl, U.: Atmospheric aerosols: Composition, transformation, climate and health effects, Angewandte Chemie-International Edition, 44, 7520–7540, 2005.

Pöschl, U., Rudich, Y., and Ammann, M.: Kinetic model framework for aerosol and cloud surface chemistry and gas-particle interactions – Part 1: General equations, parameters, and terminology, Atmos. Chem. Phys., 7, 5989–6023, 2007, http://www.atmos-chem-phys.net/7/5989/2007/.

Rincon, A. G., Guzman, M. I., Hoffmann, M. R., and Colussi, A. J.: Optical absorptivity versus molecular composition of model organic aerosol matter, J. Phys. Chem. A., 113, 10512–10520, 2009.

Rogge, W. F., Hildemann, L. M., Mazurek, M. A., Cass, G. R., and Simonelt, B. R. T.: Sources of fine organic aerosol: 1. Charbroilers and meat cooking operations, Environ. Sci. Technol., 25, 1112–1125, 1991.

Rudich, Y.: Laboratory perspectives on the chemical transformations of organic matter in atmospheric particles, Chem. Rev., 103, 5097–5124, 2003.

Rudich, Y., Donahue, N. M., and Mentel, T. F.: Aging of organic aerosol: Bridging the gap between laboratory and field studies, Ann. Rev. Phys. Chem., 58, 321–352, 2007.

Sage, A. M., Weitkamp, E. A., Robinson, A. L., and Donahue, N.

M.: Reactivity of oleic acid in organic particles: changes in oxidant uptake and reaction stoichiometry with particle oxidation, Phys. Chem. Chem. Phys., 11, 7951–62, 2009.

Schwartz, S. E. and Freiberg, J. E.: Mass-transport limitation to the rate of reaction of gases in liquid droplets – Application to oxidation of SO_2 in aqueous-solutions, Atmos. Environ., 15, 1129–1144, 1981.

Seinfeld, J. H. and Pandis, S. N.: Atmospheric chemistry and physics – From air pollution to climate change, John Wiley & Sons, Inc., New York, 1998.

Shiraiwa, M., Garland, R. M., and Pöschl, U.: Kinetic double-layer model of aerosol surface chemistry and gas-particle interactions (K2-SURF): Degradation of polycyclic aromatic hydrocarbons exposed to O_3, NO_2, H_2O, OH and NO_3, Atmos. Chem. Phys., 9, 9571–9586, 2009, http://www.atmos-chem-phys.net/9/9571/2009/.

Smith, G. D., Woods, E., DeForest, C. L., Baer, T., and Miller, R. E.: Reactive uptake of ozone by oleic acid aerosol particles: Application of single-particle mass spectrometry to heterogeneous reaction kinetics, J. Phys. Chem. A., 106, 8085–8095, 2002.

Smith, G. D., Woods, E., Baer, T., and Miller, R. E.: Aerosol uptake described by numerical solution of the diffusion – Reaction equations in the particle, J. Phys. Chem. A., 107, 9582–9587, 2003.

Springmann, M., Knopf, D. A., and Riemer, N.: Detailed heterogeneous chemistry in an urban plume box model: reversible co-adsorption of O_3, NO_2, and H_2O on soot coated with benzo[a]pyrene, Atmos. Chem. Phys., 9, 7461–7479, 2009

Swallen, S. F., Kearns, K. L., Mapes, M. K., Kim, Y. S., McMahon, R. J., Ediger, M. D., Wu, T., Yu, L., and Satija, S.: Organic glasses with exceptional thermodynamic and kinetic stability, Science, 315, 353–356, 2007.

Thornberry, T. and Abbatt, J. P. D.: Heterogeneous reaction of ozone with liquid unsaturated fatty acids: detailed kinetics and gas-phase product studies, Phys. Chem. Chem. Phys., 6, 84–93, 2004.

Titov, V. N., Konovalova, G. G., Lisitsyn, D. M., Razumovskii, S. D., Nezhdanova, I. B., and Kukharchuk, V. V.: Kinetics of fatty acid oxidation in low density lipoproteins evaluated by registration of the oxidizer consumption and reaction product yield, Bulletin of Experimental Biology and Medicine, 140, 38–40, 2005.

Vesna, O., Sax, M., Kalberer, M., Gaschen, A., and Ammann, M.: Product study of oleic acid ozonolysis as function of humidity, Atmos. Environ., 43, 3662–3669, 2009.

Vieceli, J., Roeselova, M., Potter, N., Dang, L. X., Garrett, B. C., and Tobias, D. J.: Molecular dynamics simulations of atmospheric oxidants at the air-water interface: Solvation and accommodation of OH and O_3, J. Phys. Chem. B., 109, 15876–15892, 2005.

Wiedensohler, A., Cheng, Y. F., Nowak, A., Wehner, B., Achtert, P., Berghof, M., Birmili, W., Wu, Z. J., Hu, M., Zhu, T., Takegawa, N., Kita, K., Kondo, Y., Lou, S. R., Hofzumahaus, A., Holland, F., Wahner, A., Gunthe, S. S., Rose, D., Su, H., and Pöschl, U.: Rapid aerosol particle growth and increase of cloud condensation nucleus activity by secondary aerosol formation and condensation: A case study for regional air pollution in northeastern China, J. Geophys. Res.-Atmos., 114, D00G08, doi:10.1029/2008jd010884, 2009.

Worsnop, D. R., Morris, J. W., Shi, Q., Davidovits, P., and Kolb, C. E.: A chemical kinetic model for reactive transformations of aerosol particles, Geophys. Res. Lett., 29, 20, doi:10.1029/2002GL015542, 2002.

Zahardis, J. and Petrucci, G. A.: The oleic acid-ozone heterogeneous reaction system: products, kinetics, secondary chemistry, and atmospheric implications of a model system – a review, Atmos. Chem. Phys., 7, 1237–1274, 2007, http://www.atmos-chem-phys.net/7/1237/2007/.

Ziemann, P. J.: Aerosol products, mechanisms, and kinetics of heterogeneous reactions of ozone with oleic acid in pure and mixed particles, Faraday Discuss., 130, 469–490, 2005.

Zobrist, B., Marcolli, C., Pedernera, D. A., and Koop, T.: Do atmospheric aerosols form glasses?, Atmos. Chem. Phys., 8, 5221–5244, 2008, http://www.atmos-chem-phys.net/8/5221/2008/.

B4) Shiraiwa et al., Nature Chemistry, 2011

The role of long-lived reactive oxygen intermediates in the reaction of ozone with aerosol particles

Manabu Shiraiwa[1], Yulia Sosedova[2,3], Aurélie Rouvière[2], Hong Yang[1], Yingyi Zhang[1], Jonathan P. D. Abbatt[4], Markus Ammann[2], Ulrich Pöschl[1]

1. Max Planck Institute for Chemistry, Department of Biogeochemistry, PO Box 3060, 55128, Mainz, Germany.
2. Paul Scherrer Institut, Laboratory of Radiochemistry and Environmental Chemistry, Villigen, CH-5232, Switzerland.
3. Department of Chemistry and Biochemistry, University of Bern, Freiestrasse 3, Bern CH-3012, Switzerland.
4. University of Toronto, Department of Chemistry, 80 St George Street, Toronto, Ontario M5S 3H6, Canada.

.

Nature Chemistry 3(4): 291-295, 2011.

Authors contributions.

UP, MA and MS designed the research. MS, YS, AR and MA performed tracer experiments and MS analyzed the data. HY and YZ contributed to the protein studies.MS and UP conducted the kinetic modeling. MS, UP, MA and JA discussed the results. MS, UP and MA co-wrote the paper.

nature chemistry

ARTICLES

PUBLISHED ONLINE: 20 FEBRUARY 2011 | DOI: 10.1038/NCHEM.988

The role of long-lived reactive oxygen intermediates in the reaction of ozone with aerosol particles

Manabu Shiraiwa[1], Yulia Sosedova[2,3], Aurélie Rouvière[2], Hong Yang[1], Yingyi Zhang[1], Jonathan P. D. Abbatt[4], Markus Ammann[2] and Ulrich Pöschl[1]*

The heterogeneous reactions of O_3 with aerosol particles are of central importance to air quality. They are studied extensively, but the molecular mechanisms and kinetics remain unresolved. Based on new experimental data and calculations, we show that long-lived reactive oxygen intermediates (ROIs) are formed. The chemical lifetime of these intermediates exceeds 100 seconds, which is much longer than the surface residence time of molecular O_3 ($\sim 10^{-9}$ s). The ROIs explain and resolve apparent discrepancies between earlier quantum mechanical calculations and kinetic experiments. They play a key role in the chemical transformation and adverse health effects of toxic and allergenic air-particulate matter, such as soot, polycyclic aromatic hydrocarbons and proteins. ROIs may also be involved in the decomposition of O_3 on mineral dust and in the formation and growth of secondary organic aerosols. Moreover, ROIs may contribute to the coupling of atmospheric and biospheric multiphase processes.

Reactive oxygen species (ROS) play important roles in both atmospheric chemistry and physiological processes: O_3 photochemistry, oxidative self-cleaning of the atmosphere, biological ageing, metabolism and oxidative stress[1–4]. In physiology and biochemistry, the umbrella term ROS is defined broadly to comprise a wide range of oxygen-centred and related free radicals, ions and molecules[1–3]. As illustrated in Fig. 1, different types of ROS are closely coupled by radical reactions and cyclic transformation[5–7]. The coupling and exchange of atmospheric and physiological ROS can proceed through various interfaces, such as plant surfaces and the human respiratory tract (emission and deposition of trace gases and particle deposition). Also, the biomedical definition of ROS includes reactive nitrogen species (RNS), such as NO, NO_2 and ONO_2^- (ref. 3). In atmospheric science, however, RNS are usually treated separately from oxy, hydroxy and peroxy radicals[7,8]. For clarity, we adopt the term ROIs to describe the subset of ROS potentially involved in the reaction of O_3 with aerosol particles, including organic and inorganic species, with reactive oxygen atoms or groups (O, RO, RO_2 and so on).

Heterogeneous reactions of O_3 with aerosol particles are studied extensively, but the molecular mechanism and kinetics remain unresolved[9–15]. Among the organic aerosol components that react readily with O_3, polycyclic aromatic hydrocarbons (PAHs) are one of the most prominent groups in terms of health effects. They are an integral component of soot and related carbonaceous combustion aerosol particles (in the submicron range) that can penetrate deep into human lungs[7]. Chemical transformation can change the toxicity of PAHs and modify the hygroscopic properties and climate effects of combustion aerosol particles[6,7]. PAH oxidation products (quinones, phenols and so on) are also involved in physiological processes that lead to the adverse health effects of traffic-related air pollution[3,5,16,17]. Several studies show that O_3 can also promote the nitration of protein molecules contained in primary biological aerosol particles, such as pollen and fungal spores[18–20]. This post-translational modification can enhance the allergenic potential of proteins. It provides a molecular rationale for the enhancement of allergic diseases by traffic-related air pollution in urban and rural environments observed in epidemiological studies, but the molecular mechanism remains to be elucidated[18,21,22].

Laboratory studies of the heterogeneous reaction of O_3 with PAHs adsorbed on soot and other substrates generally show a non-linear dependence of the first-order PAH decay rate coefficient on gas-phase O_3 concentration, which is consistent with a Langmuir–Hinshelwood (LH) reaction mechanism[12,23], in which an adsorbed O_3 molecule reacts with the PAH in a surface reaction. The O_3

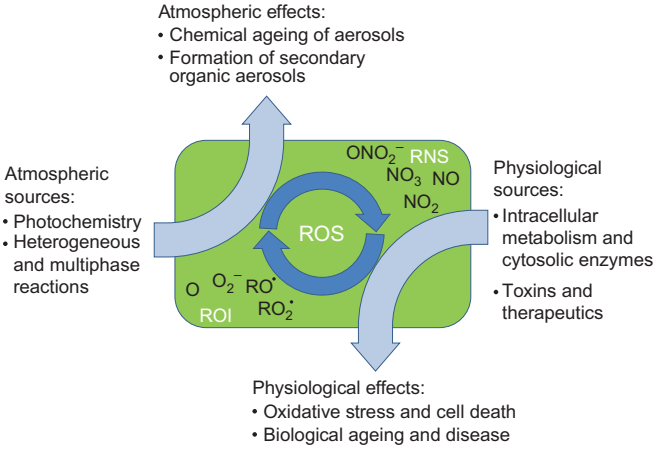

Figure 1 | Illustration of the atmospheric and physiological sources, coupling and effects of ROS. These are defined broadly to include ROIs as well as RNS.

[1]Max Planck Institute for Chemistry, Department of Biogeochemistry, PO Box 3060, 55128, Mainz, Germany, [2]Paul Scherrer Institut, Laboratory of Radiochemistry and Environmental Chemistry, Villigen, CH-5232, Switzerland, [3]Department of Chemistry and Biochemistry, University of Bern, Freiestrasse 3, Bern CH-3012, Switzerland, [4]University of Toronto, Department of Chemistry, 80 St George Street, Toronto, Ontario M5S 3H6, Canada.
*e-mail: u.poschl@mpic.de

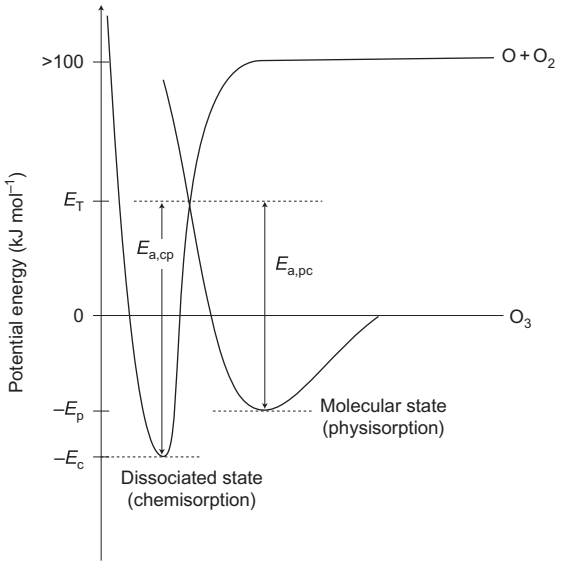

Figure 2 | Lennard-Jones potential energy diagram for the adsorption of molecular and dissociated O_3. The physisorbed O_3 molecule (binding energy E_p) can be desorbed thermally to the gas phase with a desorption lifetime of nanoseconds, or it can overcome an activation barrier ($E_{a,pc}$), go through a transition state (potential energy E_T) and enter into a dissociated state (binding energy E_c). The process can be reversed by overcoming the activation barrier from chemisorption to physisorption ($E_{a,cp}$). The horizontal axis represents the distance from the surface.

surface-residence time or desorption lifetime (τ_{d,O_3}) inferred from kinetic data, assuming a simple LH reaction between adsorbed O_3 and surface molecules, are in the range 10^{-2} s to 10 s (refs 24,25). However, according to quantum mechanical calculations based on density functional theory (DFT), the desorption lifetime of O_3 on PAH[11] or graphene[26] should be only nanoseconds, which is more than six orders of magnitude less. This indicates that the DFT simulations address a different step and state of O_3 adsorption than the reaction kinetic experiments. In this study we resolve the apparent discrepancy using a new kinetic modelling approach that takes into account intermediate processes of O_3 decomposition on the surface.

Results and discussion

ROIs in the oxidation of PAHs. Figure 2 shows a Lennard-Jones potential energy diagram[27] for the adsorption of O_3. It comprises one curve that describes the weak interaction of molecular O_3 with the surface (physisorption) and another that describes the stronger interaction and dissociation of O_3 at the surface (chemisorption). Figure 2 illustrates the thermodynamic conditions for the initial steps of the heterogeneous reaction of gaseous O_3. The weakly bound physisorbed O_3 molecule (binding energy E_p) can be desorbed thermally to the gas phase with a desorption lifetime of nanoseconds, or it can overcome an activation barrier ($E_{a,pc}$), undergo dissociation and enter into a state of stronger binding to the surface (E_c, Fig. 2). The transition state from molecular to dissociated O_3 may be a primary ozonide or a trioxyl diradical[11,28]. The dissociation products are molecular oxygen[29,30] and a ROI, such as a chemisorbed oxygen atom bound to the delocalized π-electrons of an aromatic surface[11,28]. In a further reaction step, the ROIs can form stable products, for example oxygenated PAHs with hydroxyl, carbonyl and other functional groups[7]. Alternatively, the ROIs may be lost by self-reaction or reactions with other chemical species. In surface and materials science, chemisorbed oxygen atoms on aromatic surfaces are often designated as 'epoxide-like' groups[11,26,28,31,32]. However, the oxygen atoms in these 'epoxide-like' groups reside above the aromatic system, which implies that the electronic structure and chemical properties are different from those of classical epoxides[33].

Figure 3 shows experimental data[12] and model results for the heterogeneous ozonolysis of benzo[*a*]pyrene (BaP, $C_{20}H_{12}$), one of the most toxic PAH priority pollutants[7]. The experiments were performed with soot aerosol particles coated in BaP[12] and the model calculations were performed with a kinetic double-layer surface model (K2-SURF)[24] using parameters as detailed in Supplementary Table 1. Figure 3a shows the first-order BaP decay rate coefficient ($k_{s,PAH}$) and Fig. 3b shows the adsorbate surface coverage (θ_s) plotted against the gas-phase O_3 concentration ($[O_3]_g$). The experimentally observed nonlinear dependence of $k_{s,PAH}$ and θ_s on $[O_3]_g$ can be reproduced under the assumption of a simple LH reaction between BaP and reversibly adsorbed O_3 with a very long desorption lifetime ($\tau_{d,O_3} = 16$ s) (ref. 12). If, however, we use a more reasonable very short desorption lifetime predicted by DFT calculations[11,26] ($\tau_{d,O_3} = 3$ ns) in line with the potential energy diagram of Fig. 2, the observations can be matched only with a multistep LH reaction mechanism that involves the formation of ROIs with long lifetimes ($\sim 10^2$ s, see Supplementary Section S1). A simple LH mechanism with short O_3-desorption lifetimes and without the formation of long-lived ROIs would lead to a linear concentration dependence

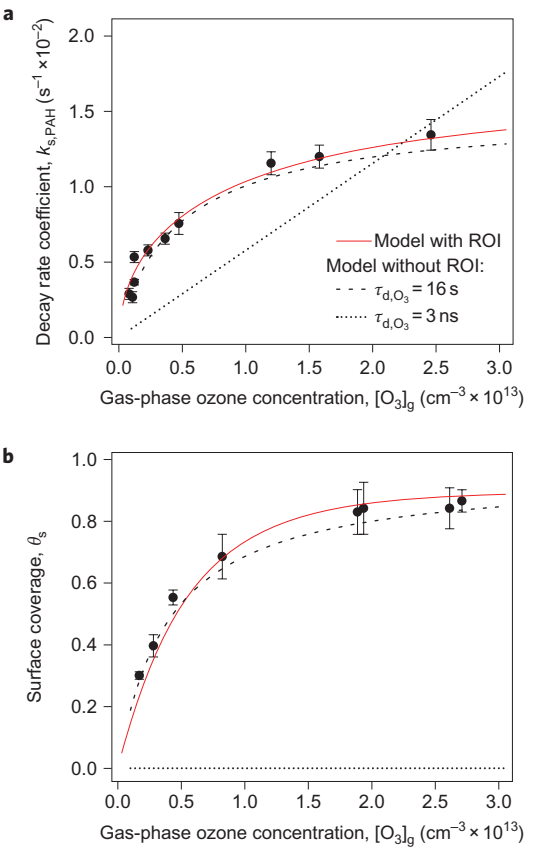

Figure 3 | Experimental and model results for heterogeneous ozonolysis of the PAH BaP on soot aerosol particles. a,b, Pseudo first-order decay rate coefficient for BaP ($k_{s,PAH}$) (**a**) and surface coverage (θ_s) (**b**) by physisorbed and chemisorbed O_3 as a function of gas-phase O_3 concentration ($[O_3]_g$). The data points and error bars represent experimental data and standard deviations[12]. The red line is from a model with ROI formation using a desorption lifetime for O_3 (τ_{d,O_3}) of 3 ns. The black lines are from models without ROI formation and with τ_{d,O_3} of 3 ns (dotted line) or 16 s (dashed line).

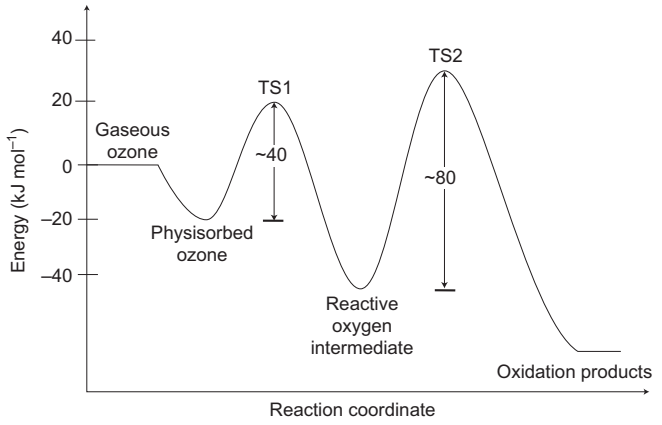

Figure 4 | Energy profile for the reaction of O_3 with the PAH BaP on soot. The ROI may be regarded as a chemisorbed oxygen atom. TS1 is the transition state from physisorbed O_3 to the ROI, which may be regarded as a trioxyl diradical or primary ozonide. TS2 is the transition state from the ROI to the oxidation products (oxygenated PAH), which may be regarded as an oxy or peroxy radical.

of $k_{s,PAH}$ on $[O_3]_g$ and to an unrealistically low surface coverage ($\theta_s = 10^{-6}$, Fig. 3b).

From the kinetic model approach using a multistep LH reaction mechanism, we derived an activation energy of $E_{a,pc} = \sim 41(\pm 7)$ kJ mol^{-1} for the transition from the physisorbed O_3 molecules to the ROI. This is consistent with the range of activation energies estimated from DFT calculations for the chemisorption of O_3 on PAHs and graphene (~40–100 kJ mol^{-1}) (refs 11,26). The activation energy from a ROI to oxidation products was estimated to be $\sim 80(\pm 9)$ kJ mol^{-1} (Supplementary Section S1.3, equation (20)). Accordingly, the energy profile of the heterogeneous reaction between O_3 and PAH that involves ROI formation can be described as shown in Fig. 4. The explicit inclusion of long-lived ROIs in a kinetic model allows us, for the first time, to reconcile the thermodynamic data of DFT calculations with the results of experimental studies to investigate the interaction of O_3 with aromatic surfaces.

ROIs in the nitration of protein. Also, strong evidence for the formation of long-lived ROIs from the interaction of O_3 with aerosol particles is provided by new experimental results on the nitration by NO_2 of the aromatic amino acid tyrosine in protein macromolecules. The uptake of NO_2 by protein particles was investigated in an aerosol flow tube using a short-lived radioactive tracer technique (^{13}N) (ref. 34) and bovine serum albumin (BSA), a globular protein with a molecular mass of 67 kDa and 21 tyrosine residues per molecule. The experimental methods are described below and in Supplementary Section S2.

As shown in Fig. 5, the NO_2 uptake coefficient (γ_{NO_2}) of BSA particles that were not in contact with O_3 was less than the detection limit ($\sim 10^{-6}$), which is consistent with previous studies that indicate protein nitration by NO_2 alone is very slow[18]. However, when the BSA particles were pretreated with O_3 (97 parts per 10^9 (ppb)) and then exposed to NO_2 in the absence of O_3, a very efficient uptake of NO_2 was observed, with uptake coefficients that decreased with increases in NO_2 concentration from $\gamma_{NO_2} \approx 5 \times 10^{-4}$ at 6 ppb NO_2 to $\gamma_{NO_2} \approx 1 \times 10^{-4}$ at 27 ppb NO_2. The high reactivity of NO_2 with O_3-pretreated particles can be explained by a nitration reaction that involves O_3-generated ROIs – most likely phenoxy radical derivatives of tyrosine (Supplemetray Section S2.6)[35,36]. The decrease of γ_{NO_2} with increasing NO_2 concentration can be explained by the increasing consumption of ROIs. With concomitant exposure to O_3 (97 ppb), NO_2 uptake was still substantial, but γ_{NO_2} was lower, which can be attributed to competitive adsorption and reaction ($\gamma_{NO_2} \approx 5 \times 10^{-5}$). The rapid NO_2 uptake by pretreated BSA particles confirms that the reaction involves O_3-generated ROIs and is not dominated by alternative reaction pathways (reaction with NO_3 and N_2O_5 formed in the gas phase).

To examine the lifetime of the ROIs formed by O_3 on the proteins, we introduced a dead volume after the removal of O_3 and before the exposure of pretreated BSA particles to NO_2. We varied the time between O_3 pretreatment and NO_2 exposure over the range 250–550 s, but we observed no significant decrease of γ_{NO_2} (Fig. 6). This implies that the ROIs are long-lived and exhibit no significant decay on a timescale of ten minutes. The observed γ_{NO_2} results imply that proteins on the surface of aerosol particles are nitrated efficiently, within minutes, under photochemical smog conditions with high concentrations of O_3 and NO_2. The final products of the nitration reaction are nitrotyrosine residues in the protein macromolecule[18,37,38].

ROIs in other atmospheric surface and multiphase processes. Besides PAH oxidation and protein nitration, long-lived ROIs also appear to influence the reaction rates of O_3 with other surfaces, including olefinic and inorganic substrates (such as mineral dust), which exhibit similar LH reaction kinetics[9,10]. The ozonolysis of olefins may involve ozonides or stabilized Criegee intermediates[39,40], and the formation of atomic oxygen and peroxides was invoked to explain the kinetics of O_3 decomposition on mineral dust[41–43]. The chemical identity of O_3-generated ROIs probably varies with the nature of the substrate, but their formation energetics, given by the decomposition of adsorbed O_3 molecules, are probably similar for many substrates. They need to be long-lived to explain the LH reaction kinetics observed on interaction of O_3 with aerosol particles.

Apart from the chemical ageing of air particulate matter, long-lived ROIs may also participate in the formation and growth of secondary organic aerosols. In particular, surface interactions of long-lived ROIs may lead to the formation of multifunctional organic substances (acids, nitrates, sulfates, dimers, oligomers and so on) with the high molecular mass and low vapour pressure required for the nucleation and growth of new particles, and they may also influence their phase state[44–48]. Further investigations are required to unravel individual molecular species and steps involved

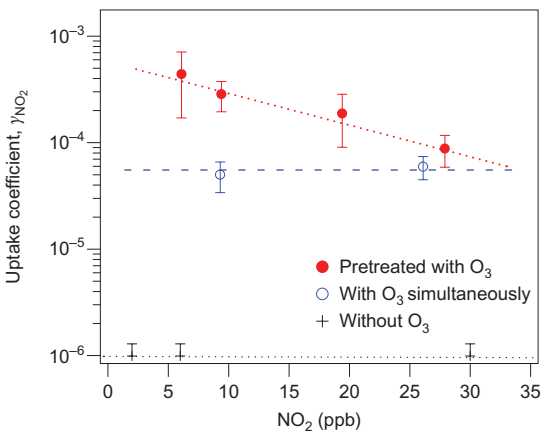

Figure 5 | Uptake coefficients of NO_2 by protein particles. These were exposed only to NO_2 (black crosses), exposed to 97 ppb O_3 and NO_2 at the same time (blue circles) or first pretreated with 97 ppb O_3 and then exposed to NO_2 (red circles). The data points and error bars represent experimental data and standard deviations. The lines are to guide the eye and illustrate that the NO_2 uptake is below the detection limit without O_3 (black), significant in the presence of O_3 (blue) and highest after pretreatment with O_3 (red).

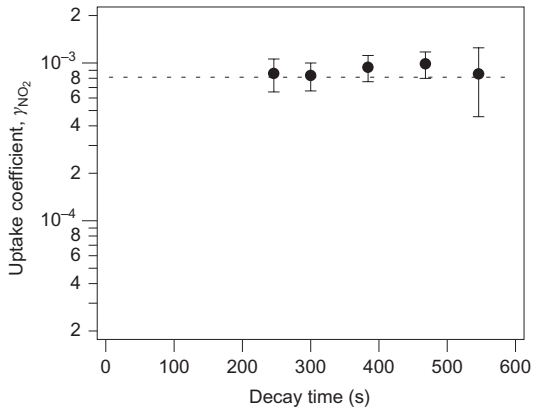

Figure 6 | Uptake coefficients of NO_2 by O_3-pretreated protein particles. These are plotted against the decay time after which the pretreated particles were exposed to NO_2. The data points and error bars represent experimental data and standard deviations. The line illustrates that the NO_2 uptake is quasi-constant up to about ten minutes, which confirms that the O_3-generated ROIs are long-lived.

in the processes outlined above, as well as their relative importance. The experimental and theoretical information currently available suggests that long-lived O_3-generated ROIs play a central role in the multiphase chemistry of atmospheric aerosols.

Methods

PAH oxidation. The kinetic double-layer model applied to model PAH oxidation (K2-SURF)[24] is based on the Pöschl–Rudich–Ammann framework for aerosol and cloud surface chemistry and gas–particle interactions[49,50]. It describes the gas–particle interface by using several compartments and molecular layers in which volatile and non-volatile species can undergo mass transport and chemical reactions: gas phase, near-surface gas phase, sorption layer and quasi-static surface layer. The chemical mechanisms and derivations of kinetic parameters are described in Supplementary Section S1. The surface mass balance and rate equations of surface species were solved numerically.

Protein nitration. Aerosols were generated by nebulizing an aqueous solution of BSA. The size distribution and surface area of particles were monitored by a scanning mobility particle sizer. Gas and particle flows were mixed in a cylindrical perfluoroalkoxy polymer flow tube. For the O_3 pretreatment experiments, O_3 was removed from the aerosol flow using potassium iodide denuder before mixing with NO_2. Afterwards, the flow entered a narrow parallel-plate diffusion denuder train coated to absorb the gas-phase NO_2 selectively, and then passed through a particle filter to collect the particles. The gamma-radiation detectors were attached to each denuder section and to the filters to detect the amount of emitted gamma quanta in the decay of ^{13}N, which corresponds to the amount of trapped ^{13}N molecules of a given species.

Received 19 October 2010; accepted 14 January 2011; published online 20 February 2011

References

1. Venkatachari, P. & Hopke, P. K. Development and evaluation of a particle-bound reactive oxygen species generator. *J. Aerosol. Sci.* **39,** 168–174 (2008).
2. Apel, K. & Hirt, H. Reactive oxygen species: metabolism, oxidative stress, and signal transduction. *Annu. Rev. Plant. Biol.* **55,** 373–399 (2004).
3. Finkel, T. & Holbrook, N. J. Oxidants, oxidative stress and the biology of ageing. *Nature* **408,** 239–247 (2000).
4. Mittler, R. Oxidative stress, antioxidants and stress tolerance. *Trends Plant Sci.* **7,** 405–410 (2002).
5. Pöschl, U. Atmospheric aerosols: composition, transformation, climate and health effects. *Angew. Chem. Int. Ed.* **44,** 7520–7540 (2005).
6. George, I. J. & Abbatt, J. P. D. Heterogeneous oxidation of atmospheric aerosol particles by gas-phase radicals. *Nature Chem.* **2,** 713–722 (2010).
7. Finlayson-Pitts, B. J. & Pitts, J. N. *Chemistry of the Upper and Lower Atmosphere* (Academic Press, 2000).
8. Seinfeld, J. H. & Pandis, S. N. *Atmospheric Chemistry and Physics – From Air Pollution to Climate Change* (John Wiley, 1998).
9. Finlayson-Pitts, B. J. Reactions at surfaces in the atmosphere: integration of experiments and theory as necessary (but not necessarily sufficient) for predicting the physical chemistry of aerosols. *Phys. Chem. Chem. Phys.* **11,** 7760–7779 (2009).
10. McCabe, J. & Abbatt, J. P. D. Heterogeneous loss of gas-phase ozone on *n*-hexane soot surfaces: similar kinetics to loss on other chemically unsaturated solid surfaces. *J. Phys. Chem. C* **113,** 2120–2127 (2009).
11. Maranzana, A. *et al.* Ozone interaction with polycyclic aromatic hydrocarbons and soot in atmospheric processes: theoretical density functional study by molecular and periodic methodologies. *J. Phys. Chem. A* **109,** 10929–10939 (2005).
12. Pöschl, U., Letzel, T, Schauer, C. & Niessner, R. Interaction of ozone and water vapor with spark discharge soot aerosol particles coated with benzo[*a*]pyrene: O_3 and H_2O adsorption, benzo[*a*]pyrene degradation, and atmospheric implications. *J. Phys. Chem. A* **105,** 4029–4041 (2001).
13. Kolb, C. E. *et al.* An overview of current issues in the uptake of atmospheric trace gases by aerosols and clouds. *Atmos. Chem. Phys.* **10,** 10561–10605 (2010).
14. Rudich, Y., Donahue, N. M. & Mentel, T. F. Aging of organic aerosol: bridging the gap between laboratory and field studies. *Annu. Rev. Phys. Chem.* **58,** 321–352 (2007).
15. Chu, S. N. *et al.* Ozone oxidation of surface-adsorbed polycyclic aromatic hydrocarbons: role of PAH–surface interaction. *J. Am. Chem. Soc.* **132,** 15968–15975 (2010).
16. Nel, A. Air pollution-related illness: effects of particles. *Science* **308,** 804–806 (2005).
17. Pöschl, U. Formation and decomposition of hazardous chemical components contained in atmospheric aerosol particles. *J. Aerosol. Med.* **15,** 203–212 (2002).
18. Franze, T., Weller, M. G., Niessner, R. & Pöschl, U. Protein nitration by polluted air. *Environ. Sci. Technol.* **39,** 1673–1678 (2005).
19. Fröhlich-Nowoisky, J., Pickersgill, D. A., Despres, V. R. & Pöschl U. High diversity of fungi in air particulate matter. *Proc. Natl Acad. Sci. USA* **106,** 12814–12819 (2009).
20. Yang, H., Zhang, Y. & Pöschl, U. Quantification of nitrotyrosine in nitrated proteins. *Anal. Bioanal. Chem.* **397,** 879–886 (2010).
21. Gruijthuijsen, Y. K. *et al.* Nitration enhances the allergenic potential of proteins. *Int. Arch. Allergy Immunol.* **141,** 265–275 (2006).
22. Traidl-Hoffmann, C., Jakob, T. & Behrendt, H. Determinants of allergenicity. *J. Allergy Clin. Immunol.* **123,** 558–566 (2009).
23. Ammann, M., Pöschl, U. & Rudich, Y. Effects of reversible adsorption and Langmuir–Hinshelwood surface reactions on gas uptake by atmospheric particles. *Phys. Chem. Chem. Phys.* **5,** 351–356 (2003).
24. Shiraiwa, M., Garland, R. M. & Pöschl, U. Kinetic double-layer model of aerosol surface chemistry and gas-particle interactions (K2-SURF): degradation of polycyclic aromatic hydrocarbons exposed to O_3, NO_2, H_2O, OH and NO_3. *Atmos. Chem. Phys.* **9,** 9571–9586 (2009).
25. Kwamena, N. O. A. *et al.* Role of the aerosol substrate in the heterogeneous ozonation reactions of surface-bound PAHs. *J. Phys. Chem. A* **111,** 11050–11058 (2007).
26. Lee, G., Lee, B., Kim, J. & Cho, K. Ozone adsorption on graphene: *ab initio* study and experimental validation. *J. Phys. Chem. C* **113,** 14225–14229 (2009).
27. Lennard-Jones, J. E. Processes of adsorption and diffusion on solid surfaces. *Trans. Faraday Soc.* **28,** 333–358 (1932).
28. Giordana, A. *et al.* Soot platelets and PAHs with an odd number of unsaturated carbon atoms and pi electrons: theoretical study of their spin properties and interaction with ozone. *J. Phys. Chem. A* **112,** 973–982 (2008).
29. Stephens, S., Rossi, M. J. & Golden D. M. The heterogeneous reaction of ozone on carbonaceous surfaces. *Int. J. Chem. Kinet.* **18,** 1133–1149 (1986).
30. Rogaski, C. A., Golden, D. M. & Williams, L. R. Reactive uptake and hydration experiments on amorphous carbon treated with NO_2, SO_2, O_3, HNO_3, and H_2SO_4. *Geophys. Res. Lett.*, **24,** 381–384 (1997).
31. Sorescu, D. C., Jordan, K. D. & Avouris, P. Theoretical study of oxygen adsorption on graphite and the (8,0) single-walled carbon nanotube. *J. Phys. Chem. B* **105,** 11227–11232 (2001).
32. Kutana, A. & Giapis, K. P. First-principles study of chemisorption of oxygen and aziridine on graphitic nanostructures. *J. Phys. Chem. C* **113,** 14721–14726 (2009).
33. Paulot, F. *et al.* Unexpected epoxide formation in the gas-phase photooxidation of isoprene. *Science* **325,** 730–733 (2009).
34. Ammann, M. Using ^{13}N as tracer in heterogeneous atmospheric chemistry experiments. *Radiochim. Acta* **89,** 831–838 (2001).
35. Truong, H., Lomnicki, S. & Dellinger, B. Potential for misidentification of environmentally persistent free radicals as molecular pollutants in particulate matter. *Environ. Sci. Technol.*, **44,** 1933–1939 (2010).
36. Harrison, M. A. J. *et al.* Nitrated phenols in the atmosphere: a review. *Atmos. Environ.*, **39,** 231–248 (2005).
37. Zhang, Y., Yang, H. & Pöschl, U. Analysis of nitrated proteins and tryptic peptides by HPLC-chip-MS/MS: site-specific quantification, nitration degree, and reactivity of tyrosine residues. *Anal. Bioanal. Chem.* **399,** 459–477 (2011).
38. Walcher, W. *et al.* Liquid- and gas-phase nitration of bovine serum albumin studied by LC-MS and LC-MS/MS using monolithic columns. *J. Proteome Res.* **2,** 534–542 (2003).

39. Baker, J., Aschmann, S. M., Arey, J. & Atkinson, R. Reactions of stabilized Criegee intermediates from the gas-phase reactions of O_3 with selected alkenes. *Int. J. Chem. Kinet.* **34,** 73–85 (2001).
40. Dubowski, Y. *et al.* Interaction of gas-phase ozone at 296 K with unsaturated self-assembled monolayers: a new look at an old system. *J. Phys. Chem. A* **108,** 10473–10485 (2004).
41. Li, W., Gibbs, G. V. & Oyama, S. T. Mechanism of ozone decomposition on a manganese oxide catalyst. I. *In situ* Raman spectroscopy and *ab initio* molecular orbital calculations. *J. Am. Chem. Soc.* **120,** 9041–9046 (1998).
42. Sullivan, R. C., Thornberry, T. & Abbatt, J. P. D. Ozone decomposition kinetics on alumina: effects of ozone partial pressure, relative humidity and repeated oxidation cycles. *Atmos. Chem. Phys.* **4,** 1301–1310 (2004).
43. Hanisch, F. & Crowley, J. N. Ozone decomposition on Saharan dust: an experimental investigation. *Atmos. Chem. Phys.* **3,** 119–130 (2003).
44. Hallquist, M. *et al.* The formation, properties and impact of secondary organic aerosol: current and emerging issues. *Atmos. Chem. Phys.* **9,** 5155–5235 (2009).
45. Jimenez, J. L. *et al.* Evolution of organic aerosols in the atmosphere. *Science* **326,** 1525–1529 (2009).
46. Virtanen, A. *et al.* An amorphous solid state of biogenic secondary organic aerosol particles. *Nature* **467,** 824–827 (2010).
47. Pöschl, U. *et al.* Rainforest aerosols as biogenic nuclei of clouds and precipitation in the Amazon. *Science* **329,** 1513–1516 (2010).
48. Kalberer, M. *et al.* Identification of polymers as major components of atmospheric organic aerosols. *Science* **303,** 1659–1662 (2004).
49. Pöschl, U., Rudich, Y. & Ammann, M. Kinetic model framework for aerosol and cloud surface chemistry and gas–particle interactions. Part 1: General equations, parameters, and terminology. *Atmos. Chem. Phys.* **7,** 5989–6023 (2007).
50. Ammann, M. & Pöschl, U. Kinetic model framework for aerosol and cloud surface chemistry and gas–particle interactions. Part 2: Exemplary practical applications and numerical simulations. *Atmos. Chem. Phys.* **7,** 6025–6045 (2007).

Acknowledgements

This work was funded by the Max Planck Society, the Swiss National Science Foundation (Grant 130175) and the European Integrated Project on Aerosol, Cloud, Climate and Air Quality Interactions (036833-2 EUCAARI). We thank M. Birrer, T. Bartels-Rausch and M. Kerbrat for support, and the staff of the Paul Scherrer Institute accelerator facilities for providing the stable proton beams used to produce ^{13}N with the PROTRAC facility. M.S. is supported by the Max Planck Graduate Center, Johannes Gutenberg University Mainz, the University of Tokyo, and the Ministry of Education, Culture, Sports, Science and Technology, Japan.

Author contributions

U.P., M.A. and M.S. designed the research. M.S., Y.S., A.R. and M.A. performed tracer experiments and M.S. analysed the data. H.Y. and Y.Z. contributed to the protein studies. M.S. and U.P. conducted the kinetic modelling. M.S., U.P., M.A. and J.A. discussed the results. M.S., U.P. and M.A. co-wrote the paper.

Additional information

The authors declare no competing financial interests. Supplementary information accompanies this paper at www.nature.com/naturechemistry. Reprints and permission information is available online at http://npg.nature.com/reprintsandpermissions/. Correspondence and requests for materials should be addressed to U.P.

nature chemistry

SUPPLEMENTARY INFORMATION

DOI: 10.1038/NCHEM.988

Supplementary information for the manuscript "The role of long-lived reactive oxygen intermediates in the reaction of ozone with aerosol particles"

Manabu Shiraiwa[a], Yulia Sosedova[b], Aurélie Rouvière[b], Hong Yang[a], Yingyi Zhang[a], Jonathan P. D. Abbatt[c], Markus Ammann[b] & Ulrich Pöschl[a]

[a] Max Planck Institute for Chemistry, Department of Biogeochemistry, J. J. Becherweg 27/29, D55128 Mainz, Germany

[b] Paul Scherrer Institute, Villigen, Switzerland, CH-5232

[c] University of Toronto, Department of Chemistry, 80 St. George Street, Toronto, ON M5S 3H6 Canada

Correspondence to: U. Pöschl (u.poschl@mpic.de)

To complement the information given in the main manuscript, the following sections provide Supplementary Text, Supplementary Tables S1, Supplementary Figures S1-S2, and Supplementary References.

DOI: 10.1038/NCHEM.988

Supplementary Figures.

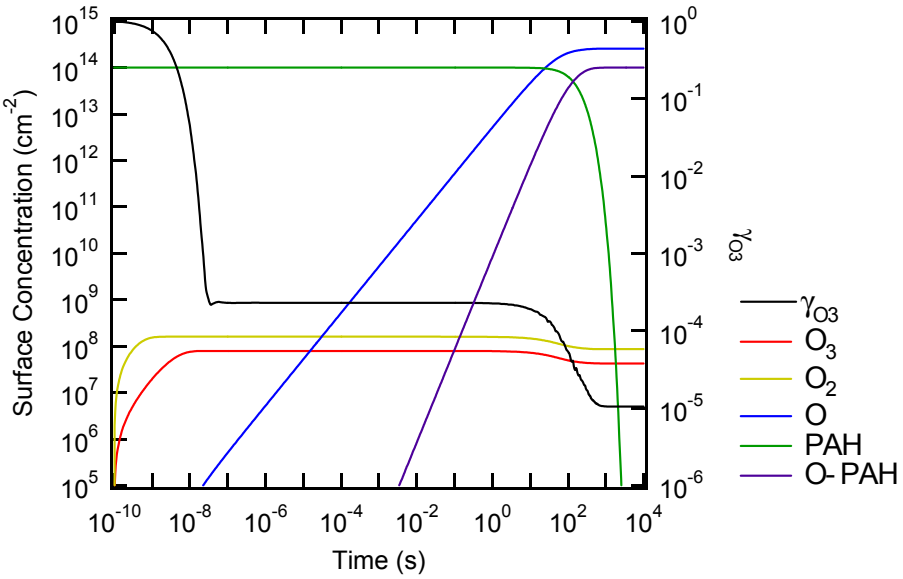

Figure S1. PAH Oxidation: Temporal evolution of the ozone uptake coefficient (γ_{O3}) and the surface concentrations of O_3, O_2, O, PAH and O-PAH according to model simulations assuming a multi-step Langmuir-Hinshelwood mechanism.

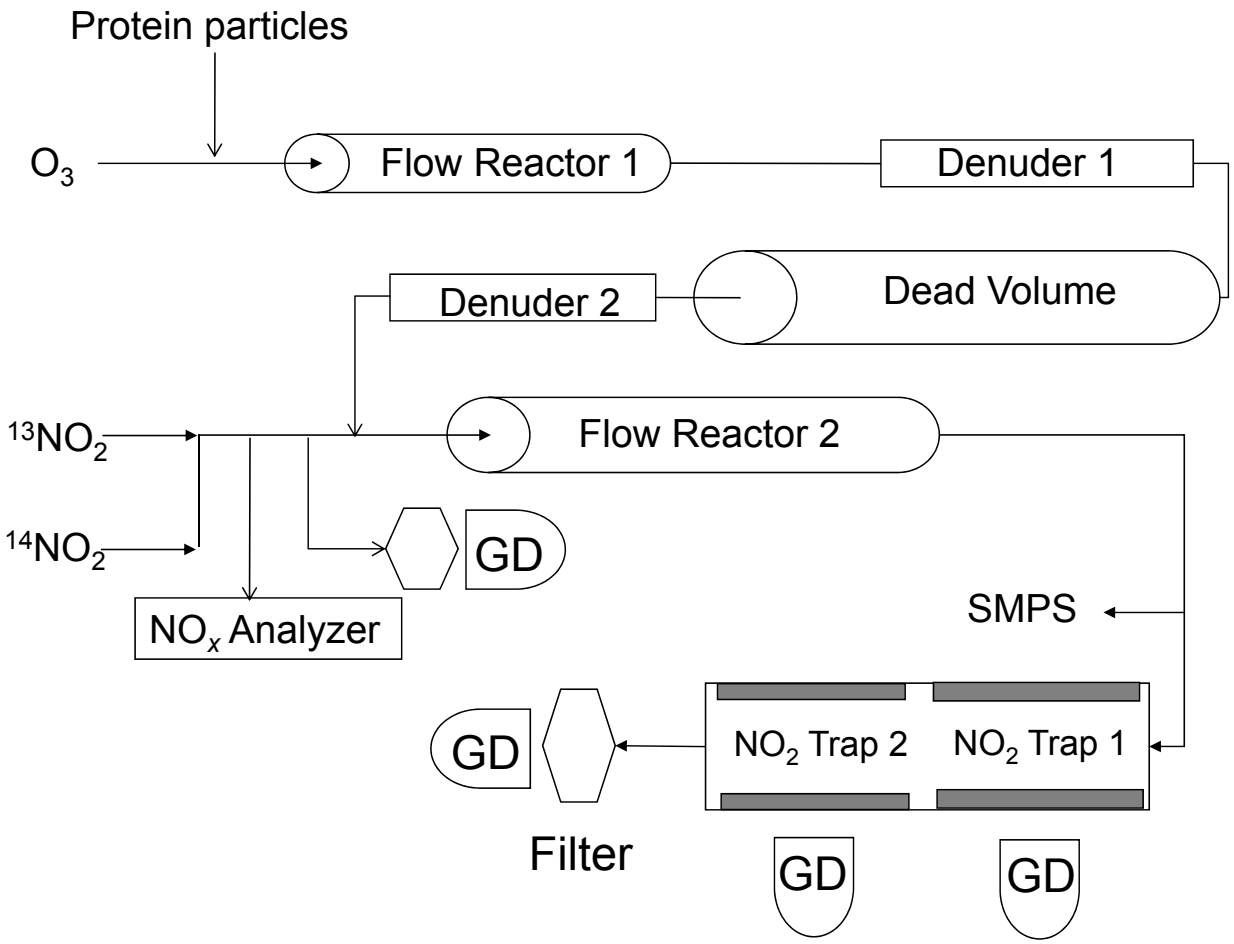

Figure S2. Protein Nitration: Experimental setup for investigation of ROI lifetime by ozone pre-treatment, removal of O_3 with KI denuders, and exposure to NO_2 after variable residence times in a dead volume before NO_2 was admixed to the aerosol (Experiment 4). The setup comprises Flow Reactor 1 for ozone pretreatment, potassium iodide denuders for ozone removal, a dead volume for ROI decay, and Flow Reactor 2 for nitration, a scanning mobility particle sizer (SMPS), NO_2 traps, particle filter, and γ-ray detectors (GD).

DOI: 10.1038/NCHEM.988

Supplementary Table.

Table S1. Kinetic parameters used in the model simulation assuming a multi-step Langmuir-Hinshelwood mechanism for the ozonolysis of benzo[a]pyrene (BaP) on soot.

Parameter	**Description**	**Value**
$\alpha_{s,0,O3}$	surface accomodation coefficient of O_3	1
$\alpha_{s,0,O2}$	surface accomodation coefficient of O_2	10^{-5}
$\tau_{d,O3}$ (s)	desorption lifetime of O_3	3.2×10^{-9}
$\tau_{d,O2}$ (s)	desorption lifetime of O_2	2.9×10^{-10}
$k_{SLR,O3}$ (s^{-1})	First-order rate coefficient for conversion of O_3 to O	7.2×10^{4}
$k_{SLR,O,PAH}$ (cm^2 s^{-1})	second-order rate coefficient for surface layer reaction between O and PAH	3.2×10^{-17}
$k_{SLR,O,O2}$ (s^{-1})	second-order rate coefficient for surface layer reaction between O and O_2	1.8×10^{-13}
$k_{SLR,O,O}$ (cm^2 s^{-1})	second-order rate coefficient for surface layer self-reaction of O	1.0×10^{-18}
$k_{SLR,O,O3}$ (cm^2 s^{-1})	second-order rate coefficient for surface layer reaction between O and O_3	1.0×10^{-18}
$\gamma_{GSR,O,O2}$	elementary gas-surface reaction probability between O and O_2	1.0×10^{-11}

Supplementary Methods and Discussion.

S1. Ozonolysis of polycyclic aromatic hydrocarbons

S1.1. K2-SURF model and chemical mechanism

The K2-SURF model[1] describes the gas-particle interface by several compartments and molecular layers in which volatile and non-volatile species can undergo mass transport and chemical reactions: gas phase (g), near-surface gas phase (gs), sorption layer (s), quasi-static surface layer (ss), near-surface bulk (bs), and particle bulk (b). Chemical reactions at the interface are classified as surface layer reactions (SLR) when they involved only species in the sorption or quasi-static surface layer and as elementary gas-surface reactions (GSR) when they proceed upon collision with a molecule from the gas phase. Thus, SLR corresponds to classical Langmuir-Hinshelwood (LH) mechanisms, whereas GSR corresponds to Eley-Rideal (ER) mechanisms[2-3]. Here we focus on mass transport (adsorption, desorption) and chemical reactions (SLR, GSR) of ozone and polycyclic aromatic compounds (PAHs) at the interface, and we neglect processes in the gas phase and in the particle bulk (diffusion, etc.[1, 4]).

The first set of chemical equations describes the simple Langmuir Hinshelwood (LH) reaction between molecular ozone and PAH[1, 5-7]:

$$O_3\,(gs) \rightarrow O_3\,(s) \qquad \alpha_{s,0,O3} \qquad (R1)$$

$$O_3\,(s) \rightarrow O_3\,(gs) \qquad \tau_{d,O3} \qquad (R2)$$

$$O_3\,(s) + PAH\,(ss) \rightarrow O\text{-}PAH\,(ss) \qquad k_{SLR,O3,PAH} \qquad (R3)$$

Molecular O_3 undergoes reversible adsorption on the surface (R1-R2), and adsorbed O_3 reacts directly with the PAH to form an oxygenated product (O-PAH, R3). For the model calculations presented in Figure 3 we used the following kinetic parameters based on a previous kinetic-double layer surface model study[1]: O_3 surface accommodation coefficient $\alpha_{s,0,O3} = 10^{-3}$, O_3

DOI: 10.1038/NCHEM.988

desorption lifetime $\tau_{d,O3}$ = 16 s, second-order rate coefficient $k_{SLR,O3,PAH}$ = 2.7×10^{-17} cm^2 s^{-1} for the dashed line; $\alpha_{s,0,O3}$ = 10^{-3}, $\tau_{d,O3}$ = 3.2×10^{-9} s, and $k_{SLR,O3,PAH}$ = 4.0×10^{-11} cm^2 s^{-1} for the dotted line. The latter value of $k_{SLR,O3,PAH}$ was chosen to match the observed order of magnitude of $k_{s,PAH}$.

The second set of chemical equations describes the multi-step Langmuir-Hinshelwood mechanism involving reactive oxygen intermediates (ROIs):

O_3 (gs) → O_3 (s)	$\alpha_{s,0,O3}$	(R4)
O_3 (s) → O_3 (gs)	$\tau_{d,O3}$	(R5)
O_2 (gs) → O_2 (s)	$\alpha_{s,0,O2}$	(R6)
O_2 (s) → O_2 (gs)	$\tau_{d,O2}$	(R7)
O_3 (s) → O (s) + O_2 (s)	$k_{SLR,O3}$	(R8)
O (s) + PAH (ss) → O-PAH (ss)	$k_{SLR,O,PAH}$	(R9)
O (s) + O_2 (s) → O_3 (s)	$k_{SLR,O,O2}$	(R10)
O (s) + O (s) → O_2(s)	$k_{SLR,O,O}$	(R11)
O (s) + O_3(s) → 2O_2(s)	$k_{SLR,O,O3}$	(R12)
O (s) + O_2(gs) → O_3(s)	$\gamma_{GSR,O,O2}$	(R13)
O (s) + O_3(gs) → 2O_2(s)	$\gamma_{GSR,O,O3}$	(R14)

Equations (R4-R7) describe the reversible adsorption of molecular O_3 and O_2 on the surface (physisorption). Ozone is stabilized at the minimum of the molecular potential energy curve (E_p, Fig. 2), which represents weak interactions with the surface. The weakly bound, physisorbed ozone molecule can be thermally desorbed to the gas phase (R5) with a desorption lifetime of nanoseconds, or it can overcome an activation barrier ($E_{a,pc}$, Fig. 2), undergo dissociation, and enter into a state of stronger binding to the surface (chemisorption: E_c, Fig. 2). The transition

state from molecular to dissociated ozone can be an ozonide or a trioxyl diradical[8-9]. The products are molecular oxygen (O_2, physisorbed) and a reactive oxygen intermediate (ROI), that may be regarded as atomic oxygen bound to the delocalized π-electrons of the aromatic surface. For brevity, we use the symbol O to represent the ROI in chemical equations.

In a second reaction step (R9), the ROI reacts with the PAH to form a stable product, i.e., an oxygenated PAH (O-PAH) with hydroxyl, carbonyl or other functional groups[10]. Alternatively, the ROI can be lost by reaction with other oxygen species and formation of molecular O_2 or O_3 through one or more of the following pathways: reverse reaction with adsorbed O_2 (R10); self-reaction (R11); reaction with adsorbed O_3 (R12); reaction with gas phase O_2 (R13); or reaction with gas phase O_3 (R14). The relative importance of the different reaction pathways will be explored and discussed in the Section S1.4, and the rate coefficients listed after the chemical equations are specified in Table S1.

S1.2. Rate equations

The surface mass balance and rate equations of O_3, O_2, O, and PAH on the surface can be expressed using mass transport fluxes (J) and chemical production and loss (P and L) as follows:

$$d[O_3]_s/dt = J_{ads,O3} - J_{des,O3} + P_{s,O3} - L_{s,O3} \quad (1)$$

$$d[O_2]_s/dt = J_{ads,O2} - J_{des,O2} + P_{s,O2} - L_{s,O2} \quad (2)$$

$$d[O]_s/dt = P_{s,O} - L_{s,O} \quad (3)$$

$$d[PAH]_{ss}/dt = -L_{ss,PAH} \quad (4)$$

$$d[O\text{-}PAH]_{ss}/dt = L_{ss,PAH} \quad (5)$$

where $J_{ads,Xi}$ is the adsorption flux, $J_{des,Xi}$ is the desorption flux, $P_{s,Xi}$ and $L_{s,Xi}$ are chemical production and loss of X_i (O_3, O_2, and O) in the sorption layer, and $L_{ss,PAH}$ is the chemical loss

DOI: 10.1038/NCHEM.988

rate of PAH in the quasi-static surface layer. The initial PAH surface concentration is set to 1×10^{14} cm^{-2}, and the initial surface concentration of gas species (O_3 and O_2) is set to zero.

The adsorption and desorption flux of gas species X_i ($J_{ads,\,Xi}$, $J_{des,\,Xi}$; $X_i = O_3, O_2$) can be expressed as follows[1-2].

$$J_{ads,Xi} = \alpha_{s,0,Xi}\,(1-\theta_s)\,J_{coll,Xi} = \alpha_{s,0,Xi}\,(1-\theta_s)\,\omega_{Xi}\,[X_i]_{gs}\,/4 \quad (6)$$

$$J_{des,Xi} = k_{d,\,Xi}\,[X_i]_s = k_{d,Xi}\,\theta_s\,/\,\sigma_{s,Xi} \quad (7)$$

where $J_{coll,Xi}$ is the collision flux, $\alpha_{s,0,O3}$ is surface accommodation coefficient of X_i on a free substrate, $[X_i]_{gs}$ is the near-surface gas phase concentration of X_i, ω_{Xi} is the mean thermal velocity ($\omega_{O3} = 3.6 \times 10^4$ cm s^{-1}, $\omega_{O2} = 4.4 \times 10^4$ cm s^{-1} at 296 K), and $\sigma_{s,Xi}$ is the effective molecular cross section of X_i, which are assumed to be 1.8×10^{-15} cm^2 [11]. The desorption lifetime $\tau_{d,Xi}$, the mean residence time on the surface in absence of a surface reaction, is the inverse of desorption rate coefficient ($\tau_{d,Xi} = k_{d,Xi}^{-1}$). θ_s is the sorption layer coverage, which is given by the sum of the fractional surface coverages of all adsorbate species X_i (O_3, O_2, and O), $\theta_{s,Xi}$, each of which is given by the ratio between the actual and the maximum surface concentration values of X_i: $\theta_{s,Xi} = [X_i]_s/[X_i]_{s,max} = \sigma_{s,Xi}[X_i]_s$.

The chemical production and loss rates of O_3, O_2 and O on the surface are given by:

$$P_{s,O3} = k_{SLR,O,O2}\,[O_2]_s\;[O]_s + \gamma_{GSR,O,O2}\,\theta_{s,O}\,J_{coll,O2} \quad (8)$$

$$L_{s,O3} = k_{SLR,O3}\,[O_3]_s + k_{SLR,O,O3}\,[O]_s\,[O_3]_s \quad (9)$$

$$P_{s,O2} = k_{SLR,O3}\,[O_3]_s + k_{SLR,O,O}\,[O]_s\,[O]_s + 2k_{SLR,O,O3}\,[O_3]_s\,[O]_s + 2\,\gamma_{GSR,O,O3}\,\theta_{s,O}\,J_{coll,O3} \quad (10)$$

$$L_{s,O2} = k_{SLR,O,O2}\,[O_2]_s\,[O]_s \quad (11)$$

$$P_{s,O} = k_{SLR,O3}\,[O_3]_s \quad (12)$$

$$L_{s,O} = k_{SLR,O,PAH}\,[O]_s\,[PAH]_{ss} + k_{SLR,O,O2}\,[O_2]_s\,[O]_s + 2k_{SLR,O,O}\,[O]_s\,[O]_s + k_{SLR,O,O3}\,[O_3]_s\,[O]_s + \gamma_{GSR,O,O2}\,\theta_{s,O}\,J_{coll,O2} + \gamma_{GSR,O,O3}\,\theta_{s,O}\,J_{coll,O3} \quad (13)$$

Here $k_{SLR,O3}$ is the first-order rate coefficient for the conversion of physisorbed into chemisorbed ozone (R8), i.e., the dissociation of molecular ozone (O_3) into atomic and molecular oxygen (O + O_2). $k_{SLR,O,O2}$ is the second-order rate coefficient for the reverse reaction (R10), i.e., the conversion of atomic oxygen (chemisorbed) into molecular ozone (physisorbed). $k_{SLR,O,O3}$ is the second-order rate coefficient for the surface layer reaction of O and O_3 on the surface (R12). $\gamma_{GSR,O,O2}$ is the reaction probability for the elementary gas-surface reaction[2] of gas phase O_2 colliding with O on the surface (R13). $k_{SLR,O,O}$, $k_{SLR,O,O3}$ and $k_{SLR,O,PAH}$ are the second-order rate coefficients for the reactions of O with O, O_3, and PAH, respectively.

The chemical loss rate of PAH in the quasi-static surface layer ($L_{ss,PAH}$) can be described by:

$$L_{ss,PAH} = k_{SLR,O,PAH}\,[O]_s\,[PAH]_{ss} = k_{s,PAH}\,[PAH]_{ss} \quad (14)$$

where $k_{s,PAH}$ is an apparent pseudo-first order rate coefficient ($d[PAH]_{ss} / dt = k_{s,PAH}\,[PAH]_{ss}$). $k_{s,PAH}$ is related to chemical half-life of PAH ($t_{PAH,1/2}$), which is defined as the time when the PAH concentration reaches half of the initial concentration.

$$k_{s,PAH} = \ln 2 / t_{PAH,1/2} \quad (15)$$

The uptake coefficient of O_3 (γ_{O3}) can be expressed as follows[1]:

$$\gamma_{O_3} = \frac{J_{ads,O_3} - J_{des,O_3}}{J_{coll,O_3}} \quad (16)$$

S1.3. Kinetic parameters

The kinetic parameters used in the multi-step Langmuir-Hinshelwood model simulations are summarized in Table S1. The parameter values were adopted from Shiraiwa et al.[1] unless mentioned otherwise.

DOI: 10.1038/NCHEM.988

The desorption lifetimes ($\tau_{d,X}$) of gas species (X = O_3, O_2) were calculated by the following Arrhenius equation[12-13]:

$$\tau_{d,X}^{-1} = \nu_{0,X} \exp(-E_{p,X} / (k_B T)) \quad (17)$$

where k_B is the Boltzmann constant (1.38×10^{-23} J K^{-1}), $\nu_{0,X}$ is the attempt frequency, and $E_{p,X}$ is the physisorption energy. According to quantum mechanical calculations, the physisorption energies of molecular oxygen and ozone on an aromatic surface are in the range of 14 kJ mol^{-1} for O_2 on graphene, 15 kJ mol^{-1} for O_3 on PAHs[8], and 24 kJ mol^{-1} on graphene[12]. In this study we use $E_{p,O2}$ = 14 kJ mol^{-1} and approximate average value of $E_{p,O3}$ = 20 kJ mol^{-1}. Assuming $\nu_{0,O3}$ = $\nu_{0,O2}$ = 1×10^{12} s^{-1}, which is a typical value for physisorbed species[14], we calculated and used $\tau_{d,O3} = 3.2\times10^{-9}$ s (3.2 ns) and $\tau_{d,O2} = 2.9\times10^{-10}$ s (0.29 ns), respectively.

The ozone dissociation rate coefficient ($k_{SLR,O3}$) was estimated using the activation energy for the conversion of physisorbed to dissociated ozone ($E_{a,pc}$) by the following equation:

$$k_{SLR,O3} = \nu_0 \exp(-E_{a,pc}/(k_B T)) \quad (18)$$

The rate coefficient for the reverse reaction ($k_{SLR,O,O2}$) was estimated using the activation energy for the conversion of chemisorbed to physisorbed ozone ($E_{a,cp}$) by the following equation:

$$k_{SLR,O,O2} = \sigma_{s,O2}\, \nu_0' \exp(-E_{a,cp}/(k_B T)) \quad (19)$$

where ν_0' is the attempt frequency of O. Here we assume $\nu_0' = 1 \times 10^{14}$ s^{-1}, which is a typical value for chemisorbed species[14]. According to density functional theory (DFT) calculations[8], the activation energies are expected to be in the range of $E_{a,pc}$ = ~40–100 kJ mol^{-1} and $E_{a,cp}$ = 67–150 kJ mol^{-1}. The second-order surface reaction rate coefficient $k_{SLR,O,PAH}$ is tightly constrained to be $\sim10^{-17}$ cm^2 s^{-1} by the observed data and linearly proportional to the ratio of $k_{s,PAH}$ and θ_s ($k_{SLR,O,PAH} = \sigma_{s,O}\, k_{s,PAH} / \theta_s$). We systematically and iteratively varied $E_{a,cp}$ and $E_{a,pc}$ together with $k_{SLR,O,PAH}$ and $\alpha_{s,0,O3}$ to match the experimental data of $k_{s,PAH}$ and θ_s shown in Figure 3. Initial

estimates for $k_{SLR,O,PAH}$ and $\alpha_{s,0,O3}$ were based on Shiraiwa et al[1], and the best estimates obtained by the procedures outlined above are listed in Table S1. The other parameters ($\alpha_{s,0,O2}$, $k_{SLR,O,O}$, $k_{SLR,O,O3}$, $\gamma_{GSR,O,O2}$, and $\gamma_{GSR,O,O3}$) have no direct influence on $k_{s,PAH}$ and were adjusted for best fit to the experimental data of θ_s (Table S1).

The activation energy from a reactive oxygen intermediate to oxidized PAH ($E_{a,ox}$) were estimated using Arrhenius equation as below.

$$k_{SLR,O,PAH} = \sigma_{ss,PAH}\, \nu_0' \exp(-E_{a,ox}/(k_B T)) \quad (20)$$

$E_{a,ox}$ was calculated to be 80(±9) kJ mol^{-1}.

S1.4. Sensitivity studies

In order to characterize the sensitivity of the model results with regard to the chosen set of kinetic input parameters, all parameters listed in Table S1 were varied systematically. $\alpha_{s,0,O3}$, $\tau_{d,O3}$, and $k_{SLR,O3}$ ($E_{a,pc}$) were found to be important parameters, as they determine the surface concentration of O_3, and thus the formation of O. If we decrease $\alpha_{s,0,O3}$ from 1 to 0.5 we can still match the experimental data of $k_{s,PAH}$ and θ_s assuming $E_{a,pc}$ = 39 kJ mol^{-1}, which is just slightly outside the range of values predicted by DFT calculations (~40–100 kJ mol^{-1})[8-9, 12]. For $\alpha_{s,0,O3}$ < 0.01, $E_{a,pc}$ would have to be <34 kJ mol^{-1} to reproduce the experimental data. This appears unrealistically low because it would reduce the potential energy of the transition state (E_T) to <14 kJ mol^{-1}, whereas the DFT calculations[8-9, 12] predict > 20 kJ mol^{-1}. Note that in our previous studies of PAH degradation modeling[1, 3] a different set of parameters with $\alpha_{s,0,O3} = 10^{-3}$ was used, because the decomposition of O_3 was not resolved (simple LH mechanism). Thus, the previously assumed value of $\alpha_{s,0,O3} = 10^{-3}$ can be regarded as an effective accommodation parameter that accounts for both the actual surface accommodation and the subsequent dissociation of O_3. For

$\tau_{d,O3}$, the range of physisorption energies predicted by DFT calculations[8-9, 12] (15–24 kJ mol^{-1}) corresponds to a range of 0.4-16 ns. Within this range the experimental data of $k_{s,PAH}$ and θ_s can be still matched by adjusting $E_{a,pc}$ in the range of 34–48 kJ mol^{-1}. As outlined above, several pairs of parameters can be mutually adjusted to match the experimental data, but the energetic constraints limit the actual range of parameters that are able to reconcile kinetic observations and DFT calculations.

The kinetic parameters of ROI loss reactions (R10-R14) were found to be much less critical than the formation rate coefficient $k_{SLR,O3}$. The surface accommodation coefficient and the desorption lifetime of molecular oxygen ($\alpha_{s,0,O2}$, $\tau_{d,O2}$) were found to be uncritical as long as $\alpha_{s,0,O2} < 10^{-2}$ and $\tau_{d,O2} < 10^{-7}$ s (corresponding $E_{p,O2}$ = ~28 kJ mol^{-1}), respectively.

In the chemical mechanism outlined above, we assumed that the ROIs are O atoms, which is the simplest possible assumption. Alternatively, our model approach would also allow describing more complex mechanisms that involve the formation of molecular organic ROIs. Note, however, that the ROI formation has to be reversible in order to explain and reconcile observations and quantum mechanical calculations (short O_3 desorption lifetime, high ROI surface coverage, slow PAH degradation). As long as the exact identity of the ROI is not fully elucidated, we consider it appropriate to use the simplest possible mechanism.

S1.5. ROI lifetime

Fig. S1 shows the temporal evolution of the ozone uptake coefficient (γ_{O3}) and the surface concentrations of all involved chemical species for the heterogeneous ozonolysis of PAH on soot using the parameters of Table S1 and an ozone gas phase concentration of 2.5×10^{12} cm^{-2} (100 ppb at 296 K, 1 atm), which is typical for polluted air masses.

The initial plateau of γ_{O3} equals $\alpha_{s,0,O3} = 1$ up to 10^{-9} s (~1 ns), which can be explained by physisorption of O_3 onto a nearly adsorbate-free surface. After ~10 ns O_3 reaches adsorption equilibrium at a surface concentration of ~10^8 cm^{-2} ($\theta_s \approx 10^{-7}$). The second plateau of γ_{O3} at ~2×10^{-4} is due to decomposition of O_3 into O and O_2. This is consistent with the experimental results of Rogaski et al.[15] and Fendel et al[16], who observed nearly constant values of $\gamma_{O3} \approx 10^{-3}$–$10^{-4}$ on amorphous carbon over more than ten seconds. After ~10^2 s, the surface reaches saturation with O at a concentration level of ~10^{14} cm^{-2} ($\theta_s \approx 0.5$). Note, as above, that we do not consider the O species to be a weakly adsorbed O atom, in which case its lifetime would be short. Instead, it likely experiences a strong chemical interaction with the surface. This is consistent with ozone-soot exposure experiments showing that the amount of ozone consumed is roughly equal to a monolayer[17]. At this point, the reaction with PAH dominates the lifetime of ROI, which is of the order of ~10^2 s. As the PAH surface concentration decreases, the lifetime of ROI increases up ~10^3 s and is then dominated by loss reactions between different oxygen species (R10-R14). These reactions also maintain γ_{O3} at a final plateau level of ~10^{-5}.

S1.6. Related studies

Many experimental chemical kinetics studies investigating the heterogeneous ozonolyis of PAHs, including anthracene[18], naphthalene[19], pyrene[20], phenanthrene[19], benzo[a]anthracene (BaA)[20], perylene[21], and fluoranthene[20], showed similar LH behaviour of $k_{s,PAH}$ as displayed in Fig. 3a for benzo[a]pyrene (BaP)[11]. The decay of several other types of surface-bound organic compounds also follows LH kinetics[22]: alkenes[23], cypermethrin[24], chlorophyll[25], oleate[26], and quinuclidine diastereomers[27]. In most cases, the surface reaction kinetics between adsorbed

DOI: 10.1038/NCHEM.988

ozone and unsaturated organic compounds can be described by a second-order rate coefficient of the order of 10^{-18} - 10^{-17} cm^2 s^{-1} [1, 17].

It has been suggested that the surface diffusion of O_3 or its dissociation and the formation of intermediates may be the rate-limiting step of the overall process[17]. In view of the short desorption lifetime of O_3 (~10^{-9} s), however, the formation of ROIs has to proceed faster (~10^{-5} s) than the decomposition of ROIs (~10^{2} s) in order to achieve the observed high surface coverages (Fig. 3b). Thus, we conclude that the second step of reaction, i.e., the reaction of ROI with PAH and the formation of stable products should be rate-limiting. This implies that not only the energetics and kinetics of the formation of the ROIs, but also their lifetimes and reactivities are similar for various unsaturated organic compounds.

Most likely, long-lived ROIs also influence the ozone uptake kinetics of other substrates like soot, metal oxides, and mineral dust[17]. Stephens et al.[28] observed the formation of an oxygen molecule for each ozone molecule lost on soot. The formation of O_2 in the heterogeneous reaction of ozone with soot was also confirmed by Rogaski et al.[15]. Similarly, the conversion of ozone into O_2 was observed on Saharan dust[29] and alumina[30], and O atoms are supposed to form upon interaction of ozone with TiO_2 surfaces[31]. The lost reactivity of alumina surface via ozone could be recovered over timescales of days[30], implying the reversibility of ROI formation. In this case, the ROI would be an inorganic species, likely involving an O-atom chemisorbed to the surface.

S2. Protein nitration

S2.1. Experimental approach

The experiments were performed using the short-lived radioactive tracer ^{13}N and an aerosol flow tube technique at Paul Scherrer Institut. The radioactive half-life of ^{13}N is ~10 min. The use of ^{13}N enabled us to perform experiments at low concentrations because of its high radioactivity to concentration ratio[32]. It also allowed us to conduct uptake experiments under atmospherically relevant pressure (960 – 990 hPa) and relative humidity (20 – 80%) and, which would interfere with several other sensitive analytical techniques such as IR spectroscopy due to water vapor's strong absorption in the infrared. The experimental setup consists of the following part described in detail in the subsections below: gas flow system, aerosol production and detection system, aerosol flow tube, and detection system.

In Experiment 1, BSA particles were exposed to NO_2 alone. . In Experiment 2, the BSA particles were pre-treated with O_3 (97 ppb); then ozone was removed from the aerosol flow, and the pre-treated particles were exposed to NO_2 in the absence of O_3. In Experiment 3, BSA particles were exposed to both NO_2 and O_3. Experiment 4 is similar to Experiment 2, but a dead volume was installed with a maximum residence time of 550 s after the removal of ozone and before the exposure of pre-treated BSA particles to NO_2 (15 ppb). Fig. S2 shows the schematics of the Experiment 4.

S2.2. Gas flow system

^{13}N was produced through the $^{16}O(p,\alpha)^{13}N$ nuclear reaction with 11 MeV protons in a gas target (20% O_2 in He) in continuous mode. It was transported as ^{13}NO with the He/O_2 mixture as carrier gas to the chemistry laboratory through a 580 m long, 4 mm inner diameter PVDF tube[33]. Note that non-labeled NO at less than about 10 ppb is also produced via radiation chemistry in the target and also transported to the laboratory. The transported labeled NO in He/O_2 was then

DOI: 10.1038/NCHEM.988

mixed with pure N_2 and a certified amount of non-labeled NO to give a defined concentration of a few ppbv to several hundred ppbv. Labeled and non-labeled NO contained in the carrier gas (~300 cm^3 s^{-1}) was converted to NO_2 by heterogeneous oxidation over firebrick granules impregnated with CrO_3[32]. The efficiency of this conversion is optimal under 30 – 70% relative humidity condition. Therefore, the ^{13}NO containing gas was passed through a vertically mounted porous Teflon tube partially immersed in water to adjust to a relative humidity (RH) of ~60% prior to oxidation.

O_3 was generated by passing a small flow of air (~100 cm^3 s^{-1}) containing O_2 and N_2 through a quartz tube irradiated by a Xe excimer lamp delivering UV light at 172 nm. By varying the volumetric ratio of the O_2 and N_2 flows, the O_3 concentration could be varied. O_3 containing air was then mixed with the NO_2 containing carrier gas. The mixed gas flow was passed through a sand-blasted glass tube coated with sodium carbonate to remove HONO upstream of the flow tube reactor.

S2.3. Aerosol production and detection system

Aerosols were generated by nebulizing an aqueous solution of the investigated pure substance at a concentration of 0.2 – 0.5 g L^{-1}. The solutions were prepared by dissolving the appropriate amounts of bovine serum albumin (BSA, >99%, Sigma) and sodium chloride in 100 mL of deionised water (18.2 MΩ cm, MilliQplus 185, Millipore). The molecular masses and density of BSA are 66.5 kg mol^{-1} and 1362 kg m^{-3}, respectively. The generated particles are dried by a diffusion dryer filled with silica gel. The dried particles are introduced into an ^{85}Kr source to establish an equilibrium charge distribution and then passed through an electrostatic precipitator

so that only uncharged particles were used for the experiments to avoid uncontrolled loss of charged particles at the wall. Then the flow was conditioned to the relative humidity of 50 - 75%.

The aerosol surface concentration was measured downstream of the flow tube reactor by diverting part of the flow to a scanning mobility particle sizer (SMPS) consisting of a differential mobility analyzer (DMA) and a condensation particle counter (CPC, TSI 3022). The same relative humidity was maintained both in the DMA sheath flow and in the flow tube reactor by using filtered carrier gas from the flow tube as the DMA sheath flow, so that the particle size is not affected by relative humidity. The diameter range was 15 – 740 nm, and the observed size distribution was mono-modal and lognormal. The observed surface distribution was fitted by a single lognormal distribution to estimate the whole distribution and surface area. A typical mode diameter of the surface area density distribution was ~350 nm, and the surface concentration was in the range of 10^{-4} – 10^{-3} cm^2 cm^{-3}.

S2.4. Aerosol flow tube

In Experiments 1-3, the gas and aerosol flows were mixed prior to the inlet of a cylindrical 7.1 cm inner diameter and 190 cm long PFA flow tube. PFA was used to minimize the loss of NO_2 on the wall. The flow was 800 – 900 cm^3 s^{-1} in the reactor, and the maximum residence time was ~10 min. The flow tube was equipped with a movable Teflon inlet of conical shape. The reactor was operated under laminar flow conditions[34]. The gas-aerosol contact time could be adjusted between 3 – 10 min depending on the position of the inlet. At the tube exit, the flow was recollected by an identical, conically shaped Teflon plug. The pressure, temperature and relative humidity in the flow reactor were generally kept at 970 – 980 hPa, 296 K, and ~60%, respectively.

DOI: 10.1038/NCHEM.988

In Experiment 4, the above flow reactor is used as a dead volume and another cylindrical flow tube reactor of 4 cm inner diameter and 90 cm long lined with a PFA foil was used for Flow Reactor 2 (Fig. S2). The reaction time was adjusted between 0.5 - 2 min by a movable injector. Pretreatment of BSA with O_3 was conducted in 140 cm long PFA tube of 0.8 cm inner diameter (Fig. S2; Flow Reactor 1).

S2.5. Detection system

After passing through the flow tube, the gas and aerosol flow entered a narrow parallel-plate diffusion denuder train coated to selectively absorb gas phase NO_2, followed by a particle filter collecting the particles[32]. The gas passes through the denuder in laminar flow. The first section was prepared to trap NO_2, coated with a solution of 1% N-(1-naphtyl) ethylenediamine dihydrochloride (NDA, Fluka, >99%), 1% KOH and 10% water in methanol. We repeated the NDA coating in the second section to make sure that all gas phase NO_2 remained trapped in the denuder train and to detect eventual breakthrough. The aerosol particles have a small diffusivity and pass through the denuder with close to 100% efficiency[32] and were retained in the glass fiber filter. An additional glass fiber filter soaked with NDA and KOH was used to monitor the total concentration of $^{13}NO_2$ by diverting a small gas flow upstream of the flow tube through it.

The γ detectors were attached to each denuder section and the filters to detect the amount of emitted gamma quanta, which are emitted in the decay of ^{13}N. The counts of γ decays were integrated over 1 min. They correspond to the amount of trapped ^{13}N molecules of a given species. They were converted to flux into the trap, which can be calculated from the difference between two consecutive activity measurements using the decay constant of ^{13}N [33-34]. The flux corresponds to the total amount of ^{13}N absorbed on the trap per unit time, hence, the

concentration of the corresponding species at the exit of the flow tube, which was used for the calculation of uptake coefficients. The relative counting efficiency of each γ detectors were investigated by exposing a certain amount of ^{13}N on a reference filter to each γ detector[32-33]. Data presented here were all corrected for the difference in counting efficiency among the traps.

Note that for the particle signal only strongly (chemically) absorbed ^{13}N species are detected, while physically adsorbed species desorbing within 30 ms and less contribute to the gas phase signal of the corresponding denuder plate, species desorbing within up to a second are trapped within the whole denuder train, and species desorbing within a few minutes are lost by desorption from the filter before they are detected by the γ detector there.

S2.6. ROIs on protein particles

The ROIs generated on protein particles by ozone are most likely phenoxy radical derivatives of tyrosine, because the final products of the protein nitration reaction are nitrotyrosine residues[35-36], and phenoxy radicals are well established intermediates in the nitration of phenolic compounds by NO_2[37-38]. Moreover, phenoxy radicals can be efficiently stabilized in condensed phases[39], which is consistent with the observed long lifetime of the ROI.

Closed shell ozonolysis products such as dihydroxy aromatic compounds are unlikely to be ROIs of protein nitration, because of their low reactivity towards NO_2. For example, Arens et al. (2002)[40] reported NO_2 uptake coefficients as low as 10^{-6} for 1,2,10-trihydroxyanthracene. Similarly low uptake coefficients have been observed for di- and trihydroxy aromatic acids (gentisic and tannic acid; Sosedova et al., in prep.). High reactivity of NO_2 with phenolic compounds is only possible in strongly basic solutions, which is not relevant for our experiments (Ammann et al., (2005)[41] and references therein).

DOI: 10.1038/NCHEM.988

Supplementary References.

1. Shiraiwa, M., R.M. Garland, and U. Pöschl, Kinetic double-layer model of aerosol surface chemistry and gas-particle interactions (K2-SURF): Degradation of polycyclic aromatic hydrocarbons exposed to O_3, NO_2, H_2O, OH and NO_3. *Atmos. Chem. Phys.*, **9**(24): p. 9571-9586, 2009.

2. Pöschl, U., Y. Rudich, and M. Ammann, Kinetic model framework for aerosol and cloud surface chemistry and gas-particle interactions - Part 1: General equations, parameters, and terminology. *Atmos. Chem. Phys.*, **7**(23): p. 5989-6023, 2007.

3. Ammann, M. and U. Pöschl, Kinetic model framework for aerosol and cloud surface chemistry and gas-particle interactions - Part 2: Exemplary practical applications and numerical simulations. *Atmos. Chem. Phys.*, **7**(23): p. 6025-6045, 2007.

4. Shiraiwa, M., C. Pfrang, and U. Pöschl, Kinetic multi-layer model of aerosol surface and bulk chemistry (KM-SUB): the influence of interfacial transport and bulk diffusion on the oxidation of oleic acid by ozone. *Atmos. Chem. Phys.*, **10**(8): p. 3673-3691, 2010.

5. Ammann, M., U. Pöschl, and Y. Rudich, Effects of reversible adsorption and Langmuir-Hinshelwood surface reactions on gas uptake by atmospheric particles. *Phys. Chem. Chem. Phys.*, **5**: p. 351-356, 2003.

6. Kwamena, N.O.A., M.E. Earp, C.J. Young, and J.P.D. Abbatt, Kinetic and product yield study of the heterogeneous gas-surface reaction of anthracene and ozone. *J. Phys. Chem. A*, **110**(10): p. 3638-3646, 2006.

7. Masel, R.I., *Principles of adsorption and reaction on solid surfaces*. 1996: John Wiley & Sons.

8. Maranzana, A., et al., Ozone interaction with polycyclic aromatic hydrocarbons and soot in atmospheric processes: Theoretical density functional study by molecular and periodic methodologies. *J. Phys. Chem. A*, **109**(48): p. 10929-10939, 2005.

9. Giordana, A., et al., Soot platelets and PAHs with an odd number of unsaturated carbon atoms and pi electrons: Theoretical study of their spin properties and interaction with ozone. *J. Phys. Chem. A*, **112**(5): p. 973-982, 2008.

10. Finlayson-Pitts, B.J. and J.N. Pitts, eds. *Chemistry of the upper and lower atmosphere*. 2000, Academic Press: San Diego, California.

11. Pöschl, U., T. Letzel, C. Schauer, and R. Niessner, Interaction of ozone and water vapor with spark discharge soot aerosol particles coated with benzo[a]pyrene: O_3 and H_2O adsorption, benzo[a]pyrene degradation, and atmospheric implications. *J. Phys. Chem. A*, **105**(16): p. 4029-4041, 2001.

12. Lee, G., B. Lee, J. Kim, and K. Cho, Ozone Adsorption on Graphene: Ab Initio Study and Experimental Validation. *J. Phys. Chem. C*, **113**(32): p. 14225-14229, 2009.

13. Frenkel, J., Theory of the adsorption and related occurrences. *Zeitschrift Für Physik*, **26**: p. 117-138, 1924.

14. Atkins, P.W., *Physical Chemistry*. 1998, Oxford: Oxford University Press.

15. Rogaski, C.A., D.M. Golden, and L.R. Williams, Reactive uptake and hydration experiments on amorphous carbon treated with NO_2, SO_2, O_3, HNO_3, and H_2SO_4. *Geophys. Res. Lett.*, **24**(4): p. 381-384, 1997.

16. Fendel, W., D. Matter, H. Burtscher, and A. Schmidtott, Interaction between carbon or iron aerosol-particles and ozone. *Atmos. Environ.*, **29**(9): p. 967-973, 1995.

17. McCabe, J. and J.P.D. Abbatt, Heterogeneous Loss of Gas-Phase Ozone on n-Hexane Soot Surfaces: Similar Kinetics to Loss on Other Chemically Unsaturated Solid Surfaces. *J. Phys. Chem. C*, **113**(6): p. 2120-2127, 2009.

18. Kwamena, N.O.A., et al., Role of the aerosol substrate in the heterogeneous ozonation reactions of surface-bound PAHs. *J. Phys. Chem. A*, **111**: p. 11050-11058, 2007.

19. Kahan, T.F., N.O.A. Kwamena, and D.J. Donaldson, Heterogeneous ozonation kinetics of polycyclic aromatic hydrocarbons on organic films. *Atmos. Environ.*, **40**(19): p. 3448-3459, 2006.

20. Alebic-Juretic, A., T. Cvitas, and L. Klasinc, Heterogeneous polycyclic aromatic hydrocarbon degradation with ozone on silica-gel carrier. *Environ. Sci. Technol.*, **24**(1): p. 62-66, 1990.

21. Wu, C.H., I. Salmeen, and H. Niki, Fluorescence spectroscopic study of reactions between gaseous ozone and surface-adsorbed polycyclic aromatic-hydrocarbons. *Environ. Sci. Technol.*, **18**(8): p. 603-607, 1984.

22. Finlayson-Pitts, B.J., Reactions at surfaces in the atmosphere: integration of experiments and theory as necessary (but not necessarily sufficient) for predicting the physical chemistry of aerosols. *Phys. Chem. Chem. Phys.*, **11**(36): p. 7760-7779, 2009.

23. Dubowski, Y., et al., Interaction of gas-phase ozone at 296 K with unsaturated self-assembled monolayers: A new look at an old system. *J. Phys. Chem. A*, **108**(47): p. 10473-10485, 2004.

24. Segal-Rosenheimer, M. and Y. Dubowski, Photolysis of thin films of cypermethrin using in situ FTIR monitoring: Products, rates and quantum yields. *J. Photochem. Photobiol. A-Chem.*, **200**(2-3): p. 262-269, 2008.

25. Clifford, D., et al., Reactive uptake of ozone by chlorophyll at aqueous surfaces. *Environ. Sci. Technol.*, **42**(4): p. 1138-1143, 2008.

26. McNeill, V.F., G.M. Wolfe, and J.A. Thornton, The oxidation of oleate in submicron aqueous salt aerosols: Evidence of a surface process. *J. Phys. Chem. A*, **111**: p. 1073-1083, 2007.

27. Stokes, G.Y., et al., Atmospheric Heterogeneous Stereochemistry. *J. Am. Chem. Soc.*, **131**(38): p. 13733-13737, 2009.

28. Stephens, S., M.J. Rossi, and D.M. Golden, The heterogeneous reaction of ozone on carbonaceous surfaces. *Int. J. Chem. Kinet.*, **18**(10): p. 1133-1149, 1986.

29. Hanisch, F. and J.N. Crowley, Ozone decomposition on Saharan dust: an experimental investigation. *Atmos. Chem. Phys.*, **3**: p. 119-130, 2003.

30. Sullivan, R.C., T. Thornberry, and J.P.D. Abbatt, Ozone decomposition kinetics on alumina: effects of ozone partial pressure, relative humidity and repeated oxidation cycles. *Atmos. Chem. Phys.*, **4**: p. 1301-1310, 2004.

31. Quiller, R.G., et al., Surface Chemistry of Organic Pollutants: Styrene, Ozone, and Water on TiO_2(110). *J. Phys. Chem. C*, **113**(6): p. 2063-2070, 2009.

32. Ammann, M., Using ^{13}N as tracer in heterogeneous atmospheric chemistry experiments. *Radiochim. Acta*, **89**(11-12): p. 831-838, 2001.

33. Sosedova, Y., A. Rouviere, H.W. Gäggeler, and M. Ammann, Uptake of NO_2 to Deliquesced Dihydroxybenzoate Aerosol Particles. *J. Phys. Chem. A*, **113**(41): p. 10979-10987, 2009.

34. Stemmler, K., et al., Light induced conversion of nitrogen dioxide into nitrous acid on submicron humic acid aerosol. *Atmos. Chem. Phys.*, **7**: p. 4237-4248, 2007.

35. Zhang, Y., H. Yang, and U. Pöschl, Analysis of nitrated proteins and tryptic peptides by HPLC-chip-MS/MS: site-specific quantification, nitration degree, and reactivity of tyrosine residues. *Anal. Bioanal. Chem.*: p. 1-13, 2010.

36. Yang, H., Y. Zhang, and U. Pöschl, Quantification of nitrotyrosine in nitrated proteins. *Anal. Bioanal. Chem.*, **397**(2): p. 879-886, 2010.

37. Harrison, M.A.J., et al., Nitrated phenols in the atmosphere: a review. *Atmos. Environ.*, **39**(2): p. 231-248, 2005.

38. Hartshorn, M.P., Reactions of substituted phenols with nitrogen dioxide; Rearrangements and addition reactions of nitrodienones. *Acta Chem. Scand.*, **52**(1): p. 2-10, 1998.

39. Truong, H., S. Lomnicki, and B. Dellinger, Potential for Misidentification of Environmentally Persistent Free Radicals as Molecular Pollutants in Particulate Matter. *Environ. Sci. Technol.*, **44**(6): p. 1933-1939, 2010.

40. Arens, F., L. Gutzwiller, H.W. Gaggeler, and M. Ammann, The reaction of NO2 with solid anthrarobin (1,2,10-trihydroxy-anthracene). *Phys. Chem. Chem. Phys.*, **4**(15): p. 3684-3690, 2002.

41. Ammann, M., E. Rossler, R. Strekowski, and C. George, Nitrogen dioxide multiphase chemistry: Uptake kinetics on aqueous solutions containing phenolic compounds. *Phys. Chem. Chem. Phys.*, **7**(12): p. 2513-2518, 2005.

B5) Shiraiwa et al., Proc. Natl. Acad. Sci., 2011

Gas uptake and chemical aging of semisolid organic aerosol particles

Manabu Shiraiwa[1], Markus Ammann[2], Thomas Koop[3] and Ulrich Pöschl[1]

[1] Max Planck Institute for Chemistry, Biogeochemistry Department, P.O. Box 3060, 55128 Mainz, Germany
[2] Paul Scherrer Institut, Laboratory of Radiochemistry and Environmental Chemistry, Villigen, CH-5232, Switzerland
[3]Faculty of Chemistry, Bielefeld University, 33615 Bielefeld, Germany

.

Proceedings of the National Academy of Sciences of the United States of America, 108, 11003-11008, 2011

Authors contributions.

MS, MA, and UP designed research. MS and MA performed research. MS and TK analyzed data. MS and UP wrote the paper.

Gas uptake and chemical aging of semisolid organic aerosol particles

Manabu Shiraiwa[a], Markus Ammann[b], Thomas Koop[c], and Ulrich Pöschl[a,1]

[a]Biogeochemistry Department, Max Planck Institute for Chemistry, P.O. Box 3060, 55128 Mainz, Germany; [b]Laboratory of Radiochemistry and Environmental Chemistry, Paul Scherrer Institut, CH-5232 Villigen, Switzerland; and [c]Faculty of Chemistry, Bielefeld University, Universitätsstraße 25, 33615 Bielefeld, Germany

Edited* by Margaret A. Tolbert, University of Colorado, Boulder, CO, and approved May 25, 2011 (received for review February 23, 2011)

Organic substances can adopt an amorphous solid or semisolid state, influencing the rate of heterogeneous reactions and multiphase processes in atmospheric aerosols. Here we demonstrate how molecular diffusion in the condensed phase affects the gas uptake and chemical transformation of semisolid organic particles. Flow tube experiments show that the ozone uptake and oxidative aging of amorphous protein is kinetically limited by bulk diffusion. The reactive gas uptake exhibits a pronounced increase with relative humidity, which can be explained by a decrease of viscosity and increase of diffusivity due to hygroscopic water uptake transforming the amorphous organic matrix from a glassy to a semisolid state (moisture-induced phase transition). The reaction rate depends on the condensed phase diffusion coefficients of both the oxidant and the organic reactant molecules, which can be described by a kinetic multilayer flux model but not by the traditional resistor model approach of multiphase chemistry. The chemical lifetime of reactive compounds in atmospheric particles can increase from seconds to days as the rate of diffusion in semisolid phases can decrease by multiple orders of magnitude in response to low temperature or low relative humidity. The findings demonstrate that the occurrence and properties of amorphous semisolid phases challenge traditional views and require advanced formalisms for the description of organic particle formation and transformation in atmospheric models of aerosol effects on air quality, public health, and climate.

Stokes-Einstein | percolation theory | glass transition | secondary organic aerosol partitioning | ozonolysis

Aerosols are ubiquitous in the atmosphere and have strong effects on climate and public health (1–3). Depending on chemical composition, phase state, and surface properties, aerosol particles can act as nuclei for cloud droplets and ice crystals, and they can affect the abundance of trace gases through heterogeneous chemical reactions (4–8). Gas-particle interactions can also significantly change the physical and chemical properties of aerosols such as toxicity, reactivity, hygroscopicity, and radiative properties (9–13). Chemical reactions and mass-transport lead to continuous transformation and changes in the composition of atmospheric aerosols ("chemical aging") (14–20).

Atmospheric aerosol particles may occur as solids or liquids or as a mixture of both depending on their composition and ambient conditions (21, 22). Carbonaceous combustion aerosol particles such as soot and related substances are known to be quasi-solid and undergo chemical reactions at the surface rather than in the bulk (black or elemental carbon, graphene, and polycyclic aromatic hydrocarbons) (1, 23–25). Until recently, secondary organic aerosol (SOA) particles formed in the atmosphere from condensable oxidation products of volatile organic compounds were assumed to be liquid (26–28). Virtanen et al. (2010) (29), however, showed that biogenic SOA particles formed in plant chamber experiments and in new particle formation events over boreal forests can adopt an amorphous semisolid state, which is in line with the observed presence of oligomers or other organic compounds with high molecular mass and low volatility in SOA (30, 31). Many organic substances, including carboxylic acids, carbohydrates, and proteins, tend to form amorphous phases upon cooling or drying of aqueous solution droplets (32–34). Depending on viscosity and microstructure, the amorphous phases can be classified as glasses, rubbers, gels, or ultraviscous liquids (32).

Amorphous substances have no long-range atomic order and are classified as solid glasses when their viscosity exceeds 10^{12} Pa s (35). Semisolid substances like rubbers, gels, or ultraviscous liquids have viscosities that are in the range of $\sim 10^{12}$ to $\sim 10^{2}$ Pa s, which is still orders of magnitude higher than the viscosity of liquid water at ambient conditions ($\sim 10^{-3}$ Pa s) (32, 36). Through the Stokes-Einstein equation, the viscosity of an amorphous organic substance can be related to its molecular self-diffusion coefficient (D_{org}):

$$D_{\mathrm{org}} = \frac{kT}{6\pi a \nu}. \quad [1]$$

Here k is the Boltzmann constant (1.38×10^{-23} J K^{-1}), T is the temperature (K), a is the effective molecular radius (m), and ν is the dynamic viscosity (Pa s). Typical viscosity values and related diffusion coefficients for liquid, semisolid, and solid phases are listed in Table 1. Note that D_{org} can vary over fifteen orders of magnitude from $\sim 10^{-5}$ cm^2 s^{-1} in a liquid to $\sim 10^{-20}$ cm^2 s^{-1} in a solid organic matrix.

Compared to the self-diffusion coefficients of the large organic molecules constituting the bulk material of amorphous organic particles (multifunctional hydrocarbon derivatives, oligomers, and macromolecules), the bulk diffusion coefficients of atmospheric photooxidants and other small gas molecules entering the organic matrix (O_3, OH, NO_x, H_2O, etc.) are usually orders of magnitude larger and less variable. Typically, the diffusion coefficients of water and photo-oxidants (D_{ox}) are around $\sim 10^{-10}$ cm^2 s^{-1} in solids (37, 38), $\sim 10^{-9}$—10^{-6} cm^2 s^{-1} in semisolid (39), and $\sim 10^{-5}$ cm^2 s^{-1} in liquid organic matrices (37, 40).

Fig. 1 shows the characteristic time of mass-transport and mixing by molecular diffusion τ_{cd} in aerosol particles (41) according to

$$\tau_{\mathrm{cd}} = \frac{{d_{\mathrm{p}}}^2}{4\pi^2 D} \quad [2]$$

as a function of particle diameter ($d_{\mathrm{p}} = 1$ nm–10 μm) and diffusion coefficient ($D = 10^{-5}$ cm^2 s^{-1} to 10^{-21} cm^2 s^{-1}). In case of nonreactive gas uptake (partitioning), τ_{cd} is the e-folding time of equilibration, i.e., the time after which the concentration in

Author contributions: M.S., M.A., and U.P. designed research; M.S. and M.A. performed research; M.S. and T.K. analyzed data; and M.S. and U.P. wrote the paper.

The authors declare no conflict of interest.

*This Direct Submission article had a prearranged editor.

[1]To whom correspondence should be addressed. E-mail: u.poschl@mpic.de.

This article contains supporting information online at www.pnas.org/lookup/suppl/doi:10.1073/pnas.1103045108/-/DCSupplemental.

Table 1. Characteristic magnitudes of viscosity for different phase states, corresponding self-diffusion coefficients of organic matrix molecules (D_{org}, Eq. 1 assuming $a = 10^{-10}$ m at 298 K), and condensed phase diffusion coefficients of small molecules like water and atmospheric oxidants (D_{ox})

Phase state	ν (Pa s)	D_{org} (cm^2 s^{-1})	D_{ox} (cm^2 s^{-1})
Liquid	$\sim 10^{-3}$	$\sim 10^{-5}$	$\sim 10^{-5}$
Semisolid	$\sim 10^{2}$–10^{12}	$\sim 10^{-10}$–10^{-20}	$\sim 10^{-7}$–10^{-9}
Solid	$\geq 10^{12}$	$\leq 10^{-20}$	$\sim 10^{-10}$

the particle core deviates by less than a factor of 1/e from the equilibrium value.

In the size range of the accumulation mode of atmospheric aerosols ($d_p \approx 10^2$ nm), τ_{cd} for nonvolatile organic species varies from microseconds to milliseconds for liquids, seconds to years for semisolids, and many years for solids. Thus, diffusion is likely to limit the kinetics of mass-transport and chemical reaction in amorphous organic aerosol particles, but so far the effects of diffusivity and their dependence on ambient conditions have hardly been quantified (29, 42–44).

The viscosity and diffusivity of water soluble and hygroscopic organic substances depend strongly on the ambient relative humidity (RH), because water can act as a plasticizer and increase the mobility of the organics (32, 43). Accordingly, the glass transition temperature of organic substances depends on RH (33, 34), and amorphous semisolids can undergo moisture-induced phase transitions (32, 43, 44). The viscosity and bulk diffusion coefficient of amorphous proteins can be estimated as a function of relative humidity, using the Stokes-Einstein relation with published viscosity and hygroscopic growth factor data (45–47) (*SI Text*). As shown in Fig. 2*A*, the phase of the protein bovine serum albumin (BSA) changes from solid to semisolid as RH increases, while D_{org} increases from 10^{-21} cm^2 s^{-1} up to 10^{-10} cm^2 s^{-1}. Fig. 2*B* shows the diffusion coefficient of ozone in the aqueous protein as estimated from percolation theory and hygroscopicity data [*SI Text*, (47–49)]. D_{ox} is $\sim 10^{-10}$ cm^2 s^{-1} at <20% RH, but it increases up to $\sim 10^{-5}$ cm^2 s^{-1} as RH increases to 100%.

Experimental and theoretical studies investigating atmospheric multiphase processes usually apply resistor model formulations that build on analogies with electric circuits (14, 15, 50, 51). The traditional resistor models, however, are usually based on simplifying assumptions such as steady state conditions, homogeneous mixing, and limited numbers of species and processes. To overcome these limitations, we use kinetic flux models to analyze measurement data of ozone uptake by amorphous semisolid organics and to elucidate the effects of bulk diffusion on gas uptake and chemical aging of atmospheric aerosols. Ozone uptake experiments were performed in a flow tube coated with the protein BSA as a proxy for semisolid organic aerosol (32, 47), and numerical simulations were performed with kinetic double- and multilayer models of aerosol surface and bulk chemistry [K2-SUB (52), KM-SUB (42)].

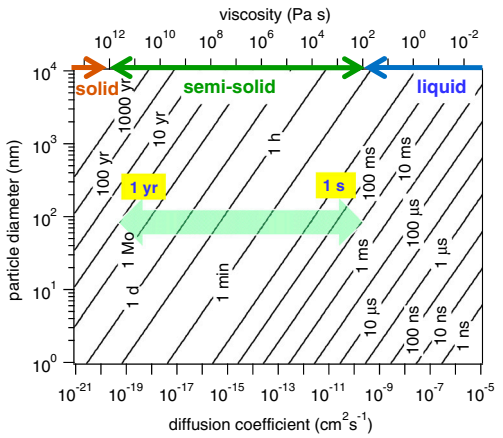

Fig. 1. Characteristic time of bulk diffusion (τ_{cd}) in liquid, semisolid, and solid particles as a function of diffusion coefficient and particle diameter. In the size range of the atmospheric aerosol accumulation mode ($d_p \approx 10^2$ nm), τ_{cd} in semisolid particles varies from seconds to years (light green arrow).

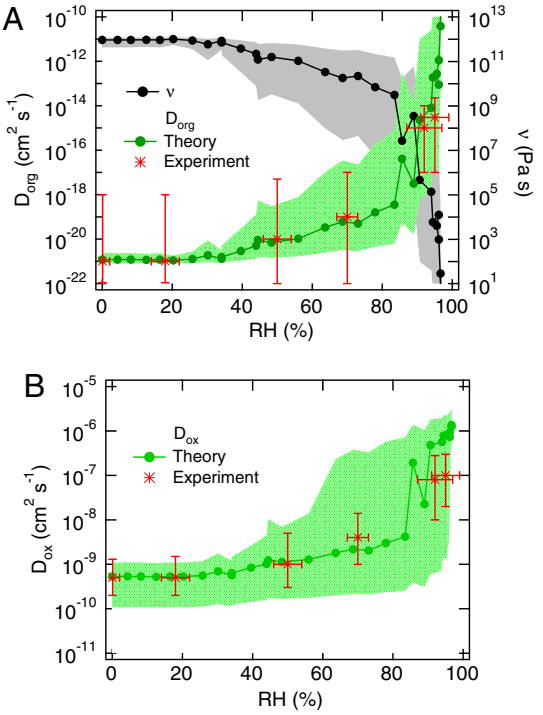

Fig. 2. (*A*) Viscosity (ν) and self-diffusion coefficient (D_{org}) of the protein BSA estimated as a function of relative humidity (RH) using the Stokes-Einstein relation with published viscosity and hygroscopic growth factor data for BSA. As RH increases, the protein phase changes from solid over semisolid to viscous liquid, while D_{org} increases from $\sim 10^{-21}$ cm^2 s^{-1} to $\sim 10^{-10}$ cm^2 s^{-1}. (*B*) Diffusion coefficient of ozone (D_{ox}) in BSA estimated as a function of RH by theoretical calculations using hygroscopic growth factor data. D_{ox} is $\sim 5 \times 10^{-10}$ cm^2 s^{-1} in solid BSA at RH <20%, but it increases up to $\sim 10^{-6}$ cm^2 s^{-1} in a viscous liquid aqueous phase at RH > 95%. The shaded areas represent uncertainties of estimation. The red stars show the D_{org} and D_{ox} values derived from the ozone uptake experiments, and the error bars indicate corresponding uncertainties.

Results and Discussion

Ozone Uptake by Amorphous Protein. Measurements of ozone uptake by amorphous protein were conducted in a coated wall flow tube for a wide range of ozone concentrations and relative humidities (42–207 ppb O_3, 0–95% RH, 296 K, 1 atm). The measurement results are ozone uptake coefficients (γ_{O_3}) which represent the probability that ozone molecules colliding with the surface are taken up by the condensed phase [net loss from the gas phase (53, 54)].

Fig. 3 shows double-logarithmic plots of γ_{O_3} plotted against reaction time (t), which exhibit a slope that is characteristic for diffusion-limited gas uptake ($\gamma \propto (D/\pi t)^{1/2}$, $\partial \ln \gamma / \partial \ln t = -0.5$) (51, 55, 56). As shown in Fig. 3*A*, the uptake coefficients observed at a given relative humidity decreased with increasing gas-phase concentration of ozone, which is due to more rapid depletion of condensed phase reactants (reactive amino acids in the protein). Fig. 3*B* shows that the uptake coefficients observed at a given ozone concentration level increased with increasing relative humidity. This behavior can be explained by a decrease of viscosity and increase of diffusivity with increasing RH, while

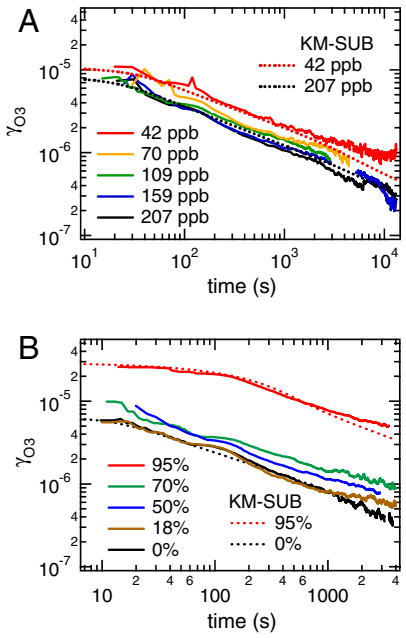

Fig. 3. Ozone uptake coefficients (γ_{O_3}) on protein films (BSA, 246 nm) observed (*A*) at 50% RH and different gas-phase O_3 concentrations (volume mixing ratios) and (*B*) at ~140 ppb O_3 and different relative humidities. The decrease of γ_{O_3} over time exhibits a double-logarithmic slope close to −0.5, which is characteristic for bulk diffusion-limited gas uptake. The time, RH, and O_3 concentration dependence of γ_{O_3} can be reproduced by the kinetic multilayer model KM-SUB (dotted lines).

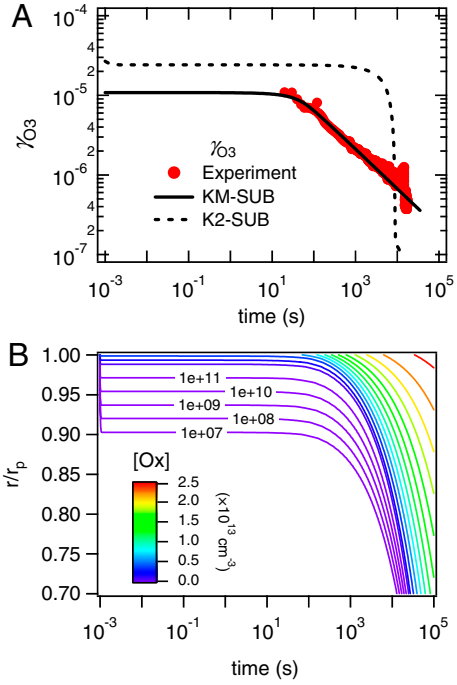

Fig. 4. Kinetic model results for the ozone uptake by semisolid protein (BSA) at 42 ppb O_3 and 50% RH. (*A*) Ozone uptake coefficients (γ_{O_3}) as observed (data points) and simulated with a multilayer model (KM-SUB, solid line) and with a resistor-based double-layer model (K2-SUB, dashed line). (*B*) Radial profile of ozone bulk concentration ([Ox]) calculated with KM-SUB; r/r_p is the distance from the particle center normalized by the particle radius ($r/r_p = 1$ at the surface).

the amorphous protein is transformed from a glassy to a semisolid state.

The time, concentration, and humidity dependence of γ_{O_3} can be reproduced by the kinetic multilayer flux model KM-SUB (42) as illustrated by the dotted lines in Fig. 3 and in Fig. S1. The model input parameters include the surface accommodation coefficient of ozone, the surface and bulk reaction rate coefficients between ozone and reactive amino acids, and the bulk diffusion coefficients of ozone and reactive amino acids (D_{ox}, D_{org}). Initial estimates of these parameters were taken from previous work (12, 24, 52), and best fit values were obtained by iterative variation as detailed in *SI Text*. The best fit values and humidity dependence of D_{ox} and D_{org} derived from the kinetic experiments are shown in Fig. 2. The experimental results agree well with the estimates obtained from theoretical calculations using literature data of protein viscosity and hygroscopic growth.

Fig. 4 displays the model simulation results for the experiment performed at 42 ppb O_3 and 50% RH. Initially γ_{O_3} equals the surface accommodation coefficient $\alpha_{s,O_3} \approx 1$ due to adsorption of ozone onto the particle surface. After $\sim 10^{-8}$ s the ozone concentration at the surface reaches a steady state level of $\sim 10^7$ cm^{-2} (Fig. S2*A*) determined by the combination of reversible adsorption, surface reaction, and surface-to-bulk transport, and γ_{O_3} decreases to the value of the bulk accommodation coefficient of $\alpha_{b,O_3} \approx 10^{-5}$ (Fig. 4*A*), indicating that the contribution of the surface reaction to the total ozone uptake is relatively minor. Up to ~10 s, γ_{O_3} remains as large as α_{b,O_3}, i.e., the uptake kinetics are limited by the transfer of ozone from the surface to the near-surface-bulk where it can readily oxidize reactive amino acids in the amorphous protein. After ~10 s, which is the time when experimental data become available, γ_{O_3} decreases below α_{b,O_3}, because the uptake is kinetically limited by diffusion in the bulk where ozone can oxidize further reactive amino acids.

In Fig. 4*B* the *y*-axis indicates the radial distance from the bottom of the protein coating (r) normalized by the film thickness (r_p), ranging from the bottom ($r/r_p \approx 0$) to the surface of the film ($r/r_p \approx 1$). The isolines in Fig. 4*B* show the radial distribution and temporal evolution of ozone in the amorphous protein matrix. Due to low diffusivity and reactive consumption, ozone initially exhibits a steep concentration gradient near the surface ($r/r_p > 0.90$), while the underlying bulk material remains essentially ozone-free. After ~10 s ozone begins to diffuse further into the bulk (Fig. 4*B*), the reactive amino acids are depleted near the surface (Fig. S2*C*), and the reaction front proceeds further into the particle bulk (Fig. S2*D*).

In contrast to the kinetic multilayer model KM-SUB, the kinetic double-layer model K2-SUB failed to reproduce the experimental results. In analogy to traditional resistor models, K2-SUB does not resolve radial profiles but approximates the effect of bulk processes by a reacto-diffusive flux term (50, 51, 53). This term accounts for the diffusion of gaseous reactants but neglects the diffusion of condensed phase reactants, assuming that the latter are homogeneously mixed. Using the same kinetic parameters as KM-SUB, K2-SUB cannot reproduce the observed time dependence of the ozone uptake coefficient. Instead, the predicted value of γ_{O_3} would remain constant over an extended period to 10^3 s and then drop off steeply due to rapid depletion of reactive amino acids throughout the homogeneously mixed protein film (dashed line in Fig. 4*A*). The results demonstrate that the assumption of homogeneous mixing and the application of the reacto-diffusive term of traditional resistor models are not appropriate for condensed phase reactants with low diffusivity in an amorphous semisolid matrix. Reliable predictions for such reaction systems require models that are able to resolve the diffusion of both gaseous and condensed phase reactants.

Atmospheric Implications. To explore and characterize the effects of bulk diffusion on the chemical aging of semisolid organic aerosols in the atmosphere, we calculated the chemical half-life ($t_{1/2}$)

of reactive amino acids in amorphous protein particles exposed to ozone under a wide range of ambient relative humidity and temperature. $t_{1/2}$ is defined as the time after which the number of reactive amino acids in the particle has decreased to half of its initial value. The particle diameter was set to 200 nm, which is typical for the accumulation mode of atmospheric aerosols, and the ozone concentration was varied in the range of zero to 200 ppb, covering clean and polluted conditions in the lower atmosphere. The kinetic parameters were the same as in the model simulation of the flow tube experiments (Table S1). The dependence of D_{ox} and D_{org} on relative humidity is shown in Fig. 2, and their temperature dependence is discussed in the supplement (*SI Text*).

The results of these calculations are shown in Fig. 5. As expected, $t_{1/2}$ decreases with increasing ozone gas-phase concentration. Fig. 5*A* shows that $t_{1/2}$ depends strongly on the ambient relative humidity at 25 °C. At 50 ppb O_3, for instance, $t_{1/2}$ is ~4 h at 20% RH, ~1.5 h at 50% RH, and only ~0.1 h at 90% RH. This variation is mainly because of the increase of D_{ox} at higher RH due to the moisture-induced phase transition of protein particles (i.e., solid at low RH, semisolid at medium RH, and viscous liquid at high RH). Fig. 5*B* shows the dependence of $t_{1/2}$ on ambient temperature at 50% RH: $t_{1/2}$ is ~1.5 h at 25 °C, and it increases to ~20 h at −60 °C due to the decrease of D_{ox}. To account for the possibility of freezing at low temperatures, we added a scenario assuming a diffusion coefficient similar to the values characteristic for small molecules in ice, i.e., $D_{ox} \approx 10^{-11}$ cm^2 s^{-1} (57), resulting in $t_{1/2} \approx 100$ h at 50 ppb O_3 and −60 °C (upper bound of shaded area). Note that a decrease of reaction rate coefficients with decreasing temperature may increase $t_{1/2}$ even further. The results show that the chemical half-life of organics can increase dramatically when particles are transported from the boundary layer to the upper free troposphere.

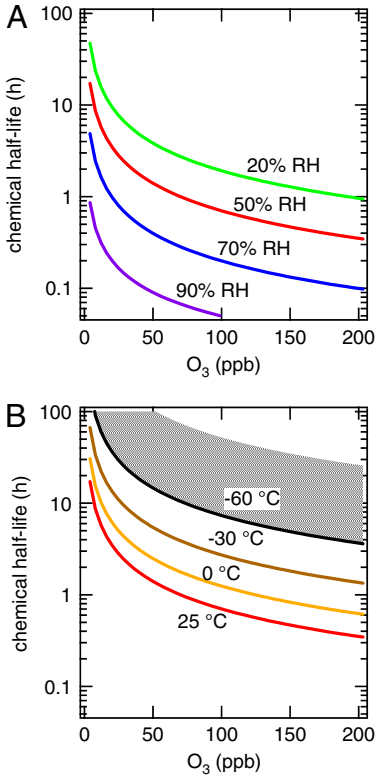

Fig. 5. Chemical half-life ($t_{1/2}$) of reactive amino acids in a protein particle of 200 nm diameter calculated as a function of gas-phase ozone concentration (volume mixing ratio, 1 atm). (*A*) $t_{1/2}$ at 25 °C for different relative humidities between 20% and 90%. (*B*) $t_{1/2}$ at 50% RH for different temperatures between 25°C and −60 °C. The shaded area shows the range of $t_{1/2}$ at −60 °C estimated for supercooled water vs. ice.

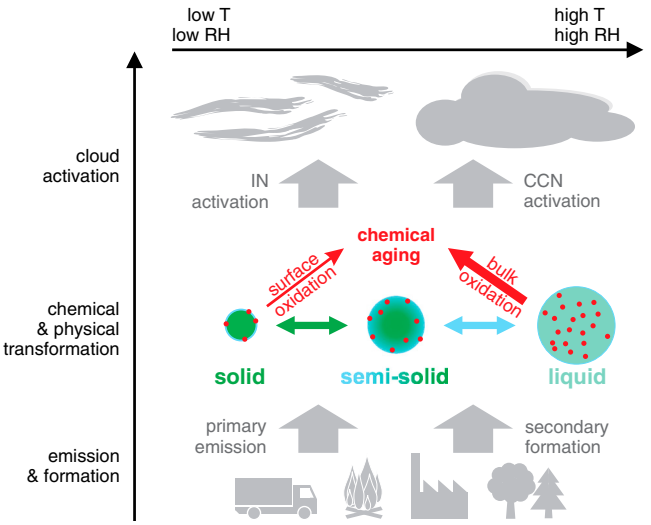

Fig. 6. Atmospheric processing of amorphous organic aerosol particles from primary emissions or secondary formation in the atmosphere. The phase state can fluctuate between glassy solid, semisolid and liquid depending on ambient relative humidity and temperature (physical transformation). Depending on phase state and diffusivity, the chemical transformation and aging upon interaction with atmospheric oxidants and other trace gases (small red circles) proceeds differently: relatively slow via surface adsorption and reaction on solid particles or relatively fast via bulk absorption and reaction in liquid particles. Upon cloud formation, solid aerosol particles are more likely to be activated as ice nuclei (IN) forming ice crystals, whereas liquid aerosol particles are more likely to be activated as cloud condensation nuclei (CCN) forming water droplets.

Fig. 6 illustrates how the phase state, viscosity, and diffusivity of atmospheric organic aerosol particle may vary upon changes in ambient relative humidity and temperature (physical transformation). Consequently, the chemical transformation and aging upon exposure to atmospheric oxidants such as O_3, OH, NO_3, N_2O_5, and halogen radicals will proceed differently (58, 59). In solid particles, the reactants are essentially confined to the surface, whereas they are rapidly mixed throughout the bulk of liquid particles. The chemical aging of semisolid organic substances is likely to be limited by the rate of molecular diffusion in the particle bulk. Our measurement and model results demonstrate that chemical reactions in amorphous semisolid aerosol particles are indeed limited by bulk diffusion, and that the rate of reaction can be strongly influenced by changes in relative humidity leading to changes in phase state and diffusivity due to hygroscopic water uptake. Thus, the chemical half-life of reactive organic compounds can change by orders of magnitude depending on ambient temperature and relative humidity, and uptake can become limited either by surface reaction, surface-bulk exchange, or bulk diffusion, underpinning the large potential effects of phase state for chemical aging (29, 42, 60, 61). The results of this study demonstrate quantitatively that mass-transport can have strong nonlinear effects on the chemical composition of atmospheric aerosols (16), and that amorphous semisolid states with high viscosity and low diffusion coefficients can effectively shield reactive organic compounds from degradation by atmospheric oxidants.

In addition to chemical aging of atmospheric aerosol particles, kinetic limitations of gas uptake by bulk diffusion may also influence the gas-particle partitioning of semivolatile organic compounds (SVOCs). In current gas-particle partitioning models, SVOCs are usually assumed to be well mixed throughout the particle (62–64). However, slow bulk diffusion may change the growth of SOA particles from absorptive to adsorptive, resulting in steep concentration gradients. On the other hand, slow trans-

port from the bulk to the surface may play an important role in the suppression of SOA evaporation (65). Moreover, aerosol hygroscopic growth and the nucleation of cloud droplets or ice crystals can be retarded or inhibited by slow diffusion (29, 32, 34, 43, 44, 47, 54, 66–69). The occurrence and properties of amorphous semisolid phases challenge traditional views and require new formalisms for the description of organic particle transformation and partitioning in atmospheric models of aerosol effects on air quality, public health, cloud physics, and climate.

Methods

BSA was obtained from Sigma-Aldrich (>96%, Sigma); it is a globular protein with a molecular mass of 67 kDa. Ozone uptake experiments with BSA were conducted in a cylindrical coated wall flow tube reactor (surface area 120 cm^2, surface-to-volume ratio 5 cm^{-1}). The sand-blasted inner surface of the pyrex tube was coated with BSA dissolved in water (18.2 MΩ cm, Milli Q plus 185, Millipore) and dried gently with a flow of nitrogen. This procedure led to about 2–4 mg of BSA deposited on the tube, which corresponds to a film thickness of BSA of 130–350 nm, assuming BSA to be evenly spread. O_3 was introduced into the flow reactor with synthetic air as carrier gas with a total flow rate of ~1 L min^{-1}. The experiments were conducted at atmospheric pressure and room temperature (~1 atm, ~296 K) and different relative humidities (0–95%). The gas-phase ozone concentration was monitored using a photometric ozone analyzer. The uptake coefficients of ozone (γ_{O_3}) were calculated using the Cooney-Kim-Davis method to concomitantly take into account radial gas-phase diffusion and first-order loss at the wall (70, 71). The model approach applied to analyze the experimental results is described in the *SI Text* [KM-SUB (42), K2-SUB (52), Figs. S3, S4, S5, and S6].

ACKNOWLEDGMENTS. We thank Y. Sosedova, A. Rouviere, S. Steimer, and M. Birrer for their help in the kinetic experiments; C. Pfrang, E. Mikhailov, T. Huthwelker, K. Binder and W. Schirmacher, J. Crowley, and T. Hoffmann for stimulating discussions. M.S. acknowledges support from the Max Planck Graduate Center—Johannes Gutenberg University Mainz, the Ministry of Education, Culture, Sports, Science and Technology—Japan (MEXT), and the University of Tokyo. This work was funded by the Max Planck Society (MPG), Swiss National Foundation (Grant no. 130175), and the European integrated project on cloud climate and air quality interactions (No 036833-2 EUCAARI).

1. Pöschl U (2005) Atmospheric aerosols: Composition, transformation, climate and health effects. *Angew Chem-Int Edit* 44:7520–7540.
2. IPCC (2007) *Climate Change 2007: The Physical Science Basis. Contribution of Working Group 1 to the 4th Assessment Report of the IPCC* (Cambridge University Press, Cambridge, United Kingdom).
3. Finlayson-Pitts BJ (2010) Atmospheric chemistry. *Proc Natl Acad Sci USA* 107:6566–6567.
4. Andreae MO, Rosenfeld D (2008) Aerosol-cloud-precipitation interactions. Part 1. The nature and sources of cloud-active aerosols. *Earth-Sci Rev* 89:13–41.
5. Fuzzi S, et al. (2006) Critical assessment of the current state of scientific knowledge, terminology, and research needs concerning the role of organic aerosols in the atmosphere, climate, and global change. *Atmos Chem Phys* 6:2017–2038.
6. Ammann M, et al. (1998) Heterogeneous production of nitrous acid on soot in polluted air masses. *Nature* 395:157–160.
7. Monge ME, et al. (2010) Light changes the atmospheric reactivity of soot. *Proc Natl Acad Sci USA* 107:6605–6609.
8. Pöschl U, et al. (2010) Rainforest aerosols as biogenic nuclei of clouds and precipitation in the Amazon. *Science* 329:1513–1516.
9. Rudich Y (2003) Laboratory perspectives on the chemical transformations of organic matter in atmospheric particles. *Chem Rev* 103:5097–5124.
10. Wiedensohler A, et al. (2009) Rapid aerosol particle growth and increase of cloud condensation nucleus activity by secondary aerosol formation and condensation: a case study for regional air pollution in northeastern China. *J Geophys Res-Atmos* 114:D00G08.
11. Shiraiwa M, et al. (2008) Radiative impact of mixing state of black carbon aerosol in Asian outflow. *J Geophys Res-Atmos* 113:D24210.
12. Shiraiwa M, et al. (2011) The role of long-lived reactive oxygen intermediates in the reaction of ozone with aerosol particles. *Nature Chemistry* 3:291–295.
13. Enami S, Hoffmann MR, Colussi AJ (2008) Acidity enhances the formation of a persistent ozonide at aqueous ascorbate/ozone gas interfaces. *Proc Natl Acad Sci USA* 105:7365–7369.
14. Hanson DR (1997) Surface-specific reactions on liquids. *J Phys Chem B* 101:4998–5001.
15. Schwartz SE, Freiberg JE (1981) Mass-transport limitation to the rate of reaction of gases in liquid droplets—Application to oxidation of SO_2 in aqueous-solutions. *Atmos Environ* 15:1129–1144.
16. Smith GD, Woods E, Baer T, Miller RE (2003) Aerosol uptake described by numerical solution of the diffusion—Reaction equations in the particle. *J Phys Chem A* 107:9582–9587.
17. Ammann M, Pöschl U (2007) Kinetic model framework for aerosol and cloud surface chemistry and gas-particle interactions—Part 2: exemplary practical applications and numerical simulations. *Atmos Chem Phys* 7:6025–6045.
18. Jimenez JL, et al. (2009) Evolution of organic aerosols in the atmosphere. *Science* 326:1525–1529.
19. Maria SF, Russell LM, Gilles MK, Myneni SCB (2004) Organic aerosol growth mechanisms and their climate-forcing implications. *Science* 306:1921–1924.
20. Kroll JH, et al. (2011) Carbon oxidation state as a metric for describing the chemistry of atmospheric organic aerosol. *Nature Chemistry* 3:133–139.
21. Martin ST (2000) Phase transitions of aqueous atmospheric particles. *Chem Rev* 100:3403–3453.
22. Marcolli C, Luo BP, Peter T (2004) Mixing of the organic aerosol fractions: liquids as the thermodynamically stable phases. *J Phys Chem A* 108:2216–2224.
23. Andreae MO, Gelencser A (2006) Black carbon or brown carbon? The nature of light-absorbing carbonaceous aerosols. *Atmos Chem Phys* 6:3131–3148.
24. Shiraiwa M, Garland RM, Pöschl U (2009) Kinetic double-layer model of aerosol surface chemistry and gas-particle interactions (K2-SURF): degradation of polycyclic aromatic hydrocarbons exposed to O_3, NO_2, H_2O, OH and NO_3. *Atmos Chem Phys* 9:9571–9586.
25. Sadezky A, Muckenhuber H, Grothe H, Niessner R, Pöschl U (2005) Raman microspectroscopy of soot and related carbonaceous materials: spectral analysis and structural information. *Carbon* 43:1731–1742.
26. Hallquist M, et al. (2009) The formation, properties and impact of secondary organic aerosol: current and emerging issues. *Atmos Chem Phys* 9:5155–5235.
27. Kanakidou M, et al. (2005) Organic aerosol and global climate modelling: a review. *Atmos Chem Phys* 5:1053–1123.
28. Pankow JF (1994) An absorption-model of the gas aerosol partitioning involved in the formation of secondary organic aerosol. *Atmos Environ* 28:189–193.
29. Virtanen A, et al. (2010) An amorphous solid state of biogenic secondary organic aerosol particles. *Nature* 467:824–827.
30. Kalberer M, et al. (2004) Identification of polymers as major components of atmospheric organic aerosols. *Science* 303:1659–1662.
31. Russell LM, Bahadur R, Ziemann PJ (2011) Identifying organic aerosol sources by comparing functional group composition in chamber and atmospheric particles. *Proc Natl Acad Sci USA* 108:3516–3521.
32. Mikhailov E, Vlasenko S, Martin ST, Koop T, Pöschl U (2009) Amorphous and crystalline aerosol particles interacting with water vapor: conceptual framework and experimental evidence for restructuring, phase transitions and kinetic limitations. *Atmos Chem Phys* 9:9491–9522.
33. Zobrist B, Marcolli C, Pedernera DA, Koop T (2008) Do atmospheric aerosols form glasses? *Atmos Chem Phys* 8:5221–5244.
34. Murray BJ (2008) Inhibition of ice crystallization in highly viscous aqueous organic acid droplets. *Atmos Chem Phys* 8:5423–5433.
35. Angell CA (1995) Formation of glasses from liquids and biopolymers. *Science* 267:1924–1935.
36. Hecksher T, Nielsen AI, Olsen NB, Dyre JC (2008) Little evidence for dynamic divergences in ultraviscous molecular liquids. *Nat Phys* 4:737–741.
37. Bird RB, Stewart WE, Lightfoot EN (2007) *Transport Phenomena* (John Wiley & Sons, Inc, New York), (2nd Ed).
38. Huthwelker T, Ammann M, Peter T (2006) The uptake of acidic gases on ice. *Chem Rev* 106:1375–1444.
39. Parker R, Ring SG (1995) Diffusion in maltose-water mixtures at temperatures close to the glass-tranition. *Carbohydr Res* 273:147–155.
40. Johnson PN, Davis RA (1996) Diffusivity of ozone in Wwater. *J Chem Eng Data* 41:1485–1487.
41. Seinfeld JH, Pandis SN (1998) *Atmospheric chemistry and physics—From air pollution to climate change* (John Wiley & Sons, Inc, New York).
42. Shiraiwa M, Pfrang C, Pöschl U (2010) Kinetic multi-layer model of aerosol surface and bulk chemistry (KM-SUB): the influence of interfacial transport and bulk diffusion on the oxidation of oleic acid by ozone. *Atmos Chem Phys* 10:3673–3691.
43. Zobrist B, et al. (2011) Ultra-slow water diffusion in aqueous sucrose glasses. *Phys Chem Chem Phys* 13:3514–3526.
44. Tong HJ, Reid JP, Bones DL, Luo BP, Krieger UK (2011) Measurements of the timescales for the mass transfer of water in glassy aerosol at low relative humidity and ambient temperature. *Atmos Chem Phys* 11:4739–4754, doi: 10.5194/acp-11-4739-2011.
45. Hottot A, Daoussi R, Andrieu J (2006) Thermophysical properties of aqueous and frozen states of BSA/water/Tris systems. *Int J Biol Macromol* 38:225–231.
46. Brownsey GJ, Noel TR, Parker R, Ring SG (2003) The glass transition behavior of the globular protein bovine serum albumin. *Biophys J* 85:3943–3950.
47. Mikhailov E, Vlasenko S, Niessner R, Pöschl U (2004) Interaction of aerosol particles composed of protein and salts with water vapor: hygroscopic growth and microstructural rearrangement. *Atmos Chem Phys* 4:323–350.
48. Murata T, Lee MS, Tanioka A (1999) An application of percolation theory to the electrolyte penetration through porous water-swollen cellulose triacetate membrane. *J Colloid Interface Sci* 220:250–254.
49. Shante VKS, Kirkpatrick S (1971) Introduction to percolation theory. *Adv Phys* 20:325–357.
50. Worsnop DR, Morris JW, Shi Q, Davidovits P, Kolb CE (2002) A chemical kinetic model for reactive transformations of aerosol particles. *Geophys Res Lett* 29:57-1–57-4.
51. Finlayson-Pitts BJ, Pitts JN, eds. (2000) *Chemistry of the upper and lower atmosphere* (Academic Press, San Diego, CA).
52. Pfrang C, Shiraiwa M, Pöschl U (2010) Coupling aerosol surface and bulk chemistry with a kinetic double layer model (K2-SUB): an exemplary study of the oxidation of oleic acid by ozone. *Atmos Chem Phys* 10:4357–4557.

53. Pöschl U, Rudich Y, Ammann M (2007) Kinetic model framework for aerosol and cloud surface chemistry and gas-particle interactions—Part 1: General equations, parameters, and terminology. *Atmos Chem Phys* 7:5989–6023.
54. Kolb CE, et al. (2010) An overview of current issues in the uptake of atmospheric trace gases by aerosols and clouds. *Atmos Chem Phys* 10:10561–10605.
55. Huthwelker T, Peter T (1996) Analytical description of gas transport across an interface with coupled diffusion in two phases. *J Chem Phys* 105:1661–1667.
56. Danckwerts PV (1951) Absorption by simultaneous diffusion and chemical reaction into particles of various shapes and into falling drops. *T Faraday Soc* 47:1014–1023.
57. Livingston FE, Smith JA, George SM (2002) General trends for bulk diffusion in ice and surface diffusion on ice. *J Phys Chem A* 106:6309–6318.
58. George IJ, Abbatt JPD (2010) Heterogeneous oxidation of atmospheric aerosol particles by gas-phase radicals. *Nature Chemistry* 2:713–722.
59. Xiao S, Bertram AK (2011) Reactive uptake kinetics of NO_3 on multicomponent and multiphase organic mixtures containing unsaturated and saturated organics. *Phys Chem Chem Phys* 13:6628–6636.
60. Knopf DA, Anthony LM, Bertram AK (2005) Reactive uptake of O_3 by multicomponent and multiphase mixtures containing oleic acid. *J Phys Chem A* 109:5579–5589.
61. Zahardis J, Petrucci GA (2007) The oleic acid-ozone heterogeneous reaction system: products, kinetics, secondary chemistry, and atmospheric implications of a model system—a review. *Atmos Chem Phys* 7:1237–1274.
62. Donahue NM, Robinson AL, Stanier CO, Pandis SN (2006) Coupled partitioning, dilution, and chemical aging of semivolatile organics. *Environ Sci Technol* 40(8): 02635–02643.
63. Robinson AL, et al. (2007) Rethinking organic aerosols: semivolatile emissions and photochemical aging. *Science* 315:1259–1262.
64. Zuend A, Marcolli C, Peter T, Seinfeld JH (2010) Computation of liquid-liquid equilibria and phase stabilities: implications for RH-dependent gas/particle partitioning of organic-inorganic aerosols. *Atmos Chem Phys* 10:7795–7820.
65. Vaden TD, Imre D, Beranek J, Shrivastava M, Zelenyuk A (2011) Evaporation kinetics and phase of laboratory and ambient secondary organic aerosol. *Proc Natl Acad Sci USA* 108:2190–2195.
66. Snider JR, et al. (2010) Intercomparison of cloud condensation nuclei and hygroscopic fraction measurements: coated soot particles investigated during the LACIS Experiment in November (LExNo). *J Geophys Res-Atmos* 115:D11205.
67. Barahona D, Rodriguez J, Nenes A (2010) Sensitivity of the global distribution of cirrus ice crystal concentration to heterogeneous freezing. *J Geophys Res-Atmos* 115:D23213.
68. Pöschl U (2011) Gas-particle interactions of tropospheric aerosols: kinetic and thermodynamic perspectives of multiphase chemical reactions, amorphous organic substances, and the activation of cloud condensation nuclei. *Atmos Res*, doi: 10.1016/j.atmosres.2010.12.12.018.
69. Murray BJ, et al. (2010) Heterogeneous nucleation of ice particles on glassy aerosols under cirrus conditions. *Nature Geoscience* 3:233–237.
70. Cooney DO, Kim SS, Davis EJ (1974) Analyses of mass-transfer in hemodialyzers for laminar blood-flow and homogeneous dialysate. *Chem Eng Sci* 29:1731–1738.
71. Ammann M, Rossler E, Strekowski R, George C (2005) Nitrogen dioxide multiphase chemistry: uptake kinetics on aqueous solutions containing phenolic compounds. *Phys Chem Chem Phys* 7:2513–2518.

Supporting Information

Shiraiwa et al. 10.1073/pnas.1103045108

SI Text

Estimation of Diffusion Coefficients. ***Estimation of D_{org}.*** In order to estimate the self-diffusion coefficient of bovine serum albumin (BSA) in BSA/water mixtures we used data of the viscosity of aqueous BSA solutions by Brownsey et al. (1) shown as red circles in Fig. S3. The data cover a range of dilute to concentrated solutions up to a BSA mass fraction of 0.5. Moreover, Brownsey et al (1) and Hottot et al (2) suggested that at room temperature aqueous BSA turns into a glass at a mass fraction between 0.6–0.8. Therefore, we chose a representative value of the viscosity at T_g of 10^{12} Pa s at a BSA mass fraction of 0.7, see blue square in Fig. S3. Using these data we can fit the viscosity (ν) of aqueous BSA over the whole concentration range, which can be estimated as follows:

$$\ln(\nu) = \ln(\nu_0) + \frac{\ln(\nu_{max})}{1+\exp(\frac{w_c - w}{s})} + Aw(1-\tanh(w-w_c)), \quad \textbf{[S1]}$$

where ν_0 is the viscosity of water (8.9×10^{-4} Pa s), ν_{max} is the characteristic viscosity in the glass transition ($\sim 10^{12}$–10^{13} Pa s, here: 7.53×10^{12} Pa s), w is the BSA mass fraction, $w_c = 0.514$ is the critical BSA mass fraction at which the BSA globules begin to come into contact with each other, $s = 0.041, A = 9.32$ is a constant characteristic of the near linear increase in $\ln(\nu)$ at small BSA mass fractions, and the term $1 - \tanh(w\text{-}w_c)$ is responsible for saturating this increase to a constant at concentration higher than about w_c.

The function in Eq. **S1** was chosen such that once the translational motion of globular BSA proteins seizes close to T_g, the viscosity remains practically constant at a value of about that at T_g (red dashed line), which is however, not relevant for the investigated concentration range investigated in Mikhailov et al. (3) and this work. Note that the steepest change in viscosity occurs around a mass fraction of 0.5–0.6, in agreement with experimental observations of Brownsey et al. (1), who observed a "glass-like kinetic arrest" at mass fractions in the region of 0.55.

The green triangles shown in Fig. S3 are inferred from the hygroscopicity tandem differential mobility analyzer (HTDMA) experiments by Mikhailov et al. (3). From these data, the water content of BSA aerosol particles as a function of relative humidity was calculated assuming a void fraction of 0.3, in agreement with a glass-transition induced fixation of BSA globules at a mass fraction of ~0.7, which is close to a dense packing of spheres. Fig. S3 implies that the BSA particles experience the entire semisolid range upon changes in humidity, with near-liquid viscosity/diffusivity at RH $\geq$ ~95% and near-solid behavior at RH $\leq$ ~30%.

The resulting viscosity values of aqueous BSA range from ν of 10^1–10^{12} Pa s depending on relative humidity. Using Eq. 1 in the main text, this viscosity can be converted to D_{org} values assuming a radius for globular BSA of $a = 2.5$ nm. As RH increased, D_{org} increases as particles take up more water.

Estimation of D_{ox}. The diffusion coefficient of ozone in the aqueous BSA film is estimated using the percolation theory (4–6), because the Stokes-Einstein equation is not applicable for small gas molecules diffusing through a highly viscous heterogeneous matrix near the glass-transition temperature (7). According to percolation and effective medium theory, the average diffusion coefficient in a mixture of two media with different diffusion can be described by the following equation:

$$D_{ox} = [D'_{ox,p} + D'_{ox,w} + [(D'_{ox,p} + D'_{ox,w})^2 + 2(Z-2)D_{ox,p}D_{ox,w}]]/(Z-2), \quad \textbf{[S2]}$$

where $D_{ox,p}$ is the diffusion coefficient of oxidant in protein globules, and $D_{ox,w}$ is the diffusion coefficient of oxidant in water ($\sim 10^{-5}$ cm^2 s^{-1}), which can be calculated by $D_{O_3,w}$ (cm^{2}s^{-1}) = $1.1 \times 10^{-4} \exp(-1{,}896/T)$ (8). $D'_{ox,p}$ and $D'_{ox,w}$ are reduced diffusion coefficients and are expressed as:

$$D'_{ox,p} = [(Z/2)(V_p/f) - 1]D_{ox,p} \quad \textbf{[S3]}$$

$$D'_{ox,w} = [(Z/2)(1 - V_p/f) - 1]D_{ox,w}. \quad \textbf{[S4]}$$

V_p is the volume fraction of protein globules, which can be directly calculated using hygroscopic growth factor (GF) data measured for BSA (3): $V_p = (1/GF)^3$. f is the packing fraction, for which we assumed a value of 0.85 (9). Z is the coordination number between water-filled pores in the protein matrix, for which we assumed a value of 12 that is characteristic for dense sphere packings (10). For $D_{ox,p}$ we assumed a value of 5×10^{-10} cm^2 s^{-1} which is of a magnitude characteristic for diffusion of small molecules solids (Table 1) and consistent with the diffusion-limited uptake of ozone observed under dry conditions (Fig. 2). For uncertainty estimates (green shaded area), f was varied from 0.65 to 1 (4, 9, 11), Z was varied between 8 and 16 (4), and $D_{ox,p}$ was varied from 10^{-10}–10^{-9} cm^2 s^{-1} (12).

The temperature dependence of D_{ox} at 50% RH was estimated using an Arrhenius-approach with an activation energy of about 15.8 kJ mol^{-1} (8) (Fig. S4).

Ozone Uptake Experiments. Fig. S5 shows the ozone uptake observed with an initial gas phase O_3 concentration of ~110 ppb at 50% RH. At the beginning of each experiment, the coated wall flow tube was bypassed to obtain a stable ozone signal ($t < 0$). When the flow was redirected through the flow tube ($t = 0$), the gas phase O_3 concentration dropped rapidly to ~60 ppb, which corresponds to an ozone uptake coefficient of $\gamma_{O_3} \approx 10^{-5}$ during the first few seconds of reaction time ($t \approx 10$ s). Then the ozone concentration recovered asymptotically towards the initial value, and the uptake coefficient exhibited a strong decrease that continued over multiple hours (Fig. 3). When the flow tube was bypassed again (e.g., at $t \approx 3{,}000$ s in Fig. S5), the gas phase ozone concentration quickly returned to the initial value, showing that the experimental conditions were stable. No significant ozone uptake was observed in an uncoated glass flow tube, confirming that the observed ozone loss was due to uptake by the protein film on the wall of the coated tube.

The magnitude and temporal evolution of γ_{O_3} did not change when the thickness of the protein film on the flow tube walls was varied between 133–346 nm. This finding indicates that the ozone uptake was kinetically limited by processes at or near the surface of the protein film. If the uptake kinetics had been affected by processes involving the entire volume of the protein film, the film thickness should have influenced the results, i.e., thicker films should have exhibited higher values or slower decrease of γ_{O_3}. Moreover, the amount of ozone taken up by the protein film ($>1 \times 10^{14}$ cm^{-2} after 1 h) clearly exceeded the surface capacity of reaction sites ($\leq 3 \times 10^{13}$ cm^{-2}). Thus, the most plausible explanation for the observed behavior is that the uptake of ozone was limited by diffusion and reaction near the surface of the protein film.

Kinetic Models and Parameters. Two kinetic flux models were applied to analyze the experimental results: the kinetic multilayer model (KM-SUB) (13) and the kinetic double-layer model (K2-SUB) (14) for aerosol surface and bulk chemistry, both of which build on the formalism and terminology of the PRA framework (15, 16). The uptake coefficient of ozone (γ_{O_3}) is defined as the ratio between the net flux of O_3 from the gas phase to the condensed phase and the gas kinetic flux of O_3 colliding with the surface (13, 14). The temporal evolution of γ_{O_3} and the particle surface and bulk composition were modeled by numerically solving the differential equations for the mass balance of each model compartment with Matlab (ode23tb solver with 999 time steps).

KM-SUB consists of multiple model compartments and layers: gas phase, near-surface gas phase, sorption layer, quasi-static surface layer, near-surface bulk, and a number of bulk layers as detailed below. KM-SUB explicitly treats all steps of mass transport (gas phase diffusion, gas-surface transport, and bulk diffusion) and chemical reactions from the gas-particle interface to the particle core, resolving concentration gradients and diffusion throughout the particle bulk. Unlike traditional resistor models, KM-SUB does not require simplifying assumptions about steady-state conditions and radial mixing. Surface-bulk transport and bulk diffusion of volatile and nonvolatile reactants are treated as the mass transport from one bulk layer to the next by describing the mass transport fluxes between different layers of the bulk by first-order transport velocities, which are calculated from the bulk diffusion coefficients (13). Bulk reaction rates are calculated assuming that bulk reactions proceed with second-order rate dependencies on the concentrations within each bulk layer. In the numerical simulations presented in this study, the number of model layers was set to $n = 200$ unless mentioned otherwise. Test calculations using smaller or higher values of n gave very similar results. The maximum relative deviations were 10% for $n < 20$, reconfirming the robustness of the KM-SUB model approach (13).

Instead of explicitly resolving radial profiles of bulk diffusion and reaction, K2-SUB (14) uses just one layer for the bulk, and the effects of bulk diffusion and reaction are represented by the reacto-diffusive flux ($J_{b,rd}$) based on traditional resistor model formulations (15,17–19). In this approach, the nonvolatile reactant is assumed to be well mixed in the bulk of the condensed phase (14). While the original K2-SUB model presented by Pfrang et al. (2009) (14) also assumed steady-state conditions for O_3 on the surface and in the bulk, we used the modified K2-SUB model of Shiraiwa et al. (2010) (13) without these steady-state assumptions (13).

The initial concentrations of ozone at the surface and in the bulk were set to zero, and the kinetic input parameters are listed in Table S1: surface accommodation coefficient of ozone for the clean substrate ($\alpha_{s,0}$), desorption lifetime of ozone (τ_d), bulk diffusion coefficients of ozone and reactive amino acids (D_{ox}, D_{org}), and second-order rate coefficients for the reaction between ozone and amino acids at the surface and in the bulk (k_{SLR} and k_{BR}), and the Henry's law coefficient of ozone ($K_{sol,cc}$). Additional input parameters are the mean thermal velocity of ozone ($\omega = 3.6 \times 10^4$ cm s^{-1}) and the effective molecular diameter of ozone ($\delta_{O_3} = 0.4$ nm) (14).

Among the 20 standard amino acids occurring in proteins, five are known to react with ozone: cysteine [35], methionine [5], tryptophan [3], tyrosine [21], and histidine [16] (20–22); the number in brackets shows the number of amino acid residues in one BSA molecule. The second-order rate coefficients of the reaction between these reactive amino acids and ozone in water at around pH7 vary by about three orders of magnitude from 10^5–10^7 M^{-1} s^{-1} (20, 23). For simplicity, we assume that ozone reacts with these amino acids with the same reactivity of 10^6 M^{-1} s^{-1} (1.6×10^{-15} cm^3 s^{-1}). Considering the BSA molecular mass (67 kDa) and density (1.36 g cm^{-3}) and assuming that the BSA protein molecules are densely packed, the BSA concentration is calculated to be 4.5×10^{18} cm^{-3}. Here we assume that one quarter of the reactive amino acids in the protein can be reacted (24, 25), resulting in the initial surface and bulk concentrations of these reactive amino acids of 3.3×10^{13} cm^{-2} and 9.0×10^{19} cm^{-3}, respectively.

Initial estimates for the required kinetic parameters are based on our previous studies (13, 14, 16, 26) and typical ranges for the interactions between ozone and organic surfaces: $\alpha_{s,0} = 10^{-3} - 1$, $\tau_d = 10^{-10} - 1$, $k_{SLR} = 10^{-18} - 10^{-11}$ cm^2 s^{-1}, and $K_{sol,cc} = 10^{-5}$–10^{-3} mol cm^{-3} atm^{-1}. These parameters were systematically and iteratively varied using Matlab software to find a best fit solution as summarized in Table S1. As specified below, the optimized parameter combination given in Table S1 is not a unique solution and other parameter combinations can also match the observed uptake coefficients. However, the key results presented in our study remain unchanged. In particular, the range of available literature data on the reaction rate coefficients and Henry's law coefficients of ozone in organic matrices does limit the range of diffusion coefficients that we extracted by applying KM-SUB to the experimental data observed as a function of time, O_3, and RH. The corresponding ranges of uncertainty are indicated by the error bars in Fig. 2.

Sensitivity Studies. In order to characterize the sensitivity of the model results with regard to the chosen set of kinetic input parameters, all parameters in Table S1 were varied systematically. The sensitivity studies revealed that $\alpha_{s,0}$, τ_d, and k_{SLR} are not critical for describing the observations of γ_{O_3} over the time scales of the experiments performed (>10 s); much higher time resolution would be required to resolve the surface processes. Even if the surface reaction is switched off (i.e., $k_{SLR,X,Y} = 0$), the model can reproduce the observed γ_{O_3} because uptake kinetics was limited by surface-bulk transport and bulk diffusion of ozone. The uptake of O_3 is insensitive to k_{BR} as long as it exceeds 10^{-16} cm^2 s^{-1}, indicating that for the reaction of ozone with amino acids under our experimental conditions, uptake was not kinetically limited by bulk reaction. If both the surface and bulk reactions are switched off, the calculated ozone concentration profiles (Fig. S6) reflects a nonreactive saturation process with a characteristic diffusion time as discussed in the main text (Fig. 1 and Eq. 1).

The most sensitive parameter is found to be D_{ox}, confirming that bulk diffusion of ozone is the rate-limiting step. The sensitivity study suggests that D_{ox} should be in the range of 5×10^{-10} – 10^{-8} cm^2 s^{-1} at 50% RH, which is consistent with predictions of Fig. 2*B*. D_{ox}, $K_{sol,cc}$, and k_{BR} can be mutually adjusted to match the observed γ_{O_3}; for example, the data can be also reproduced with $D_{ox} = 10^{-8}$ cm^2 s^{-1}, $K_{sol,cc} = 10^{-4}$ mol cm^{-3} atm^{-1}, and $k_{BR} = 1.6 \times 10^{-14}$ cm^3 s^{-1}. The reported k_{BR} (10^{-17}–10^{-14} cm^3 s^{-1}) and $K_{sol,cc}$ ($\sim 10^{-4}$ mol cm^{-3} atm^{-1}) limit the range of D_{ox} to match the kinetic observations and modeling.

The sensitivity study suggests that D_{org} should be below 10^{-17} cm^2 s^{-1} at 50% RH in order to be consistent with the experimental data. For values smaller than 10^{-17} cm^2 s^{-1}, the actual value becomes unimportant. This result implies that a potential breakdown of the Stokes-Einstein near the glass-transition is not relevant for the self-diffusion coefficient D_{org}. If a larger value for D_{org} is used, the second plateau of γ_{O_3} extends, showing similar behavior as K2-SUB in Fig. 5*A*. In this case Org is transported to the near-surface bulk to react with ozone there, so that diffusion of ozone is not the limiting step any more.

1. Brownsey GJ, Noel TR, Parker R, Ring SG (2003) The glass-transition behavior of the globular protein bovine serum albumin. *Biophys J* 85:3943–3950.

2. Hottot A, Daoussi R, Andrieu J (2006) Thermophysical properties of aqueous and frozen states of BSA/water/Tris systems. *Int J Biol Macromol* 38:225–231.

3. Mikhailov E, Vlasenko S, Niessner R, Pöschl U (2004) Interaction of aerosol particles composed of protein and salts with water vapor: hygroscopic growth and microstructural rearrangement. *Atmos Chem Phys* 4:323–350.
4. Murata T, Lee MS, Tanioka A (1999) An application of percolation theory to the electrolyte penetration through porous water-swollen cellulose triacetate membrane. *J Colloid Interface Sci* 220:250–254.
5. Shante VKS, Kirkpatrick S (1971) Introduction to percolation theory. *Adv Phys* 20:325–357.
6. Sherman RD, Middleman LM, Jacobs SM (1983) Electron-transport processes in conductior-filled polymers. *Polym Eng Sci* 23:36–46.
7. Champion D, Le Meste M, Simatos D (2000) Towards an improved understanding of glass-transition and relaxations in foods: molecular mobility in the glass-transition range. *Trends Food Sci Technol* 11:41–55.
8. Johnson PN, Davis RA (1996) Diffusivity of ozone in water. *J Chem Eng Data* 41:1485–1487.
9. Farr RS, Groot RD (2009) Close packing density of polydisperse hard spheres. *J Chem Phys* 131:244104.
10. Kittel C (1996) *Introduction to Solid State Physics* (Wiley, New York).
11. Fitzpatrick J, Malt RB, Spaepen F (1974) Percolation theory and conductivity of random close packed mixtures of hard spheres. *Phys Lett A* 47:207–208.
12. Huthwelker T, Ammann M, Peter T (2006) The uptake of acidic gases on ice. *Chem Rev* 106:1375–1444.
13. Shiraiwa M, Pfrang C, Pöschl U (2010) Kinetic multilayer model of aerosol surface and bulk chemistry (KM-SUB): the influence of interfacial transport and bulk diffusion on the oxidation of oleic acid by ozone. *Atmos Chem Phys* 10:3673–3691.
14. Pfrang C, Shiraiwa M, Pöschl U (2010) Coupling aerosol surface and bulk chemistry with a kinetic double-layer model (K2-SUB): an exemplary study of the oxidation of oleic acid by ozone. *Atmos Chem Phys* 10:4357–4557.
15. Pöschl U, Rudich Y, Ammann M (2007) Kinetic model framework for aerosol and cloud surface chemistry and gas-particle interactions—Part 1: general equations, parameters, and terminology. *Atmos Chem Phys* 7:5989–6023.
16. Ammann M, Pöschl U (2007) Kinetic model framework for aerosol and cloud surface chemistry and gas-particle interactions—Part 2: exemplary practical applications and numerical simulations. *Atmos Chem Phys* 7:6025–6045.
17. Danckwerts PV (1951) Absorption by simultaneous diffusion and chemical reaction into particles of various shapes and into falling drops. *Trans Faraday Soc* 47:1014–1023.
18. Hanson DR (1997) Surface-specific reactions on liquids. *J Phys Chem B* 101:4998–5001.
19. Worsnop DR, Morris JW, Shi Q, Davidovits P, Kolb CE (2002) A chemical kinetic model for reactive transformations of aerosol particles. *Geophys Res Lett* 29:57-1–57-4.
20. Sharma VK, Graham NJD (2010) Oxidation of amino acids, peptides and proteins by ozone: a review. *Ozone Sci Eng* 32:81–90.
21. Mudd JB, Leavitt R, Ongun A, McManus TT (1969) Reaction of ozone with amino acids and proteins. *Atmos Environ* 3:669–681.
22. Pryor WA, Giamalva DH, Church DF (1984) Kinetics of ozonation. 2. Amino acids and model compounds in water and comparisons to rates in nonpolar solvents. *J Am Chem Soc* 106:7094–7100.
23. Ignatenko AV, Cherenkevich SN (1985) Reactivity of amino-acids and proteins in reactions with ozone. *Kinet Catal* 26:1145–1148.
24. Zhang Y, Yang H, Pöschl U (2011) Analysis of nitrated proteins and tryptic peptides by HPLC-chip-MS/MS: site-specific quantification, nitration degree, and reactivity of tyrosine residues. *Anal Bioanal Chem* 399:459–471.
25. Yang H, Zhang Y, Pöschl U (2010) Quantification of nitrotyrosine in nitrated proteins. *Anal Bioanal Chem* 397:879–886.
26. Shiraiwa M, Garland RM, Pöschl U (2009) Kinetic double-layer model of aerosol surface chemistry and gas-particle interactions (K2-SURF): degradation of polycyclic aromatic hydrocarbons exposed to O_3, NO_2, H_2O, OH and NO_3. *Atmos Chem Phys* 9:9571–9586.

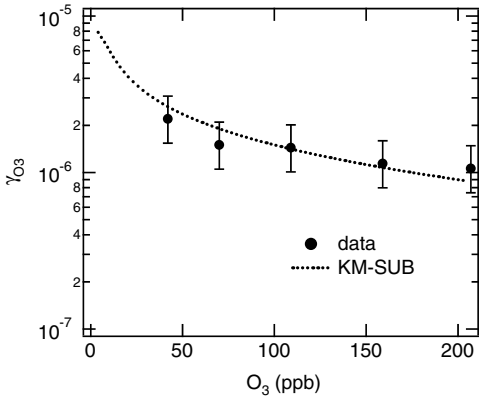

Fig. S1. Ozone uptake coefficients (γ_{O_3}) on BSA films (246 nm) at 50% RH as a function of gas phase ozone concentration after a reaction time of $t = 10^3$ s. The data points and error bars represent experimental data and standard deviations. The dotted line was calculated with the kinetic multilayer model KM-SUB using input parameters from Table S1.

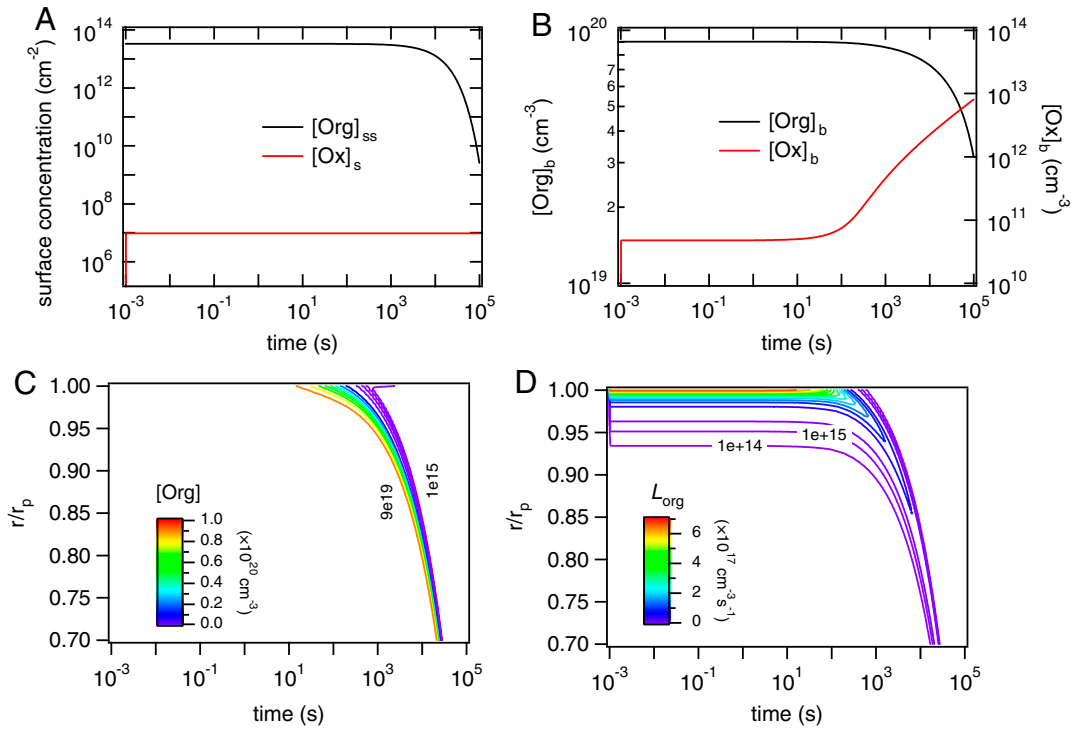

Fig. S2. Kinetic model results for the ozone uptake by semisolid protein (BSA) at 42 ppb O_3 and 50% RH at 296 K calculated with KM-SUB using input parameters from Table S1. (*A*) Surface concentrations and (*B*) average bulk concentrations of ozone ([Ox], red line) and reactive amino acids ([Org], black line). (*C*) Radial profile of reactive amino acid bulk concentration ([Org]); r/r_p is the distance from the particle center normalized by the particle radius ($r/r_p = 1$ at the surface). (*D*) Loss rate profile of reactive amino acids (L_{org}), showing that the reaction front (region of maximum loss rate) progresses from $r/r_p = 0.99$ up to ~10 s to $r/r_p = 0.80$ after ~10^4 s.

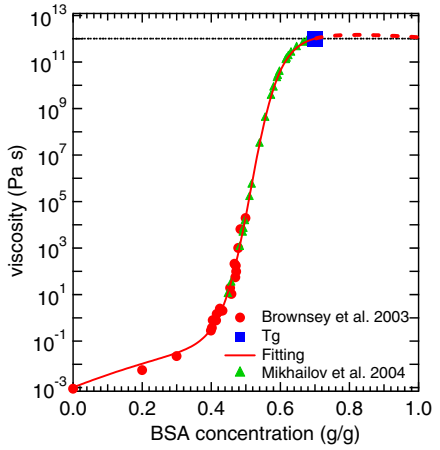

Fig. S3. Viscosity of aqueous BSA as a function of BSA mass fraction at 298 K. Experimental data from Brownsey et al. (1) (red circles) and at T_g of aqueous BSA at room temperature (blue square) were fitted using Eq. **S1** (red line). The green data points indicate the range of concentration and viscosity of aqueous BSA aerosol particles in the HTDMA experiments by Mikhailov et al. (2).

1 Brownsey GJ, Noel TR, Parker R, Ring SG (2003) The glass-transition behavior of the globular protein bovine serum albumin. *Biophys J* 85:3943–3950.

2 Mikhailov E, Vlasenko S, Niessner R, Pöschl U (2004) Interaction of aerosol particles composed of protein and salts with water vapor: hygroscopic growth and microstructural rearrangement. *Atmos Chem Phys* 4:323–350.

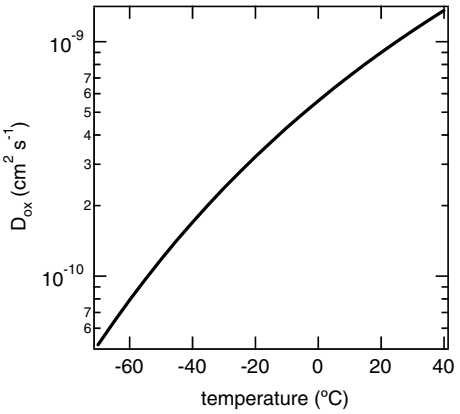

Fig. S4. Diffusion coefficient of ozone in aqueous BSA at 50% RH calculated as a function of temperature.

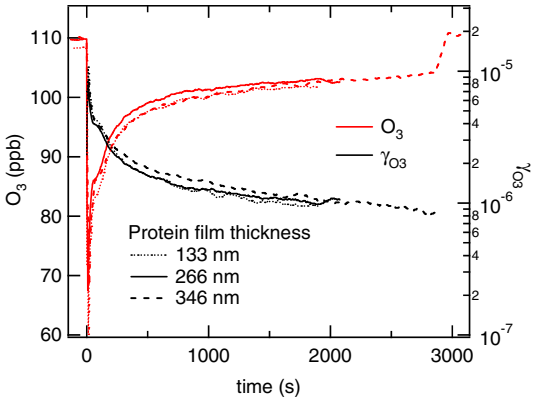

Fig. S5. Measurement data of ozone uptake experiments with protein films (BSA) at 50% RH. The uptake coefficient (γ_{O_3}) did not change when the protein film thickness was increased from 133 nm to 346 nm, indicating that the ozone uptake was kinetically limited by processes at or near the surface of the protein film.

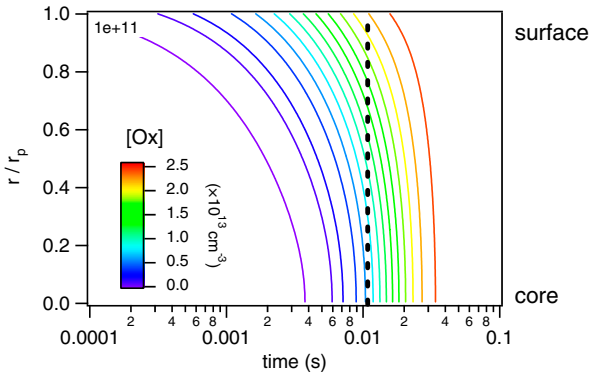

Fig. S6. Radial profile of ozone bulk concentration ([Ox]) for nonreactive uptake into a particle with 200 nm diameter and $D_{ox} = 10^{-9}$ cm^2 s^{-1} at 42 ppb O_3 and 50% RH calculated with KM-SUB using input parameters from Table S1; r/r_p is the distance from the particle center normalized by the particle radius ($r/r_p = 1$ at the surface). After the characteristic time of diffusion, $\tau_{cd} \approx 0.01$ s (black dotted line), the concentration at the particle core ($\approx 8 \times 10^{12}$ cm^{-3}) reaches $\sim 1/e$ of that in the near-surface bulk ($\approx 2.4 \times 10^{13}$ cm^{-3}).

Table S1. Kinetic parameters for the interaction of ozone and reactive amino acids in amorphous protein at 50% RH and 296 K

Parameter (Unit)	Value	Reference
$\alpha_{s,0}$	1	(1)
τ_d (s)	10^{-9}	(1)
k_{SLR} ($cm^2\ s^{-1}$)	10^{-11}	(2)
k_{BR} ($cm^3\ s^{-1}$)	1.6×10^{-15}	(3)
$K_{sol,cc}$ ($mol\ cm^{-3}\ atm^{-1}$)	10^{-3}	(4)
D_{ox} ($cm^2\ s^{-1}$)	10^{-9}	*SI Text*
D_{org} ($cm^2\ s^{-1}$)	10^{-20}	*SI Text*

*$\alpha_{s,0}$: surface accommodation coefficient of ozone on adsorbate-free substrate, τ_d: desorption lifetime of ozone, k_{SLR}: second-order rate coefficients of surface reaction between ozone and reactive amino acids, k_{BR}: second-order rate coefficients of bulk reaction between ozone and reactive amino acids, $K_{sol,cc}$: Henry's law coefficient of ozone, D_{ox} and D_{org}: bulk diffusion coefficients of ozone and reactive amino acids.

1 Shiraiwa M, et al (2011) The role of long-lived reactive oxygen intermediates in the reaction of ozone with aerosol particles. *Nature Chemistry* 3:291–295.
2 Pfrang C, Shiraiwa M, Pöschl U (2010) Coupling aerosol surface and bulk chemistry with a kinetic double-layer model (K2-SUB): an exemplary study of the oxidation of oleic acid by ozone. *Atmos Chem Phys* 10:4357–4557.
3 Sharma VK, Graham NJD (2010) Oxidation of amino acids, peptides, and proteins by ozone: a review. *Ozone Sci Eng* 32:81–90.
4 Ammann M, Pöschl U (2007) Kinetic model framework for aerosol and cloud surface chemistry and gas-particle interactions—Part 2: exemplary practical applications and numerical simulations. *Atmos Chem Phys* 7:6025–6045.

B6) Pfrang et al., Atmos. Chem. Phys., 2011

Chemical ageing and transformation of diffusivity in semi-solid multi-component organic aerosol particles

Christian Pfrang[1,2], Manabu Shiraiwa[2], and Ulrich Pöschl[2]

1. University of Reading, Department of Chemistry, P.O. BOX 224, Whiteknights, Reading RG6 6AD, UK

2. Max Planck Institute for Chemistry, Department of Biogeochemistry
J.J. Becherweg 27/29, D55128, Mainz, Germany

Atmospheric Chemistry and Physics 11, 7343-7354, 2011.

Authors contributions.

CP, UP and MS designed research. MS developed a new kinetic model. CP performed a kinetic modeling. CP, MS and UP discussed the results. CP wrote the paper.

Atmos. Chem. Phys., 11, 7343–7354, 2011
www.atmos-chem-phys.net/11/7343/2011/
doi:10.5194/acp-11-7343-2011

Atmospheric Chemistry and Physics

Chemical ageing and transformation of diffusivity in semi-solid multi-component organic aerosol particles

C. Pfrang[1,2], M. Shiraiwa[2], and U. Pöschl[2]

[1]University of Reading, Department of Chemistry, PO BOX 224, Whiteknights, Reading RG6 6AD, UK
[2]Max Planck Institute for Chemistry, Biogeochemistry Department, PO BOX 3060, 55128 Mainz, Germany

Received: 24 March 2011 – Published in Atmos. Chem. Phys. Discuss.: 27 April 2011
Revised: 12 July 2011 – Accepted: 13 July 2011 – Published: 26 July 2011

Abstract. Recent experimental evidence underlines the importance of reduced diffusivity in amorphous semi-solid or glassy atmospheric aerosols. This paper investigates the impact of diffusivity on the ageing of multi-component reactive organic particles approximating atmospheric cooking aerosols. We apply and extend the recently developed KM-SUB model in a study of a 12-component mixture containing oleic and palmitoleic acids. We demonstrate that changes in the diffusivity may explain the evolution of chemical loss rates in ageing semi-solid particles, and we resolve surface and bulk processes under transient reaction conditions considering diffusivities altered by oligomerisation. This new model treatment allows prediction of the ageing of mixed organic multi-component aerosols over atmospherically relevant timescales and conditions. We illustrate the impact of changing diffusivity on the chemical half-life of reactive components in semi-solid particles, and we demonstrate how solidification and crust formation at the particle surface can affect the chemical transformation of organic aerosols.

1 Introduction

Aerosols are highly variable components of the Earth's atmosphere that have a substantial impact on hydrological cycle, climate and public health (e.g. Seinfeld and Pankow, 2003; Pöschl, 2005; Fuzzi et al., 2006; Andreae and Rosenfeld, 2008). Gas-particle interactions can significantly change the physical and chemical properties of aerosols such as toxicity, reactivity, hygroscopicity and radiative properties (e.g. Rudich, 2003; Enami et al., 2008; Shiraiwa et al., 2011a). Thus, full understanding of the properties and transformation of aerosol particles is of key importance for atmospheric science. Aerosols may be present as solids or liquids depending on their compositions and ambient conditions (Martin, 2000; Marcolli et al., 2004; Shiraiwa et al., 2011b; Vaden et al., 2011). Until recently, secondary organic aerosol (SOA) particles formed in the atmosphere were assumed to be liquid (Hallquist et al., 2009). Virtanen et al. (2010), however, showed that biogenic SOA particles produced both in chamber experiments and during particle-formation events over boreal forests can adopt an amorphous semi-solid state, which is in line with the observed presence of oligomers with high molecular mass and low volatility in SOA (Kalberer et al., 2004). Many organic compounds, e.g. carboxylic acids, form amorphous phases upon cooling or drying of aqueous solution droplets (Murray, 2008; Zobrist et al., 2008; Mikhailov et al., 2009). These solid or semi-solid amorphous phases can be classified as glasses, rubbers, gels, or ultraviscous liquids (Mikhailov et al., 2009). The occurrence of highly viscous, glassy or gel-like substances can impact on the atmospheric fate of reactive aerosol components. The oxidation of organic substances in the atmosphere is mainly initiated by hydroxyl radicals (OH), nitrate radicals (NO_3) and ozone (O_3) (Wayne, 2000). While atmospheric lifetimes of volatile organic compounds are largely determined by the rate coefficients of the chemical reactions with OH, NO_3, and O_3 (e.g. King et al., 1999; Pfrang et al., 2006, 2007, 2008; McGillen et al., 2011), mass transport parameters of reactants are important additional factors for organic aerosols. Chemical reactions can occur at the surface and in the bulk of aerosol particles (e.g. Pfrang et al., 2010; Xiao and Bertram, 2011). Rates and relative proportions of surface and bulk reactions as well as the evolution of diffusivity during atmospheric ageing of multi-component aerosol particles are poorly understood.

Cooking aerosol has been recognised to contribute substantially to the urban aerosol burden. The aerosol-mass spectrometer spectra of one of its most prominent reactive components have strong similarity to oleic acid (Allan et al.,

Correspondence to: C. Pfrang
(c.pfrang@reading.ac.uk)

2010). Oxidation of oleic acid and related compounds has been subject to intense experimental investigation (e.g. Ziemann, 2005; Zahardis and Petrucci, 2007; Gonzalez-Labrada et al., 2007; Lee and Chan, 2007; King et al., 2008, 2009, 2010; Vesna et al., 2009; Thompson et al., 2010; Pfrang et al., 2011) and been established as a model system for atmospheric aerosol ageing. While single-component aerosol oxidation studies provide very useful mechanistic and kinetic insight, real atmospheric aerosols consist of much more complex multi-component and multi-phase mixed particles. Recent studies of mixed particles report that the changes in viscosity and phase significantly affect atmospheric aerosol ageing (e.g. Xiao and Bertram, 2011 and references therein; Tong et al., 2011; Zobrist et al., 2011; Shiraiwa et al., 2011b). Xiao and Bertram (2011) studied a mixture of the oleic acid methyl ester, methyl oleate, in a multi-component matrix. Kinetic parameters were derived following a resistor model approach aiming to distinguish between surface and bulk reactivity. A range of laboratory studies report an impact of diffusivity changes on the ageing of aerosols containing oleic acid (e.g. Moise and Rudich, 2002; Nash et al., 2006; Zahardis et al., 2008; Last et al., 2009). Most of these studies found physical changes leading to the solidification (e.g. drying and deliquescence). A few studies reported reduced reactivity with increasing reaction time that suggests an oxidation-induced change in viscosity (e.g. Huff Hartz et al., 2007). To date, the large majority of laboratory studies provide evidence for physical – not chemical – processes altering diffusivity, but this might be due to the higher complexity of the added chemical reactions that have to be considered in studies of chemical ageing.

Moise and Rudich (2002) studied oleic acid ozonolysis in liquid and solid particles. They contrast liquid particles where sub-surface layers participate in the uptake with frozen oleic acid particles where uptake is limited exclusively to the surface. Lee and Chan (2007) studied ozonolysis of oleic acid particles in an electrodynamic balance with Raman spectroscopy. They report formation of peroxidic compounds and an increasing hygroscopicity of aged particles. They propose reaction pathways leading to formation of diperoxides and polymeric peroxides. Vesna et al. (2009) also report predominance of peroxides as secondary reaction products (Ziemann, 2005 estimated organic peroxides to contribute 68 % to the total product aerosol mass) and include polymerisation channels in their reaction schemes. They found that the product distribution depends strongly on ambient relative humidity. Last et al. (2009) studied products from oleic acid ozonolysis and found that oligomer chain lengths increased with ozone exposure. Zahardis et al. (2008) studied mixed particles containing oleic acid and particulate amines. They also report stabilised Criegee intermediates and found direct evidence for the formation of a surface reaction barrier during ozonolysis of mixed oleic acid/octadecylamine particles. This reaction barrier leads to retention of oleic acid in the mixed particle even at very high ozone concentrations. Zahardis et al. (2008) propose that this effect is caused by surface or near-surface reactions that produce high molecular weight products and that these surface active species may impede the diffusion of ozone into the particle as well as limiting the diffusion of oleic acid to the surface: this effectively shuts down oleic acid ozonolysis. Similar effects of formation of solid or highly viscous surface layers have been observed by Nash et al. (2006) for ozonised mixed oleic acid-myristic acid particles. Zahardis et al. (2008) propose that condensed phase thermochemical effects like gel or semi-solid formation that may prolong oleic acid lifetimes need to be explored.

Huff Hartz et al. (2007) applied a relative rate technique to follow the kinetics of multi-component reactive organic aerosol particles. They found a retardation of the decay of oleic and palmitoleic acids and report initial and final rate coefficients differing by more than one order of magnitude. This investigation was chosen for simulation in the present modelling study, since these experimental data are very well suited for detailed analysis with our modelling tools promising new mechanistic insight by exploring diffusivity effects.

Description of the behaviour of multi-component aerosols that are realistic models for atmospheric particles remains a major challenge. In the present modelling study we applied three approaches for description of 12-component mixed organic aerosol particles: a simple model variant based on resistor model formulations (K2-SUB; Pfrang et al., 2010) is compared with a more sophisticated model (KM-SUB; Shiraiwa et al., 2010) to establish the significance of diffusion processes in semi-solid aerosol particles that cannot be resolved in resistor model formulations. In the KM-SUB modelling approach we either assume a semi-solid matrix with constant diffusivity or describe the diffusivity evolution caused by highly viscous reaction products.

2 Methodology

We applied two kinetic flux models to analyze the experimental results of ozone uptake by semi-solid multi-component organic aerosol particles: the kinetic multi-layer model (KM-SUB: Shiraiwa et al., 2010) and the kinetic double-layer model (K2-SUB: Pfrang et al., 2010) for aerosol surface and bulk chemistry, both of which are based on Pöschl-Rudich-Ammann framework (Pöschl et al., 2007; Ammann and Pöschl, 2007). KM-SUB explicitly treats all steps of mass transport and chemical reaction from the gas-particle interface to the particle core, resolving concentration gradients and diffusion throughout the particle bulk. Unlike traditional resistor models, KM-SUB does not require simplifying assumptions about steady-state conditions and radial mixing. Instead of explicit treatments of bulk diffusion and reaction, K2-SUB uses one layer for bulk and the diffusion and reaction in the bulk is represented by the reacto-diffusive flux ($J_{\mathrm{b,rd,O_3}}$) based on traditional resistor model

formulations (Pöschl et al., 2007). In this approach, the non-volatile reactant is assumed to be well mixed in the bulk of the condensed phase.

KM-SUB consists of multiple model compartments and layers: gas phase, near-surface gas phase, sorption layer, quasi-static surface layer, near-surface bulk, and a number of n bulk layers. The following processes are considered in KM-SUB: gas phase diffusion and gas-surface transport (reversible adsorption) of ozone, surface and bulk reactions between ozone and each organic component, surface-bulk transport and bulk diffusion of ozone and organic multi-components.

Surface-bulk transport and bulk diffusion of volatile and nonvolatile reactants are explicitly treated as the mass transport from one bulk layer to the next by describing the mass transport fluxes between different layers of the bulk by first-order transport velocities, which are calculated from the bulk diffusion coefficients (Shiraiwa et al., 2010). Bulk reaction rates are calculated assuming that bulk reactions proceed with straightforward second-order rate dependences on the concentrations within each bulk layer. In the numerical simulations presented in this study, the number of model layers was set to $n = 250$ for the 275 nm-radius particle. Test calculations using a wide range of values for n gave very similar results (see Fig. S5 in the Supplement).

The evolution of bulk diffusion coefficients upon products formation are implemented to KM-SUB in this study. The diffusion coefficient of ozone in the multi-component organics is evolved using the theory for diffusion in heterogeneous media, known as obstruction theory (Stroeve, 1975). Assuming the reaction products are dimmers and polymers which have much lower diffusivity compared to parent organics, the obstruction theory gives the expression for the diffusion coefficients of ozone and the organic reactant, Y, in a medium containing a concentration fraction $f_{b,n}$ of products in each layer n as follows:

$$D_{b,O_3,n}(t) = D_{b,O_3,0}(2-2f_{b,n})/(2+f_{b,n}) \quad (1)$$

$$D_{b,Y,n}(t) = D_{b,Y,0}(2-2f_{b,n})/(2+f_{b,n}) \quad (2)$$

where $D_{b,O_3,0}$ and $D_{b,Y,0}$ are the initial diffusion coefficients of ozone and Y in the 12-component mixture, respectively. The concentration fraction of products in the quasi-static surface layer (f_{ss}) is used analogously for calculation of the surface diffusion coefficients $D_{s,O_3}(t)$ and $D_{s,Y}(t)$. The reaction products are assumed to be (semi-)solid, so that the concentration fractions f_{ss} and f_b may be interpreted as degrees of solidification with a value of unity corresponding to complete conversion of reactants into (semi-)solid products. f_{ss} or f_b approaching unity thus leads to a shut down of transport due to massively decreasing diffusivity.

While we follow the obstruction theory approach throughout the paper, we tested the sensitivity of our modelling approach on the method used to describe the evolution of diffusivity as detailed in the Supplement material (see Fig. S4). The alternative approach uses a linear combination expression for the time-dependent diffusion coefficients assuming a product diffusivity of 1/4 of the initial value (based on a M^2 dependence for dimmer formation). There is a measurable, but not substantial difference between the two approaches. Another alternative approach, percolation theory, has been applied by Shiraiwa et al. (2011b), but constraining parameters required for application of this theory are not available for the multi-component system investigated in the present study. We thus used the obstruction theory approach which has been applied in the past (Stroeve, 1975). However, we would like to point out that representation of viscosity and diffusion in multi-component mixtures is highly uncertain: lack of miscibility may lead to phase heterogeneity and separation into domains of very different compositions and viscosities. There is no direct experimental evidence suggesting only radial heterogeneity in viscosity and discrete domains analogous to micelle formation by surfactant material in aqueous solutions may be equally as possible as formation of complete crusts.

In both models the uptake coefficients of ozone (γ_{O_3}) is expressed as the ratio of the net flux of O_3 from the gas phase to the condensed phase to the gas kinetic flux of ozone colliding with the surface (Pöschl et al., 2007). The temporal evolution of the particle surface and bulk composition and uptake coefficient of ozone were modelled by numerically solving the differential equations for the mass balance for each model compartment with Matlab (using the ode23tb solver with 999 time steps). The initial concentrations of ozone at the surface and in the bulk were set to zero and those of the 12-mixture components are based on Huff Hartz et al. (2007). The 12 components (9.9 % unreactive alkanes, 14.9 % palmitoleic acid, 13.1 % oleic acid, 1 % nervonic acid, 2.8 % cholesterol, 2.0 % decanoic acid, 17.7 % palmitic acid, 22.4 % stearic acid, 1.3 % arachadic acid, 2.6 % glutaric acid, 6.6 % adipic acid, 5.8 % suberic acid) have been chosen to mimic meat-cooking emission profiles in dry conditions containing the key unsaturated compounds commonly used as markers, in particular cholesterol as well as palmitoleic and oleic acids (Huff Hartz et al., 2007 and references therein). Product volatilization in the complex 12-component aerosol mixture is not considered here, mainly because of the lack of experimental data to constrain any modelling attempt. Re-condensation of components is unlikely to be of importance in the experimental conditions where gaseous components originate from the particles only. All components are assumed to be initially homogeneously mixed throughout the particle. The required kinetic parameters are listed in Table 1. The values were chosen based on previous work (Pfrang et al., 2010; Shiraiwa et al., 2011a) and to match the experimental data. Initial surface accommodation coefficient of ozone ($\alpha_{s,0,O_3} = 1$) and desorption lifetime of ozone ($\tau_{d,O_3} = 10^{-9}$ s) are based on previous studies (Shiraiwa et al., 2011a, b). Additional input parameters are: the mean thermal velocity of

Table 1. Kinetic parameters for the interaction of ozone and multi-component organics (compare List of symbols in Appendix A).

Parameters	Values
$\alpha_{s,0,O_3}$	1
τ_{d,O_3} (s)	10^{-9}
K_{sol,cc,O_3} (mol cm^{-3} atm^{-1})	4.8×10^{-4}
$D_{b,O_3,0}$ (cm^2 s^{-1})	5.5×10^{-8}
$D_{b,Y,0}$ (cm^2 s^{-1})	3.0×10^{-15}
$k_{SLR,O_3,ole}$ (cm^2 s^{-1})	1.0×10^{-10}
$k_{SLR,O_3,pal}$ (cm^2 s^{-1})	1.6×10^{-10}
$k_{BR,O_3,ole}$ (cm^3 s^{-1})	1.0×10^{-16}
$k_{BR,O_3,pal}$ (cm^3 s^{-1})	1.6×10^{-16}

$\alpha_{s,0,O_3}$: surface accommodation coefficient of ozone on free substrate, τ_d: desorption lifetime of ozone, K_{sol,cc,O_3}: Henry's law coefficient of ozone, $D_{b,O_3,0}$ and $D_{b,Y,0}$: bulk diffusion coefficients of ozone and organics, $k_{SLR,O_3,ole}$, $k_{SLR,O_3,pal}$: second-order rate coefficients of surface reaction between ozone, and oleic acid and palmitoleic acids, respectively, $k_{BR,O_3,ole}$, $k_{BR,O_3,pal}$: second-order rate coefficients of bulk reaction between ozone, and oleic acid and palmitoleic acids, respectively.

ozone ($\omega_{O_3} = 3.6 \times 10^4$ cm s^{-1}), the Henry's law coefficient of ozone ($K_{sol,cc,O_3} = 4.8 \times 10^{-4}$ mol cm^{-3} atm^{-1}), and the molecular diameter of ozone and organics ($\delta_{O_3} = 0.4$ nm, $\delta_Y = 0.8$ nm) (Shiraiwa et al., 2009; Pfrang et al., 2010). Second-order rate coefficients for the reaction between ozone and oleic and palmitoleic acid in the bulk (k_{BR}) are taken from Huff Hartz et al. (2007) and those at the surface (k_{SLR}) are based on Pfrang et al. (2011). The initial estimates of bulk diffusion coefficients of ozone and organics ($D_{b,O_3,0}$ and $D_{b,Y,0}$) are based on Shiraiwa et al. (2011b) and they were systematically and iteratively varied using Matlab software to find the best fits. The sensitivity of each parameter on model results is discussed in the Supplement material. While experimental data are only available for the first ca. 13 000 s, the model was run for 10^5 s since this is an atmospherically relevant timescale for this type of aerosol matrix.

3 Results and discussion

Figure 1 shows the time evolution of oleic and palmitoleic acids, the most reactive species in the 12-component mixture approximating cooking aerosols. Surface and bulk concentrations are converted into numbers of molecules to be able to show the decays in a single figure. The fitted data were obtained using variants of the detailed kinetic multi-layer flux model (KM-SUB) at 130 ppb [O_3] with the kinetic parameters listed in Table 1. The best fits (illustrated as solid lines) to experimental data from Huff Hartz et al. (2007)

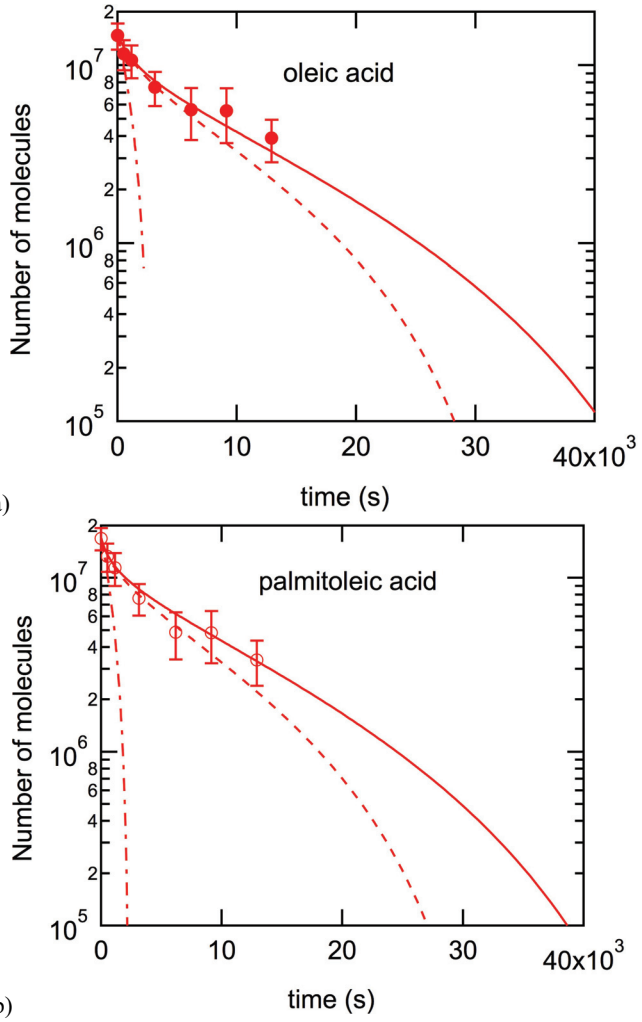

Fig. 1. Decays of numbers of molecules of **(a)** oleic and **(b)** palmitoleic acids in a 12-component aerosol matrix as a function of time. Symbols correspond to experimental data (Huff Hartz et al., 2007). The solid line is our best model fit with solidification (diffusivity-evolution model variant). The dashed line is a model fit of the semi-solid matrix assuming constant diffusivity (constant-diffusivity variant). The dot-dashed line[1] represents a fit using a resistor-model formulation (K2-SUB).

are achieved when assuming successive solidification of the mixed particle (diffusivity-evolution model variant). At short reaction times, a fit that assumes a semi-solid matrix with constant diffusivity (dashed lines) matches the experimental data equally well. The constant-diffusivity fits lie outside the error limits of the experimental data for reaction times above ca. 10^4 s. The discrepancy between the two model variants is substantial for longer reaction times: complete consumption of the reactive acids (concentration <1 % of initial value) takes ca. 10^4 s longer and the relative differences in concentrations increase progressively (>50 % at t: 2×10^4 s) if the viscosity of the mixed aerosol increases during the ageing

[1]Only a limited timescale is accessible with standard Matlab solvers (see end of dot-dashed line in Fig. 1a) due to the steep decays. The deviation from experimental data is clearly demonstrated on the available timescale and we expect the dot-dashed line in Fig. 1a to behave like that in Fig. 1b.

processes. The massive importance of the diffusivity of the particle matrix is illustrated in a comparison with the resistor-model formulation based K2-SUB model variant (Pfrang et al., 2010) where diffusion of the organic species in the bulk is not resolved (see dot-dashed lines in Fig. 1). This comparison illustrates that the assumption of homogeneous mixing and the application of the reacto-diffusive term of traditional resistor models are not appropriate for condensed phase reactants with low diffusivity in an amorphous semi-solid multi-component aerosol matrix (confirming very recent findings by Shiraiwa et al., 2011b for protein ozonolysis). While there is clear experimental evidence for a retardation of the losses of oleic and palmitioleic acids (Huff Hartz et al., 2007), it should be noted that volatilization of reaction products – which is not considered in our approach – might affect the experimental data. The chemical composition of the particle will change during reaction and the extent of the deviation from initial particle composition will become increasingly significant for longer reaction timescales. Dominant initial products from the ozonolysis of oleic acid are known to be nonanal, which is likely to evaporate, as well as 9-oxononanoic, nonanoic, and azelaic acids in the liquid phase (e.g. Rudich et al., 2007; Vesna et al., 2009). We expect first-generation products of oleic acid ozonolysis other than nonanal to remain in the particle phase. No data is available on the product volatility or properties for the specific 12-component organic aerosol matrix simulated, so that the evaporation of products from particle to gas phase could not be considered in the current model. However, if crust formation is occurring the loss of volatiles would be restricted to the surface and near-surface bulk, i.e. the amount of volatile molecules relative to the total number of oleic and palmitoleic acid molecules in the particle would be small. The influence of the changing chemical composition of the particle surface on adsorbate–surface interactions i.e. on the surface accommodation coefficient can be taken into account by adjusting $\alpha_{s,0,O_3}$ (see Pöschl et al., 2007, Pfrang et al., 2010 and Shiraiwa et al., 2010). For long reaction times, the increasing proportion of second- and third-generation products in the particle will also introduce additional uncertainties since branching ratios and molecular properties in such complex multi-component and multi-phase matrices are entirely unknown. Reliable predictions for such reaction systems require models able to resolve diffusivity of both gaseous and condensed phase reactants together with constraining experimental data.

Figure 2 compares surface and bulk accommodation with the uptake coefficient of ozone for constant-diffusivity (dashed lines) and diffusivity-evolution (solid lines) model variants. Surface accommodation, α_{s,O_3}, remains at the initial surface accommodation value of unity throughout all model runs. Bulk accommodation, α_{b,O_3}, is time independent as long as the diffusivity remains constant. At long reaction times, lower diffusion coefficients lead to a substantial reduction in bulk accommodation. This causes an earlier, but more gradual drop in γ_{O_3}. Crust formation on the particle surface is illustrated by the plateau in α_{b,O_3} at long reaction times in the diffusivity-evolution model variant.

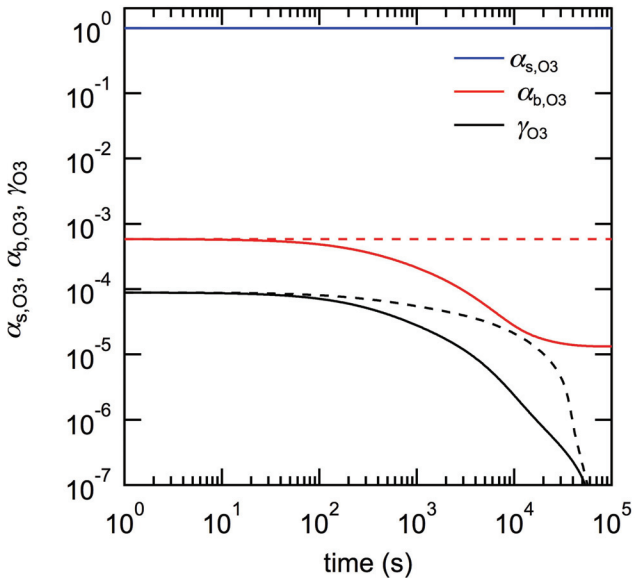

Fig. 2. Time evolution of surface and bulk accommodation as well as uptake coefficient for ozone for constant-diffusivity (dashed lines) and diffusivity-evolution (solid lines) model variants.

Figure 3 illustrates model surface parameters. Figure 3a shows the time evolution of surface concentrations of the reactants for both KM-SUB variants. While surface ozone is not affected by crust formation, the surface loss of the reactive organic species is significantly faster if the evolution of diffusivity is considered. In this case, transport between surface and bulk is slowed down due to the changes in diffusivity: transport is impeded 2-fold ∼500 s oxidative ageing, 3-fold ∼1000 s, 10-fold ∼5000 s and 20-fold ∼10000 s. The decay of reactive species on the particle surface is enhanced, because the surface cannot be renewed as bulk to surface transport of organics is inhibited by crust formation. Figure 3b illustrates surface parameters for the diffusivity-evolution model variant. The concentration fractions of products in the quasi-static surface layer (f_{ss}) and in the particle bulk (f_b) are illustrated in Figs. 3b and 6, respectively. Since the products are assumed to be (semi-)solid, we interpret these fractions as degrees of solidification with a value of unity corresponding to a complete conversion of reactants into products. f_{ss} approaching unity thus corresponds to the formation of a surface crust which would effectively shut down transport into the particle core due to the massively decreased diffusivity in the quasi-static surface layer. The degree of solidification (f_{ss}) is shown as blue line, while diffusivities at the surface for ozone and the organic species (Y; here oleic acid) are represented by black and red lines, respectively. One third of the surface solidifies already ∼500 s oxidative ageing; half of the surface ∼1000 s, 60 % ∼1800 s,

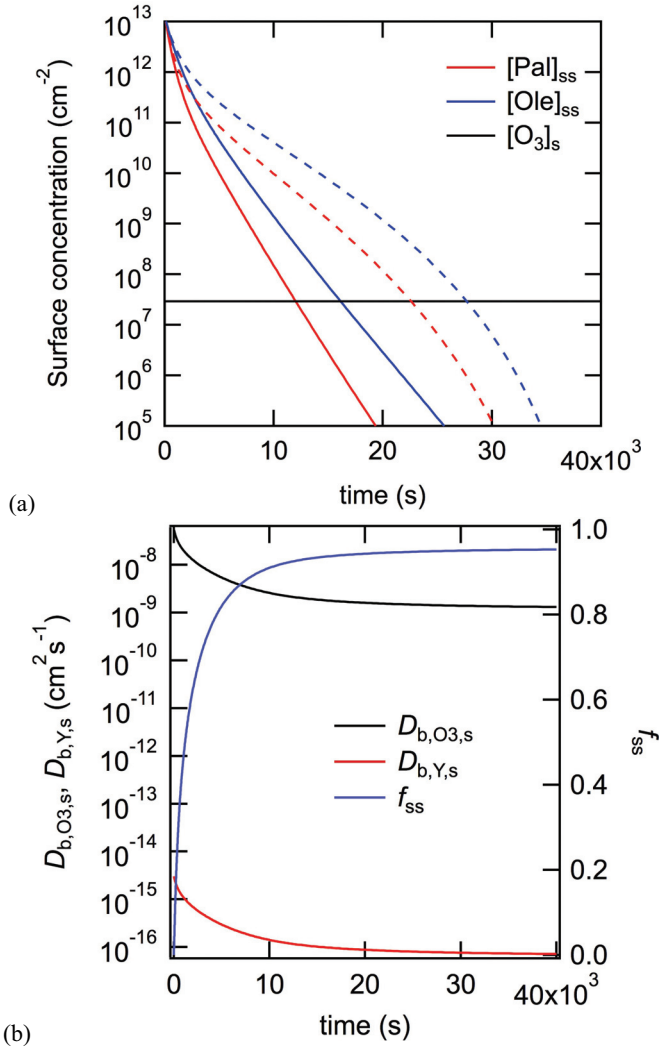

Fig. 3. **(a)** Time profiles of concentrations in the quasi-static surface layer of the reactive acids and ozone for constant-diffusivity (dashed lines) and diffusivity-evolution (solid lines) model variants. **(b)** Time evolution of diffusion coefficients for ozone and oleic acid as well as extent of solidification (f_{ss}) at the particle surface for the diffusivity-evolution model variant.

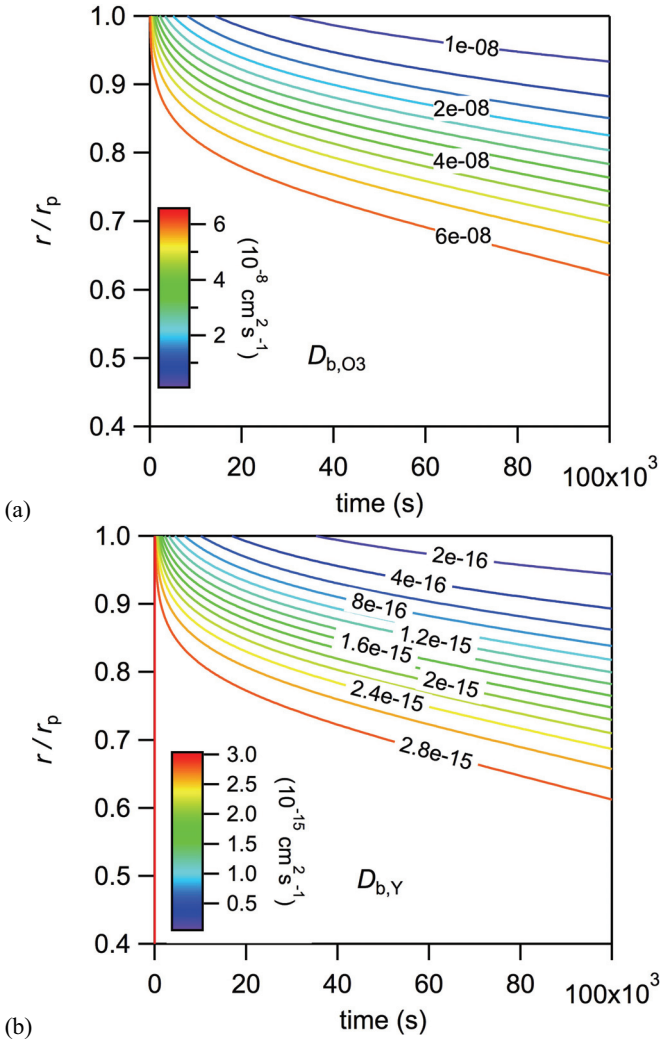

Fig. 4. Bulk diffusion coefficients of **(a)** ozone and **(b)** oleic acid as a function of time and depth in the 275 nm-radius particle.

80 % ∼4500 s, 90 % ∼9100 s, and: 95 % ∼30000 s. Note that 30 000 s correspond to about 8 h, which is still much shorter than the typical atmospheric residence time of aerosol particles in the accumulation size range (several days). The solidification reduces the diffusivity of ozone and organic species at the particle surface by more than one order of magnitude.

Figure 4 shows the evolution of diffusivity in the bulk of the mixed particle for the best fit to the experimental data from Huff Hartz et al. (2007). The y-axis indicates the radial distance from the core of the aerosol particle (r) normalized by the particle radius (r_p), ranging from the core ($r/r_p \approx 0$; not shown) to the particle surface ($r/r_p \approx 1$). The isolines in Fig. 4 illustrate the radial distribution and temporal evolution of the bulk diffusion coefficients of ozone (Fig. 4a) and the reactive organic species (here oleic acid; Fig. 4b) in the semi-solid aerosol matrix. It is apparent that the diffusivities of both ozone and the organic species near the surface (up to: 120 nm into the particle) show considerable gradients while the diffusivities in the inner half of the particle remain largely unaffected by the oxidative ageing processes. Diffusion in the surface region is slowed down substantially: after 10-h ageing we observe a 6-fold drop in the diffusion coefficient for ozone and a 10-fold reduction for oleic acid comparing the top to a depth of 75 nm in the 275 nm-radius particle. The crust formation clearly reduces the diffusivity. This effect becomes more pronounced at long reaction times.

Figure 5 displays the time evolution of the bulk concentrations of ozone and oleic acid. It is apparent that both ozone and organic species are not well-mixed and subject to considerable concentration gradients. The O_3 gradient remains fairly large throughout the model run (ca. two orders

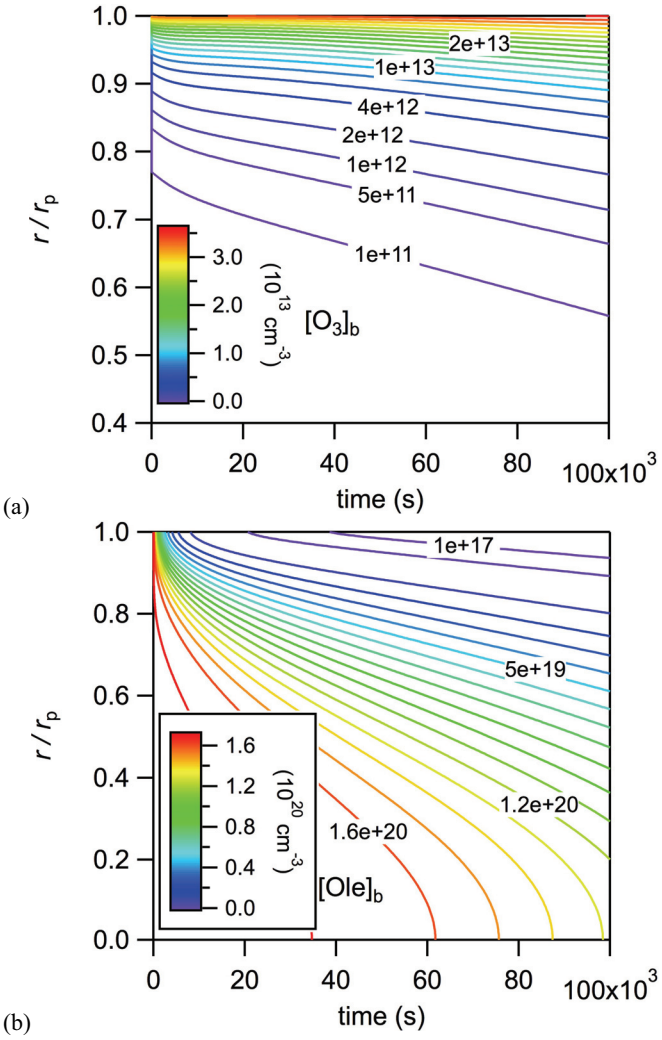

Fig. 5. Bulk concentration profiles of **(a)** ozone and **(b)** oleic acid for the diffusivity-evolution model. Equivalent plots for the constant-diffusivity model variant are presented in the Supplement in Fig. S1a and b.

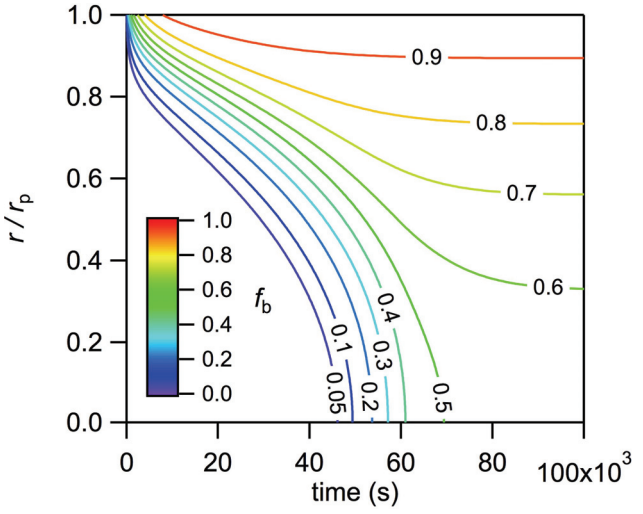

Fig. 6. Extent of solidification in the particle bulk, f_b, as a function of time and depth in the 275 nm-radius particle.

of magnitude in the top 75 nm of the particle). Gradients in the organic compounds are generated very rapidly due to initially efficient loss at and near the particle surface. The oleic acid gradient in the top 75 nm reaches ca. three orders of magnitude and then decreases to ca. two orders of magnitude after one day of ageing. In particular the concentration gradient of the organic species leads to the breakdown of the resistor model treatment (see deviation of the dot-dashed lines in Fig. 1 from the experimental data) where organics are assumed to remain homogeneously mixed throughout the particle.

Figure 6 illustrates the extent of solidification in the particle bulk. Values close to unity illustrate the crust formation near the particle surface. 90 % of the aerosol matrix becomes solid in the top 30nm of the 275 nm-radius particle already after 10-h ageing. However, only 60 % of the particle core solidifies even after long-term atmospheric ageing (>1 day) illustrating that the solid crust does not allow the reaction to continue efficiently inside the particle. This suggests that reactive species in the particle bulk are protected underneath a solid crust and may thus survive much longer in the atmosphere than anticipated based on chemical reactivity.

We demonstrate that our model allows flexible description of chemical and physical processes in multi-component aerosol matrices with evolving diffusivity. The best fit to experimental data is achieved for a solidifying aerosol forming a crust on the surface of the mixed particle. The impact of crust formation and diffusivity change on the reactive decay becomes larger with increasing reaction times. On typical atmospheric timescales crust formation would strongly affect the fate of reactive organic species with substantially extended lifetimes near the particle core. On the shorter timescales of experimental data (up to 10^4 s), a semi-solid matrix with constant diffusivity can also describe the observed reactive decays. Resistor model assumptions are inadequate even at short timescales, since limited diffusion of the organic species strongly affects particle ageing. These diffusivity effects cannot be described with traditional resistor-model formulations (compare Shiraiwa et al., 2011b). We demonstrate this directly by comparison of models with opposing assumptions for description of diffusivity. Chemical loss and physical retardation of composition changes in semi-sold aerosol matrices can be de-convoluted with our modelling approach. Solidification plays a substantial role at long reaction times highly relevant on atmospheric timescales.

4 Atmospheric implications

In order to explore the effects of the diffusivity evolution on the chemical aging of semi-solid multi-component organic aerosols in the atmosphere, we have calculated the chemical half-life ($t_{1/2}$) of the reactive fatty acids in the 12-component mixed particles exposed to atmospherically relevant gas-phase ozone mixing ratios. $t_{1/2}$ is defined as the time after which the number of reactive fatty acid molecules in the particle has decreased to half of its initial value. The particle radius was set to 275 nm, which corresponds to the size used in the simulated experiments (Huff Hartz et al., 2007) and is typical for the accumulation mode of atmospheric aerosols. [O_3] was varied in the range of 4 to 150 ppb, covering clean and polluted conditions in the lower atmosphere. The kinetic parameters were the same as in the model simulation of the experimental data (see Table 1).

For atmospheric interpretation of the results presented below, it should be noted that the model used in the present study has been optimized to simulate laboratory data for a 12-species organic aerosol matrix in dry conditions (Huff Hartz et al., 2007). While the 12 components have been chosen to mimic meat-cooking emission profiles containing the key unsaturated compounds commonly used as markers, in particular cholesterol as well as palmitoleic and oleic acids (Huff Hartz et al., 2007 and references therein), real meat cooking emissions are complex mixtures of hundreds of compounds and likely to interact with moisture present in the atmosphere. Particularly in highly humid conditions we would expect considerable deviations between our model results and the behaviour of cooking aerosol in the atmosphere, since hygroscopic growth can impact substantially on chemical ageing and atmospheric lifetimes of aerosols. Product volatilization in the complex 12-component aerosol mixture is also not considered here, mainly because of the lack of experimental data to constrain any modelling attempt. The evaporation and re-condensation of components and the resulting evolution of the chemical matrix may have considerable effects on chemical processes in these multi-species and multi-phase mixtures. While re-condensation is unlikely to be of importance in the experimental conditions where gaseous components originate from particles only, it may be important in complex atmospheric aerosol matrices.

Figure 7 shows the chemical half-life for oleic and palmitoleic acids contrasting diffusivity-evolution (solid lines) and constant-diffusivity (dashed lines) model variants. Model parameters are identical to those used in our best-fit scenario (see Table 1). As expected, $t_{1/2}$ decreases with increasing ozone gas phase concentration. Below 50 ppb, oleic and palmitoleic acids have half lives of several hours (up to >0.5 days at 4 ppb). At 150 ppb, half lives are below one hour. There are clear differences between the half lives obtained when assuming constant or evolving diffusivities. In clean and low-pollution environments, crust formation caused by diffusivity evolution of semi-solid aerosol matrices would lead to almost identical half lives of the reactive species while under polluted conditions (>40 ppb for palmitoleic acid and >50 ppb for oleic acid), lifetimes of reactive organics are increased significantly. The half-life increase becomes more pronounced at high [O_3]. Overall, the half lives are increased when considering the crust formation which illustrates that reactive organic species can be protected underneath a surface crust in multi-component reactive aerosol matrices. This is consistent with atmospheric residence times of reactive species (in particular oleic acid) that are substantially longer than those obtained when considering chemical reactivity alone. The evolution of diffusivity in multi-component aerosol matrices clearly impacts on the fate of reactive components of organic aerosols.

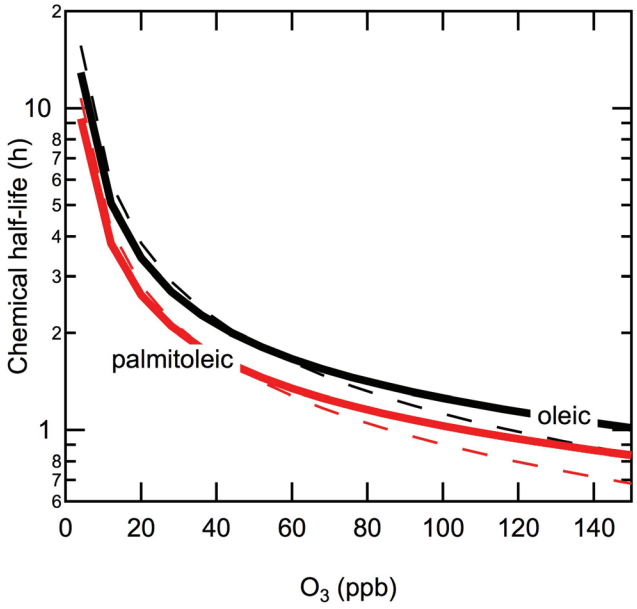

Fig. 7. Chemical half-life of oleic and palmitoleic acids, the most reactive components of the 12-component mixed aerosol matrix with a particle radius of 275 nm as a function of gas phase ozone mixing ratio. Bold solid lines represent results from the diffusivity-evolution model variant and the dashed lines are obtained assuming constant diffusivity of the semi-solid aerosol matrix.

The importance of diffusivity for the lifetime of the reactive species in multi-component aerosols is further illustrated in Fig. 8. Diffusion coefficients of water and photo-oxidants are typically $<10^{-10}$ cm^2 s^{-1} in solid (Bird et al., 2007; Huthwelker et al., 2006), 10^{-10}–10^{-6} cm^2 s^{-1} in semi-solid (Parker and Ring, 1995), and 10^{-6}–10^{-5} cm^2 s^{-1} in liquid organic matrices (Bird et al., 2007; Johnson and Davis, 1996). We varied diffusivity of ozone between 10^{-5} cm^2 s^{-1} (liquid matrix) to 10^{-10} cm^2 s^{-1} in Fig. 8a. In Fig. 8b we varied the initial diffusivity of the organic species in the range for semi-solids of 10^{-13}–10^{-20} cm^2 s^{-1} (compare Shiraiwa et al., 2011b).

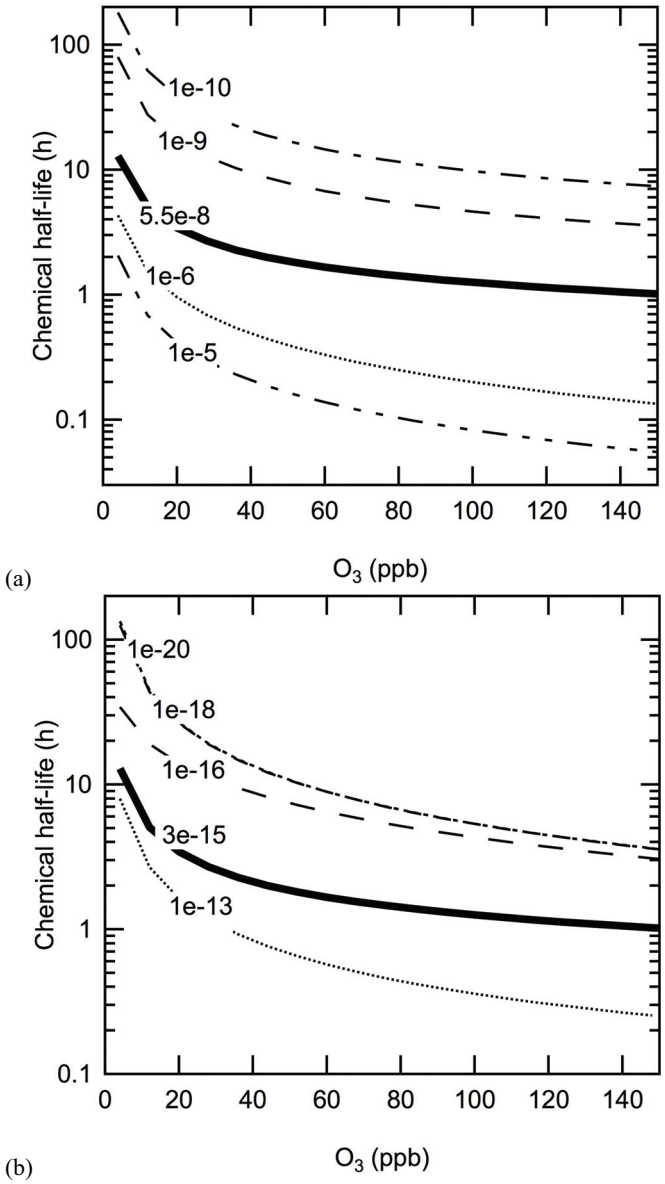

Fig. 8. Chemical half-life of oleic acid in the 12-component mixed aerosol matrix with a particle radius of 275 nm as a function of gas phase ozone mixing ratio. **(a)** With fixed $D_{b,Y,0}$ (3×10^{-15} cm^2 s^{-1}) and $D_{b,O_3,0}$ are varied between 10^{-10}–10^{-5} cm^2 s^{-1}. **(b)** With fixed $D_{b,O_3,0}$ (5.5×10^{-8} cm^2 s^{-1}) and $D_{b,Y,0}$ are varied between 10^{-20}–10^{-13} cm^2 s^{-1}.

The chemical lifetimes converge for diffusivities of the organic species (see Fig. 8b) above 10^{-18} cm^2 s^{-1} while they remain sensitive to the diffusivity of ozone (see Fig. 8a). The half lives span ca. three orders of magnitude for a given [O_3] depending on the diffusivity of the aerosol matrix. This underlines the importance of a detailed understanding of aerosol diffusivity to be able to establish lifetimes of reactive aerosol components in semi-solid matrices.

The importance of the phase state of aerosol particles (solid, semi-solid, or liquid) has been pointed out in previous studies (Knopf et al., 2005; Zahardis and Petrucci, 2007; Virtanen et al., 2010; Shiraiwa et al., 2011b). Recent kinetic model simulations showed that the atmospheric chemical lifetime of oleic acid in a liquid is only a few minutes, and it may increase to many hours if organic species are embedded in semi-solid aerosol matrices with low diffusivity (Shiraiwa et al., 2010). Our present study demonstrates that chemical reactions are hindered in amorphous semi-solid aerosol particles so that chemical half lives of many hours to a few days can be reached even for reactive unsaturated fatty acids in multi-component matrices (similar effects during protein ozonolysis have been described very recently by Shiraiwa et al., 2011b). The results of this study confirm that highly viscous semi-solid aerosol matrices with low diffusivity can effectively shield reactive organic compounds from degradation by atmospheric oxidants (Shiraiwa et al., 2010; George and Abbatt, 2010; Zobrist et al., 2011). Amorphous semi-solid or gel-like phases present in multi-component organic aerosol matrices thus require new formalisms for description of particle transformation.

5 Conclusions

Synthesising previous work in a detailed model analysis we demonstrate how variations in aerosol diffusivity can be described in multi-component semi-solid aerosol matrices. By extending the recently developed kinetic model (KM-SUB) for description of a 12-component mixture approximating atmospheric cooking aerosols we demonstrate how this model may be used to resolve flexibly surface and bulk processes in varying phases considering diffusivities altered by oligomerisation of reaction products.

We successfully resolve bulk diffusion and temporal change of diffusivity in a complex reactive multi-component aerosol matrix. We confirm that resistor-model formulations break down for the semi-solid aerosols and illustrate under which conditions changes in diffusivity play a key role for the fate of aged multi-component aerosol mixtures.

Atmospheric half lives for several components of a complex semi-solid aerosol matrix have been calculated for a wide range of [O_3] illustrating the impact of diffusivity and its evolution on the ageing of multi-component aerosols in atmospheric conditions. Impeded diffusivity in semi-solid matrices needs to be considered when estimating lifetimes for reactive species present in atmospheric aerosols.

Discrepancies between laboratory and field derived lifetimes of reactive aerosol components can be explained by trapping of the reactive species underneath a surface crust that limits diffusion into the aerosol core. We illustrate and quantify crust formation on the surface and in the near-surface bulk as well as its impact on the reactive loss of components of the semi-solid aerosol matrix. Slow diffusion in a

semi-solid aerosol matrix can explain the reduced bulk reactivity reported in Huff Hartz et al. (2007) without introducing an arbitrary change of chemical reaction rate coefficients.

While there is qualitative evidence for oligomer formation upon chemical ageing of atmospheric aerosols, further investigations are required to elucidate the importance of these processes both in the laboratory and in the atmosphere. Future studies should resolve the interactions and relative contributions of physical and chemical processes leading to changes in phase and diffusivity, i.e. the interplay of chemical reaction and transformation with changes in temperature and relative humidity.

Appendix A

List of symbols

Symbol	Meaning	Unit
α_{b,O_3}	Bulk accommodation coefficient of O_3	
α_{s,O_3}	Surface accommodation coefficient of O_3	
$\alpha_{s,0,O_3}$	Surface accommodation coefficient of O_3 on an adsorbate-free surface	
$\alpha_{s,0,O_3,Y_j}$	Surface accommodation coefficient of O_3 on an adsorbate-free surface composed of Y_j	
γ_{O_3}	Uptake coefficient of O_3 (normalized by gas kinetic flux of surface collisions)	
τ_{d,O_3}	Desorption lifetime of O_3	s
$\tau_{d,O_3,Yj}$	Desorption lifetime of O_3 on a surface composed of Y_j	s
ω_{O_3}	Mean thermal velocity of O_3 in the gas phase	$cm\,s^{-1}$
$D_{b,O_3,0}$, $D_{b,Y,0}$	Initial bulk diffusion coefficient of O_3 and Y	$cm^2\,s^{-1}$
$D_{b,O_3,0}(t)$, $D_{b,Y,0}(t)$	Time-dependent bulk diffusion coefficient of O_3 and Y	$cm^2\,s^{-1}$
$D_{s,O_3,0}(t)$, $D_{s,Y,0}(t)$	Time-dependent surface diffusion coefficient of O_3 and Y	$cm^2\,s^{-1}$
$f_{b,n}$	Extent of solidification in bulk layer n	
f_{ss}	Extent of solidification in the surface layer	
J_{b,rd,O_3}	Reacto-diffusive flux of 0_3 in the particle bulk	$cm^{-2}\,s^{-1}$
k_{BR,O_3,Y_j}	Second-order rate coefficients for bulk reactions of O_3 with Y_j	$cm^3\,s^{-1}$
k_{SLR,O_3,Y_q}	Second-order rate coefficients for surface layer reactions of O_3 with Y_q	$cm^2\,s^{-1}$
K_{sol,cc,O_3}	Gas-particle partitioning coefficient of O_3	
n	Number of bulk layers	
N_Y	Total number of Y molecules	
r_p	Particle radius	cm
$[Ole]_b$	Bulk phase number concentration of oleic acid	cm^{-3}
$[Ole]_{ss}$	Surface number concentration of oleic acid (quasi-static surface layer)	cm^{-2}
$[O_3]_b$	Bulk phase number concentration of O_3	cm^{-3}
$[O_3]_g$	Gas phase number concentration of O_3	cm^{-3}
$[O_3]_{gs}$	Near-surface gas phase number concentration of O_3	cm^{-3}
$[O_3]_s$	Surface number concentration of O_3 (sorption layer)	cm^{-2}
$[Pal]_{ss}$	Surface number concentration of palmitoleic acid (quasi-static surface layer)	cm^{-2}

Supplementary material related to this article is available online at: http://www.atmos-chem-phys.net/11/7343/2011/acp-11-7343-2011-supplement. Dateinamevonsupplement.

Acknowledgements. This work was supported by the Royal Society, NERC (grant no. NE/G000883/1), the European Integrated Project on Aerosol, Cloud, Climate and Air Quality Interactions (036833-2 EUCAARI), and the Pan-European Gas-Aerosols-Climate Interaction Study (PEGASOS). MS is supported by the Max Planck Graduate Center – Johannes Gutenberg University Mainz and the Ministry of Education, Culture, Sports, Science and Technology, Japan.

The service charges for this open access publication have been covered by the Max Planck Society.

Edited by: V.-M. Kerminen

References

Allan, J. D., Williams, P. I., Morgan, W. T., Martin, C. L., Flynn, M. J., Lee, J., Nemitz, E., Phillips, G. J., Gallagher, M. W., and Coe, H.: Contributions from transport, solid fuel burning and cooking to primary organic aerosols in two UK cities, Atmos. Chem. Phys., 10, 647–668, doi:10.5194/acp-10-647-2010, 2010.

Ammann, M. and Pöschl, U.: Kinetic model framework for aerosol and cloud surface chemistry and gas-particle interactions - Part 2: Exemplary practical applications and numerical simulations, Atmos. Chem. Phys., 7, 6025–6045, doi:10.5194/acp-7-6025-2007, 2007.

Andreae, M. O. and Rosenfeld, D.: Aerosol-cloud-precipitation interactions. Part 1. The nature and sources of cloud-active aerosols, Earth-Sci. Rev., 89, 13–41, 2008.

Bird, R. B., Stewart, W. E., and Lightfoot, E. N.: Transport Phenomena (2nd Ed.) (John Wiley & Sons, Inc., New York), 2007.

Enami, S., Hoffmann, M. R., and Colussi, A. J.: Acidity enhances the formation of a persistent ozonide at aqueous ascorbate/ozone gas interfaces, P. Natl. Acad. Sci. USA, 105, 7365–7369, 2008.

Fuzzi, S., Andreae, M. O., Huebert, B. J., Kulmala, M., Bond, T. C., Boy, M., Doherty, S. J., Guenther, A., Kanakidou, M., Kawamura, K., Kerminen, V.-M., Lohmann, U., Russell, L. M., and Pöschl, U.: Critical assessment of the current state of scientific knowledge, terminology, and research needs concerning the role of organic aerosols in the atmosphere, climate, and global change, Atmos. Chem. Phys., 6, 2017–2038, doi:10.5194/acp-6-2017-2006, 2006.

George, I. J. and Abbatt, J. P. D.: Heterogeneous oxidation of atmospheric aerosol particles by gas-phase radicals, Nature Chem., 2, 713–722, 2010.

Gonzalez-Labrada, E., Schmidt, R., and DeWolf, C. E.: Kinetic analysis of the ozone processing of an unsaturated organic monolayer as a model of an aerosol surface, Phys. Chem. Chem. Phys., 9, 5814–5821, 2007.

Hallquist, M., Wenger, J. C., Baltensperger, U., Rudich, Y., Simpson, D., Claeys, M., Dommen, J., Donahue, N. M., George, C., Goldstein, A. H., Hamilton, J. F., Herrmann, H., Hoffmann, T., Iinuma, Y., Jang, M., Jenkin, M. E., Jimenez, J. L., Kiendler-Scharr, A., Maenhaut, W., McFiggans, G., Mentel, Th. F., Monod, A., Prévôt, A. S. H., Seinfeld, J. H., Surratt, J. D., Szmigielski, R., and Wildt, J.: The formation, properties and impact of secondary organic aerosol: current and emerging issues, Atmos. Chem. Phys., 9, 5155–5236, doi:10.5194/acp-9-5155-2009, 2009.

Huff Hartz, K. E. H., Weitkamp, E. A., Sage, A. M., Donahue, N. M., and Robinson, A. L.: Laboratory measurements of the oxidation kinetics of organic aerosol mixtures using a relative

rate constants approach, J. Geophys. Res.-Atmos., 112, D04204, doi:10.1029/2006jd007526, 2007.

Huthwelker, T., Ammann, M., and Peter, T.: The uptake of acidic gases on ice, Chem. Rev., 106, 1375–1444, 2006.

Johnson, P. N. and Davis, R. A.: Diffusivity of Ozone in Water, J. Chem. Eng. Data, 41, 1485–1487, 1996.

Kalberer, M., Paulsen, D., Sax, M., Steinbacher, M., Dommen, J., Prévôt, A. S. H., Fisseha, R., Weingartner, E., Frankevich, V., Zenobi, R. and Baltensperger, U.: Identification of polymers as major components of atmospheric organic aerosols, Science, 303, 1659–1662, 2004.

King, M. D., Canosa-Mas, C. E., and Wayne, R. P.: Frontier molecular orbital correlations for predicting rate constants between alkenes and the tropospheric oxidants NO_3, OH and O_3, Phys. Chem. Chem. Phys., 1, 2231–2238, 1999.

King, M. D., Thompson, K. C., Ward, A. D., Pfrang, C., and Hughes, B. R.: Oxidation of biogenic and water-soluble compounds in aqueous and organic aerosol droplets by ozone: a kinetic and product analysis approach using laser Raman tweezers, Faraday Discuss., 137, 173–192, 2008.

King, M. D., Rennie, A. R., Thompson, K. C., Fisher, F. N., Dong, C. C., Thomas, R. K., Pfrang, C., and Hughes, A. V.: Oxidation of oleic acid at the air-water interface and its potential effects on cloud critical supersaturations, Phys. Chem. Chem. Phys., 11, 7699–7707, 2009.

King, M. D., Rennie, A. R., Pfrang, C., Hughes, A. V., Thomas, R. K., Dong, C. C., and Thompson, K. C.: Interaction of nitrogen oxide with a monolayer of oleic acid at the air-water interface: a simple proxy for atmospheric aerosol, Atmos. Environ., 44, 1822–1825, 2010.

Knopf, D. A., Anthony, L. M., and Bertram, A. K.: Reactive uptake of O_3 by multicomponent and multiphase mixtures containing oleic acid, J. Phys. Chem. A, 109, 5579–5589, 2005.

Last, D. J., Nájera, J. J., Wamsley, R., Hilton, G., McGillen, M., Percival, C. J., and Horn, A. B.: Ozonolysis of organic compounds and mixtures in solution. Part I: Oleic, maleic, nonanoic and benzoic acids, Phys. Chem. Chem. Phys., 11, 1427–1440, 2009.

Lee, A. K. Y. and Chan, C. K.: Single particle Raman spectroscopy for investigating atmospheric heterogeneous reactions of organic aerosols, Atmos. Environ., 41, 4611–4621, 2007.

Marcolli, C., Luo, B. P., and Peter, T.: Mixing of the organic aerosol fractions: Liquids as the thermodynamically stable phases, J. Phys. Chem. A, 108, 2216–2224, 2004.

Martin, S. T.: Phase transitions of aqueous atmospheric particles, Chem. Rev., 100, 3403-3453, 2000.

McGillen, M. R., Archibald, A. T., Carey, T., Leather, K. E., Shallcross, D. E., Wenger, J. C., and Percival, C. J.: Structure-activity relationship (SAR) for the prediction of gas-phase ozonolysis rate coefficients: an extension towards heteroatomic unsaturated species, Phys. Chem. Chem. Phys., 13, 2842–2849, 2011.

Mikhailov, E., Vlasenko, S., Martin, S. T., Koop, T., and Pöschl, U.: Amorphous and crystalline aerosol particles interacting with water vapor: conceptual framework and experimental evidence for restructuring, phase transitions and kinetic limitations, Atmos. Chem. Phys., 9, 9491–9522, doi:10.5194/acp-9-9491-2009, 2009.

Moise, T. and Rudich, Y.: Reactive uptake of ozone by aerosol-associated unsaturated fatty acids: Kinetics, mechanism, and products, J. Phys. Chem. A, 106, 6469–6476, 2002.

Murray, B. J.: Inhibition of ice crystallisation in highly viscous aqueous organic acid droplets, Atmos. Chem. Phys., 8, 5423–5433, doi:10.5194/acp-8-5423-2008, 2008.

Nash, D. G., Tolocka, M. P., and Baer, T.: The uptake of O_3 by myristic acid – oleic acid mixed particles: Evidence for solid surface layers, Phys. Chem. Chem. Phys., 8, 4468–4475, 2006.

Parker, R. and Ring, S. G.: Diffusion in maltose-water mixtures at temperatures close to the glass-transition, Carbohyd. Res., 273, 147–155, 1995.

Pfrang, C., King, M. D., Canosa-Mas, C. E., and Wayne, R. P.: Correlations for gas-phase reactions of NO_3, OH and O_3 with alkenes: an update, Atmos. Environ., 40, 1170–1179, 2006.

Pfrang, C., King, M. D., Canosa-Mas, C. E., Flugge, M., and Wayne, R. P.: Gas-phase rate coefficients for the reactions of NO_3, OH and O_3 with α, β-unsaturated esters and ketones: structure-activity relations (SARs), Atmos. Environ., 41, 1792–1802, 2007.

Pfrang, C., King, M. D., Braeckevelt, M., Canosa-Mas, C. E., and Wayne, R. P., Gas-phase rate coefficients for reactions of NO_3, OH, O_3 and $O(^3P)$ with unsaturated alcohols and ethers: Correlations and structure-activity relations (SARs), Atmos. Environ., 42, 3018–3034, 2008.

Pfrang, C., Shiraiwa, M., and Pöschl, U.: Coupling aerosol surface and bulk chemistry with a kinetic double layer model (K2-SUB): oxidation of oleic acid by ozone, Atmos. Chem. Phys., 10, 4537–4557, doi:10.5194/acp-10-4537-2010, 2010.

Pfrang, C. et al.: Kinetics and mechanism of the reaction of ozone with a monolayer of d-methyl oleate at the air-water interface studied by fast neutron reflectometry, in preparation, 2011.

Pöschl, U.: Atmospheric aerosols: Composition, transformation, climate and health effects, Angew. Chem. Int. Edit., 44, 7520–7540, 2005.

Pöschl, U., Rudich, Y., and Ammann, M.: Kinetic model framework for aerosol and cloud surface chemistry and gas-particle interactions Part 1: General equations, parameters, and terminology, Atmos. Chem. Phys., 7, 5989–6023, doi:10.5194/acp-7-5989-2007, 2007.

Rudich, Y.: Laboratory perspectives on the chemical transformations of organic matter in atmospheric particles, Chem. Rev., 103, 5097–5124, 2003.

Rudich, Y., Donahue, N. M., and Mentel, T. F.: Aging of organic aerosol: Bridging the gap between laboratory and field studies, Annu. Rev. Phys. Chem., 58, 321–352, 2007.

Seinfeld, J. H. and Pankow, J. F.: Organic atmospheric particulate material, Annu. Rev. Phys. Chem., 54, 121–140, 2003.

Shiraiwa, M., Garland, R. M., and Pöschl, U.: Kinetic double-layer model of aerosol surface chemistry and gas-particle interactions (K2-SURF): Degradation of polycyclic aromatic hydrocarbons exposed to O_3, NO_2, H_2O, OH and NO_3, Atmos. Chem. Phys., 9, 9571–9586, doi:10.5194/acp-9-9571-2009, 2009.

Shiraiwa, M., Pfrang, C., and Pöschl, U.: Kinetic multi-layer model of aerosol surface and bulk chemistry (KM-SUB): the influence of interfacial transport and bulk diffusion on the oxidation of oleic acid by ozone, Atmos. Chem. Phys., 10, 3673–3691, doi:10.5194/acp-10-3673-2010, 2010.

Shiraiwa, M., Sosedova, Y., Rouviere, A., Yang, H., Zhang, Y., Abbatt, J. P. D., Ammann, M., and Pöschl, U.: Long-lived reactive oxygen intermediates controlling the reaction

of ozone with aerosol particles, Nature Chem., 3, 291–295, doi:10.1038/nchem.988, 2011a.

Shiraiwa, M., Ammann, M., Koop, T., and Pöschl, U.: Gas uptake and chemical aging of semi-solid organic aerosol particles, P. Natl. Acad. Sci. USA, 108(27), 11003–11008, 2011b.

Stroeve, P.: On the Diffusion of Gases in Protein Solutions, Ind. Eng. Chem. Fund., 14, 140-141, 1975.

Thompson, K., Rennie, A., King, M., Hardman, S., Lucas, C., Pfrang, C., Hughes, B., and Hughes, A.: Reaction of a phospholipid monolayer with gas-phase ozone at the air-water interface: measurement of surface excess and surface pressure in real time, Langmuir, 26, 17295–17303, 2010.

Tong, H.-J., Reid, J. P., Bones, D. L., Luo, B. P., and Krieger, U. K.: Measurements of the timescales for the mass transfer of water in glassy aerosol at low relative humidity and ambient temperature, Atmos. Chem. Phys., 11, 4739–4754, doi:10.5194/acp-11-4739-2011, 2011.

Vaden, T. D., Imre, D., Beránek, J., Shrivastava, M., and Zelenyuk, A.: Evaporation kinetics and phase of laboratory and ambient secondary organic aerosol, P. Natl. Acad. Sci. USA, 108, 2190–2195, 2011.

Vesna, O., Sax, M., Kalberer, M., Gaschen, A., and Ammann, M.: Product study of oleic acid ozonolysis as function of humidity, Atmos. Environ., 43, 3662–3669, 2009.

Virtanen, A., Joutsensaari, J., Koop, T., Kannosto, J., Yli-Pirilä, P., Leskinen, J., Mäkelä, J. M., Holopainen, J. K., Pöschl, U., Kulmala, M., Worsnop, D. R., and Laaksonen, A.: An amorphous solid state of biogenic secondary organic aerosol particles, Nature, 467, 824–827, 2010.

Wayne, R. P.: Chemistry of Atmospheres, third ed., Oxford University Press, Oxford, 2000.

Xiao, S. and Bertram, A. K.: Reactive uptake kinetics of NO_3 on multicomponent and multiphase organic mixtures containing unsaturated and saturated organics, Phys. Chem. Chem. Phys., 13, 6628–6636, doi:10.1039/c0cp02682d, 2011.

Zahardis, J. and Petrucci, G. A.: The oleic acid-ozone heterogeneous reaction system: products, kinetics, secondary chemistry, and atmospheric implications of a model system a review, Atmos. Chem. Phys., 7, 1237–1274, doi:10.5194/acp-7-1237-2007, 2007.

Zahardis, J., Geddes, S., and Petrucci, G. A.: The ozonolysis of primary aliphatic amines in fine particles, Atmos. Chem. Phys., 8, 1181–1194, doi:10.5194/acp-8-1181-2008, 2008.

Ziemann, P. J.: Aerosol products, mechanisms, and kinetics of heterogeneous reactions of ozone with oleic acid in pure and mixed particles, Faraday Discuss., 130, 469–490, 2005.

Zobrist, B., Marcolli, C., Pedernera, D. A., and Koop, T.: Do atmospheric aerosols form glasses?, Atmos. Chem. Phys., 8, 5221–5244, doi:10.5194/acp-8-5221-2008, 2008.

Zobrist, B., Soonsin, V., Luo, B. P., Krieger, U. K., Marcolli, C., Peter, T., and Koop, T.: Ultra-slow water diffusion in aqueous sucrose glasses, Phys. Chem. Chem. Phys., 13, 3514–3526, 2011.

6 Supplementary Material

Supplement S1: Sensitivity studies

Figure S1 illustrates the concentration profiles for ozone and oleic acid when assuming constant diffusivity in the semi-solid 12-component aerosol matrix. The differences to the diffusivity-evolution model variant (see Fig. 5) are subtle, but accumulate to considerable differences in the total loss in particular at long reaction times.

The sensitivity of our best-fit scenario (see solid lines in Fig. 1) are tested towards a wide range of input parameters. Fig. S2 illustrates the impact of a 10-fold change of the surface rate coefficients and Fig. S3 shows the impact of a 10-fold change of the bulk reactivity. The surface reactivity has only a small impact on the total number of molecules lost (partly caused by the surface to volume ratio of a 275nm-radius particle). The faster the surface reaction the slower is the loss of the reactive component: this suggests that the loss is not limited by surface reactivity, but by transport to the aerosol bulk. Surface rate coefficients are constrained by experimental data (Pfrang et al., 2011) for ozonolysis of a monolayer of the oleic acid methyl ester, methyl oleate. This new experimental evidence demonstrates considerably higher reactivity at the surface than assumed previously (e.g. Pfrang et al., 2010) based on earlier experimental work. The bulk rate coefficients affect the loss of reactive species significantly. Please note that the coefficients used for the best-fit scenario are constrained by experimental data from Huff Hartz et al. (2007).

We also tested the sensitivity of our modelling approach on the method used to describe the evolution of diffusivity. Throughout the paper we follow the obstruction theory approach (Stroeve, 1975). In Fig. S4 we present an alternative approach using a linear combination expression for the time-dependent diffusion coefficients assuming a product diffusivity of ¼ of the initial value (based on a M^2 dependence for dimer formation; compare Bird et al., 2007). There is a measurable, but not substantial difference between the two approaches (compare Figs. 4 and S4) and we thus used the obstruction theory approach which has been applied in the past (Stroeve, 1975).

The robustness of the model to the thickness of the layers representing the 275nm-radius aerosol particle is illustrated in Fig. S5. The results converge from ca. 100 layers with the chosen 250 layers being both physically meaningful and computationally affordable.

References

Bird, R. B., Stewart, W. E., & Lightfoot, E. N.: *Transport Phenomena (2nd Ed.)* (John Wiley & Sons, Inc., New York), 2007.

Huff Hartz, K. E. H., Weitkamp, E. A., Sage, A. M., Donahue, N. M. and Robinson, A. L.: Laboratory measurements of the oxidation kinetics of organic aerosol mixtures using a relative rate constants approach, J. Geophys. Res.-Atmos., 112, D04204, 10.1029/2006jd007526, 2007.

Pfrang, C., Shiraiwa, M. and Pöschl, U.: Coupling aerosol surface and bulk chemistry with a kinetic double layer model (K2–SUB): an exemplary study of the oxidation of oleic acid by ozone, Atmos. Chem. Phys., 10, 4357-4557, 2010.

Pfrang, C. et al.: Kinetics and mechanism of the reaction of ozone with a monolayer of *d*-methyl oleate at the air-water interface studied by fast neutron reflectometry, in preparation, 2011.

Stroeve, P.: On the Diffusion of Gases in Protein Solutions, Industrial & Engineering Chemistry Fundamentals, 14, 140-141, 10.1021/i160054a017, 1975.

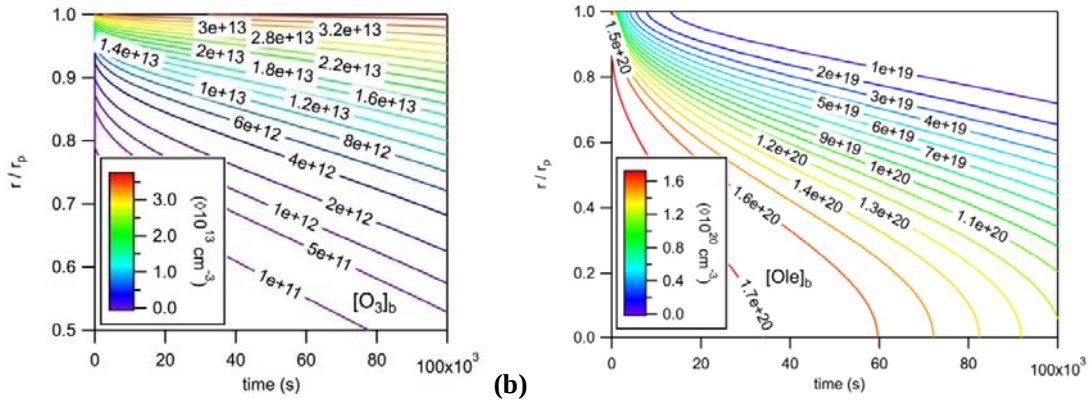

Figure S1 Concentration profiles of ozone ((a)) and oleic acid ((b)) when assuming constant-diffusivity of the semi-solid aerosol matrix. Equivalent profiles for the diffusivity-evolution model variant are displayed in Fig. 5 (a) and (b).

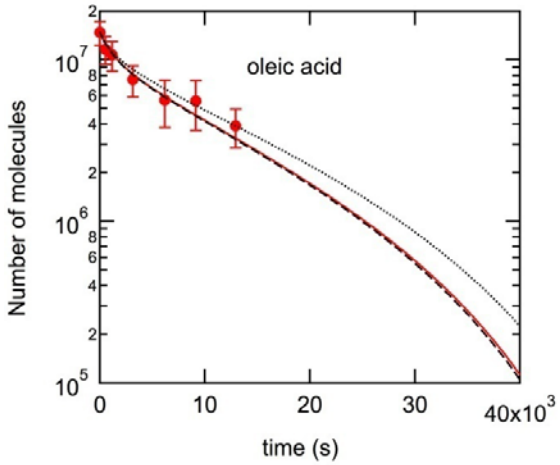

Figure S2 Decays of numbers of molecules of oleic acid in a 12-component aerosol matrix as a function of time. Symbols correspond to experimental data (Huff Hartz et al., 2007). Surface rate coefficients are set to be 10-fold higher (dotted line) and 10-fold lower (dashed line) than in our best-fit scenario (red solid line).

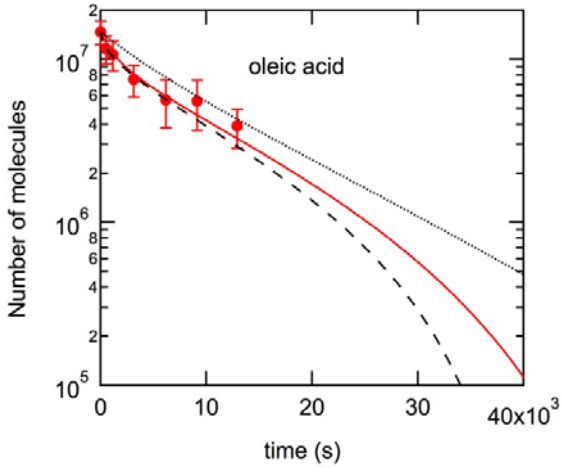

Figure S3 Decays of numbers of molecules of oleic acid in a 12-component semi-solid aerosol matrix as a function of time. Symbols correspond to experimental data (Huff Hartz et al., 2007). Bulk rate coefficients are set to be 10-fold higher (dashed line) and 10-fold lower (dotted line) than in our best-fit scenario (red solid line).

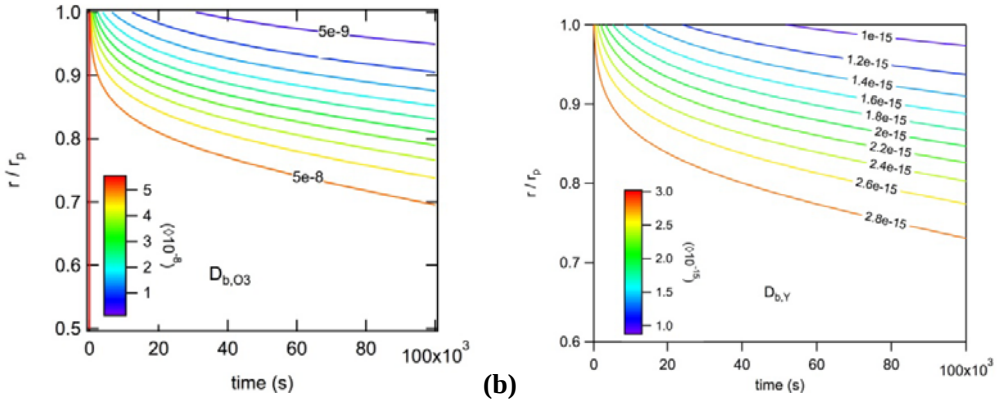

Figure S4 Bulk diffusion coefficients of (a) ozone and (b) oleic acid as a function of time and depth in the 275nm-radius particle. The diffusivity evolution is represented here by a linear combination assuming a final diffusion coefficient at ¼ of the initial coefficient. Fig. 4 shows the equivalent plots with the diffusivity expressed by obstruction theory (Stroeve, 1975).

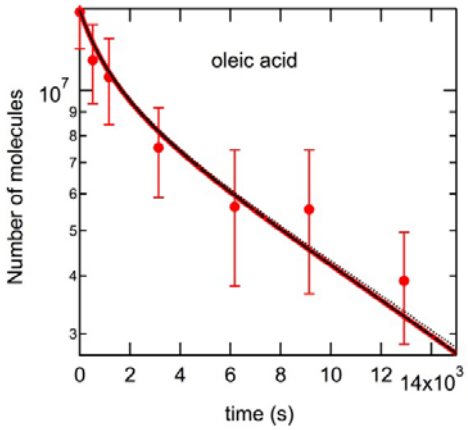

Figure S5 Decays of numbers of molecules of oleic acid in a 12-component aerosol matrix as a function of time. Symbols correspond to experimental data (Huff Hartz et al., 2007). Numbers of layers representing the aerosol particle in the model are varied (n = 50-275; black lines; the dotted line slightly above the other lines is for n = 50). The bold red line corresponds to the model representation used for all other runs (see also solid line in Fig. 1 (a)) with n = 250.

B7) Shiraiwa et al., to be submitted

Reaction kinetics and mechanism of the nitration of aerosolized protein by O_3 and NO_2

Manabu Shiraiwa[1], Kathrin Selzle[1], Hong Yang[1], Yulia Sosedova[2], Markus Ammann[2], and Ulrich Pöschl[1]

1. Max Planck Institute for Chemistry, Department of Biogeochemistry, J. J. Becherweg 27/29, 55128 Mainz, Germany
2. Paul Scherrer Institute, Laboratory for Radio and Environmental Chemistry, 5232 Villigen PSI, Switzerland

to be submitted

Authors contributions.

MS, MA and UP designed research. MS conducted experiments with help of MA and YS. KS and HY conducted protein analysis. MS wrote the paper.

Abstract.

Protein is nitrated by O_3 and NO_2 in polluted air. The protein nitration can enhance allergic responses, which may contribute to an increased prevalence of allergic diseases in modern societies. The heterogeneous reaction kinetics and mechanism of the nitration of aerosolized protein (bovine serum albumin) exposed to O_3 and NO_2 at atmospherically relevant concentration was investigated in an aerosol flow tube. The experiments were performed using the short-lived radioactive tracer ^{13}N and a denuder technique. In the absence of O_3, NO_2 uptake by protein particles was below detection limit ($\gamma_{NO2} < \sim 10^{-6}$). In the presence of O_3, however, the γ_{NO2} were of the order of 10^{-5} and enhance up to $\sim 1 \times 10^{-4}$ with the increase of the O_3 concentration. The additional experiments and kinetic modeling confirm the formation of long-lived reactive oxygen intermediates (ROIs) upon ozone exposure, which are reactive towards NO_2. The products analysis of protein exposed to ozone suggests phenoxy radical derivatives of amino acid tyrosine as chemical identity of ROI.

1. Introduction

Airborne particulates and gaseous pollution are important environmental issues because they affect human health. Asthma and allergy are major health problems in most modern societies and numerous studies indicate that allergic diseases have been increasing during the past decades (Krämer et al., 1999; 2000). Immune responses can be affected by air pollutants including atmospheric particles, semi-volatile hydrocarbons and exhaust gases, which drive proallergic inflammation through the generation of oxidative stress (Saxon and Diaz-Sanchez, 2005). Traffic-related air pollution such as ozone and nitrogen dioxide and particulate matter less than 10 or 2.5 μm in size appears to link allergic diseases and childhood respiratory health (Miguel et al., 1999; Brunekreef and Sunyer, 2003; Janssen et al., 2003). However, the effects of air pollution on the occurrence of allergic diseases are not yet well-understood (Ring et al., 2001).

Proteins contained in biogenic aerosol particles account for up to 5% of urban air particulate matter (Fröhlich-Nowoisky et al., 2009; Huffman et al., 2009). They are not only contained in coarse biological particles (e.g., pollen, spores) but also in the fine fraction of air particulate matter (Schäppi et al., 1997; Jaenicke, 2005). Several studies have shown that ozone can also promote the nitration of protein molecules contained in primary biological aerosol particles (Franze et al., 2005; Shiraiwa et al., 2011b). Nitration of protein leads to the formation

of 3-nitrotyrosine residues, which is a posttranslational modification (Yang et al., 2010; Zhang et al., 2010). Indeed, nitrated proteins were detected in dust samples from various urban environments (Franze et al., 2005). Inhalation and deposition of these nitrated proteins in the human respiratory tract may lead to the adverse health effects. Accumulating data suggest a strong link between protein 3-nitrotyrosine and the mechanism involved in disease development (Souza et al., 2008). This posttranslational modification provides a molecular rationale for the enhancement of allergic diseases by traffic-related air pollution in urban and rural environments, which has been observed in epidemiological studies but remains to be elucidated on a molecular level (Franze et al., 2005; Gruijthuijsen et al., 2006; Traidl-Hoffmann et al., 2009).

The purpose of this study is to investigate the kinetics and reaction mechanism of nitration of aerosolized protein. The uptake experiments of nitrogen dioxide by protein particles were conducted at atmospherically relevant concentration of nitrogen dioxide, ozone, and water vapor. Bovine serum albumin (BSA) is chosen as a well-defined model substance for proteins, which is a globular protein with a molecular mass of 67 kDa and 21 tyrosine residues per molecule. The experiments were also done using deliquesced sodium chloride (NaCl) particles as reference.

2. Experimental method

2.1. NO_2 uptake experiments

The experiments were performed using the short-lived radioactive tracer ^{13}N and an aerosol flow tube technique at the Paul Scherrer Institute, Switzerland. The radioactive half-life of ^{13}N is ~10 min. The use of the ^{13}N enables us to perform experiments at low concentrations because of its high radioactivity to concentration ratio (Ammann, 2001). Fig. 1 shows the schematics of the experimental setup. It consists of the production system of O_3 and labeled $^{13}NO_2$, an aerosol generation system, a flow tube reactor, and a detection system. The detail of the experimental setup is described in Shiraiwa et al. (2011b).

^{13}NO were produced through the $^{16}O(p,\alpha)^{13}N$ nuclear reaction with 11 MeV protons in a gas target (20% O_2 in He) in continuous mode at Paul Scherrer Institute (Ammann, 2001). They were converted to NO_2 by heterogeneous oxidation over firebrick granules impregnated with CrO_3 (Levaggi et al., 1972; Ammann, 2001). O_3 was generated by passing O_2/N_2 air through a

quartz tube irradiated by a Xe excimer lamp. The gas flow was passed through a sand-blasted glass tube coated with sodium carbonate to remove HONO upstream of the flow tube reactor.

Aerosols were generated by nebulizing an aqueous solution of the investigated pure substance at a concentration of 0.2 – 0.5 g L^{-1}. The solutions were prepared by dissolving the appropriate amounts of bovine serum albumin (BSA, fraction V, >96%, Sigma) and sodium chloride in 100 mL of deionised water (18.2 MΩ cm, Milli Q plus 185, Millipore). The generated particles are dried by a diffusion dryer filled with silica gel. The dried particles are introduced into an ^{85}Kr source to attain an equilibrium charge distribution and then passed through an electrostatic precipitator so that only uncharged particles were used for the experiments to avoid uncontrolled loss of charged particles at the wall. Then the flow was conditioned to the relative humidity of 50 - 75%. For NaCl particles, the flow was humidified to 75% to achieve complete deliquescence.

The aerosol surface concentration was measured downstream of the flow tube reactor by diverting part of the flow to a scanning mobility particle sizer. The same relative humidity was maintained both in the DMA sheath flow and in the flow tube reactor by using filtered carrier gas from the flow tube as the DMA sheath flow, so that the particle size is not affected by relative humidity. The diameter range was 15 – 740 nm, and the observed size distribution was mono-modal and lognormal. The observed surface distribution was fitted by a single lognormal distribution to estimate the whole distribution and surface area. A typical mode diameter of the surface area density distribution was ~350 nm, and the surface concentration was in the range of $10^{-4} – 10^{-3}$ cm^2 cm^{-3}.

The gas and aerosol flows were mixed prior to the inlet of a cylindrical 7.1 cm inner diameter and 190 cm long PFA flow tube. PFA is used to minimize the loss of NO_2 on the wall. The flow was 800 – 900 cm^3 s^{-1} in the reactor and the maximum residence time was ~10 min. The gas-aerosol contact time could be adjusted between 3 – 10 min depending on the position of the inlet. At the tube exit, the flow was recollected by an identical Teflon plug. The pressure of the flow reactor was kept constant 970 – 980 hPa and the temperature was kept at 296 K by an efficient air conditioning system.

After passing through the flow tube, the gas and aerosol flow entered a narrow parallel-plate diffusion denuder train coated to selectively absorb gas phase HONO and NO_2, followed by a particle filter collecting the particles (Ammann, 2001). The gas passes through the denuder in

laminar flow. The first and second sections of the denuder were coated with a sulphanilamide which trapped HONO. Some amount of NO_2 was also absorbed or temporarily retained in the SA coating. To take this interference by NO_2 into account, we repeated the SA coating in the second section. The third section was prepared to trap NO_2, coated with N-(1-naphtyl) ethylenediamine dihydrochloride (NDA, Fluka, >99%). We repeated the NDA coating in the fourth section to make sure that all gas phase NO_2 remained trapped in the denuder train and to detect eventual breakthrough. The aerosol particles have a small diffusivity and pass through the denuder with close to 100% efficiency (Ammann, 2001; Stemmler et al., 2007) and were retained in the glass fiber filter.

The gamma-radiation detectors were attached to each denuder section and to the filters to detect the amount of emitted gamma quanta in the decay of ^{13}N, which corresponds to the amount of trapped ^{13}N molecules of a given species. Note that for the particle signal only strongly (chemically) absorbed ^{13}N species are detected, while physically adsorbed species desorbing within 30 ms and less contribute to the gas phase signal of the corresponding denuder plate, species desorbing within up to a second are trapped within the whole denuder train, and species desorbing within a few minutes are lost by desorption from the filter before they are detected by the γ detector there (Kalberer et al., 1999).

2.2. Ozone uptake experiments

Ozone uptake experiments on bulk BSA were conducted with a sand-blasted cylindrical coated wall flow tube reactor (surface = 120 cm^2, surface to volume ratio = 5 cm^{-1}) (Shiraiwa et al., 2011a). The tube was coated with bovine serum albumin (BSA) dissolved into water (18.2 MΩ cm, Milli Q plus 185, Millipore) and dried gently with nitrogen flow. Consequently 2 – 4 mg of BSA was deposited on the tube, which corresponds to a film thickness of BSA of 130 – 350 nm, if assumed to be evenly spread. O_3 was introduced into the flow reactor with synthetic air as carrier gas with a total flow rate of ~1 l min^{-1}. The experiments were conducted at atmospheric pressure and room temperature (296 K) and 50(±5) % of relative humidity. The gas phase ozone concentration was monitored using a photometric ozone analyzer. The uptake coefficients were calculated using the Cooney-Kim-Davis method to concomitantly take into account radial gas-phase diffusion and first-order loss at the wall (Cooney et al., 1974; Murphy and Fahey, 1987; Ammann et al., 2005).

The ozone uptake experiments were also conducted on pure tyrosine coatings to judge whether tyrosine is responsible for the reactivity of proteins towards O_3. As tyrosine is not water soluble, the tyrosine solutions were prepared by dissolving 0.05 g of tyrosine (BSA, fraction V, >96%, Sigma) in 10 mL of 1M HCl. The coated wall flow tube was coated with 0.5 ml of this solution and dried gently under a flow of nitrogen. Accordingly, 2.1 mg of tyrosine are deposited on the tube, which corresponds to a film thickness of 120 nm.

Protein samples were extracted from the tube using MiliQ water for products analysis. The extracted samples were dried using a freeze dryer. The intact protein samples were analyzed with a HPLC-chip MS/MS system consisting of a nano pump (G2226A, Agilent) with 4-channel micro-vacuum degasser (G1379B, Agilent), a microfluidic chip cube (G4240-64000, Agilent) interfaced to a Q-TOF mass spectrometer (6520, Agilent; nominal mass resolution 20000 at a scan rate of 5 s^{-1}), a capillary pump (G1376A, Agilent) with degasser (G1379B, Agilent), and an autosampler with thermostat (G1377A, Agilent). All modules were controlled by Mass Hunter software (version B.02.00, Agilent. A microfluidic reversed phase HPLC chip (Zorbax 300SB-C8, 5µm particle size, 75µm i.d., and 75 mm length) was used for protein separation. For each chromatographic run, the solvent gradient started with 97% water with formic acid (HCOOH volume fraction 0.1%, Chromasolv, Sigma, Seelze, Germany) and 3% acetonitrile at 400 nL min^{-1} (3min). Then the acetonitrile (Chromasolv, Sigma, Seelze, Germany) content was increased to 50% within 11 min and then to 70% within 1 min. Finally, the mobile phase was reset to initial conditions within 0.1 min, and the chip was equilibrated for 2 min before the next run. The ESI-Q-TOF instrument was operated in the positive ionization mode (ESI+) with an ionization voltage of 1750 V and a fragmentor voltage of 175 V at 300 °C. The MS mode was used and the selected m/z ranges were 200 to 3000 Da. The acquisition rate was 1.02 spectra s^{-1}. Reference correction of detected ions was enabled during the whole analysis. Protein identification and deconvolution was performed with Agilent MassHunter Bioconfirm Software (version B.03) using Large Molecular Feature Extraction (MFE).

3. Results and discussion

3.1. Uptake of NO_2 under absence of O_3

Protein (BSA) and deliquesced NaCl particles were exposed to NO_2 (6, 30 ppb) under humid condition (25, 60% RH). Figure 2(a) shows the experimental profile when BSA particles

were exposed to 30 ppb NO_2 at 60% RH. The signal from particle filter did not show any enhancement in the investigated range of NO_2 concentration and relative humidity. The estimated upper limit of uptake coefficient of NO_2 (γ_{NO2}) for BSA particles is $\sim 1\times10^{-6}$. This indicates NO_2 itself cannot nitrate protein efficiently, consistent with a previous study (Franze et al., 2005).

NO_2 uptake was also not observed on deliquesced NaCl particles with an estimated upper limit of γ_{NO2} of $\sim 1\times10^{-7}$. Abbatt and Waschewsky (1998) reported an upper limit of γ_{NO2} by liquid NaCl aerosol of $\sim 1\times10^{-4}$. Our results are consistent with their results and give better estimates. This is in line with some earlier studies indicating that the bulk aqueous phase reaction of NO_2 with chloride to form NOCl and nitrate is very slow (Cape et al., 1993; Behnke et al., 1997; Karlsson and Ljungstrom, 1998). It however also contrasts with other experiments, though performed at significantly higher concentrations of NO_2, where uptake coefficients of up to 10^{-4} have been reported (Harrison and Collins, 1998; Yabushita et al., 2009). Yabushita et al. (2009) propose a surface complex $NO_2{*}Cl^-$ to play a significant role at millimolar chloride concentration, i.e., for more dilute solutions than the deliquesced particles of the present study.

3.2. Uptake of NO_2 in presence of O_3

The initial gas phase concentrations of NO_2 and O_3 were in the range of 5 – 110 ppb and 0 – 160 ppb, respectively. For most of the experiments a relative humidity (RH) of 60 ± 5% was chosen unless mentioned otherwise. Kinetic experiments usually involved measurements of NO_2 uptake at five different contact times in the range 2 – 10 min (40 – 100 cm injector displacements).

Typical experimental profiles are shown in Figure 2(b) with mixing ratios of NO_2 and O_3 of 10 ppb and 120 ppb, respectively, at 25% RH. The NDA denuder signal represents gas phase NO_2 (red line), and the signal from the particle filter represents NO_2 on the particles (green line). The black line with markers gives the surface area of particles measured by the SMPS. In absence of aerosol (surface area ≈ 0, nebulizer was switched off), only a NDA signal is observed and the particle filter signal remained at the detection limit. When the nebulizer was switched on to generate aerosols, the surface area increased, along with the enhancement of a ^{13}N signal on the particle filter, which is by factor of ~20 smaller than the gas phase $^{13}NO_2$ signal. This indicates that a small fraction of labeled $^{13}NO_2$ molecules had been taken up by the particles. The

signal from the particle filter decreased for shorter reaction times, whereas the gas phase $^{13}NO_2$ signal remained almost unchanged. The HONO signal did not show an increase at any O_3 and NO_2 concentration, indicating that HONO was not produced by this reaction system in detectable amounts ($\gamma_{HONO} < 10^{-6}$).

The uptake coefficient of NO_2 (γ_{NO2}) is defined by the following equation:

$$\frac{d[NO_2]_g}{dt} = -\gamma_{NO_2} \frac{\omega_{NO_2}}{4} [NO_2]_g S \quad (1)$$

where ω_{NO2} is the mean thermal velocity (3.69×10^4 cm s^{-1} at 296 K, 1013 hPa) of NO_2 molecules and S is the aerosol surface concentration (cm^2 cm^{-3}). Eq (1) results in:

$$\gamma_{NO_2} t = -\frac{4}{\omega_{NO_2} S} \ln\left(\frac{[^{13}NO_2]_{g,t}}{[^{13}NO_2]_{g,0}}\right) = -\frac{4}{\omega_{NO_2} S} \ln\left(1 - \frac{[\text{particle } ^{13}N]}{[^{13}NO_2]_{g,0}}\right) \quad (2)$$

Here we assume $[^{13}NO_2]_{g,t} = [^{13}NO_2]_{g,0} - [\text{particle } ^{13}N]$, which is justified as ^{13}N on the particle originates from gas phase $^{13}NO_2$.

Figure 3 shows the uptake coefficients of NO_2 (γ_{NO2}) on BSA and deliquesced NaCl particles as a function of NO_2 mixing ratio with fixed RH (60%) and O_3 mixing ratio: (a) 30 ppb, (b) 70 ppb, and (c) 150 ppb. γ_{NO2} was almost constant in the 0 – 40 ppb NO_2 range at 30 and 70 ppb O_3. As the NO_2 concentration increases to 100 ppb, γ_{NO2} decreases by factor of ~4. γ_{NO2} on deliquesced NaCl particles are by a factor of ~5 smaller than that by BSA and showed only a small dependence on the NO_2 mixing ratio.

Figure 4 shows the γ_{NO2} on BSA and deliquesced NaCl particles as a function of O_3 mixing ratio with fixed RH (60%) and NO_2 mixing ratio: (a) 9 ppb, (b) 26 ppb, (c) 75 ppb, and (d) 100 ppb. γ_{NO2} showed pronounced non-linear increases with increasing O_3 mixing ratio. For example, at 9 ppb NO_2 γ_{NO2} on BSA is 4.4×10^{-6} at 16 ppb O_3, which is enhanced by factor of ~30 to 1.0×10^{-4} at 158 ppb O_3. The γ_{NO2} on deliquesced NaCl is one order of magnitude smaller, which is likely to be attributed to the formation of gas phase NO_3 and N_2O_5, as neither O_3 nor NO_2 is expected to rapidly react with deliquesced NaCl.

NO_2 can be oxidized by O_3 to form the highly reactive NO_3 in the gas phase. NO_3 radicals could further react with NO_2 to form N_2O_5. Generally NO_3 radical could directly react with particles to cause oxidation/nitration. The reactive uptake coefficients of NO_3 on liquid and solid surfaces of unsaturated organic are reported to be in the range of 10^{-3} – 0.1 (Moise et al., 2002; Gross et al., 2009). N_2O_5 undergoes heterogeneous hydrolysis to form HNO_3 on the

surface. There have been extensive laboratory investigations of the reactive uptake coefficients of N_2O_5 on aqueous inorganic particles, which showed reactive uptake coefficients between 0.02 - 0.15 (Hu and Abbatt, 1997; Knopf et al., 2007; Cosman and Bertram, 2008).

To evaluate the influence of NO_3 and N_2O_5 in the flow reactor, the temporal evolution of gas phase species and uptake of NO_3 and N_2O_5 in the flow reactor was modeled within the experimental reaction time (~10 min).using a kinetic double-layer model (Shiraiwa et al., 2009). The gas phase reactions considered in the model are listed in Table 1. The kinetic parameters were taken from Finlayson-Pitts and Pitts (2000). The photolysis rate of NO_3 (GPR2 and GPR3) is hard to determine as the reported value is the value under sunlight, while the experiment was done under undefined light intensity in the laboratory. For simplicity the photolysis rates were assumed to be 0, which may have led to an overestimation of the NO_3 concentration. The reactive uptake of NO_3 and N_2O_5 by particles was considered by using the elementary gas-surface reaction probabilities (γ_{gsr}) (Pöschl et al., 2007; Shiraiwa et al., 2009), which is assumed to be equivalent to the reactive uptake coefficient. To estimate the possible maximum contribution of NO_3 and N_2O_5 to the apparent NO_2 uptake, γ_{gsr} are assumed to be the maximum reported values: $\gamma_{gsr,NO3} = 0.1$, $\gamma_{gsr,N2O5} = 0.15$. The loss of NO_3 and N_2O_5 by the wall was also not considered for simplicity, which also led to an overestimation of their concentration.

The initial mixing ratios of O_3 and NO_2 were set to 120 and 10 ppb, respectively, as an exemplary simulation, whereas those of NO_3, N_2O_5, and NO were set to 0. The model results show that the steady-state condition was achieved in less than 1 min. The mixing ratios of O_3 and NO_2 showed only a slight decrease (< 3%) and remained practically unchanged. The NO_3 and N_2O_5 mixing ratios were comparable and between of 0.1 and 1 ppt, whereas NO mixing ratio remained low at ~0.01 ppt. The model underestimates the observed uptake of NO_2 by BSA significantly as shown in Fig. 5(a). NO_3 and N_2O_5 uptake could explain only ~30% of the observed uptake, indicating gas phase NO_3 and N_2O_5 is not the main contributor. This is certainly a conservative upper limit, since we do not take into account wall losses, which likely reduce this contribution significantly. On the other hand, the model can successfully reproduce the observed NO_2 uptake by deliquesced NaCl particles as shown in Fig. 5(b), indicating that gas phase NO_3 and N_2O_5 is the main contributor.

The dependence of uptake of NO_2 on relative humidity (RH) in the range of 24 – 75% is shown in Figure 6 with two concentration sets of O_3 and NO_2 (10 ppb NO_2, 120 ppb O_3 and 9

ppb NO_2, 30 ppb O_3). In both cases, there were no clear effects of RH on NO_2 uptake. Shiraiwa et al. (2011a) emphasized the strong effects of relative humidity on ozone uptake by protein due to the moisture-induced phase transition (Mikhailov et al., 2009). The ozone uptake by protein at 70% RH is ca. 50% higher than that at 70 % RH. This implies that the NO_2 uptake is not limited by the formation of reactive oxygen intermediates, but limited by reaction between intermediates and NO_2. Note that Franze et al. (2005) reported that under dry condition the degree of protein nitration was very low compared to under 40% RH, suggesting the importance of hygroscopic growth of BSA on nitration. Generally, competitive adsorption of water vapor could reduce the uptake by particles (Pöschl et al., 2001), which is not clearly seen in this study. The promoting effects of hydration may be counteracted by the competing effects of water adsorption at the surface.

3.3. Uptake of NO_2 by pretreated BSA with O_3

To further investigate the mechanism of the protein nitration, we conducted additional experiments with O_3 as a possibly competing oxidant on the aerosol surface (Shiraiwa et al., 2011b). Protein particles were pretreated by 97 ppb O_3 in the first flow reactor with variable reaction time in the range of 0 - 2 min. O_3 was then removed from the aerosol in a denuder coated with potassium iodide (KI). The aerosol flow was further introduced into a second reactor with maximum residence time of ~10 min to investigate the decay of intermediates. They were again introduced to a KI denuder in case some O_3 should have desorbed from the particle phase to the gas phase in this reactor. The gas phase O_3 free aerosol flow was finally mixed with NO_2 in the third flow reactor with 4 - 5 different reaction times within ~10 min. All experiments were performed at 50 (±3)% RH.

As reported in Shiraiwa et al. (2011b), the obtained γ_{NO2} is larger than for the case when O_3 and NO_2 coexist in the flow reactor, confirming that the uptake route via NO_3 and N_2O_5 are not the main pathways, by which labelled NO_2 is ending up in the protein particles, as neither NO_3 nor N_2O_5 could be formed in this system. Moreover, Shiraiwa et al. (2011b) did not observe significant decrease of γ_{NO2} when the decay time of intermediates in the second reactor was varied up to 550 s, confirming the long lifetime of intermediates.

The reaction time between O_3 and BSA particles in the first reactor was varied between 0 – 2 min. As shown in Fig. 8, the observed γ_{NO2} did not show any significant increase as reaction

time increases, and is rather independent on the reaction time with O_3. This indicates that BSA could react with O_3 quickly to form reactive oxygen intermediates (ROIs), and the reaction between ROIs and NO_2 is the limiting step. Indeed, NO_2 uptake by ROI showed strong time dependence, i.e., the longer reaction time between ROI and NO_2 lead to higher uptake of NO_2.

3.4. Uptake of O_3 by BSA

Figure 7 illustrates the results of one such experiment of BSA and tyrosine exposed to 200 ppbv of O_3. A constant value of γ_{O3} on tyrosine at ~10^{-4} was observed during the first ~5 min, which was by one order of magnitude higher than the initial uptake coefficient on BSA and clearly indicating that tyrosine is very reactive towards O_3. Shiraiwa et al. (2011a) observed that the magnitude and temporal evolution of γ_{O3} did not change when the thickness of the protein film on the flow tube walls was varied between 133–346 nm, indicating that the ozone uptake was kinetically limited by processes at or near the surface of the protein film. If the uptake kinetics had been affected by processes involving the entire volume of the protein film, the film thickness should have influenced the results, i.e., thicker films should have exhibited higher values or slower decrease of γ_{O3}. Moreover, Fig. 7 exhibit a slope that is characteristic for diffusion-limited gas uptake uptake ($\gamma \propto (D/\pi t)^{1/2}$, $\partial \ln\gamma / \partial \ln t = -0.5$) (Huthwelker and Peter, 1996). Thus, the most plausible explanation for the observed behavior is that the uptake of ozone was limited by bulk diffusion. The time, dependence of γ_{O3} can be reproduced by the kinetic multilayer flux model KM-SUB (Shiraiwa et al., 2010), as shown in dotted lines in Fig. 7.

Shiraiwa et al. (2011a) shows that the uptake coefficients observed at a given ozone concentration level increased with increasing relative humidity. This can be explained by a decrease of viscosity and increase of diffusivity with increasing RH, while the amorphous protein is transformed from a glassy to a semi-solid state.

Figure 9 shows the molecular weight of native BSA and BSA exposed to O_3 at dry and 95% RH conditions, obtained by HPLC-chip MS/MS system. The molecular weight of native BSA is 66.4 kDa, and after the exposure of O_3 the molecular weight shifted due to the modification. The degree of modification is more prominent at 95% RH condition, consistent with ozone uptake results. Some products have smaller molecular mass probably due to decomposition of molecules via ozonolysis. Interestingly the formation of dimer is observed. At wet conditions some products pose larger molecular weight than dimer of 13.3 kDa, which may

due to dimerization between modified monomers or secondary reactions between dimer and decomposed protein.

The phenoxy radical derivatives of tyrosine residues are known to undergo dimerization (Bartesaghi et al., 2007). Moreover, the final products of the protein nitration reaction are nitrotyrosine residues, and phenoxy radicals are well established intermediates in the nitration of phenolic compounds by NO_2 (Harrison et al., 2005). In addition, phenoxy radicals can be efficiently stabilized in condensed phases (Truong et al., 2010), which is consistent with the observed long lifetime of the ROI. Thus, as shown in Fig. 10 the identity of ROI is most likely phenoxy radical derivatives, as speculated by Shiraiwa et al. (2011b).

4. Conclusions

Reaction kinetics and mechanism of the nitration of the aerosolized protein by O_3 and NO_2 was investigated at atmospherically relevant concentration. In the absence of O_3, NO_2 uptake by both protein and deliquesced NaCl particles were below detection limit ($\gamma_{NO2} < \sim 10^{-6}$). In the presence of O_3, however, the γ_{NO2} of BSA were of the order of 10^{-5}, which is one order of magnitude larger than that of deliquesced NaCl, indicating the higher reactivity of protein particles. The γ_{NO2} of BSA enhance up to $\sim 1 \times 10^{-4}$ with the increase of the O_3 concentration, while they decrease with the increase of the NO_2 concentration.

The additional experiments confirm that gas phase NO_3 or N_2O_5 have small contribution to NO_2 uptake. Rather, O_3 reacts with protein to form reactive oxygen intermediates (ROIs), which could further react with NO_2 efficiently. The kinetic results suggest that protein contained bio particles such as pollen can be efficiently nitrated in urban polluted air masses. The products analysis of ozone exposed protein strongly indicates phenoxy radical derivatives of tyrosine amino acid residues as chemical identities of ROI.

Acknowledgements.

This work was funded by the Swiss National Science Foundation (grant no. 200020-109341), the Max Planck Society (MPG) and the European integrated project on cloud climate and air quality interactions (No 036833-2, EUCAARI). MS is supported by the Max Planck Graduate Center – Johannes Gutenberg University Mainz (MPGC - JOGU) and the Ministry of Education, Culture, Sports, Science and Technology – Japan (MEXT). We thank M. Birrer for technical support and

T. Bartels-Rausch, M. Kerbrat, Y. Zhang for support and stimulating discussions. The staffs of the PSI accelerator facilities are appreciated for providing the stable proton beams.

References.

Abbatt, J. P. D. and Waschewsky, G. C. G.: Heterogeneous interactions of HOBr, HNO_3, O_3, and NO_2 with deliquescent NaCl aerosols at room temperature, J. Phys. Chem. A, 102, 3719-3725, 1998.

Ammann, M.: Using ^{13}N as tracer in heterogeneous atmospheric chemistry experiments, Radiochimica Acta, 89, 831-838, 2001.

Ammann, M., Rossler, E., Strekowski, R. and George, C.: Nitrogen dioxide multiphase chemistry: Uptake kinetics on aqueous solutions containing phenolic compounds, Phys. Chem. Chem. Phys., 7, 2513-2518, 2005.

Bartesaghi, S., Ferrer-Sueta, G., Peluffo, G., Valez, V., Zhang, H., Kalyanaraman, B. and Radi, R.: Protein tyrosine nitration in hydrophilic and hydrophobic environments, Amino Acids, 32, 501-515, 10.1007/s00726-006-0425-8, 2007.

Behnke, W., George, C., Scheer, V. and Zetzsch, C.: Production and decay of ClNO2, from the reaction of gaseous N2O5 with NaCl solution: Bulk and aerosol experiments, J. Geophys. Res.-Atmos., 102, 3795-3804, 1997.

Brunekreef, B. and Sunyer, J.: Asthma, rhinitis and air pollution: is traffic to blame?, European Respiratory Journal, 21, 913-915, 10.1183/09031936.03.00014903, 2003.

Cape, J. N., Storetonwest, R. L., Devine, S. F., Beatty, R. N. and Murdoch, A.: The reaction of nitrogen dioxide at low concentrations with natural waters, Atmospheric Environment Part a-General Topics, 27, 2613-2621, 1993.

Cooney, D. O., Kim, S. S. and Davis, E. J.: Analyses of mass-transfer in hemodialyzers for laminar blood-flow and homogeneous dialysate, Chem. Eng. Sci., 29, 1731-1738, 1974.

Cosman, L. M. and Bertram, A. K.: Reactive uptake of N_2O_5 on aqueous H_2SO_4 solutions coated with 1-component and 2-component monolayers, J. Phys. Chem. A, 112, 4625-4635, 10.1021/jp8005469, 2008.

Franze, T., Weller, M. G., Niessner, R. and Pöschl, U.: Protein nitration by polluted air, Environ. Sci. Technol., 39, 1673-1678, 10.1021/es0488737, 2005.

Fröhlich-Nowoisky, J., Pickersgill, D. A., Despres, V. R. and Pöschl, U.: High diversity of fungi in air particulate matter, Proc Natl Acad Sci USA, 106, 12814-12819, 10.1073/pnas.0811003106, 2009.

Gross, S., Iannone, R., Xiao, S. and Bertram, A. K.: Reactive uptake studies of NO_3 and N_2O_5 on alkenoic acid, alkanoate, and polyalcohol substrates to probe nighttime aerosol chemistry, Phys Chem Chem Phys, 11, 7792-7803, 2009.

Gruijthuijsen, Y. K., Grieshuber, I., Stocklinger, A., et al.: Nitration enhances the allergenic potential of proteins, Int. Arch. Allergy Immunol., 141, 265-275, 10.1159/000095296, 2006.

Harrison, M. A. J., Barra, S., Borghesi, D., Vione, D., Arsene, C. and Olariu, R. L.: Nitrated phenols in the atmosphere: a review, Atmos. Environ., 39, 231-248, 10.1016/j.atmosenv.2004.09.044, 2005.

Harrison, R. M. and Collins, G. M.: Measurements of reaction coefficients of NO2 and HONO on aerosol particles, Journal of Atmospheric Chemistry, 30, 397-406, 1998.

Hu, J. H. and Abbatt, J. P. D.: Reaction probabilities for N_2O_5 hydrolysis on sulfuric acid and ammonium sulfate aerosols at room temperature, J. Phys. Chem. A, 101, 871-878, 1997.

Huffman, J. A., Treutlein, B. and Pöschl, U.: Fluorescent biological aerosol particle concentrations and size distributions measured with an ultraviolet aerodynamic particle sizer (UV-APS) in Central Europe, Atmos. Chem. Phys. Discuss., 9, 17705-17751, 2009.

Huthwelker, T. and Peter, T.: Analytical description of gas transport across an interface with coupled diffusion in two phases, J. Chem. Phys., 105, 1661-1667, 1996.

Jaenicke, R.: Abundance of cellular material and proteins in the atmosphere, Science, 308, 73-73, 10.1126/science.1106335, 2005.

Janssen, N. A. H., Brunekreef, B., van Vliet, P., Aarts, F., Meliefste, K., Harssema, H. and Fischer, P.: The relationship between air pollution from heavy traffic and allergic sensitization, bronchial hyperresponsiveness, and respiratory symptoms in Dutch schoolchildren, Environ. Health Perspect., 111, 1512-1518, 10.1289/ehp.6243, 2003.

Kalberer, M., Ammann, M., Arens, F., Gäggeler, H. W. and Baltensperger, U.: Heterogeneous formation of nitrous acid (HONO) on soot aerosol particles, J. Geophys. Res.-Atmos., 104, 13825-13832, 1999.

Karlsson, R. and Ljungstrom, E.: A laboratory study of the interaction of NH3 and NO2 with sea salt particles, Water Air and Soil Pollution, 103, 55-70, 1998.

Knopf, D. A., Cosman, L. M., Mousavi, P., Mokamati, S. and Bertram, A. K.: A novel flow reactor for studying reactions on liquid surfaces coated by organic monolayers: Methods, validation, and initial results, J. Phys. Chem. A, 111, 11021-11032, 10.1021/jp075724c, 2007.

Krämer, U., Behrendt, H., Dolgner, R., Ranft, U., Ring, J., Willer, H. and Schlipkoter, H. W.: Airway diseases and allergies in East and West German children during the first 5 years after reunification: time trends and the impact of sulphur dioxide and total suspended particles, Int. J. Epidemiol., 28, 865-873, 1999.

Levaggi, D. A., Siu, W., Feldstei.M and Kothny, E. L.: Quantitative separation of nitri-oxide from nitrogen-dioxide at atmospheric concentration ranges, Environ. Sci. Technol., 6, 250-&, 1972.

Miguel, A. G., Cass, G. R., Glovsky, M. M. and Weiss, J.: Allergens in paved road dust and airborne particles, Environ. Sci. Technol., 33, 4159-4168, 1999.

Mikhailov, E., Vlasenko, S., Martin, S. T., Koop, T. and Pöschl, U.: Amorphous and crystalline aerosol particles interacting with water vapor: conceptual framework and experimental evidence for restructuring, phase transitions and kinetic limitations, Atmos. Chem. Phys., 9, 9491-9522, 2009.

Moise, T., Talukdar, R. K., Frost, G. J., Fox, R. W. and Rudich, Y.: Reactive uptake of NO_3 by liquid and frozen organics, J. Geophys. Res.-Atmos., 107, 10.1029/2001jd000334, 2002.

Murphy, D. M. and Fahey, D. W.: Mathematical treatment of the wall loss of a trace species in denuder and catalytic-converter tubes, Anal. Chem., 59, 2753-2759, 1987.

Pöschl, U., Letzel, T., Schauer, C. and Niessner, R.: Interaction of ozone and water vapor with spark discharge soot aerosol particles coated with benzo[a]pyrene: O_3 and H_2O adsorption, benzo[a]pyrene degradation, and atmospheric implications, J. Phys. Chem. A, 105, 4029-4041, 2001.

Pöschl, U., Rudich, Y. and Ammann, M.: Kinetic model framework for aerosol and cloud surface chemistry and gas-particle interactions - Part 1: General equations, parameters, and terminology, Atmos. Chem. Phys., 7, 5989-6023, 2007.

Ring, J., Kramer, U., Schafer, T. and Behrendt, H.: Why are allergies increasing?, Curr. Opin. Immunol., 13, 701-708, 2001.

Saxon, A. and Diaz-Sanchez, D.: Air pollution and allergy: you are what you breathe, Nat. Immunol., 6, 223-226, 10.1038/ni0305-223, 2005.

Schäppi, G. F., Suphioglu, C., Taylor, P. E. and Knox, R. B.: Concentrations of the major birch tree allergen Bet v 1 in pollen and respirable fine particles in the atmosphere, J. Allergy Clinical Immunol., 100, 656-661, 1997.

Shiraiwa, M., Garland, R. M. and Pöschl, U.: Kinetic double-layer model of aerosol surface chemistry and gas-particle interactions (K2-SURF): Degradation of polycyclic aromatic hydrocarbons exposed to O_3, NO_2, H_2O, OH and NO_3, Atmos. Chem. Phys., 9, 9571-9586, 2009.

Shiraiwa, M., Pfrang, C. and Pöschl, U.: Kinetic multi-layer model of aerosol surface and bulk chemistry (KM-SUB): the influence of interfacial transport and bulk diffusion on the oxidation of oleic acid by ozone, Atmos. Chem. Phys., 10, 3673-3691, 2010.

Shiraiwa, M., Ammann, M., Koop, T. and Pöschl, U.: Gas uptake and chemical aging of semi-solid organic aerosol particles, Proc Natl Acad Sci USA, 2011a.

Shiraiwa, M., Sosedova, Y., Rouviere, A., Yang, H., Zhang, Y., Abbatt, J. P. D., Ammann, M. and Pöschl, U.: The role of long-lived reactive oxygen intermediates in the reaction of ozone with aerosol particles, Nature Chem., 3, 291-295, 10.1038/nchem.988, 2011b.

Souza, J. M., Peluffo, G. and Radi, R.: Protein tyrosine nitration - Functional alteration or just a biomarker?, Free Radical Biol. Med., 45, 357-366, 10.1016/j.freeradbiomed.2008.04.010, 2008.

Stemmler, K., Ndour, M., Elshorbany, Y., Kleffmann, J., D'Anna, B., George, C., Bohn, B. and Ammann, M.: Light induced conversion of nitrogen dioxide into nitrous acid on submicron humic acid aerosol, Atmos. Chem. Phys., 7, 4237-4248, 2007.

Traidl-Hoffmann, C., Jakob, T. and Behrendt, H.: Determinants of allergenicity, J. Allergy Clinical Immunol., 123, 558-566, 10.1016/j.jaci.2008.12.003, 2009.

Truong, H., Lomnicki, S. and Dellinger, B.: Potential for Misidentification of Environmentally Persistent Free Radicals as Molecular Pollutants in Particulate Matter, Environ. Sci. Technol., 44, 1933-1939, 10.1021/es902648t, 2010.

Wahn, U.: What drives the allergic march?, Allergy, 55, 591-599, 2000.

Yabushita, A., Enami, S., Sakamoto, Y., Kawasaki, M., Hoffmann, M. R. and Colussi, A. J.: Anion-Catalyzed Dissolution of NO_2 on Aqueous Microdroplets, J. Phys. Chem. A, 113, 4844-4848, 10.1021/jp900685f, 2009.

Yang, H., Zhang, Y. and Pöschl, U.: Quantification of nitrotyrosine in nitrated proteins, Anal. Bioanal. Chem., 397, 879-886, 10.1007/s00216-010-3557-3, 2010.

Zhang, Y., Yang, H. and Pöschl, U.: Analysis of nitrated proteins and tryptic peptides by HPLC-chip-MS/MS: site-specific quantification, nitration degree, and reactivity of tyrosine residues, Anal. Bioanal. Chem., 1-13, 10.1007/s00216-010-4280-9, 2010.

Table 1. Gas phase reaction (GPR) included in the box model.

	Gas phase reaction	Rate coefficient (296 K)
GPR1	$NO_2 + O_3 \rightarrow NO_3 + O_2$	3.2×10^{-17} cm^3 molecule^{-1} s^{-1}
GPR2	$NO_3 + h\nu \rightarrow NO + O_2$	0 – 0.016 s^{-1}
GPR3	$NO_3 + h\nu \rightarrow NO_2 + O$	0 – 0.19 s^{-1}
GPR4	$NO + O_3 \rightarrow NO_2 + O_2$	1.8×10^{-14} cm^3 molecule^{-1} s^{-1}
GPR5	$NO + NO_3 \rightarrow 2NO_2$	2.6×10^{-11} cm^3 molecule^{-1} s^{-1}
GPR6	$NO_2 + NO_3 + M \leftrightarrow N_2O_5 + M$	$K_{eq} = 2.9 \times 10^{-11}$ cm^3 molecule^{-1}
GPR7	$NO_3 + M \rightarrow NO + O_2 + M$	3.0×10^{-3} s^{-1}

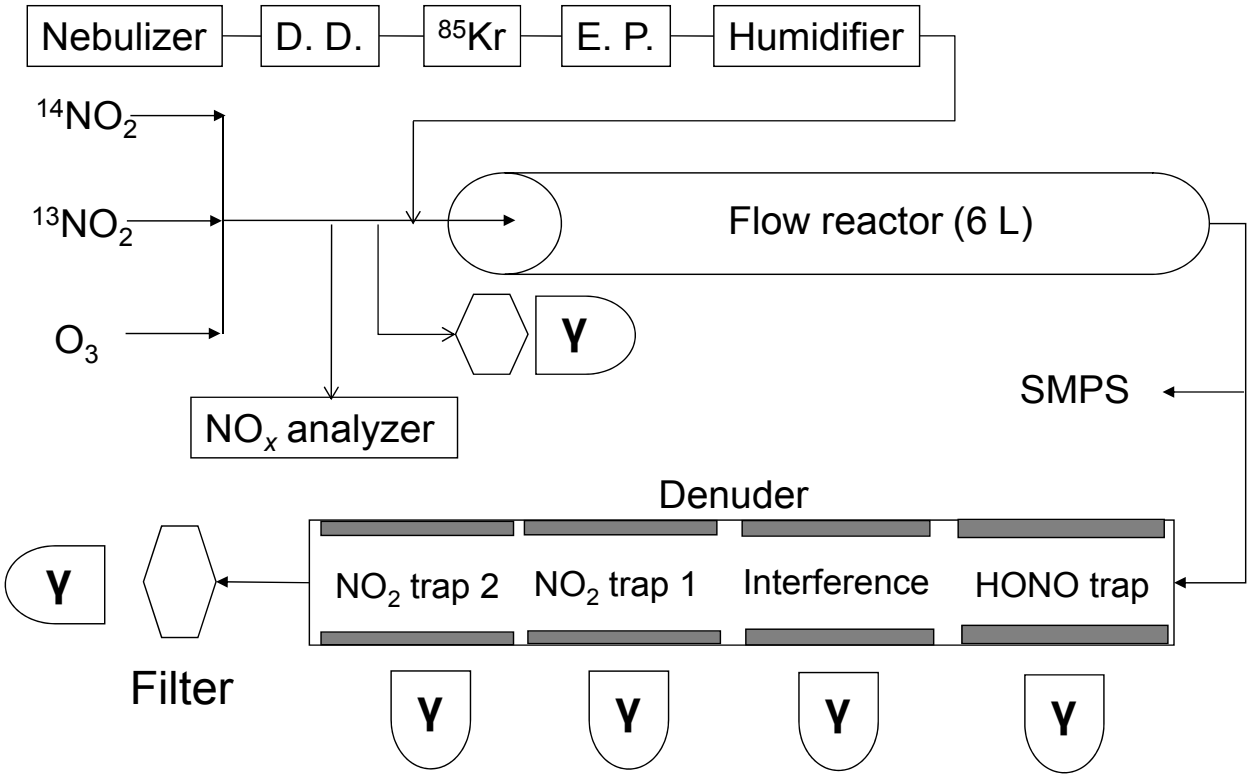

Figure 1. Scheme of the experimental setup: D. D. – Diffusion dryer, E. P. – Electrostatic precipitator.

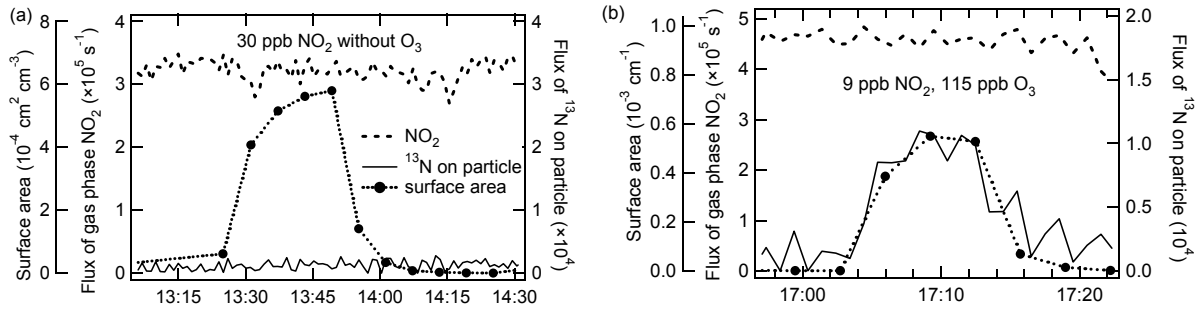

=

Figure 2. Experimental profiles of NO_2 interacting with protein (BSA) particles: NDA denuder signal representing gas phase NO_2 (dashed line), signal from particle filter representing NO_2 on particle (solid line), and surface area measured by SMPS (dotted line with markers): (a) 30 ppb NO_2 at 60% RH, (b) 9 ppb NO_2, 120 ppb O_3 at 25% RH.

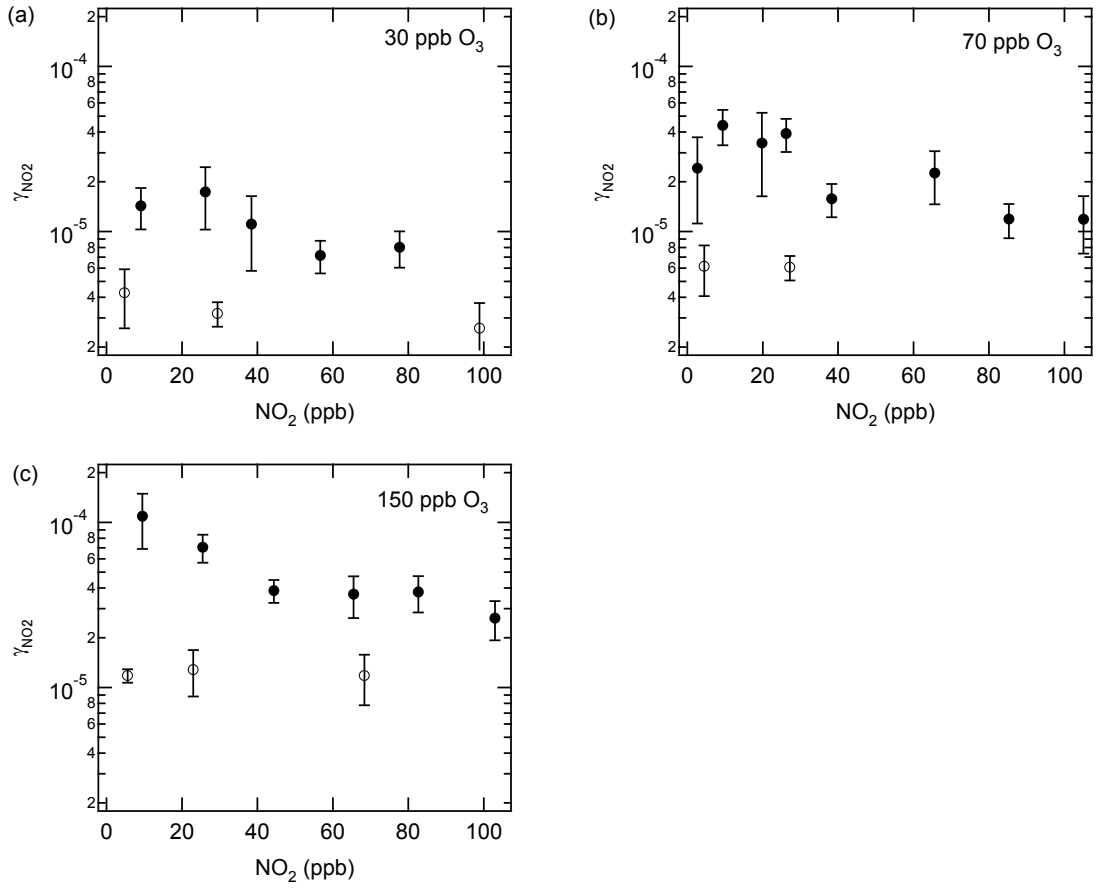

Figure 3. Uptake coefficients of NO_2 (γ_{NO2}) by BSA (circle) and deliquesced NaCl (open circle) particles under 60% RH as a function of NO_2 mixing ratio with fixed O_3 mixing ratio: (a) 30 ppb, (b) 70 ppb, and (c) 150 ppb.

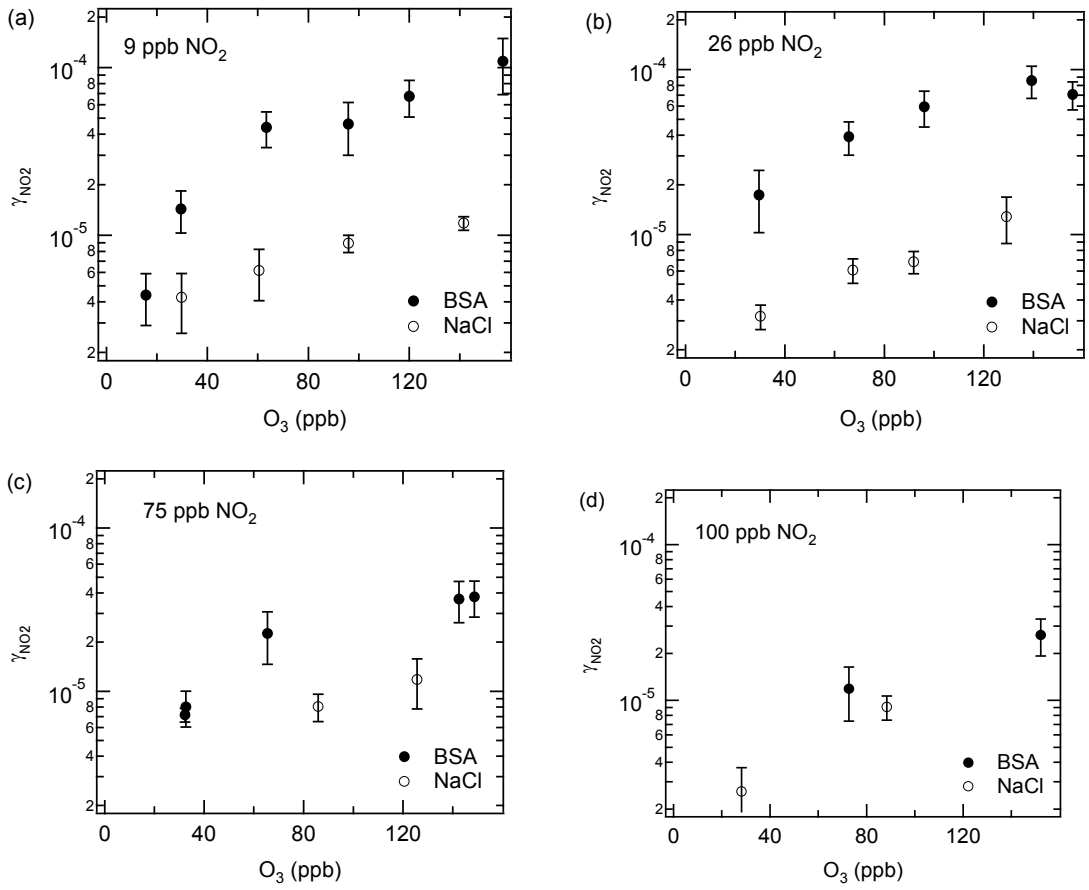

Figure 4. Uptake coefficients of NO_2 (γ_{NO2}) by BSA (circle) and deliquesced NaCl (open circle) particles under 60% RH as a function of O_3 mixing ratio with fixed NO_2 mixing ratio: (a) 9 ppb, (b) 26 ppb, (c) 75 ppb, and (d) 100 ppb.

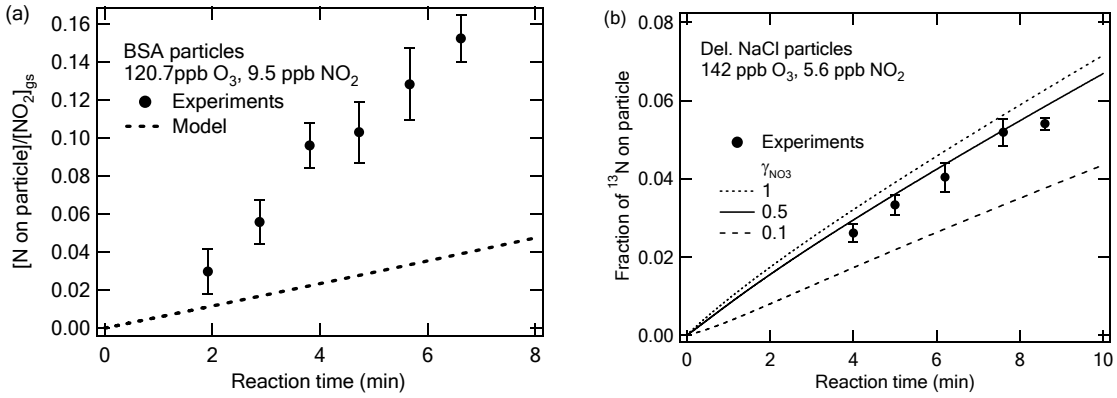

Figure 5. The measured fraction of NO_2 ([NO_2 on particle]/[NO_2]$_g$) on (a) BSA particles and (b) deliquesced NaCl particles as function of reaction time. The dotted lines are modeled considering the contribution from gas phase NO_3 formation and their uptake to particles.

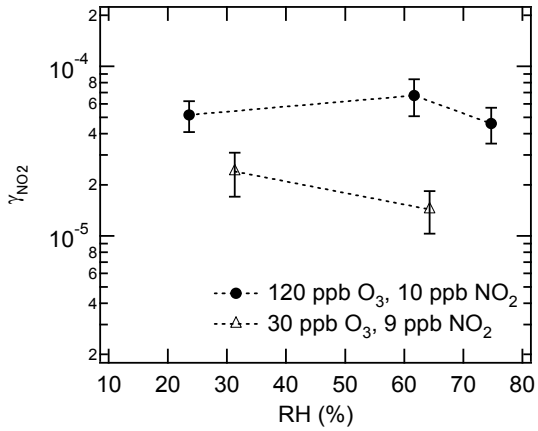

Figure 6. Uptake coefficients of NO_2 (γ_{NO2}) by BSA particles as a function of relative humidity (RH).

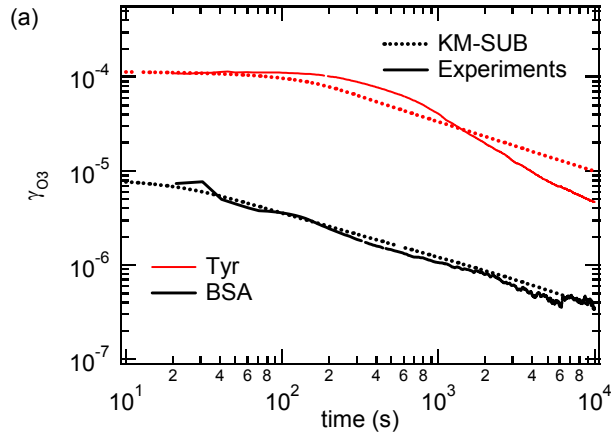

Figure 7. O_3 uptake coefficients (γ_{O3}) by tyrosine and BSA film at 200 ppb O_3 and 50% RH.

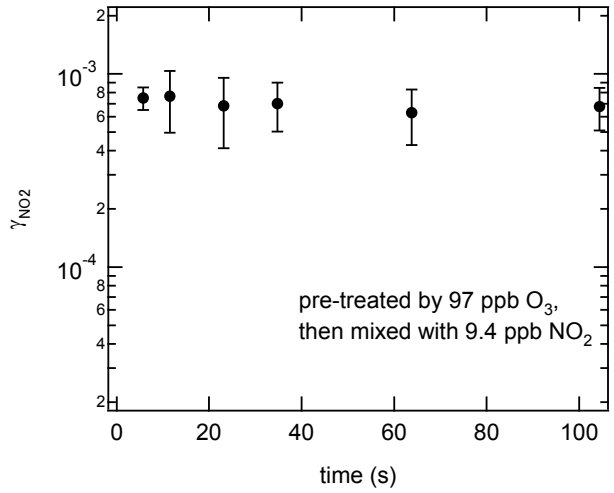

Figure 8. Uptake coefficients of NO_2 (γ_{NO2}) by BSA particles, which was first exposed to 97 ppb O_3 and then exposed to NO_2 as function of reaction time between O_3 and BSA particles.

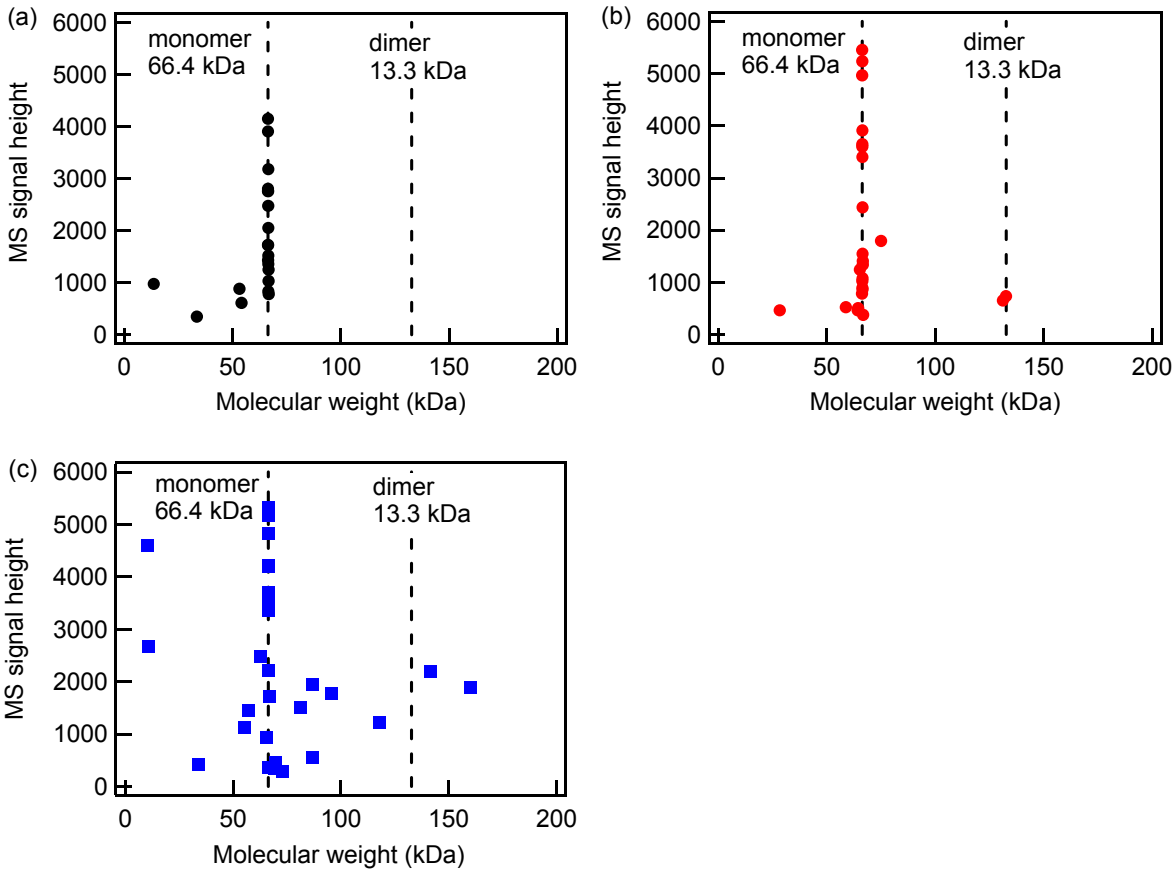

Figure 9. The molecular weight of (a) native BSA and BSA exposed to O_3 at (b) dry and (c) wet conditions (95% RH). The molecular weight of native BSA is 66.4 kDa. Due to the reaction with O_3, dimerization and decomposition of BSA are observed and the degree of modification is larger at wet condition.

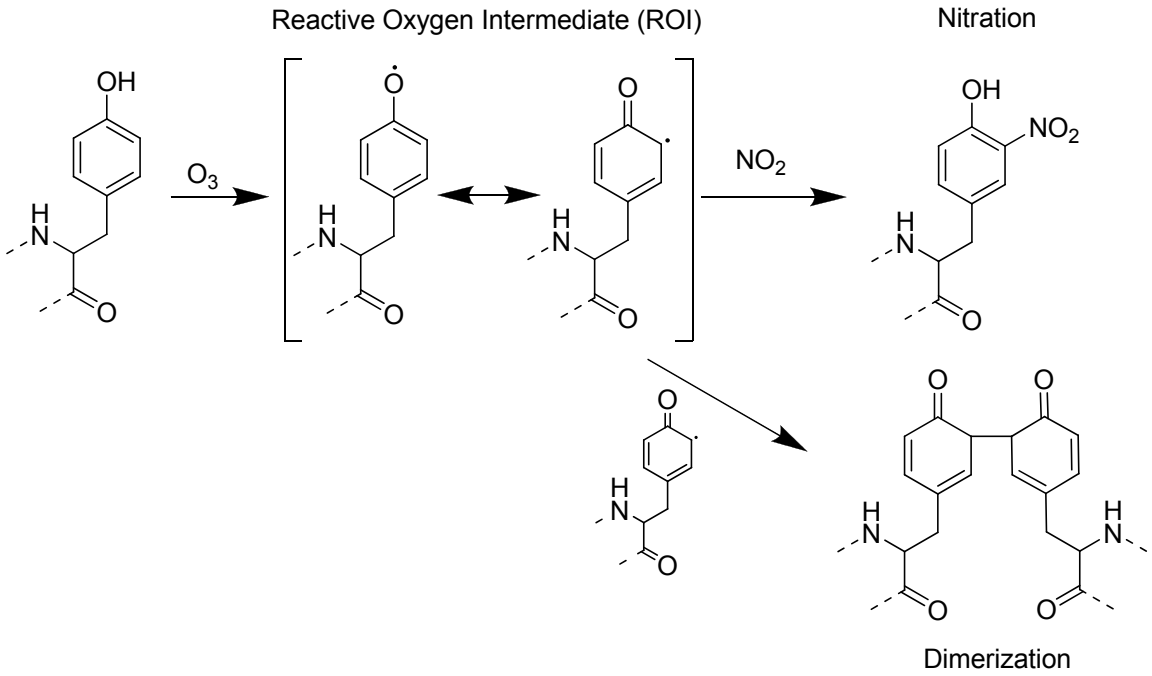

Figure 10. Schematics of reaction pathways of protein BSA and ozone and nitrogen dioxide.

Appendix C. Media Reports

Shiraiwa et al. Nature Chem., 2011 (Appendix B4) was widely reported by medias including newspapers, radio, and TV over Europe and in Japan.

Below are the lists of media reports in German newspapers and radios.

- Allgemeine Zeitung vom 21.02.2011, Seite 0, „Mehr Ozon, mehr Allergien“
- Berliner Zeitung vom 22.02.2011, Seite 12, „Schadstoffe verändern Oberfläche von Pollen Grund für Allergiehäufigkeit“
- dapd Nachrichtendienste vom 20.02.2011, Seite 0, „(Sperrfrist 19.00 Uhr) Allergien: Sauerstoffverbindungen machen Pollen und Feinstaub scharf“
- FOCUS online vom 21.02.2011, Seite online, „Warum Allergien auf dem Vormarsch sind“
- Frankfurter Rundschau vom 22.02.2011, Seite 22, „Schadstoffe verändern Oberfläche von Pollen”
- Gränzbote vom 22.02.2011, Seite 7„Wissenschaftler sind Allergien auf der Spur ”
- Neue OZ Osnabrücker Zeitung vom 21.02.2011, Seite, „Scharfmacher in der Luft“
- pressetext vom 22.02.2011, Seite 0, „Reaktive Sauerstoffformen begünstigen Allergien“
- WELT ONLINE vom 23.02.2011, „Sauerstoffverbindungen lassen Allergien steigen“
- Recklinghäuser Zeitung vom 24.02.2011, Seite 33, Ohne Titelangabe
- Recklinghäuser Zeitung vom 03.03.2011, Seite 35, „Verstärkte Allergien“
- RP Online (Rheinische Post) vom 25.02.2011, Seite Online 25.02.2011, 21:17 Uhr, „Abgase gefährlicher als bisher bekannt“
- Stuttgarter Nachrichten - Stadtausgabe vom 23.02.2011, Seite 32, „Auch im hohen Alter für Heuschnupfen anfällig“
- Süddeutsche Zeitung vom 23.02.2011, Seite 16, „Eine unheilige Allianz“
- Thüringer Allgemeine vom 22.02.2011, Seite 0, „Abgase als häufige Ursachevon Allergien“
- Westfalenpost vom 21.02.2011, Seite 4
- Schwäbische Zeitung Laupheim vom 25.02.2011, Seite 2, „Wissenschaftler sind Allergien auf der Spur“
- Frankfurter Allgemeine Zeitung vom 11.03.2011, „Der Scharfmacher für Pollenkörner“

- Süd West Rundfunk vom 22.02.2011, „Warum Allergien zur Volkskrankheit werden“
- Campus Radio Köln vom 09:10 Uhr, 28.02.2011, „Dangerous Oxygen“

Below are the lists of media reports in Japanese newspapers and TV.

- The NIKKEI Shimbun（日本経済新聞）,朝刊,23.02.2011,「大気汚染　花粉症悪化、仕組み解明」
- The ASAHI Shimbun（朝日新聞）, 朝刊, 04.03.2011,「大気中のオゾン　変化の過程解明　発がん性に影響」
- Tokyo Broadcast System Television (TBS テレビ), 09.03.2011,　N スタ、「大気汚染で花粉症が」

Curriculum Vitae

Personal information

NAME	Manabu Shiraiwa
BIRTH	27 April 1983 in Niigata, Japan
MARITAL STATUS	Married with one daughter

EDUCATION

2008–2011	PhD study, Max Planck Institute for Chemistry, Department of Biogeochemistry, Mainz, Germany Max Planck Graduate Center - Johannes-Gutenberg University, Mainz PhD project: "Kinetic modeling and experiments on gas uptake and chemical transformation of organic aerosol in the atmosphere" Supervisor: PD Dr. Ulrich Pöschl
2006 – 2008	Master study, The University of Tokyo, Department of Earth and Planetary Science, Graduate School of Science, Tokyo, Japan Master project: "Experimental and observational studies on mixing state of black carbon aerosol" Supervisor: Prof. Yutaka Kondo
2002 – 2006	Bachelor study, The University of Tokyo, Department of Chemistry, School of Science, Tokyo, Japan Bachelor project: "Observation of a rutile TiO_2 (110) ultra-smooth surface using a ultrahigh vacuum – scanning tunneling microscope" Supervisor: Prof. Tetsuya Hasegawa

AWARDS and SCHOLARSHIPS

2009 – 2011	Scholarship of Max Planck Graduate Center – Johannes Gutenberg University Mainz (MPGC-JOGU)
2008 – 2011	Scholarship of Ministry of Education, Culture, Sports, Science and Technology – Japan (MEXT)
2010	*Poster Award* at the International Max Planck Research School (IMPRS) days, Frankfurt
2009	*Best Poster Award* at the European Aerosol Conference (EAC) 2009, Karlsruhe
2008 – 2009	Scholarship of International Max Planck Research School for Atmospheric Chemistry and Physics (IMPRS-ACP)
2008	*Best Poster Award* at the IMPRS autumn school on Climate Change, Cyprus
2008	*Research Encouragement Award*, School of Science, the University of Tokyo